

**Reconstructing the Pleistocene depositional environments
at Schöningen (northern Germany):
Insights from 3D subsurface modelling and numerical
simulation**

Von der Naturwissenschaftlichen Fakultät
der Gottfried Wilhelm Leibniz Universität Hannover
zur Erlangung des Grades

DOKTOR DER NATURWISSENSCHAFTEN

Dr. rer. nat.

genehmigte Dissertation

von

Dipl.-Geow. Jörg Lang

geboren am 22.09.1982 in Hannover

2014

Referentin: Prof. Dr. Jutta Winsemann

Korreferentin: Prof. Dr. Andrea Hampel

Korreferent: Prof. Dr. Richard Pott

Tag der Promotion: 05.02.2014

Table of content

Abstract	3
Zusammenfassung	4
1. Introduction	5
1.1 Generation of the accommodation space	7
1.2 Middle Pleistocene glacigenic and interglacial depositional environments	10
1.3 The reaction of salt structures to ice-sheet loading	12
2. Study area	14
2.1 The Central European Basin System	14
2.2 The Subhercynian Basin	16
2.3 The Pleistocene glaciations	17
3. Methods	18
3.1 Field work	18
3.2 Acquisition and interpretation of shear-wave seismic data	19
3.3 3D subsurface modelling	20
3.4 Finite-element simulation	21
4. Overview of this thesis ó Publications and their content	22
5. References	23
Publication 1	37
The Pleistocene of Schöningen, Germany: a complex tunnel valley fill revealed from 3D subsurface modelling and shear-wave seismics	
Publication 2	75
The Middle Pleistocene tunnel valley at Schöningen as a Palaeolithic archive	
Publication 3	91
Lateral and vertical facies relationships of bedforms deposited by aggrading supercritical flows: from cyclic steps to humpback dunes	

Publication 4	127
Do salt structures react to ice-sheet loading? Insights from two-dimensional finite-element modelling	
6. Synthesis	157
6.1 Generation of the accommodation space	157
6.2 Interglacial depositional environments	159
6.3 Ice-marginal deposition in front of tunnel valleys	162
6.4 The reaction of salt structures to ice-sheet loading	164
7. Conclusions	166
8. References	167
Acknowledgements	173
Curriculum vitae	175
List of publications	177

Abstract

The Pleistocene deposits of Schöningen represent an outstanding geological and archaeological archive, where an up to 45 m thick, almost complete Middle Pleistocene to Holocene succession has been preserved and unique Lower Palaeolithic artefacts have been discovered. However, the geological setting remained yet poorly understood. The aims of this study are to understand the formation of the Pleistocene depocentre and to reconstruct the glacial and interglacial depositional processes and environments. The new model is based on the integration of outcrop data, borehole data, shear-wave seismic sections, 3D subsurface modelling and finite-element simulations.

The geometry and dimensions of the Pleistocene depocentre are characteristic of a subglacial tunnel valley, which is 300-850 m wide and 40 m deep. The basal tunnel-valley fill consists of Elsterian meltwater deposits and subglacial till. During the subsequent Holsteinian interglacial (MIS 9) a lake formed within the underfilled tunnel valley and was laterally infilled by delta deposits. Climatically controlled lake-level fluctuations led to the formation of laterally and vertically stacked delta systems. The long-lived interglacial lake provided an attractive site for animals and early humans ambushing them. Artefacts were mainly recovered from delta plain deposits, where they were embedded during lake-level rise. During the Saalian Drenthe ice advance the last remnant of the tunnel valley was completely filled by meltwater deposits and subsequently overlain by subglacial till.

Meltwater deposits offer the rare opportunity to study the facies architecture of bedforms related to aggrading supercritical to transcritical flows. The observed sandy bedforms include deposits of cyclic steps, chutes-and-pools, breaking antidunes, aggrading stationary antidunes and humpback dunes, which were deposited during ice-sheet retreat on ice-contact subaqueous fans and by glacial lake-outburst floods. The large-scale lateral and vertical facies architecture is controlled by the temporal and spatial evolution of the initial supercritical flows, which was strongly affected by the occurrence of hydraulic jumps. Small-scale facies changes and the formation of individual bedforms are related to fluctuating discharge, bed topography and pulsating unstable flows.

Finite-element simulations were applied to test the influence of ice-load induced salt flow in the Helmstedt-Staßfurt salt wall and its effect on the generation of accommodation space in the rim synclines. The model comprises a simplified geological 2D cross-section, which was loaded at the surface to simulate the weight of an ice sheet. The input parameters were systematically varied to detect the controlling factors. All simulations indicate that salt structures respond to ice-sheet loading. Salt structures rise in front of an ice-sheet and are pushed down beneath an ice sheet. The resulting displacements are in a range of few decimetres to several metres and will probably affect glacial erosion and deposition near the salt structure, but are too low to have a marked effect on the advance or retreat pattern of the ice sheet.

Keywords: Tunnel valley, interglacial deposition, Schöningen

Zusammenfassung

Schöningen stellt durch die Erhaltung einer ~45 m mächtigen mittelpleistozänen bis holozänen Abfolge ein hervorragendes geologisches und archäologisches Archiv dar, in dem einzigartige Artefakte überliefert wurden. Die geologische Gesamtsituation allerdings blieb bisher nur unzureichend geklärt. Das Ziel dieser Studie ist die Bildung des pleistozänen Ablagerungszentrums zu klären und die glazialen und interglazialen Ablagerungsprozesses und Ablagerungsräume zu rekonstruieren. Das neue Modell basiert auf Aufschlussbeobachtungen, Bohrlochdaten, scherwellenseismischen Profilen, 3D-Untergrundmodellierungen und Finite-Elemente Simulationen.

Die Geometrie und Dimensionen des pleistozänen Ablagerungszentrums sind typisch für eine subglaziale Rinne. Die subglaziale Rinne ist 300-850 m breit und 40 m tief, ihre basale Füllung besteht aus Schmelzwasserablagerungen und Grundmoräne. Während des Holstein-Interglazials bildete sich in der unvollständig verfüllten subglazialen Rinne ein See, welcher lateral durch Deltaablagerungen aufgefüllt wurde. Klimatisch gesteuerte Seespiegelschwankungen führten zur lateralen und vertikalen Stapelung der Deltaablagerungen. Artefakte stammen hauptsächlich aus Ablagerungen der Deltaebene. Während des Drenthe-Eisvorstoßes der Saale-Eiszeit wurde der letzte Rest der subglazialen Rinne durch Schmelzwasserablagerungen aufgefüllt und anschließend durch Grundmoräne überlagert.

Schmelzwasserablagerungen bieten die seltene Gelegenheit, Ablagerungen aggradierender superkritischer und transkritischer Strömungen zu untersuchen, welche für Eiskontaktfächer und Eisstauseeausbrüche typisch sind. Die untersuchten Abfolgen umfassen *cyclic steps*, *chutes-and-pools*, brechende Antidünen, aggradierende stationäre Antidünen und *humpback dunes*. Die übergeordnete laterale und vertikale Faziesarchitektur wurde durch die zeitliche und räumliche Entwicklung der ursprünglichen superkritischen Strömungen kontrolliert, die stark durch hydraulische Sprünge beeinflusst wurde. Kleinräumige Fazieswechsel wurden durch wechselnden Abflussraten, die Topographie des Untergrunds und pulsierende instabile Strömung kontrolliert.

Eine mögliche Reaktivierung der Helmstedt-Staßfurt Salzmauer durch Eisauflast und ihr Einfluss auf den Akkommodationsraum in den Randsenken wurde mit der Finiten-Elemente Modellierung untersucht. Das Model besteht aus einem vereinfachten geologischen 2D Schnitt, welcher an der Oberfläche belastet wird, um das Gewicht des Gletschers zu simulieren. Die Ausgangsbedingungen wurden systematisch variiert, um die Kontrollfaktoren zu bestimmen. Alle Simulationen zeigen an, dass Salzstrukturen auf Eisauflast reagieren. Salzstrukturen steigen vor dem Gletscher auf und werden subglazial nach unten gedrückt. Die resultierenden Versätze erreichen einige Dezimeter bis mehrere Meter und können wahrscheinlich glaziale Erosions- und Ablagerungsprozesse im Umfeld der Salzstruktur beeinflussen, sind aber zu niedrig, um einen deutlicheren Effekt auf den Verlauf von Eisvorstößen zu haben.

Schlagnworte: Subglaziale Rinne, interglaziale Ablagerungen, Schöningen

1. Introduction

The Pleistocene succession of Schöningen (Fig. 1) represents an outstanding geological and archaeological archive, where an up to 45 m thick, almost complete Middle Pleistocene to Holocene succession has been preserved and unique Lower Palaeolithic artefacts have been discovered. The preservation of such complete successions is rare in the terrestrial record of northern central Europe, where repeated ice advances (Fig. 1) caused the erosion of older deposits and successions are thus usually incomplete. Especially the preservation of Middle Pleistocene interglacial successions is rare and the recovery of the Palaeolithic artefacts offers an extraordinary chance for archaeology. The hunting spears, which were discovered in Holsteinian deposits (MIS 9; Urban *et al.*, 2011), belong to the oldest known wooden tools and represent a technological stage previously not attributed to Lower Palaeolithic humans (Thieme, 1997). Although the area of Schöningen has for almost 30 years been in the focus of archaeological research (Thieme, 1995, 2007; Serangeli *et al.*, 2012), the geological setting of the sites remained poorly understood and previous work focussed mainly on the palaeo-ecology of the interglacial deposits. Considering the importance of the artefact-bearing strata for archaeological research and their implications for the reconstruction of Lower Palaeolithic human behaviour, it is crucial to understand the geological setting that allowed for the preservation of the artefact-bearing strata. Schöningen also represents an unusually complete and well preserved sedimentary succession, reflecting the complex interaction between climate, sedimentation and possibly also salt tectonics under constantly changing conditions from the Middle Pleistocene to the Holocene.

Schöningen is located in the Subhercynian Basin in northern Germany, near the inverted southern margin of the Central European Basin System. The Pleistocene succession forms the uppermost part of the infill of the rim synclines of the Helmstedt-Staßfurt salt wall. The main fill of the rim synclines comprises lignite-bearing Palaeogene deposits, overlying Triassic bedrock (Look, 1984). The study area was twice transgressed by the Pleistocene ice sheets, which terminated approximately 40 km further south. The Pleistocene succession comprises Elsterian and Saalian glacial deposits, Weichselian periglacial deposits and Holsteinian, Eemian and Holocene interglacial deposits (Urban *et al.*, 1988, 1991a, b; Mania, 1998, 2006; Elsner, 2003; Lang & Winsemann, 2012). The glacial successions include glacialfluvial, glaciallacustrine and subglacial deposits, while the interglacial successions comprise fluvial and lacustrine deposits (Mania, 1998; Elsner, 2003; Lang & Winsemann, 2012). The reconstruction of the glacial depositional processes and environments will help to unravel the Middle Pleistocene evolution of the study area and improve the understanding of glacial depositional processes. Analysing the Pleistocene succession as a part of the infill of the salt rim synclines will provide insight into the reaction of salt structures to ice-sheet loading. An analysis of the depositional environments during the formation of the archaeological sites encompasses the distribution, embedding and preservation of the artefacts and forms the basis for any palaeo-environmental reconstruction.



Fig. 1: Location of the study area and maximum extent of the major Pleistocene ice advances (modified after Ehlers *et al.*, 2011).

Central questions of this study

The aim of this study is to present a comprehensive geological model for the study area, placing the emphasis on the formation and preservation of Middle Pleistocene succession at Schöningen, by answering the following central questions:

- **Which mechanism provided the accommodation space for the deposition and preservation of the Middle Pleistocene succession?** The preservation of such a thick and complete glacial/interglacial succession requires a mechanism, which allows not only for the deposition of the succession, but also prevents subsequent erosion. A variety of processes may have formed the depocentre, including both endogenic and exogenic processes. Potential endogenic processes are subsidence in the rim syncline of the salt wall, differential compaction of the underlying Palaeogene deposits and subsurface salt dissolution in the Triassic bedrock. Exogenic processes may include fluvial, glacial or meltwater erosion, the melting of dead-ice blocks or syn-sedimentary diapirism of unconsolidated sediment.
- **Which processes controlled the landscape evolution of the study area during the Middle Pleistocene?** The Middle Pleistocene succession reflects changing environmental conditions, spanning two continental-scale glaciations with multiple ice advances and a prolonged warm phase in between. The ice advances formed large-scale depositional and erosional features and had a huge impact on the landscape of the study area. Ice-sheet loading may further have caused the reactivation of salt structures. The depositional environments

during the glaciations include subglacial, glacialfluvial and glaciallacustrine settings, which changed rapidly through space and time. Smaller-scale changes affected the interglacial deposition and controlled the formation of the archaeological sites. Reconstructing these different depositional environments allows for a better understanding of the landscape evolution during the Middle Pleistocene.

- **How were the artefact-bearing strata deposited and preserved?** The archaeological findings indicate the recurring presence of Lower Palaeolithic humans, which suggests that favourable conditions made the site attractive for both animals and humans ambushing them. Reconstructing the evolution of depositional environment of the artefact-bearing, interglacial strata is the prerequisite to understand the palaeo-environmental conditions and the formation of the archaeological sites. The depositional model will also help to explain the spatial and temporal distribution of the different archaeological sites.

1.1 Generation of the accommodation space

The Pleistocene succession of Schöningen was deposited within a relatively small depocentre. Previous studies focussed on the formation of the depocentre of the interglacial succession. Elsner (1987) proposed the formation of shallow kettle-hole lakes by dead-ice melting, while Mania (1998, 2006) assumed a combination of fluvial incision and salt dissolution in the subsurface, leading to the development of broad channels. Mania (1998, 2006) postulated repeated phases of subsidence and formation of separate depocentres, accommodating successively younger interglacial deposits.

A variety of endogenic and exogenic processes are capable of forming such depocentres. The position of the Pleistocene depocentre in the rim syncline of a salt wall suggests ongoing subsidence as a long-term mechanism. The subsidence of the rim syncline was probably re-activated by ice-sheet loading, interacting with the salt wall (cf., Chapter 1.3).

Other potential subsidence mechanisms are differential compaction of the underlying Palaeogene succession and subsurface salt dissolution in the Triassic bedrock. Alternatively, the formation of the depocentre may relate to differential compaction, the melting of dead-ice blocks, syn-sedimentary diapirism of unconsolidated sediment or to fluvial, glacial or meltwater erosion.

1.1.1 Differential compaction

The original volume of unconsolidated sediment is strongly reduced by compaction. The reduction in volume depends on the lithology and is highest in peat and mud (Van Asselen, 2010). In peat-bearing successions up to 40 % of the accommodation space may be created by peat compaction (Van Asselen, 2010). Lateral facies variations between compressible and non-compressible lithologies may create pronounced changes in elevation of the overlying surface.

1.1.2 Subsurface salt dissolution

The dissolution of salt in the subsurface causes the overburden to subside and form collapse structures (Ge & Jackson, 1998). Salt dissolution is favoured by thick accumulations of salt in diapirs and other salt structures, but may also affect tabular salt bodies close to the surface (Ge & Jackson, 1998; Gutiérrez, 2004). Salt dissolution may be a very long lasting process and consume vast volumes of salt (Cartwright *et al.*, 2001). Collapse structures are typically circular, but may also emulate the shape of the salt structures. Deformation related to collapse structures is extensional at their margins (ring-faulting) and contractional in their centres (Ge & Jackson, 1998).

1.1.3 Dead ice melting

Kettle holes in till or outwash plains are formed by the melting of dead-ice blocks. Dead-ice blocks detach from the glacier during deglaciation and may be buried by meltwater deposits, eventually causing delayed melting (Fleisher, 1986; Böse, 1995). Kettle holes formed by the melting of dead ice commonly accommodate fluvial or lacustrine deposits (Fleisher, 1986; Kaiser *et al.*, 2012). Dead-ice blocks, remaining in overdeepened basins during ice-sheet decay, may also prevent the basins from being rapidly filled during deglaciation (Kuster & Meyer, 1979; Böse, 1995).

1.1.4 Syn-sedimentary diapirism of unconsolidated deposits

Density inversion may cause the diapiric rise of mud, peat and lignite analogous to salt diapirism and occurs when water-saturated mud, peat or lignite is buried beneath denser sediment, leading to an upward displacement of the overburdened sediment (Mills 1983; Aber & Ber 2007). The process is amplified by the differential load applied by the weight of an advancing ice sheet (Aber & Ber, 2007) and by freezing and thawing processes in periglacial environment (Eissmann, 1987). The expulsion of ductile material in the subsurface may form shallow, localised depocentres (Eissmann, 1987; Strahl *et al.*, 2011).

1.1.5 Fluvial erosion

Fluvial incision, especially abandoned channels in meandering systems, may provide excellent sedimentary and environmental archives. During the Pleistocene rivers were affected by high-amplitude and high-frequency environmental changes, causing changes in both channel style and aggradational and degradational behaviour (e.g., Vandenberghe, 1995; Blum & Törnquist, 2000). The behaviour of fluvial systems is controlled by a variety of controlling factors acting both in the downstream and upstream reaches of a river. The downstream control is exerted by the base level, which is ultimately tied to sea-level change (Holbrook *et al.*, 2006). The upstream control is more complex, depending largely on climate, sediment supply, bank stability and local uplift, and commonly acts on time scales at least one order of magnitude smaller than the downstream control (Blum & Törnquist, 2000; Holbrook *et al.*, 2006). Incision of channels in the downstream reaches occurs in response to base-level fall and

lowstand (Posamentier & Vail, 1988). In the upstream reaches incision is generally favoured during phases of high discharge and low sediment supply (Blum & Törnquist, 2000; Bogaart & Van Balen, 2000).

1.1.6 Glacigenic erosional processes

In glaciated settings the generation and destruction of accommodation space are in large parts controlled by the advance or retreat of ice sheets. Beneath an ice sheet accommodation space is basically non-existent (Brookfield & Martini, 1999) and glacial ice and meltwater are strong erosive agents. Glacigenic erosion is highly effective in creating accommodation space. Subglacial erosion is one of the deepest-reaching erosional processes and is responsible for the formation of glacial basins and tunnel valleys. These subglacial basins are regarded as overdeepened if a locally-reversed subglacial slope is present and the products of glacial erosion have been transported along this slope by ice or meltwater (Cook & Swift, 2012). Overdeepening creates basins, which are well below the base level of other erosional processes as for example fluvial incision. Overdeepened basins therefore provide excellent sedimentary archives with a high preservation potential (Cook & Swift, 2012). The climatic conditions during deglaciation exert a major control if glacial basins or tunnel valleys are formed. Warmer conditions with higher supraglacial meltwater production favour the incision of tunnel valleys, while colder conditions enhance the basal coupling of the ice, favouring glacitectonics and the formation of erosional glacial basins (Van Dijke & Veldkamp, 1996; Kehew *et al.*, 2012).

Glacial basins

Glacial basins are irregular-shaped, wide depressions, which are excavated directly by glaciers (Eissmann, 1967; Van der Wateren, 1987). The width and length of glacial basins may be up to several tens of kilometres, while the depths are up to 150 m (Van Dijke & Veldkamp, 1996). Glacial basins typically form beneath advancing ice lobes or ice streams, protruding from the main ice sheet (Van der Wateren, 1994). Because the formation of glacial basins is caused by glacitectonic thrusting, they are commonly associated with push-moraine ridges (Van der Wateren, 1987, 1994) and may even form hill-hole pairs of equal volume (Aber & Ber, 2007). The removal of larger volumes of sediment from the glacial basin requires additional erosion by meltwater (Van der Wateren, 1994; Cook & Swift, 2012). The glacigenic infill of glacial basins comprises till and meltwater deposits, which are commonly deformed and incorporated into the push-moraines during re-advances of the glacier (van der Wateren, 1994). After deglaciation glacial basins may accommodate and preserve post-glacial successions (Hahne *et al.*, 1994; Cleveringa *et al.*, 2000; de Gans *et al.*, 2000).

Tunnel valleys

Tunnel valleys are elongated incisions, which are carved by subglacial meltwater under high hydrostatic pressure (Ó Cofaigh, 1996; Huuse & Lykke-Andersen, 2000; Kehew *et al.*, 2012). Individual

tunnel valleys have undulating basal profiles, are up to 500 m deep, up to 5 km wide and are composed of 1 to 40 km long segments (Van der Vegt *et al.*, 2012). The incision of tunnel valleys is most likely controlled by a combination of time-transgressive steady-state drainage processes (Boulton & Hindmarsh, 1987; Ó Cofaigh, 1996; Praeg, 2003; Janszen *et al.*, 2012a; Stewart *et al.*, 2013) and catastrophic drainage events (Wingfield, 1990; Hooke & Jennings, 2006; Jørgensen & Sandersen, 2006). Additionally, direct erosion by the glacier may also contribute to the formation of tunnel valleys (Ehlers & Linke, 1989; Huuse & Lykke-Andersen, 2000; Stewart *et al.*, 2013). In general, tunnel valleys form during phases of ice-sheet retreat in a position relatively close to the ice margin (100s of km; Huuse & Lykke-Andersen, 2000; Praeg, 2003). Tunnel valley networks are oriented sub-parallel to the patterns of ice-sheet advance and retreat (Stackebrandt, 2009; Van der Vegt *et al.*, 2012; Stewart *et al.*, 2013). Cross-cutting networks are related to multiple ice advances during one or more several glaciations (Stackebrandt, 2009; Stewart & Lonergan, 2011; Kehew *et al.*, 2012; Stewart *et al.*, 2013). Tunnel-valley networks are regarded as equivalent to esker networks in bedrock areas, where incision is prevented by the resistance of the substratum to erosion (Boulton *et al.*, 2009; Kehew *et al.*, 2012). The erodibility and permeability of the substratum exerts a major control on the location and shape of tunnel valleys (Huuse & Lykke-Andersen, 2000; Boulton *et al.*, 2009; Stackebrandt, 2009; Janszen *et al.*, 2012b). Tunnel valleys commonly act as depocentres for both syn-glacial and post-glacial deposition. Subglacial meltwater deposits and till are deposited during or immediately after the incision of the tunnel valley (e.g., Piotrowski *et al.*, 1999; Jørgensen & Sandersen, 2006; Praeg, 2003; Russell *et al.*, 2003). Composite tunnel valley fills, indicating several phases of incision and infill during a single ice advance, are interpreted as pointing to repeated closure and re-opening of the subglacial meltwater conduit during repeated meltwater outburst events (Jørgensen & Sandersen, 2006; Kehew *et al.*, 2012). During deglaciation tunnel valleys commonly accommodate glacialacustrine successions, which are deposited in ice-dammed lakes in front of the retreating ice margin (Kuster & Meyer, 1979; Ehlers & Linke, 1989; Piotrowski, 1994; Krohn *et al.*, 2009; Janszen *et al.*, 2012a). Tunnel valleys commonly remain underfilled after deglaciation and provide depocentres for post-glacial deposition (Turner, 1970; Kuster & Meyer, 1979; Piotrowski, 1994; Eissmann, 2002; Preece, 2006; Janszen *et al.*, 2012a).

1.2 Middle Pleistocene glacial and interglacial depositional environments

1.2.1 Glacial depositional environments

The Middle Pleistocene glacial successions at Schöningen reflect changing environmental conditions and depositional environments, including subglacial, glacialfluvial and glacialacustrine settings. Reconstructing the spatial and temporal evolution of these depositional environments allows for a better understanding of the Middle Pleistocene landscape evolution. Glacial depositional processes are mainly controlled by the action of either glacial ice or meltwater. The ice is responsible for the formation of basal till by subglacial lodgement, melt-out and deformation of pre-existing sediment

(Evans *et al.*, 2006). Meltwater is the main agent for the transport and deposition of sediment in glaci-fluvial and glacialacustrine environments, but is also of importance for subglacial processes.

Deposition by supercritical flows

Glacigenic depositional environments are commonly characterised by high-energy, sediment-laden, rapidly waning meltwater flows. Therefore, deposits of aggradational supercritical flows represent a typical feature of subaqueous ice-contact fans, tunnel-valley fills, glaci-fluvial deltas and glacial-lake outburst flood successions (e.g., Russell & Arnott, 2003; Russell *et al.*, 2003, 2007; Johnsen & Brennand, 2004, 2006; Hornung *et al.*, 2007; Duller *et al.*, 2008; Carling *et al.*, 2009; Ghienne *et al.*, 2010; Winsemann *et al.*, 2009, 2011; Clerc *et al.*, 2012; Hirst, 2012; Lang *et al.*, 2012). Deposits of supercritical flows include upper-stage plane beds, antidunes, chutes-and-pools and cyclic steps (Allen, 1984; Alexander *et al.*, 2001; Fielding, 2006; Cartigny *et al.*, *in press*), although in many known examples of deposits by supercritical flows no further distinction has been drawn between the various depositional processes. However, the correct identification and interpretation of these bedforms is a prerequisite to reconstruct the flow processes. Deposits of supercritical flows in glacigenic settings are frequently related to high-discharge events in ice-proximal settings and their recognition is therefore relevant for the reconstruction of depositional processes and palaeo-flows near the palaeo-ice margins.

1.2.2 Interglacial environments and the formation of archaeological sites

The archaeological findings indicate the recurring presence of Lower Palaeolithic humans at Schönin-gen throughout the warm phase between the Elsterian and Saalian glaciations. There are at least three important Palaeolithic sites in the Schönin-gen area (Sites 12-II, 13-I and 13-II; cf., Serangeli *et al.*, 2012). Each of these sites consists of several archaeological horizons, indicating that the individual sites required a considerable amount of time for their formation. Site 13-II for example comprises five individual horizons that all bear Palaeolithic artefacts although the density of finds varies (Thieme, 1999, 2007; Serangeli, *et al.*, 2012). Site 13-II has recently been dated using $^{230}\text{Th}/\text{U}$ and age determinations range from 280 to 343 ka (Urban *et al.*, 2011) and 294 +/-10 to 297 +/-12 ka (Sierralta *et al.*, 2012). However, absolute ages providing a chronological framework for the different archaeological sites are still unavailable due to the methodical problems of dating such old samples with the required temporal resolution (Geyh & Müller, 2005; Geyh & Krbetschek, 2012; Richter & Thieme, 2012). However, the palaeoecological data indicate that the sites evolved under changing climatic conditions, suggesting a considerable duration of the site formation (Urban, 2007).

So far, a huge amount of palaeoecological data has been collected, spanning almost the whole period from the end of the Elsterian glaciation to the onset of the Saalian glaciation (e.g., Urban *et al.*, 1988, 1991b, 2011; Urban, 1995, 2007; Van Kolfschoten, 1995, 2007, 2012; Böhme, 2000; Jechorek, 2000), and include stadial, interstadial and full interglacial phases. Reconstructing the depositional environments of the artefact-bearing strata is the prerequisite to understand the palaeo-environmental condi-

tions and the formation of the archaeological sites. The correlation of the interglacial deposits within a sequence stratigraphic framework will allow understanding the relative chronology and spatial distribution of the archaeological sites.

1.3 The reaction of salt structures to ice-sheet loading

The preservation of a thick Pleistocene succession within the southwestern rim syncline of the Helmstedt-Staßfurt salt wall implies ongoing salt rise and associated subsidence in the rim synclines during the Pleistocene. The evolution of secondary rim synclines is characterised by the migration of the depocentres towards the central salt structure (Trusheim, 1960; Alsop, 1996; Waldron & Rygel, 2005; Brandes *et al.*, 2012). According to Mania (1998) the shift of the Pleistocene depocentres towards the centre of the rim syncline is an expression of the ongoing subsidence in the rim syncline. The high thickness of the Pleistocene succession suggests an interaction between the salt structure and ice-sheet loading.

Field examples

Evidence for the interaction of subsurface salt bodies and ice sheets has previously been observed along the margins of former ice sheets. A correlation of salt structures and push-moraine ridges related to Late Pleistocene ice advances has been observed at a variety of locations in northern Germany (Gripp, 1952; Schirrmeister, 1999) and Poland (Liszkowski, 1993). Most salt structures in the North German Basin that have penetrated the surface or show indications for Pleistocene or Holocene rise are also placed in the proximity of the palaeo-ice margins (Teichmüller, 1946; Illies, 1955; Hurtig, 1965; Sirocko *et al.*, 2002; Stackebrandt, 2005). Lateral and vertical displacement of salt within a sheet-like salt body is reported from parts of the Michigan Basin that were beneath the margin of the Laurentide ice sheet in the northeastern USA (White, 1992; Aber & Ber, 2007).

Conceptual model

Based on such field observations conceptual models for the interaction of ice sheets and salt structures have been developed by Liszkowski (1993) and Sirocko *et al.* (2008). These conceptual models propose that (i) salt structures will rise in front of an advancing ice sheet due to the additional load applied by the weight of the ice sheet (Fig. 2A), (ii) beneath an ice sheet the rise will be blocked due to the ice load applied to the top of the salt structure (Fig. 2B) and (iii) after the removal of the ice load the salt structure will rise again (Fig. 2C). This process may be accompanied by the reactivation of faults above the salt structure, although the sense of fault slip may switch during the different stages of the process (Liszkowski, 1993; Lehné & Sirocko, 2007; Sirocko *et al.*, 2008) During the ice advance thick glacial successions may be deposited between the ice margin and the salt structure, which may be deformed into push-moraines during further ice advance (Sirocko *et al.*, 2008). The reactivation of

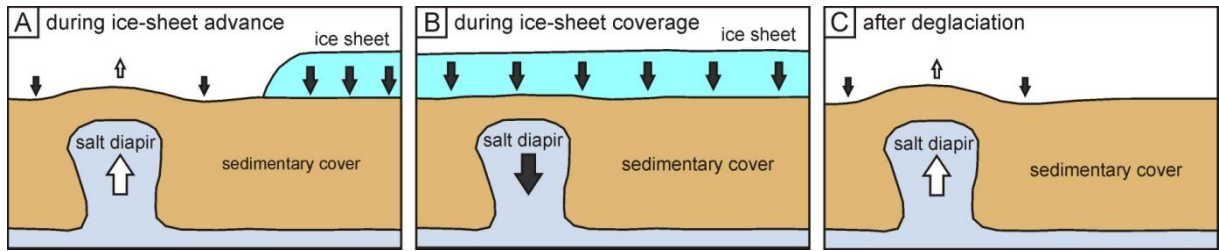


Fig. 2: Conceptual model of the interaction of salt diapirs and ice sheets (compiled from Liszkowski, 1993; Lehné & Sirocko, 2007; Sirocko *et al.*, 2008). **A)** During the ice advance the diapir rises due to the load applied to the salt source layer by the ice sheet. **B)** During ice coverage the diapir is pushed down by the load of the ice sheet applied to the top of the diapir. **C)** After deglaciation the diapir may rise again.

salt rise after deglaciation may cause subsidence in the rim synclines, providing the accommodation space for subsequent deposition.

1.3.1 Salt tectonic processes

Salt tectonic processes constitute an important controlling factor for the structural and stratigraphic evolution of many sedimentary basins. Rock salt is distinguished from other sedimentary rocks by its rheological properties. Under typical geologic strain rates salt behaves like a viscous Newtonian fluid with no yield strength (Jackson & Talbot, 1986; Weijermars *et al.*, 1993). Salt is relatively incompressible and has a constant density ($\sim 2200 \text{ kg/m}^3$ for slightly impure rock salt) at burial depths between 0.2 to 8 km (Warren, 2006; Hudec & Jackson, 2007). The viscous rheology and the incompressibility make salt rocks inherently unstable and mobile, which causes salt tectonics that significantly influence the structure and stratigraphy of salt-bearing basins. The variety of structures formed by salt tectonics is huge and includes for example salt diapirs, pillows, walls and sheets. Within sedimentary basins salt structures represent zones of weakness and thus accumulate strain during regional deformation (Hudec & Jackson, 2007).

Driving forces

Differential loading, which causes viscous flow from areas of higher load to areas of lower load, is considered as the main driving force of salt tectonics (Hudec & Jackson, 2007). Salt tectonics may be driven purely by gravity, if lateral tectonic forces are absent, or by regional extension, shortening or wrenching. Purely gravitational loading is caused either by differential pressure exerted on a salt layer due to lateral variations of the thickness of the salt and the overburden rocks or by the force of gravity affecting a salt layer resting on a tilted basal surface (Jackson & Talbot, 1986; Waltham, 1997; Brun & Fort, 2011). Displacement loading is triggered by forced displacement of the boundaries of a salt body due to regional shortening or extension (Jackson & Vendeville, 1994; Hudec & Jackson, 2007; Dooley *et al.*, 2009). High thermal gradients may also lead to thermal loading (Jackson & Talbot, 1986).

Gravitational differential loading of a salt layer is for example caused by the infill of supra-salt basins (Trusheim, 1960; Waldron & Rygel, 2005; Hudec *et al.* 2009; Trudgill *et al.*, 2011; Brandes *et al.*, 2012) or by the progradation of sedimentary wedges above a salt layer (Wu *et al.*, 1990; Ge *et al.*,

1997; Vendeville, 2005). Salt tectonics related to differential loading triggered by prograding sediment wedges have been studied by both analogue (e.g., Koyi, 1996; Ge *et al.*, 1997) and numerical (e.g., Cohen & Hardy, 1996; Albertz *et al.*, 2010) modelling to investigate the controlling factors and the resulting geometries of salt structures and overburden deformation. These salt movements do not require the overburden to be denser than the salt, but occur solely in response to differential thickness of the overburden (Jackson & Talbot, 1986; Cohen & Hardy, 1996). The viscosity of the salt exerts a first order control on the salt flow rate, the efficiency of salt expulsion from the source layer and the resulting geometries. Salt with lower viscosities will flow faster and be more efficiently expelled (Cohen & Hardy, 1996; Gemmer *et al.*, 2004; Albertz & Ings, 2012). Salt expulsion from an initially thick source layer will be faster and more effective than from a thin source layer (Cohen & Hardy, 1996). The rate and style of the progradation of the overburden also influences salt movement, low rates of progradation will cause low rates of salt flow (Cohen & Hardy, 1996; Koyi, 1996; Vendeville, 2005). Slow progradation of the overburden will promote efficient salt evacuation and the formation of welds (Gemmer *et al.*, 2004). Phases of aggradation counteract the rise of salt structures (Koyi, 1996).

Salt-ice interaction

The advance of an ice sheet into a salt-bearing basin causes differential loading similar to a prograding sediment wedge (Jackson & Talbot, 1986; White, 1992). While the density of ice is lower ($\sim 900 \text{ kg/m}^3$) than the density of unconsolidated siliciclastic sediments ($\sim 2000 \text{ kg/m}^3$), the rates of ice-sheet advance are much faster than the progradation rates in sedimentary systems. The Pleistocene ice sheets advanced at rates of 75-150 m/a (Ehlers, 1990; Lunkka *et al.* 2001; Clark *et al.*, 2012), while sedimentary wedges at passive continental margins typically prograde at rates of several centimetres per year (Carvajal *et al.*, 2009). Therefore, an advancing ice sheet is able to apply the same load several hundred times faster than a prograding sediment wedge. Ice sheets advancing into salt-bearing basins may thus cause rise or fall of existing salt structures (Liszkowski *et al.*, 1993; Sirocko *et al.*, 2008) or, in the absence of salt structures, cause displacement within sheet-like salt bodies (White, 1992).

2. Study area

2.1 The Central European Basin System

The study area is located in the Subhercynian Basin, which is a subbasin of the North German Basin, forming part of the Central European Basin System (CEBS; Fig. 3A). The formation of the CEBS commenced in the latest Carboniferous to Early Permian after the Variscian Orogeny and was characterised by east-west directed extension controlled by dextral transtension along northwest-southeast trending strike-slip faults. Subsequently, the faulting waned and thermal subsidence took over (Kley *et al.*, 2008). During the Mesozoic changing tectonic regimes led to the formation of various subbasins and increasing basin complexity. From the Early Triassic until the Middle Jurassic east-west directed

2. Study area

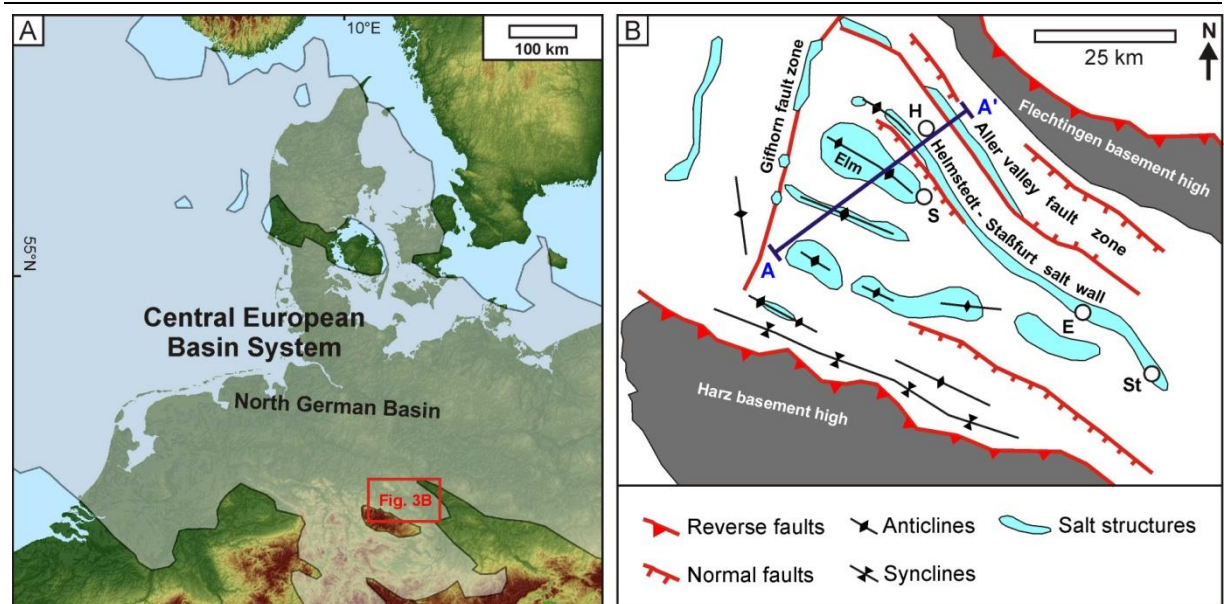


Fig. 3: **A)** Overview map of the Central European Basin System (CEBS). The Subhercynian Basin is located within the red box. The CEBS is outlined by the present day extent of Permian deposits (shaded area; modified after Maystrenko *et al.*, 2013). **B)** Structural map of the Subhercynian Basin (based on Stackebrandt, 1986; modified after Brandes *et al.*, 2012; E: Egeln, H: Helmstedt, S: Schöningen, St: Staßfurt). The blue line AA' indicates the cross-section shown in Fig. 4.

extension along north-south trending normal faults controlled the basin evolution (Kley *et al.*, 2008). Strong extension continued from the Late Jurassic to the early Late Cretaceous with a change in the direction of extension to northwest-southeast (Kley *et al.*, 2008). During the Late Cretaceous to the Palaeogene the stress regime changed to a northeast-southwest directed contraction, which was caused by the onset of convergence between the European and the African plates (Betz *et al.*, 1987; Ziegler, 1990; Kley & Voigt, 2008), and lead to basin inversion (Lohr *et al.*, 2007; Voigt *et al.*, 2006, 2008; Brandes *et al.*, 2013). The main phase of inversion occurred between 80 to 85 Ma (Santonian to Campanian) and focussed on the northeastern and southwestern margins of the CEBS (Voigt *et al.*, 2008). Pre-existing normal faults were commonly reactivated as reverse faults during the basin inversion (Betz *et al.*, 1987; Lohr *et al.*, 2007). The WNW-ESE trending Harz Boundary Fault is one of the major fault zones in the CEBS, where the folded Palaeozoic rocks of the Harz Mountains were thrust onto Mesozoic rocks (Fig. 3B). Seismic data display a steeply southwest dipping fault that flattens at a depth of ~10 km (DEKORP-BASIN Research Group, 1999). During the main phase of inversion an offset of ~7 km occurred within only 4 Ma at the Harz boundary fault, causing the removal of 2-3 km of Mesozoic overburden (von Eynatten *et al.*, 2008) and the deposition of a ~2.5 km thick syn-tectonic succession in the Subhercynian basin (Voigt *et al.*, 2008).

The evolution and the present day geometries within the CEBS are strongly influenced by rises of Upper Permian salt. During the Late Permian 1500-2500 m thick evaporites of the Zechstein Group were deposited (Ziegler, 1990; Stollhofen *et al.*, 2008; Maystrenko *et al.*, 2013). The Zechstein Group comprises six stacked evaporation cycles, representing third-order depositional sequences. Each cycle starts with basal marine clay overlain by carbonates, calcium-sulphates and rock salt, which is dominated by halite (Stollhofen *et al.*, 2008). Salt movement in the CEBS was initially triggered by exten-

sional faulting during the Early Triassic. Subsequent rifting pulses during the Late Triassic initiated the second phase of salt movement. The third phase of salt movement was caused by the Late Cretaceous to Palaeogene compression (Jaritz, 1973; Mohr *et al.*, 2005; Kley *et al.*, 2008; Stollhofen *et al.*, 2008; Maystrenko *et al.*, in press). Salt movements further complicated the structural evolution of the CEBS by decoupling between the basement and the Mesozoic to Cenozoic cover (Lohr *et al.*, 2007; Maystrenko *et al.*, 2013).

The Cenozoic evolution of the CEBS is characterised by major subsidence and the passive rise of salt diapirs (Lohr *et al.*, 2007). In the North German Basin the Cenozoic subsidence axis is formed by the northwest-southeast trending Central European Subsidence Zone (Stackebrandt, 2004, 2009). The orientation of the major horizontal stress in the CEBS is northwest-southeast since the Neogene (Kley *et al.*, 2008).

2.2 The Subhercynian Basin

The Subhercynian Basin is a relatively small basin at the southern margin of the CEBS, which emerged as separate basin during the Cretaceous to Palaeogene basin inversion. The Subhercynian Basin is bounded by the Gifhorn fault zone to the west, by the Harz Mountains to the southwest and the Flechtingen High to the northeast (Fig. 3B). The Harz Mountains and the Flechtingen High both consist of Palaeozoic basement rocks, which were uplifted during basin inversion. The 2-3 km thick basin fill has the highest thickness at the southwestern basin margin and pinches-out towards the northeastern basin margin (DEKORP-Basin Research Group, 1999). The lower part of the basin fill comprises Permian to Lower Cretaceous pre-inversion deposits, which are dominated by Triassic deposits (Fig. 4). Up to 2.5 km thick Upper Cretaceous syn-inversion deposits occur at the southern basin margin. Palaeogene deposits are restricted to salt-related mini-basins, as the rim synclines of the Helmstedt-Staßfurt salt wall. The Subhercynian Basin is subdivided into several northwest-southeast trending synclines and anticlines by rises of salt of the Upper Permian Zechstein Group (Figs. 3B, 4). Salt movement in the Subhercynian Basin was initiated by the extensional tectonics of the Late Triassic and later reactivated by Late Cretaceous compression (Niebuhr & Ernst, 1991; Karpe, 1994; Best, 1996; Brandes *et al.*, 2012).

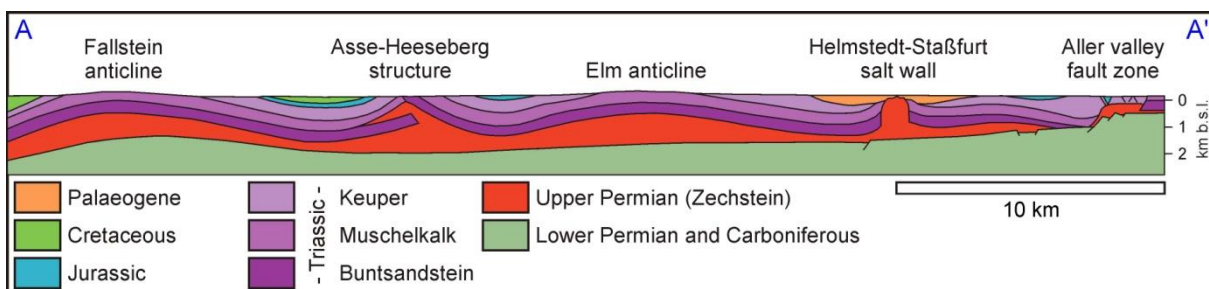


Fig. 4: Geological cross-section of the study area (modified after Baldschuhn *et al.*, 1996). The location of the cross-section is given in Fig. 3B (blue line AA ϕ).

2.2.1 The Helmstedt-Staßfurt salt wall and its rim synclines

The Helmstedt-Staßfurt salt wall trends northwest-southeast, is ~70 km long and on both sides accompanied by rim synclines (Fig. 4). The rim synclines bear economically important Palaeogene lignites in the Helmstedt-Schöningen and Egelst-Staßfurt mining districts with one remaining open-cast mine near Schöningen. Karpe (1994) classified the rim synclines as secondary rim synclines, where subsidence is controlled by salt withdrawal and the depocentres migrate towards the salt wall. The basement of the rim syncline is formed by Triassic sand-, mud- and limestone (Manger, 1952; Look, 1984; Baldschuhn *et al.*, 1996). The oldest deposits within the rim synclines of the Helmstedt-Staßfurt salt wall are Campanian in age and were deposited at the northwestern termination of the structure (Niebuhr & Ernst, 1991). The deposits within the rim synclines become successively younger towards the centre of the structure (Niebuhr & Ernst, 1991; Karpe, 1994; Brandes *et al.*, 2012). The main fill of the rim-syncline consists of an up to 360 m thick succession of unconsolidated sand, silt, clay and lignite, interpreted as marginal marine Palaeogene deposits (Behrend, 1927; Manger, 1952; Look, 1984; Brandes *et al.*, 2012; Osman *et al.*, *in press*).

A sub-salt normal fault below the Helmstedt-Staßfurt salt wall suggests initial reactive salt rise during Late Triassic extension (Baldschuhn *et al.*, 1996; Brandes *et al.*, 2012; Fig. 4). The main phase of salt rise and subsidence in the rim synclines occurred during the Palaeogene and was diachronous along strike (Niebuhr & Ernst, 1991; Karpe, 1994; Brandes *et al.*, 2012). According to Brandes *et al.* (2012) the salt wall was initiated by diapirs defining the terminations of the structure, which were subsequently connected by the rising salt to form the salt wall. For the southwestern rim-syncline near Schöningen, Brandes *et al.* (2012) modelled maximum subsidence rates of 76-80 m/Ma between 57 and 50 Ma, which subsequently ceased due to the depletion of the salt layer. A causal relationship between the ongoing rise of the salt wall, subsidence in the rim synclines and the migration of the Pleistocene depocentres has been postulated by Mania (1998). In the inner part of the rim synclines the Holocene lacustrine and peat bog deposits may attain unusual high thicknesses of up to 7 m, which was considered an indicator for ongoing subsidence by Manger (1952).

2.3 The Pleistocene glaciations

During the Pleistocene large parts of the Central European Basin System were affected by the repeated advances of the Fennoscandian ice sheets (Litt *et al.*, 2008; Ehlers *et al.*, 2011; Houmark-Nielsen, 2011; Laban & Van der Meer, 2011; Marks, 2011). In northern Germany these glaciations are known as the Elsterian, Saalian and Weichselian glacial periods and the intervening interglacial periods as Holsteinian and Eemian (Litt *et al.*, 2007; Fig. 1). The Elsterian ice sheet covered most of northern Germany (Ehlers *et al.*, 2004, 2011) and there are indications for two major ice advances, which advanced to approximately the same maximum position (Eissmann, 2002; Litt *et al.* 2007). Discussion is still ongoing, if the Elsterian glaciation occurred during MIS 10 (e.g., Geyh & Müller, 2005; Litt *et al.*, 2008; Lee *et al.*, 2010) or MIS 12 (e.g., Gibbard & Cohen, 2008; Toucanne *et al.*, 2009; Ehlers *et al.*,

2011). The Holsteinian interglacial probably occurred during MIS 9 (Geyh & Müller, 2005; Litt *et al.*, 2007, 2008) and was characterised by slightly warmer but less stable climatic conditions than the Eemian or Holocene interglacials (Kühl & Litt, 2007). The Saalian Complex spans MIS 8 to MIS 6 and is characterised by several pronounced climatic fluctuations in the Early Saalian prior to the initial ice advance (Krbetschek *et al.*, 2008; Litt *et al.*, 2008). An alternation between several warm and cold phases has been ascribed to the Early Saalian (Litt *et al.* 2007; Urban, 2007; Kleinmann *et al.*, 2011; Urban *et al.*, 2011). The maximum extent of the Saalian ice cover in northwestern Germany was reached during the older Saalian Drenthe ice advance, while the younger Saalian Warthe ice advance had a lesser maximum extent (Ehlers *et al.*, 2004, 2011; Litt *et al.*, 2007). Both Saalian ice advances occurred during MIS 6 (Lambeck *et al.*, 2006; Busschers *et al.*, 2008). The Saalian subglacial tills are separated by glacialacustrine and glacialfluvial deposits and no interglacial sediments have been found (Litt *et al.*, 2007). The subsequent Eemian interglacial occurred during MIS 5 (Litt *et al.*, 2008). The ice sheet of the Weichselian glaciation had the lowest maximum extent of the Pleistocene glaciations (Ehlers *et al.*, 2004, 2011). Up to three Weichselian ice advances are known, which occurred during MIS 2 (Litt *et al.*, 2007, 2008)

The Subhercynian Basin was transgressed by both the Elsterian and the older Saalian Drenthe ice advances (Fig. 1). The younger Saalian Warthe ice advance and the Weichselian ice advances did not reach the Subhercynian Basin (Look, 1984; Ehlers *et al.*, 2011).

3. Methods

3.1 Field work

Field work was carried out at different locations within the Schöningen open-cast mine and at a number of sand pits. Ongoing excavation helped to gain insight into the three-dimensional architecture of the studied outcrops. The outcrops were characterised from vertical sedimentological logs measured at the scale of individual beds and two-dimensional photo panels of the outcrop walls. Sedimentary facies were defined from grain size, bed thickness, bed contacts, bed geometry, internal sedimentary structures and soft-sediment deformation structures, and interpreted in terms of depositional processes. The sedimentary facies were grouped into facies associations and interpreted in terms of depositional environments. Photos and line drawings document further details of the sedimentary facies and deformation structures. The larger-scale facies architecture was mapped from the photo panels, observing the spatial distribution of the sedimentary facies and facies associations, the dimensions of architectural elements, the bounding surfaces and the occurrence of large-scale deformation structures. Palaeoflow directions were obtained from cross-stratification, corrected for deformed sections and plotted in rose diagrams. Soft-sediment deformation structures were measured in the field and plotted in stereographic projection (lower hemisphere equal area projection).

3.2 Acquisition and interpretation of shear-wave seismic data

To gain insight into the large-scale depositional architecture at Schöningen two 2D shear-wave seismic reflection profiles were acquired. Shear-wave seismics provide a very high-resolution image of the shallow subsurface and have successfully been applied for sedimentological and structural studies of the near surface geology (Pugin *et al.*, 2004; Haines & Ellefsen, 2010; Winsemann *et al.*, 2009, 2011; Brandes *et al.*, 2011; Hansen *et al.*, 2013; Polom *et al.*, 2013). The acquisition configuration and procedure used in this study are described in more detail in Publication 1. The resolution achieved in this study was ~0.5 m vertically and ~0.5 m horizontally near the surface, decreasing to ~1.5 m vertically and ~12 m horizontally in a depth of 50 m. The acquisition set-up was parameterised for a maximum target depth of 50 m.

The seismic interpretation includes the definition of seismic facies, the construction of a seismic-stratigraphic framework and the transformation into an arbitrary chronostratigraphic chart (c.f., Mitchum & Vail, 1977). Seismic facies are defined by external geometry, internal reflector configuration and seismic facies parameters, which include the amplitude, continuity and density of the individual reflectors (Mitchum *et al.*, 1977). Seismic facies can be interpreted in terms of depositional environment, depositional processes and lithology (Mitchum *et al.*, 1977; Sangree & Widmier, 1979; Veeken & Van Moerkerken, 2013). To construct the seismic-stratigraphic framework the seismic facies were grouped together into seismic-stratigraphic units. Seismic stratigraphic-units are enveloped by reflectors or discontinuities, which are defined by reflector terminations, and represent distinct depositional events (Brown & Fisher, 1977). The interpreted seismic sections allowed for the reconstructing the depositional processes and the understanding of the relative stratigraphic framework. The interpretation of the seismic data was corroborated by the lithological control provided by the outcrop and borehole data.

Seismic reflections that represent depositional surfaces can be regarded as approximate timelines (Brown & Fisher, 1977; Vail *et al.* 1977). Interpreted seismic sections can therefore be transformed into arbitrary chronostratigraphic charts, which allow recognising time-equivalent deposits, the relative importance of unconformities and reconstructing relative sea-level curves (Vail *et al.*, 1977; Veeken & Van Moerkerken, 2013). The relative lake-level changes for the interglacial lacustrine succession at Schöningen were reconstructed in this way (cf., Publication 1). The seismic-stratigraphic unit representing the interglacial succession was extracted and plotted into an arbitrary chronostratigraphic chart. The occurrence of unconformities and the onlap pattern (öcoastal onlapö, c.f., Vail *et al.*, 1977) point to fluctuating lake-levels. The foreset-topset transition indicates the location of the shoreline (Helland-Hansen & Hampson, 2009; Winsemann *et al.*, 2011). The trajectory of foreset-topset transition can be extracted from the arbitrary chronostratigraphic chart and represents a relative lake-level curve.

3.3 3D subsurface modelling

Outcrop and borehole data were integrated into a 3D geological subsurface model (GOCAD®, Version 2009.2, Paradigm) to reconstruct the large-scale depositional architecture of the studied succession. Surfaces in Gocad are approximated by nodes, which span triangular facets, and are modelled by applying the discrete smooth interpolation (DSI) algorithm (Mallet, 1992). The DSI algorithm solves for the optimal position of the nodes to minimise the roughness and constraint misfit of the resulting surface (Mallet, 1992; Caumon *et al.*, 2009). The input data for the surface triangulation are 3D point sets derived from well markers and a bounding box to define the extent of the surface. Input data, as stratigraphic markers from boreholes (well markers), are considered as hard constraints (control nodes) and must not be moved when the surface is triangulated. In contrast, nodes created during the triangulation are soft constraints (control points) that may be moved during the further interpolation of the surface. To maximise the mesh quality the triangulation honours the Delaunay condition, stating that the circumscribed circle of every triangle should not contain any other node of the surface (Mallet, 1992; Caumon *et al.*, 2009).

Altogether, three individual 3D subsurface models were built. The subsurface models are primarily based on the interpretation of logs from boreholes originally drilled for lignite, sand, gravel and groundwater exploration. Borehole data were provided by Brinkmeyer Kieswerk GmbH & Co. KG., E.ON-Kraftwerke GmbH, E.ON Westfalen Weser AG, Niedersächsisches Landesamt für Bergbau, Energie und Geologie and Geologischer Dienst NRW. The boundaries of the modelled areas were defined by the availability of borehole data. Most borehole logs are limited to a description of the lithology, comprising grain size, clast composition and colour. For the interpretation of the borehole logs the software GeODin® (Fugro) was used, allowing for the rapid display of logs and construction of arbitrary cross-sections. Sections measured in the outcrops were integrated into the models as logs and facilitated the interpretation of the borehole data. From the outcrop observations and borehole logs stratigraphic markers (well markers) were defined, which represent the boundaries (top or base) of the individual depositional unit. High-resolution digital elevation models (DEM) were integrated as reference surfaces, but were of restricted use due to the presence of active and abandoned open-cast mines and tailings in large parts of the study areas. The bounding surfaces of the depositional units were triangulated individually from the well markers and subsequently used to calculate the thickness of the depositional units. The geometry of the stratigraphic surfaces and thickness of depositional units were visualised on maps and 2D cross-sections.

For the Schöningen area one large-scale model of the whole studied area and one detailed model of the Buschhaus subaqueous fan in the northern part of the study area were constructed. The interpretation of the borehole logs was supported by accompanying studies by Pollok (2010) and Steinmetz (2010). The larger subsurface model is based on the interpretation of 744 borehole logs, while the model of the Buschhaus subaqueous fan is based on the interpretation of data from 165 boreholes.

For the Porta subaqueous fan the model published by Winsemann *et al.* (2009) was used with some minor modifications. The subsurface model is based on the data from 102 boreholes; the newly measured sections from the outcrops were integrated into the existing model.

3.4 Finite-element simulation

To simulate the reaction of salt structures to ice-sheet loading a finite-element model was built using ABAQUS™ (Version 6.12, Dassault Systèmes Simulia). The finite-element method is an approximate numerical modelling technique to solve differential equations, which describe a given physical problem and is independent of spatial or temporal scale. The applied equations are based on the constitutive relations between the physical parameters the preservation of energy and mass (e.g., Goering *et al.*, 2010; Braess, 2013). The actual geometry of a structure is discretised into a set of finite set of elements, which are joined by shared nodes to form a mesh. The element equations are joined by matrix techniques to form a global equations system. Boundary conditions are prescribed to reduce the number of variables and permit a solution of the equation system, for example by setting the displacement of certain nodes in a strain and stress analysis to zero. For a strain and stress analysis the displacements of the individual nodes are the fundamental variables calculated in Abaqus and subsequently extrapolated for each finite-element (Dassault Systèmes, 2012).

Model set-up

The model section represents a 50 km long and 10 km deep cross-section through the uppermost crust. The model domain was meshed using triangular plane-strain elements with a maximum edge length of ~50 m. Boundary conditions were defined to fix the bottom of the model in both the horizontal and vertical directions and the two sides of the model in the horizontal direction.

The internal geometries of the modelled layers were chosen to resemble the geometries of salt structures and their overburden in intra-continental basins. Models with different internal geometries were tested to investigate the effects of the diapir size, depth to the source layer and thickness of the source layer. One model was set-up with a geometry adapted from a regional geological cross-section of the Helmstedt-Staßfurt salt wall (Baldschuhn *et al.*, 1996), providing a realistic model for the Schöningen sites. The model layers represent sedimentary overburden rocks of elastoplastic rheologies, a viscoelastic salt structure and elastic basement rocks. The physical parameters, including density, elastic modulus, Poisson's ratio, viscosity and yield stress, are defined for the individual layers in the model and represent values typical of sedimentary rocks. The systematic variation of the input parameters (e.g., geometry and rheology of the model layers, magnitude, spatial distribution and timing of loading) allows for a detection of the controlling factors. The model set-up and the material parameters are described in more detail in Publication 4.

Simulation of ice-sheet loading

The load was adjusted to reflect ice-sheet loading and unloading during the Pleistocene ice advances and was applied as a pressure, corresponding to the weight of the ice sheet. The durations of the loading and unloading phases were adjusted to represent realistic glacial episodes. Variations of the simulated ice load include the maximum ice extent, thickness of the ice sheet, duration of the maximum ice extent and the number of ice advances (cf., Publication 4).

4. Overview of this thesis ó Publications and their content

The results of this study are subdivided into four publications, which have been submitted to international, peer-reviewed journals.

Publication 1: The Pleistocene of Schöningen, Germany: a complex tunnel valley fill revealed from 3D subsurface modelling and shear-wave seismics by J. Lang, J. Winsemann, D. Steinmetz, U. Polom, L. Pollok, U. Böhner, J. Serangeli, C. Brandes, A. Hampel and S. Winghart, published in *Quaternary Science Reviews* (2012), 39, 86-105.

This publication presents a comprehensive geological model for the Middle Pleistocene succession of Schöningen, examining how the accommodation space was provided and which depositional environments contributed to the succession. The new geological model is based on outcrop data, borehole data and high-resolution shear-wave seismics, which were integrated into a 3D geological subsurface model. The 3D reconstruction clearly shows that the accommodation space for the Middle Pleistocene succession was provided by an Elsterian tunnel valley. During the Holsteinian a lake formed in the remnant tunnel valley, which provided an attractive site for animals and early humans ambushing them. Small deltas were shed into the lake from the west and Palaeolithic artefacts were embedded in the delta plain deposits. During the course of the interglacial repeated lake-level changes controlled the location of delta deposition and thus the formation of the archaeological sites. A sequence stratigraphic analysis allows for the reconstruction of the lake-level curve and the spatial and temporal correlation of the different archaeological sites.

Publication 2: The Middle Pleistocene tunnel valley at Schöningen as a Palaeolithic archive by J. Lang, J. Winsemann, U. Polom, U. Böhner and J. Serangeli, submitted to *Journal of Human Evolution*.

This publication focuses on the importance of the geological setting for the formation and preservation of Palaeolithic archaeological sites. The basic requirement for Palaeolithic archaeological sites are accommodation space and the potential for preservation, but also favourable palaeo-environmental conditions. All these requirements were met by the interglacial lake, which formed in an underfilled tunnel valley at Schöningen. The lake represented an attractive site for early humans, who kept frequenting the shores in face of changing environmental conditions through-out the Holsteinian intergla-

cial. In general, underfilled tunnel valleys provide accommodation space for post-glacial deposition and have a high preservation potential due to their great depth. The interglacial infills of tunnel valleys should therefore be regarded as potential environmental and archaeological archives.

Publication 3: Lateral and vertical facies relationships of bedforms deposited by aggrading supercritical flows: from cyclic steps to humpback dunes by J. Lang and J. Winsemann, published in *Sedimentary Geology* (2013), 296, 36-54.

Depositional processes related to supercritical flows constitute an important aspect of sedimentation in glacial settings, which commonly occur at the ice margin or during the filling of tunnel valleys. This publication provides new insights into the anatomy of bedforms deposited by supercritical to transcritical flows under highly aggradational conditions. The observed bedforms comprise laterally and vertically stacked deposits of cyclic steps, chutes-and-pools, breaking antidunes, aggrading stationary antidunes and humpback dunes. The criteria for the recognition of the various bedforms are specified and field evidence for supercritical flows are discussed and linked to flow conditions. These deposits are interpreted as representing characteristic facies of subaqueous ice-contact fan and glacial lake-outburst flood settings and their recognition is relevant for the reconstruction of depositional processes and palaeo-flows near the palaeo-ice margins.

Publication 4: Do salt structures react to ice-sheet loading? Insights from two-dimensional finite-element modelling by J. Lang, A. Hampel, C. Brandes and J. Winsemann, submitted to *Quaternary Science Reviews*.

The reaction of salt structures to ice-sheet loading and unloading is yet poorly understood. This study aims to test conceptual models by finite-element modelling. The input parameters were systematically varied to detect the controlling factors. All simulations indicate that salt structures respond to the load applied by an ice sheet. An ice advance towards the diapir causes flow of salt from the source layer into the diapir and results in diapir uplift. When the diapir is transgressed by the ice sheet the diapir is pushed downwards. Larger displacements are observed in models with deep-rooted diapirs, high thickness of the ice sheet, high thickness of the salt source layer and low viscosity of the salt. The results of the simulations are discussed in terms of their implications for the behaviour of salt structures, rim synclines and ice sheets.

5. References

- Aber, J.S., Ber, A., 2007: Glaciotectonism. *Developments in Quaternary Science* 6, 1-246.
- Albertz, M., Ings, S.J., 2012: Some consequences of mechanical stratification in basin-scale numerical models of passive-margin salt tectonics. *In: Alsop, G.I., Archer, S.G., Hartley, A.J., Grant, N.T., Hodgkinson, R. (Eds.), Salt tectonics, sediments and prospectivity. Geological Society Special Publications*, 363, pp. 303-330.

- Albertz, M., Beaumont, C., Shimeld, J.W., Ings, S.J., Gradmann, S., 2010: An investigation of salt tectonic structural styles in the Scotian Basin, offshore Atlantic Canada: 1. Comparison of observations with geometrically simple numerical models. *Tectonics* 29, 1-29.
- Alexander, J., Bridge, J.S., Cheel, R.J., Leclair, S.F., 2001: Bedforms and associated sedimentary structures formed under supercritical water flows over aggrading sand beds. *Sedimentology* 48, 133-152.
- Allen, J.R.L., 1984: Sedimentary structures: their character and physical basis. *Developments in Sedimentology* 30, 1-663.
- Alsop, G.I., 1996: Physical modelling of fold and fracture geometries associated with salt diapirism. *In: Blundell, G.I., Davison, I. (Eds.), Salt tectonics. Geological Society Special Publications* 100, 227-241.
- Baldschuhn, R., Binot, F., Fleig, S., Kockel, F., 1996: Geotektonischer Atlas von Nordwest-Deutschland und dem deutschen Nordsee-Sektor. *Geologisches Jahrbuch A* 153, 1-55.
- Behrend, F., 1927: Erläuterungen zur geologischen Karte von Preußen und benachbarten deutschen Ländern 1:25.000, Blatt Schöningen. Preußische geologische Landesanstalt, Berlin, 40 pp.
- Best, G., 1996: Floßtektonik in Norddeutschland: Erste Ergebnisse reflexionsseismischer Untersuchungen an der Salzstruktur. *Zeitschrift der Deutschen Geologischen Gesellschaft* 147, 455-464.
- Betz, D., Führer, F., Greiner, G., Plein, E., 1987: Evolution of the Lower Saxony Basin. *Tectonophysics* 137, 127-170.
- Blum, M.D., Törnqvist, T.E., 2000: Fluvial responses to climate and sea-level change: a review and look forward. *Sedimentology* 47, 2-48.
- Böhme, G., 2000: Reste von Fischen, Amphibien und Reptilien aus der Fundstelle Schöningen 12 bei Helmstedt (Niedersachsen) ó Erste Ergebnisse. *Praehistoria Thuringica* 4, 18-27.
- Böse, M., 1995: Problems of dead ice and ground ice in the central part of the North European Plain. *Quaternary International* 28, 13-125.
- Bogaart, P.W., Van Balen, R.T., 2000: Numerical modeling of the response of alluvial rivers to Quaternary climate change. *Global and Planetary Change* 27, 147-163.
- Boulton, G.S., Hindmarsh, R.C.A., 1987: Sediment deformation beneath glaciers: rheology and geological consequences. *Journal of Geophysical Research: Solid Earth* 92, 9059-9082.
- Boulton, G.S., Hagedorn, M., Maillot, P.B., Zatsepin, S., 2009: Drainage beneath ice sheets: groundwateróchannel coupling, and the origin of esker systems from former ice sheets. *Quaternary Science Reviews* 28, 621-638.
- Braess, D., 2013: Finite Elemente ó Theorie, schnelle Löser und Anwendungen in der Elastizitätstheorie. Springer Spektrum, Berlin, 394 pp.
- Brandes, C., Polom, U., Winsemann, J., 2011: Reactivation of basement faults: interplay of ice-sheet advance, glacial lake formation and sediment loading. *Basin Research* 23, 53-64.

- Brandes, C., Pollok, L., Schmidt, C., Riegel, W., Wilde, V., Winsemann, J., 2012: Basin modelling of a lignite-bearing salt rim syncline: insights into rim syncline evolution and salt diapirism in NW Germany. *Basin Research* 24, 699-716.
- Brandes, C., Schmidt, C., Tanner, D.C., Winsemann, J., 2013: Paleostress pattern and salt tectonics within a developing foreland basin (northwestern Subhercynian Basin, northern Germany). *International Journal of Earth Sciences* 102, 2239-2254.
- Brookfield, M.E., Martini, I.P., 1999: Facies architecture and sequence stratigraphy in glacially influenced basins: basic problems and water-level/glacier input-point controls (with an example from the Quaternary of Ontario, Canada). *Sedimentary Geology* 123, 183-197.
- Brown, L.F., Fisher, W.L., 1977: Seismic-stratigraphic interpretation of depositional systems: examples from Brazilian rift and pull-apart basins. *In: Payton, C.E. (Ed.), Seismic Stratigraphy ó applications to hydrocarbon exploration. AAPG Memoir* 26, pp. 117-133.
- Brun, J.P., Fort, X., 2011: Salt tectonics at passive margins: Geology versus models. *Marine and Petroleum Geology* 28, 1123-1145.
- Busschers, F.S., Van Balen, R.T., Cohen, K.M., Kasse, C., Weerts, H.J.T., Wallinga, J., Bunnik, F.P.M., 2008: Response of the Rhine-Meuse fluvial system to Saalian ice-sheet dynamics. *Boreas* 37, 329-468.
- Carling, P.A., Burr, D.M., Johnsen, T.F., Brennand, T.A., 2009: A review of open-channel megaflood depositional landforms on Earth and Mars. *In: Burr, D.M., Carling, P.A., Baker, V.R. (Eds.), Megaflooding on Earth and Mars. Cambridge University Press, Cambridge*, pp. 33-49.
- Cartigny, M.J.B., Ventra, D., Postma, G. and van den Berg, J.H., *in press*: Morphodynamics and sedimentary structures of bedforms under supercritical-flow conditions: new insights from flume experiments. *Sedimentology*, doi: 10.1111/sed.12076.
- Cartwright, J., Stewart, S., Clark, J., 2001: Salt dissolution and salt-related deformation of the Forth Approaches Basin, UK North Sea. *Marine and Petroleum Geology* 18, 757-778.
- Carvajal, C., Steel, R., Petter, A., 2009: Sediment supply: The main driver of shelf-margin growth. *Earth-Science Reviews* 96, 221-248.
- Caumon, G., Collon-Drouaillet, P., de Veslud, C.L.C., Viseur, S., Sausse, J., 2009: Surface-based 3D modeling of geological structures. *Mathematical Geosciences* 41, 927-945.
- Clark, C.D., Hughes, A.L.C., Greenwood, S.L., Jordan, C., Sejrup, H.P., 2012: Pattern and timing of retreat of the last British-Irish Ice Sheet. *Quaternary Science Reviews* 44, 112-146.
- Clerk, S., Buonchristiani, J.-F., Guiraud, M., Desaubliaux, G., Portier, E., 2012: Depositional model in subglacial cavities, Killiney Bay, Ireland. Interactions between sedimentation, deformation and glacial dynamics. *Quaternary Science Reviews* 33, 142-164.
- Cleveringa, P., Meijer, T., Van Leeuwen, R.J.W., De Wolf, H., Pouwer, R., Lissenberg, T., Burger, A.W., 2000: The Eemian stratotype locality at Amersfoort in the central Netherlands: a re-evaluation of old and new data. *Geologie en Mijnbouw* 79, 197-216.

- Cohen, H.A., Hardy, S., 1996: Numerical modelling of stratal architectures from differential loading of a mobile substratum. *In*: Blundell, G.I., Davison, I. (Eds.), Salt tectonics. Geological Society Special Publications 100, pp. 265-273.
- Cook, S.J., Swift, D.A., 2012: Subglacial basins: Their origin and importance in glacial systems and landscapes. *Earth-Science Reviews* 115, 332-372.
- Dassault Systèmes, 2012: ABAQUS 6.12 Online Documentation. Dassault Systèmes Simulia Corp., Providence, RI, USA.
- DEKORP Basin Research Group 1999: The deep structure of the NE German Basin – constraints on the controlling mechanisms of intracontinental basin development. *Geology* 27, 55-58.
- Dooley, T.P., Jackson, M., Hudec, M.R., 2009: Inflation and deflation of deeply buried salt stocks during lateral shortening. *Journal of Structural Geology* 31, 582-600.
- Duller, R.A., Mountney, N.P., Russell, A.J., Cassidy, N.C., 2008: Architectural analysis of a volcaniclastic jökulhlaup deposit, southern Iceland: sedimentary evidence for supercritical flow. *Sedimentology* 55, 939-964.
- Ehlers, J., 1990: Reconstructing the dynamics of the north-west European Pleistocene ice-sheets. *Quaternary Science Reviews* 9, 71-83.
- Ehlers, J., Linke, G., 1989: The origin of deep buried channels of Elsterian age in northwest Germany. *Journal of Quaternary Science* 4, 255-265.
- Ehlers, J., Eissmann, L., Lippstreu, L., Stephan, H.-J., Wansa, S., 2004: Pleistocene glaciations of North Germany. *In*: Ehlers, J., Gibbard, P.L. (Eds.), Quaternary Glaciations. Extent and Chronology Part I, Europe. *Developments in Quaternary Science* 2, pp. 135-146.
- Ehlers, J., Grube, A., Stephan, H.-J., Wansa, S., 2011: Pleistocene Glaciations of North Germany – New Results. *In*: Ehlers, J., Gibbard, P.L., Hughes, P.D. (Eds.), Quaternary Glaciations – Extent and Chronology – A Closer Look. *Developments in Quaternary Science* 15, pp. 149-162.
- Eissmann, L., 1967: Glaziäre Destruktionszonen (Rinnen, Becken) im Altmoränengebiet des Norddeutschen Tieflandes. *Geologie* 16, 804-833.
- Eissmann, L., 1987: Lagerungsstörungen im Lockergebirge: Endogene und exogene Tektonik im Lockergebirge des nördlichen Mitteleuropas. *Geophysik und Geologie* 3, 1987, 7-78.
- Eissmann, L., 2002: Quaternary geology of eastern Germany (Saxony, Saxon-Anhalt, South Brandenburg, Thuringia), type area of the Elsterian and Saalian Stages in Europe. *Quaternary Science Reviews* 21, 1275-1346.
- Elsner, H., 1987: Das Quartär im Tagebau Schöningen der Braunschweigischen Kohlenbergwerke AG, Helmstedt. University of Hannover, unpublished diploma thesis, 126 pp.
- Elsner, H., 2003: Verbreitung und Ausbildung Elster-zeitlicher Ablagerungen zwischen Elm und Flechtinger Höhenzug. *Eiszeitalter und Gegenwart* 52, 91-116.
- Evans, D.J.A., Philipps, E.R., Hiemstra, J.F., Auton, C.A., 2006: Suglacial till: Formation, sedimentary characteristics and classification. *Earth Science Reviews* 78, 115-176.

- von Eynatten, H., Voigt, T., Meier, A., Franzke, H. J., Gaupp, R., 2008: Provenance of Cretaceous clastics in the Subhercynian Basin: constraints to exhumation of the Harz Mountains and timing of inversion tectonics in Central Europe. *International Journal of Earth Sciences* 97, 1315-1330.
- Fielding, C.R., 2006: Upper flow regime sheets, lenses and scour fills: Extending the range of architectural elements for fluvial sediment bodies. *Sedimentary Geology* 190, 227-240.
- Fleisher, P.J., 1986: Dead-ice sinks and moats: Environments of stagnant ice deposition. *Geology* 14, 39-42.
- de Gans, W., Beets, D.J., Centineo, M.C., 2000: Late Saalian and Eemian deposits in the Amsterdam glacial basin. *Geologie en Mijnbouw* 79, 147-160.
- Ge, H., Jackson, M.P.A., 1998: Physical modeling of structures formed by salt withdrawal: implications for deformation caused by salt dissolution. *AAPG Bulletin* 82, 228-250.
- Ge, H., Jackson, M.P., Vendeville, B.C., 1997: Kinematics and dynamics of salt tectonics driven by progradation. *AAPG Bulletin* 8, 398-423.
- Gemmer, L., Ings, S.J., Medvedev, S., Beaumont, C., 2004: Salt tectonics driven by differential sediment loading: stability analysis and finite-element experiments. *Basin Research* 16, 199-218.
- Geyh, M.A., Müller H., 2005: Numerical $^{230}\text{Th}/\text{U}$ dating and a palynological review of the Holsteinian/Hoxnian Interglacial. *Quaternary Science Reviews* 24, 1861-1872.
- Geyh, M.A., Krbetschek, M., 2012: Zum radiometrischen Alter des Holstein-Interglazials. *In: Behre, K.-E. (Ed.), Forschungen zur Urgeschichte im Tagebau von Schöningen 1*, pp. 155-170.
- Gibbard, P.L., Cohen, K.M., 2008: Global chronostratigraphical correlation table for the last 2.7 million years. *Episodes* 31, 243-247.
- Ghienne, J.-F., Girard, F., Moreau, J., Rubino, J.-L., 2010: Late Ordovician climbing-dune cross-stratification: a signature of outburst floods in proglacial outwash environments? *Sedimentology* 57, 1175-1198.
- Goering, H., Roos, H.-G., Tobiska, L., 2010: *Die Finite-Elemente Methode für Anfänger*. Wiley-VCH, Weinheim, 219 pp.
- Gripp, K., 1952: Inlandeis und Salzaufstieg. *Geologische Rundschau* 40, 74-81.
- Gutiérrez, F., 2004: Origin of the salt valleys in the Canyonlands section of the Colorado Plateau: Evaporite-dissolution collapse versus tectonic subsidence. *Geomorphology* 57, 423-435.
- Hahne, J., Kemle, S., Merkt, J., 1994: Eem-, weichsel- und saalezeitliche Ablagerungen der Bohrung šQuakenbrück GE 2ö. *In: Meyer, K.-D. (Ed.), Neuere Untersuchungen an Interglazialen in Niedersachsen. ó Geologisches Jahrbuch A 134*, 9-69.
- Haines, S.S., Ellefsen, K.J., 2010: Shear-wave seismic reflection studies of unconsolidated sediments in the near surface. *Geophysics* 75, 59-66.
- Hansen, L., L'Heureux, J.S., Sauvin, G., Polom, U., Lecomte, I., Vanneste, M., Longva, O., Krawczyk, C.M., 2013, Effects of mass-wasting on the stratigraphic architecture of a fjord-valley fill: Corre-

- lation of onshore, shear-wave seismic and marine seismic data at Trondheim, Norway. *Sedimentary Geology* 289, 1-18.
- Helland-Hansen, W., Hampson, G.J., 2009: Trajectory analysis: concepts and applications. *Basin Research* 21, 454-483.
- Hirst, J.P.P., 2012: Ordovician proglacial sediments in Algeria: insights into the controls on hydrocarbon reservoirs in the In Amenas field, Illizi Basin. *In: Huuse, M., Redfern, J., Le Heron, D.P., Dixon, R.J., Moscariello, A., Craig, J. (Eds.), Glaciogenic Reservoirs. Geological Society of London Special Publication 368, pp. 319-353.*
- Holbrook, J., Scott, R.W., Oboh-Ikuenobe, F.E., 2006: Base-level buffers and buttresses: a model for upstream versus downstream control on fluvial geometry and architecture within sequences. *Journal of Sedimentary Research* 76, 162-174.
- Hooke, R.L., Jennings, C.E., 2006: On the formation of the tunnel valleys of the southern Laurentide ice-sheet. *Quaternary Science Reviews* 25, 1364-1372.
- Hornung, J.J., Asprion, U., Winsemann, J., 2007: Jet-efflux deposits of a subaqueous ice-contact fan, glacial Lake Rinteln, northwestern Germany. *Sedimentary Geology* 193, 167-192.
- Houmark-Nielsen, M., 2011: Pleistocene Glaciations in Denmark: A closer look at Chronology, Ice Dynamics and Landforms. *In: Ehlers, J., Gibbard, P.L., Hughes, P.D. (Eds.), Quaternary Glaciations ó Extent and Chronology ó A Closer Look. Developments in Quaternary Science 15, pp. 47-58.*
- Hudec, M.R., Jackson, M.P.A., 2007: Terra infirma: Understanding salt tectonics. *Earth-Science Reviews* 82, 1-28.
- Hudec, M.R., Jackson, M.P., Schultz-Ela, D.D., 2009: The paradox of minibasin subsidence into salt: Clues to the evolution of crustal basins. *GSA Bulletin* 121, 201-221.
- Hurtig, E., 1965: Beziehungen zwischen Oberflächenmorphologie und Salzstrukturen. *Geologie & Geophysik* 7, 42-56.
- Huuse, M., Lykke-Andersen, H., 2000: Overdeepened Quaternary valleys in the eastern Danish North Sea: morphology and origin. *Quaternary Science Reviews* 19, 1233-1253.
- Illies, H., 1955: Pleistozäne Salzstockbewegungen in Norddeutschland und ihre regionale Anordnung. *Geologische Rundschau* 43, 70-78.
- Jackson, M.P.A., Talbot, C.J., 1986: External shapes, strain rates, and dynamics of salt structures. *GSA Bulletin* 97, 305-323.
- Jackson, M.P.A., Vendeville, B.C., 1994: Regional extension as a geologic trigger for diapirism. *GSA Bulletin* 106, 57-73.
- Janszen, A., Moreau, J., Moscariello, A., Ehlers, J., Kröger, J., 2012a: Time-transgressive tunnel-valley infill revealed by a three-dimensional sedimentary model, Hamburg, north-west Germany. *Sedimentology* 60, 693-719.

- Janszen, A., Spaak, M., Moscariello, A., 2012b: Effects of the substratum on the formation of glacial tunnel valleys: an example from the Middle Pleistocene of the southern North Sea. *Boreas* 41, 629-643.
- Jaritz, W., 1973: Zur Entstehung der Salzstrukturen Norddeutschlands. *Geologisches Jahrbuch A* 10, 1-77.
- Jechorek, H., 2000: Die fossile Flora des Reinsdorf-Interglazial. *Paläokarpologische Untersuchungen an mittelpleistozänen Ablagerungen im Braunkohlentagebau Schöningen. Praehistoria Thuringica* 4, 7-17.
- Johnsen, T.F., Brennand, T.A., 2004: Late-glacial lakes in the Thompson Basin, British Columbia: paleogeography and evolution. *Canadian Journal of Earth Sciences* 41, 1367-1383.
- Johnsen, T.F., Brennand, T.A., 2006: The environment in and around ice-dammed lakes in the moderately high relief setting of the southern Canadian Cordillera. *Boreas* 35, 106-125.
- Jørgensen, F., Sandersen, P.B.E., 2006: Buried and open tunnel valleys in Denmark - erosion beneath multiple ice sheets. *Quaternary Science Reviews* 25, 1339-1363.
- Kleinmann, A., Müller, H., Lepper, J., Waas, D., 2011: Nachtigall: A continental sediment and pollen sequence of the Saalian Complex in NW-Germany and its relationship to the MIS-framework. *Quaternary International* 241, 97-110.
- Kaiser, K., Lorenz, S., Germer, S., Juschus, O., Küster, M., Libra, J., Bens, O., Hüttl, R.F., 2012: Late Quaternary evolution of rivers, lakes and peatlands in northeast Germany reflecting past climatic and human impact - an overview. *E&G Quaternary Science Journal* 61, 103-132.
- Karpe, W., 1994: Zur Dynamik halokinetischer Randsenken auf der Subherzynen Scholle. *Hallesches Jahrbuch für Geowissenschaften* 16, 79-93.
- Kehew, A.E., Piotrowski, J.A., Jørgensen, F., 2012: Tunnel valleys: Concepts and controversies ó A review. *Earth-Science Reviews* 113, 33-58.
- Kley, J., Voigt, T., 2008: Late Cretaceous intraplate thrusting in central Europe: Effect of Africa-Iberia-Europe convergence, not Alpine collision. *Geology* 36, 839-842.
- Kley, J., Franzke, H. J., Jähne, F., Krawczyk, C., Lohr, T., Reicherter, K., Scheck-Wenderoth, M., Sippel, J., Tanner, D., van Gent, H., 2008: Strain and stress. *In: Littke, R., Bayer, U., Gajewski, D., Nelskamp, S. (Eds.), Dynamics of Complex Intracontinental Basins ó The Central European Basin System. Springer, Berlin, pp. 97-124.*
- Koyi, H., 1996: Salt flow by aggrading and prograding overburdens. *In: Blundell, G.I., Davison, I. (Eds.), Salt tectonics. Geological Society Special Publications* 100, pp. 243-258.
- Krbetschek, M.R., Degering, G., Alexowsky, W., 2008: Infrarot-Radiofluoreszenz-Alter (IR-RF) unter-saalezeitlicher Sedimente Mittel- und Ostdeutschlands. *Zeitschrift der Deutschen Gesellschaft für Geowissenschaften* 159, 133-140.

- Krohn, C.F., Larsen, N.K., Kronborg, C., Nielsen, O.B., Knudsen, K.L., 2009: Litho- and chronostratigraphy of the Late Weichselian in Vendsyssel, northern Denmark, with special emphasis on tunnel-valley infill in relation to a receding ice margin. *Boreas* 38, 811-833.
- Kühl, N., Litt, T., 2007: Quantitative time-series reconstructions of Holsteinian and Eemian temperatures using botanical data. *In: Sirocko, F., Claussen, M., Goni, M.F.S., Litt, T. (Eds.), The climate of past interglacials; Developments in Quaternary Science* 7, pp. 418-444.
- Kuster, H., Meyer, K.-D., 1979: Glaziäre Rinnen im mittleren und nordöstlichen Niedersachsen. *Eiszeitalter und Gegenwart* 29, 135-156.
- Laban, C., van der Meer, J.J.M., 2011: Pleistocene Glaciation in the Netherlands. *In: Ehlers, J., Gibbard, P.L., Hughes, P.D. (Eds.), Quaternary Glaciations ó Extent and Chronology ó A Closer Look. Developments in Quaternary Science* 15, pp 247-260.
- Lambeck, K., Purcell, A., Funder, S., Kjær, K., Larsen, E., Moller, P.E.R., 2006: Constraints on the Late Saalian to early Middle Weichselian ice sheet of Eurasia from field data and rebound modeling. *Boreas* 35, 539-575.
- Lang, J., Winsemann, J., 2012: The 12II DB outcrop section at Schöningen: Sedimentary Facies and Depositional Architecture. *In: Behre, K.-E. (Ed.), Forschungen zur Urgeschichte im Tagebau von Schöningen* 1, pp. 39-59.
- Lang, J., Dixon, R.J., Le Heron, D.P., Winsemann, J., 2012: Depositional architecture and sequence stratigraphic correlation of Upper Ordovician glacigenic deposits, Illizi Basin, Algeria. *In: Huuse, M., Redfern, J., Le Heron, D.P., Dixon, R.J., Moscariello, A., Craig, J. (Eds.), Glaciogenic Reservoirs. Geological Society of London Special Publication* 368, pp. 293-317.
- Lehné, R., Sirocko, F., 2007: Rezente Bodenbewegungspotenziale in Schleswig-Holstein (Deutschland) ó Ursachen und ihr Einfluss auf die Entwicklung der rezenten Topographie. *Zeitschrift der deutschen Gesellschaft für Geowissenschaften* 158, 329-347.
- Liszkowski, J., 1993 The effects of Pleistocene ice-sheet loading-deloadng cycles on the bedrock structure of Poland. *Folia Quaternaria* 64, 7-23.
- Litt, T., Behre, K.-E., Meyer, K.-D., Stephan, H.-J., Wansa, S., 2007: Stratigraphische Begriffe für das Quartär des norddeutschen Vereisungsgebietes. *Eiszeitalter und Gegenwart* 56, 7-65.
- Litt, T., Schmincke, H.-U., Frechen, M., Schlüchter, C., 2008: Quaternary. *In: McCann, T. (Ed.), The Geology of Central Europe, Vol. 2: Mesozoic and Cenozoic. The Geological Society, London*, pp. 1287-1340.
- Lohr, T., Krawczyk, C.M., Tanner, D.C., Samiee, R., Endres, H., Oncken, O., Trappe, H., Kukla, P.A., 2007: Strain partitioning due to salt: insights from interpretation of a 3D seismic data set in the NW German Basin. *Basin Research* 19, 579-597.
- Look, E.-R., 1984: Geologie und Bergbau im Braunschweiger Land. *Geologisches Jahrbuch A* 78, 1-467.

- Lunkka, J.P., Saarnisto, M., Gey, V., Demidov, I., Kiselova, V., 2001: Extent and age of the Last Glacial Maximum in the southeastern sector of the Scandinavian Ice Sheet. *Global and Planetary Change* 31, 407-425.
- Mallet, J.L., 1992: Discrete smooth interpolation in geometric modelling. *Computer-Aided Design* 24, 178-191.
- Manger, G., 1952: Der Zusammenhang von Salztektunik und Braunkohlenbildung bei der Entstehung der Helmstedter Braunkohlenlagerstätten. *Mitteilungen geologisches Staatsinstitut Hamburg* 21, 7-45.
- Mania, D., 1998: Zum Ablauf der Klimazyklen seit der Elstervereisung im Elbe-Saalegebiet. *Praehistoria Thuringica* 2, 5-21.
- Mania, D., 2006: Stratigraphie, Klima- und Umweltentwicklung der letzten 400 000 Jahre im Saalegebiet und Harzvorland (Forschungsstand 2006). *Hercynia N.F.* 39, 155-194.
- Marks, L., 2011: Quaternary Glaciations in Poland. *In: Ehlers, J., Gibbard, P.L., Hughes, P.D. (Eds.), Quaternary Glaciations ó Extent and Chronology ó A Closer Look. Developments in Quaternary Science* 15, pp 299-303.
- Maystrenko, Y.P., Bayer, U., Scheck-Wenderoth, M., 2013: Salt as a 3D element in structural modelling ó example from the Central European Basin System. *Tectonophysics* 591, 62-82.
- Mills, P.C., 1983: Genesis and diagnostic value of soft-sediment deformation structures ó a review. *Sedimentary Geology* 35, 1983, 83-104.
- Mitchum, R.M., Vail, P.R., 1977: Seismic stratigraphy and global changes of sea level, Part 7: Seismic stratigraphic interpretation procedure. *In: Payton, C.E. (Ed.): Seismic Stratigraphy ó applications to hydrocarbon exploration. AAPG Memoir* 26, pp. 135-143.
- Mitchum, R.M., Vail, P.R., Sangree, J.B., 1977. Seismic stratigraphy and global changes of sea-level, Part 6: stratigraphic interpretation of seismic reflection patterns in depositional sequences. *In: Payton, C.E. (Ed.): Seismic Stratigraphy ó applications to hydrocarbon exploration. AAPG Memoir* 26, pp. 117-133.
- Mohr, M., Kukla, P.A., Urai, J.L., Bresser, G., 2005: Multiphase salt tectonic evolution in NW Germany: seismic interpretation and retro-deformation. *International Journal of Earth Sciences* 94, 917-940.
- Niebuhr, B., Ernst, G., 1991: Faziesgeschichte und Entwicklungsdynamik von Campan, Maastricht und Eozän im Beienroder Becken (E-Niedersachsen). *Zeitschrift der Deutschen Geologischen Gesellschaft* 142, 251-283.
- Ó Cofaigh, C., 1996: Tunnel valley genesis. *Progress in Physical Geography* 20, 1-19.
- Osman, A., Pollok, L., Brandes, C., Winsemann, J., *in press*: Sequence stratigraphy of a Paleogene coal bearing rim syncline: interplay of salt dynamics and sea-level changes, Schöningen, Germany. *Basin Research*, doi: 10.1111/bre.12021.

- Piotrowski, J., 1994: Tunnel-valley formation in northwest Germany ó geology, mechanisms of formation and subglacial bed conditions for the Bornhöved tunnel valley. *Sedimentary Geology* 89, 107-141.
- Piotrowski, J., Geletneky, J., Vater, R., 1999: Soft-bedded subglacial meltwater channel from the Welzow-Süd open-cast lignite mine, Lower Lusatia, eastern Germany. *Boreas* 28, 363-374.
- Pollok, L., 2010: 3D-Untergrundmodellierung der tertiären Schichtfolge im Bereich der Salzrandsenken von Schöningen. Leibniz Universität Hannover, unpublished diploma thesis, 116 pp.
- Polom, U., Bagge, M., Wadas, S., Winsemann, J., Brandes, C., Binot, F., Krawczyk, C. M., 2013: Surveying near-surface depocentres by means of shear wave seismics. *First Break* 31, 67-79.
- Posamentier, H.W., Vail, P.R., 1988: Eustatic controls on clastic deposition II ó sequence and systems tract models. *In: Wilgus, C.K., Hastings, B.S., Kendall, C.G.S.C., Posamentier, H.W., Ross, C.A., van Wagoner, J.C. (Eds.), Sea-Level Changes: An Integrated Approach: SEPM Special Publication* 42, pp. 125-154.
- Praeg, D., 2003: Seismic imaging of mid-Pleistocene tunnel-valleys in the North Sea Basin ó high resolution from low frequencies. *Journal of Applied Geophysics* 53, 273-298.
- Preece, R.C., Gowlett, J.A.J., Parfitt, S.A., Bridgland, D.R., Lewis, S.G., 2006: Humans in the Hoxnian: habitat, context and fire use at Beeches Pit, West Stow, Suffolk, UK. *Journal of Quaternary Science* 21, 485-496.
- Pugin, A.J.M., Larson, T.H., Sargent, S.L., McBride, J.H., Bexfield, C.E., 2004: Near-surface mapping using SH-wave and P-wave seismic land streamer data acquisition in Illinois, U.S. *The Leading Edge* 23, 677-682.
- Richter, D., Thieme, H., 2012: One first chronometric date for the Lower Palaeolithic occupation at Schöningen 13 I. *In: Behre, K.-E. (Ed.), Forschungen zur Urgeschichte im Tagebau von Schöningen* 1, pp. 171-182.
- Russell, H.A.J., Arnott, R.W.C., 2003: Hydraulic jump and hyperconcentrated-flow deposits of a glacial subaqueous fan: Oak Ridges Moraine, Southern Ontario, Canada. *Journal of Sedimentary Research* 73, 887-905.
- Russell H.A.J., Arnott, R.W.C., Sharpe, D.R., 2003: Evidence for rapid sedimentation in a tunnel channel, Oak Ridges Moraine, southern Ontario, Canada. *Sedimentary Geology* 160, 33-55.
- Russell, H.A.J., Sharpe, D.R., Bajk, A.F., 2007: Sedimentary signatures of the Waterloo Moraine, Ontario, Canada. *In: Hambrey, M., Christoffersen, P., Glasser, N., Hubbard, B. (Eds.), Glacial Processes and Products. International Association of Sedimentologists Special Publication* 39, pp. 85-108.
- Sangree, J.B., Widmier, J.M., 1979: Interpretation of depositional facies from seismic data. *Geophysics* 44, 131-160.
- Schirrmeister, L., 1999: Die Positionen weichselzeitlicher Eisrandlagen in Norddeutschland und ihr Bezug zu unterlagernden Salzstrukturen. *Zeitschrift für geologische Wissenschaften* 27, 111-120.

- Serangeli, J., Böhner, U., Haßmann, H., Conard, N.J., 2012: Die Pleistozänen Fundstellen in Schöningen ó eine Einführung. *In*: Behre, K.-E. (Ed.), *Forschungen zur Urgeschichte im Tagebau von Schöningen 1*, pp. 1-22.
- Sierralta, M., Frechen, M., Urban, B., 2012: $^{230}\text{Th}/\text{U}$ dating results from opencast mine Schöningen. *In*: Behre, K.-E. (Ed.), *Forschungen zur Urgeschichte im Tagebau von Schöningen 1*, 134-154.
- Sirocko, F., Szeder, T., Seelos, C., Lehné, R., Rein, B., Schneider, W.M., Dimke, M., 2002: Young tectonic and halokinetic movements in the North-German Basin: its effect on formation of modern rivers and surface morphology. *Netherlands Journal of Geosciences* 81, 431-441.
- Sirocko, F., Reicherter, K., Lehné, R., Hübscher, Ch., Winsemann, J., Stackebrandt, W., 2008: Glaciation, salt and the present landscape. *In*: Littke, R., Bayer, U., Gajewski, D., Nelskamp, S. (Eds.), *Dynamics of Complex Intracontinental Basins ó The Central European Basin System*. Springer, Berlin, pp. 233-245.
- Stackebrandt, W., 1986: Beiträge zur tektonischen Analyse ausgewählter Bruchzonen der Subherzynen Senke und angrenzender Gebiete (Aufrichtungszone, Flechtinger Scholle). *Veröffentlichungen des Zentralinstituts für Physik der Erde* 79, 1-81.
- Stackebrandt, W., 2004: Zur Neotektonik in Norddeutschland. *Zeitschrift für Geologische Wissenschaften* 32, 85-95.
- Stackebrandt, W., 2005: Neotektonische Aktivitätsgebiete in Brandenburg (Norddeutschland). *Brandenburger geowissenschaftliche Beiträge* 12, 165-172.
- Stackebrandt, W., 2009: Subglacial channels of Northern Germany ó a brief review. *Zeitschrift der Deutschen Gesellschaft für Geowissenschaften* 60, 203-210.
- Steimetz, D., 2010: 3D-Untergrundmodellierung (GoCAD) der pleistozänen Schichtfolge im Bereich der südlichen Salzrandsenke von Schöningen. Leibniz Universität Hannover, unpublished diploma thesis, 93 pp.
- Stewart, M.A., Lonergan, L., 2011: Seven glacial cycles in the middle-late Pleistocene of northwest Europe: Geomorphic evidence from buried tunnel valleys. *Geology* 39, 283-286.
- Stewart, M.A., Lonergan, L., Hampson, G., 2013: 3D seismic analysis of buried tunnel valleys in the central North Sea: morphology, cross-cutting generations and glacial history. *Quaternary Science Reviews* 72, 1-17.
- Stollhofen, H., Bachmann, G.H., Barnasch, J., Bayer, U., Beutler, G., Franz, M., Kästner, M., Legler, B., Mutterlose, J., Radies, D., 2008: Upper Rotliegend to Early Cretaceous basin development. *In*: Littke, R., Bayer, U., Gajewski, D., Nelskamp, S. (Eds.), *Dynamics of Complex Intracontinental Basins ó The Central European Basin System*. Springer, Berlin, pp. 181-210.
- Strahl, J., Luckert, J., Krbetschek, M., Machalet, B., Meng, S., Oches, E.A., Rappsilber, I., Wansa, S., Zöller, L., 2011: Geologie, Paläontologie und Geochronologie des Eem-Beckens Neumark-Nord 2 und Vergleich mit dem Becken Neumark-Nord 1 (Geiseltal, Sachsen-Anhalt). *E&G ó Quaternary Science Journal* 59, 120-167.

- Teichmüller, R., 1946: Das Oberflächenbild des Salzdoms von Segeberg in Holstein. *Zeitschrift der Deutschen Geologischen Gesellschaft* 98, 7-29.
- Thieme, H., 1997: Lower Palaeolithic hunting spears from Germany. *Nature* 385, 307-310.
- Thieme, H., 1999: Altpaläolithische Holzgeräte aus Schöningen, Lkr. Helmstedt. Bedeutsame Funde zur Kulturentwicklung des frühen Menschen. *Germania* 77, 451-487.
- Thieme, H., 2007: Die ältesten Speere der Menschheit: Funde von Weltrang. *In*: Thieme, H. (Ed.): *Die Schöninger Speere ó Mensch und Jagd vor 400 000 Jahren*. Theiss, Stuttgart, pp. 13-16.
- Toucanne, S., Zaragosi, S., Bourillet, J.F., Cremer, M., Eynaud, F., Van Vliet-Lanoë, B., Penaud, A., Fontanier, C., Turon, J.L., Cortijo, E., Gibbard, P.L., 2009: Timing of massive Æleuve Mancheø discharges over the last 350 kyr: insights into the European ice-sheet oscillations and the European drainage network from MIS 10 to 2. *Quaternary Science Reviews* 28, 1238-1256.
- Trudgill, B.D., 2011: Evolution of salt structures in the northern Paradox Basin: controls on evaporite deposition, salt wall growth and supra-salt stratigraphic architecture. *Basin Research* 23, 208-238.
- Trusheim, F., 1960: Mechanism of salt migration in northern Germany. *AAPG Bulletin* 44, 1519-1540.
- Turner, C., 1970: The Middle Pleistocene deposits at Marks Tey, Essex. *Philosophical Transactions of the Royal Society of London. Series B, Biological Sciences* 257, 373-437.
- Urban, B., 1995: Palynological evidence of younger Middle Pleistocene Interglacials (Holsteinian, Reinsdorf, Schöningen) in the Schöningen open cast lignite mine (eastern Lower Saxony, Germany). *Mededelingen Rijks Geologische Dienst* 52, 175-186.
- Urban, B., 2007: Interglacial Pollen Records from Schöningen, North Germany. *In*: Sirocko, F., Claussen, M., Goni, M.F.S., Litt, T. (Eds.): *The Climate of Past Interglacials; Developments in Quaternary Science* 7, pp. 418-444.
- Urban, B., Thieme, H., Elsner, H., 1988: Biostratigraphische, quartärgeologische und und urgeschichtliche Befunde aus dem Tagebau ŠSchöningenø, Ldkr. Helmstedt. *Zeitschrift der deutschen geologischen Gesellschaft* 139, 123-154.
- Urban, B., Elsner, H., Hölzer, A., Mania, D., Albrecht, B., 1991a: Eine eem- und frühweichselzeitliche Abfolge im Tagebau Schöningen, Landkreis Helmstedt. *Eiszeitalter und Gegenwart* 41, 85-99.
- Urban, B., Lenhard, R., Mania, D., Albrecht, B., 1991b: Mittelpleistozän im Tagebau Schöningen, Ldkr. Helmstedt. *Zeitschrift der deutschen geologischen Gesellschaft* 142, 351-372.
- Urban, B., Sierralta, M., Frechen, M., 2011: New evidence for vegetation development and timing of Upper Middle Pleistocene interglacials in Northern Germany and tentative correlations. *Quaternary International* 241, 125-142.
- Vandenbergh, J., 1995: Timescales, climate and river development. *Quaternary Science Reviews*, 14, 631-638.
- Van Asselen, S., 2010: The contribution of peat compaction to total basin subsidence: implications for the provision of accommodation space in organic-rich deltas. *Basin Research* 23, 239-255.

- Van der Vegt, P., Janszen, A., Moscariello, A., 2012. Tunnel valleys: current knowledge and future perspectives. *In*: Huuse, M., Redfern, J., Le Heron, D.P., Dixon, R.J., Moscariello, A., Craig, J. (Eds.), Glaciogenic reservoirs. Geological Society of London Special Publication 368, pp. 75-97.
- Van der Wateren, F.M., 1987: Structural geology and sedimentology of the Dammer Berge push moraine, FRG. *In*: van der Meer, J.J.M. (Ed.), Tills and Glaciotectonics. A.A. Balkema, Rotterdam, pp. 157-182.
- Van der Wateren, F.M., 1994: Proglacial subaquatic outwash fan and delta sediments in push moraines ó Indicators of subglacial meltwater activity. *Sedimentary Geology* 91, 145-172.
- Van Dijke, J.J., Veldkamp, A., 1996: Climate-controlled glacial erosion in the unconsolidated sediments of northwestern Europe, based on a genetic model for tunnel valley formation. *Earth Surface Processes and Landforms* 21, 327-340.
- Van Kolfschoten, T., 1995: Faunenreste des altpaläolithischen Fundplatzes Schöningen 12 (Reinsdorf-Interglazial). *In*: Thieme, H., Maier, R. (Eds.): Archäologische Ausgrabungen im Braunkohlentagebau Schöningen. Hannover, pp. 85-94.
- Van Kolfschoten, T. 2007: Die Kleinsäugerreste aus dem Reinsdorf-Interglazial von Schöningen. *In*: Hartmut Thieme (Ed.): Die Schöninger Speere ó Mensch und Jagd vor 400 000 Jahren. Theiss, Stuttgart, pp. 112-117.
- Van Kolfschoten, T., 2012: The Schöningen mammalian Fauna in biostratigraphical perspective. *In*: Behre, K.-E. (Ed.), Forschungen zur Urgeschichte im Tagebau von Schöningen 1, pp. 113-124.
- Vail, P.R., Mitchum, R.M., Thompson, S., 1977: Seismic stratigraphy and global changes of sea level, Part 3: relative changes of sea level from coastal onlap. *In*: Payton, C.E. (Ed.): Seismic Stratigraphy ó applications to hydrocarbon exploration. AAPG Memoir 26, pp. 63-81.
- Veeken, P.C.H., Van Moerkerken, B., 2013: Seismic Stratigraphy and Depositional Facies Models. EAGE Publications, Houten, 494 pp.
- Vendeville, B.C., 2005: Salt tectonics driven by sediment progradation: Part I ó Mechanics and kinematics. *AAPG Bulletin* 89, 1071-1079.
- Voigt, T., Wiese, F., von Eynatten, H., Franzke, H. J., Gaupp, R., 2006: Facies evolution of syntectonic Upper Cretaceous deposits in the Subhercynian Cretaceous Basin and adjoining areas (Germany). *Zeitschrift der deutschen Gesellschaft für Geowissenschaften*, 157, 203-243.
- Voigt, T., Reicherter, K., von Eynatten, H., Littke, R., Voigt, S., Kley, J., 2008: Sedimentation during basin inversion. *In*: Littke, R., Bayer, U., Gajewski, D., Nelskamp, S. (Eds.), Dynamics of Complex Intracontinental Basins ó The Central European Basin System. Springer, Berlin, pp. 211-232.
- Waldron, J.W.F., Rygel, M.C., 2005: Role of evaporite withdrawal in the preservation of a unique coal-bearing succession: Pennsylvanian Joggins Formation, Nova Scotia. *Geology* 33, 337-340.
- Waltham, D., 1997: Why does salt start to move? *Tectonophysics* 282, 117-128.
- Warren, J.K., 2006: Evaporites: sediments, resources and hydrocarbons. Springer, Berlin, 1035 pp.

- Weijermars, R., Jackson, M.P.A., Vendeville, B.C., 1993: Rheological and tectonic modeling of salt provinces. *Tectonophysics* 217, 143-174.
- White, W.A., 1992: Displacement of salt by the Laurentide Ice Sheet. *Quaternary Research* 38, 305-315.
- Wingfield, R., 1990: The origin of major incisions within the Pleistocene deposits of the North Sea. *Marine Geology* 91, 31-52.
- Winsemann, J., Hornung, J.J., Meinsen, J., Asprion, U., Polom, U., Brandes, C., Bußmann, M., Weber, C., 2009: Anatomy of a subaqueous ice-contact fan and delta complex, Middle Pleistocene, North-west Germany. *Sedimentology* 56, 1041-1076.
- Winsemann, J., Brandes, C., Polom, U., 2011: Response of a proglacial delta to rapid high-amplitude lake-level change: an integration of outcrop data and high-resolution shear wave seismic. *Basin Research* 23, 22-52.
- Wu, S., Bally, A.W., Cramez, C., 1990: Allochthonous salt, structure and stratigraphy of the north-eastern Gulf of Mexico. Part II: Structure. *Marine and Petroleum Geology* 7, 334-370.
- Ziegler, P. A., 1990: Collision related intra-plate compression deformations in Western and Central Europe. *Journal of Geodynamics*, 11, 357-388

This chapter has been published as Lang et al., 2012, Quaternary Science Reviews 39, 86-105, doi: 10.1016/j.quascirev.2012.02.009 and can be found at:
<http://www.sciencedirect.com/science/article/pii/S0277379112000820>

The Pleistocene of Schöningen, Germany: a complex tunnel valley fill revealed from 3D subsurface modelling and shear-wave seismics

Jörg Lang¹⁾, Jutta Winsemann¹⁾, Dominik Steinmetz¹⁾, Ulrich Polom²⁾, Lukas Pollok¹⁾, Utz Böhner³⁾, Jordi Serangeli⁴⁾, Christian Brandes¹⁾, Andrea Hampel¹⁾ & Stefan Winghart³⁾

- 1) Institut für Geologie, Leibniz Universität Hannover, Callinstraße 30, 30167 Hannover, Germany
- 2) Leibniz Institut für Angewandte Geophysik (LIAG), Stilleweg 2, 30655 Hannover, Germany
- 3) Niedersächsisches Landesamt für Denkmalpflege, Scharnhorststraße 1, 30175 Hannover, Germany
- 4) Institut für Ur- und Frühgeschichte, Eberhardt Karls Universität Tübingen, Burgsteige 11, 72070 Tübingen, Germany

Abstract

The Pleistocene deposits of Schöningen represent an outstanding geological and archaeological archive, where an up to 45 m thick Middle to Late Pleistocene succession has been preserved and unique artefacts from the Lower Palaeolithic have been discovered. The preservation of such a thick and complete glacial/interglacial succession is very rare in the geological record and requires a specific depositional setting. We will present a new depositional model for the Pleistocene succession of Schöningen, integrating outcrop data, borehole data and high-resolution shear-wave seismics. A total of four outcrop sections and 744 borehole logs were examined to document the complex facies architecture. All collected sedimentological and geophysical data sets were integrated into a high-resolution 3D geological model (GOCAD[®]) for reconstructing the spatial distribution of facies associations and the large-scale depositional architecture. The spatial distribution of the artefacts will be discussed with respect to the depositional environment.

The Elsterian and Holsteinian deposits are restricted to a NNW-SSE trending, elongated trough, which is deeply incised into unconsolidated lignite-bearing Palaeogene deposits. The geometry of this erosional structure points to a tunnel valley origin that was incised below the Elsterian ice sheet. The basal tunnel valley fill consists of cross-stratified pebbly sand and gravel overlain by till. After deglaciation the tunnel valley remained underfilled and acted as a depocentre for interglacial deposition. During the subsequent Holsteinian interglacial (MIS 9) a lake formed within this depocentre and lacustrine sediments accumulated. This interglacial succession consists of peat, organic-rich silt and

fine-grained sand interpreted as lake-bottom and deltaic sediments fed by surface run-off shed from the Elm ridge. The lacustrine deposition was controlled by repeated lake-level fluctuations in the range of 1 to 6 metres leading to the formation of laterally stacked delta systems. These lake-level changes were probably triggered by climate, causing variations of precipitation and surface run-off. During the late Saalian glaciation the remnant tunnel valley was completely filled with meltwater deposits. The sedimentary facies and depositional architecture point to a shallow-water delta. Subsequently the meltwater deposits were overlain by till.

The deposition of the Middle Pleistocene sediments within an Elsterian tunnel valley explains the unique preservation of the sedimentary succession of Schöningen. The long-lived interglacial lake provided an attractive site for animals and early humans ambushing them. Artefacts mainly became embedded on the delta plain, which rapidly was transgressed during lake-level rise and artefacts were thus preserved.

Introduction

Schöningen is one of the most important archaeological sites in central Europe, where unique Lower Palaeolithic artefacts have been discovered, including the famous hunting spears (Thieme, 1997). Due to the preservation of a complete Middle Pleistocene succession the Pleistocene deposits of Schöningen represent an outstanding geological and archaeological archive. The preservation of such a thick and complete glacial/interglacial succession is very rare in the geological record and requires a specific depositional and tectonic setting. The Schöningen open-cast lignite mine (Fig. 1) has for more than three decades been the focus of intensive archaeological and palaeoecological research, especially since the discovery of the hunting spears in 1995 (Thieme, 1997, 1999). During the Holsteinian (MIS 9, Urban *et al.*, 2011) the spears and other objects became embedded into wet and anaerobic sediment and remained under the water table up until the present day. This allowed for an excellent preservation of organic materials, such as bones, wood, leaves, seeds, fish scales and insect wings. The climatic changes within this succession are demonstrated by the variable occurrence of animal and plant species (e.g. Urban, 1995, 2007; Van Kolfschoten, 1995, 2007).

Of the different sites within the excavation area (Fig. 1C), the most important one is Schöningen 13 II, level 4, for the discovery of eight spears, the remains of nearly twenty butchered horses and nearly 1500 stone artefacts (Thieme, 1997, 1999, 2007). Another important site is Schöningen 12 II, level 1, where several possible wooden shafts were discovered, together with more than 1000 bones of large mammals, numerous fragments of wood and several stone tools (Thieme, 1999, 2007).

The numerous other Middle Pleistocene open air sites in Schöningen bear fewer remains and therefore should be considered as sites with a low density of finds (Serangeli & Böhner, 2012). However, the evidence of human presence in the Middle Pleistocene open air sites of Schöningen is unmistakable and, thanks to the exceptionally good organic preservation, unique for layers this old. The spears, the possible wooden shafts and the stone tools are evidence for complex planning and traditions. The nu-

merous animal bones with cut- and impact-marks are evidence for repeated, complex hunting and butchering activities. Therefore, the Schöningen sites represent a milestone in the history of human culture. In this context, geological analysis of the sites is fundamental for the research of the settlement dynamics amongst Lower Palaeolithic humans in central Europe, and more generally for the understanding of human cultural evolution.

Although a lot of research has been conducted concerning the geology of certain strata or areas as well as the palaeoecology, especially palynology, of this important site (e.g. Urban *et al.*, 1988, 1991a, b; Urban 1995, 2007; Elsner, 2003), existing geological models (Mania, 1995, 1998, 2006) do not yet satisfactorily explain the formation and preservation of the glacial and interglacial deposits. The aim of our study is to provide a comprehensive geological model, solving the most important, but up to now poorly understood, questions:

- Which mechanism provided accommodation space for the thick, almost complete Middle Pleistocene succession?
- How were the Elsterian and subsequent interglacial deposits preserved from later erosion, especially during the Saalian glaciation?
- What was the depositional environment of the Middle Pleistocene interglacial deposits that contain the unique artefacts, plants and fossils?
- What made the site so attractive for animals and early human hunters during the Lower Palaeolithic?

Regional setting and previous research

The study area is located in the Subhercynian Basin of northern Germany, which is bounded by the Harz Mountains to the southwest and the Flechtingen High to the northeast (Fig. 1B). The Subhercynian Basin is subdivided into several northwest to southeast trending synclines and anticlines, which are related to domes of Upper Permian salt (Fig. 1B; Walter, 2007). The Schöningen open-cast mine is located at the outer margin of the south-western rim syncline of the Helmstedt-Staßfurt salt wall, which forms a ~70 km long, northwest to southeast trending salt structure. The basement of the rim syncline is formed by Mesozoic mud- and limestone (Look, 1984). The main fill of the rim-syncline consists of an up to 360 m thick succession of unconsolidated sand, silt, clay and lignite, interpreted as terrestrial to marine Palaeogene deposits (Behrend, 1927; Manger, 1952; Look, 1984; Brandes *et al.*, 2012). The Palaeogene deposits are unconformably overlain by an up to 45 m thick Pleistocene and Holocene succession (Urban *et al.*, 1988; Elsner, 2003; Lang & Winsemann, 2012).

During the Pleistocene northern Germany was affected by three major glaciations of the Elsterian, Saalian and Weichselian glacial periods. The Elsterian ice sheet covered most of northern Germany (Fig. 1A, Ehlers *et al.*, 2004). Discussion is still ongoing if the Elsterian glaciation occurred during MIS 10 (e.g., Geyh & Müller, 2005; Litt *et al.*, 2007, 2008; Lee *et al.*, 2010) or MIS 12 (e.g. Toucanne

et al., 2009; Ehlers *et al.*, 2011). For the Elsterian glaciation two major ice advances are known from northeast Germany, which advanced to approximately the same maximum position (Fig. 1A; Eissmann, 2002; Litt *et al.*, 2007). The Elsterian tills are separated by glacialacustrine and glacialfluvial deposits (Eissmann, 2002; Litt *et al.*, 2007). From the Saalian glaciation two major ice advances are known. Tills are separated by meltwater deposits (Ehlers *et al.*, 2004, 2011; Litt *et al.*, 2007; Fig. 1). There are no organic deposits known to occur in the warmer phases between the Saalian ice advances (Ehlers *et al.*, 2011). The maximum extent of the Saalian ice cover in northern Germany (Fig. 1A) was reached during the Older Saalian ice advance (“Drenthe” cf. Litt *et al.*, 2007), which occurred during MIS 6 (Litt *et al.*, 2007; Busschers *et al.*, 2008; Krbetschek *et al.*, 2008). The Schöningen area has been transgressed by both the Elsterian and Older Saalian (Drenthe) ice sheets. The Younger Saalian ice advance (“Warthe” cf. Litt *et al.*, 2007) and the Weichselian ice advance did not reach the study area (Fig. 1A; Ehlers *et al.*, 2004, 2011).

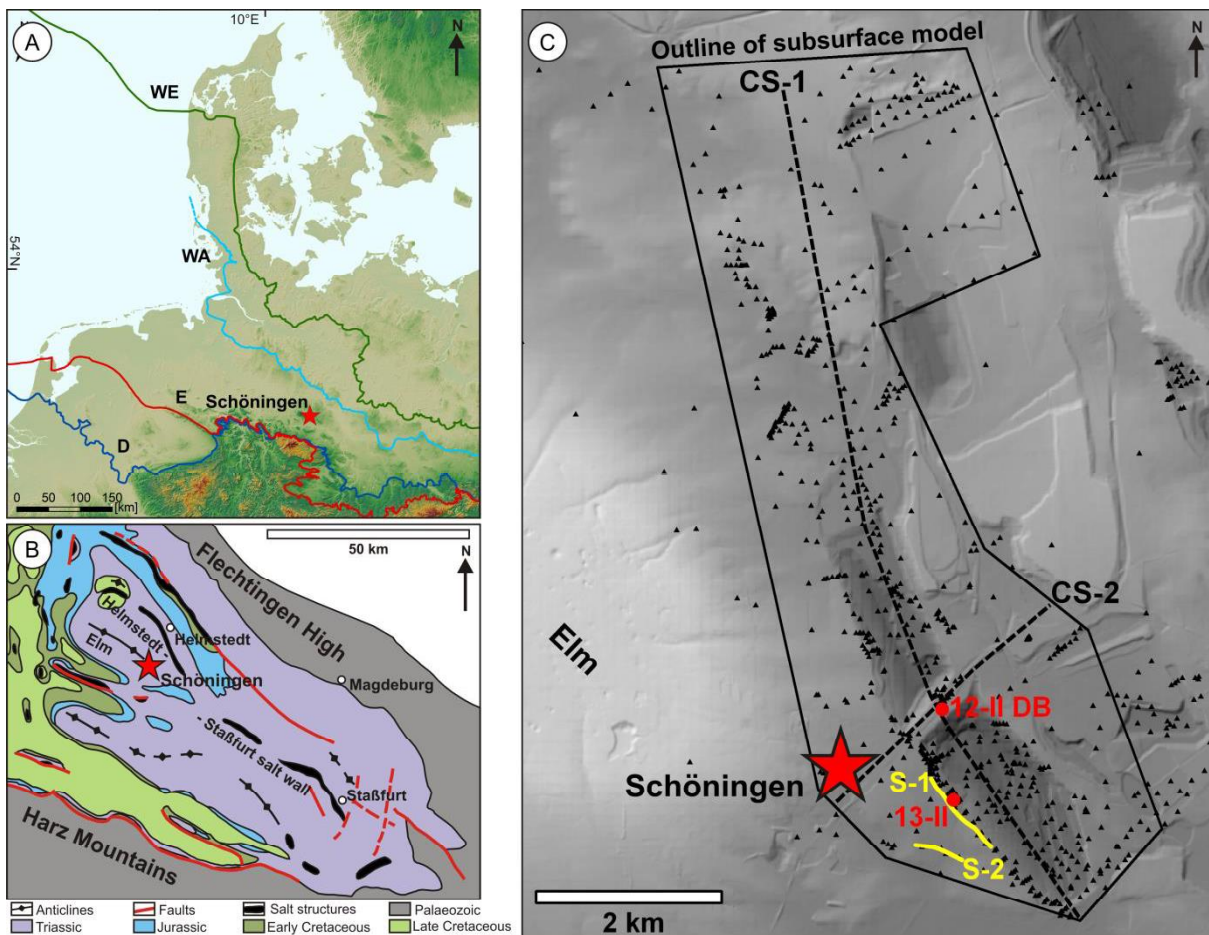


Fig. 1: A) Location of the study area and maximum extent of the Pleistocene ice sheets (modified after Ehlers *et al.*, 2004; Winsemann *et al.*, 2011b). B) Simplified geological map of the study area, located in the Subhercynian Basin (modified after Walter, 2007). C) Hill-shaded relief model of the study area, showing the locations of the excavation sites 12-II and 13-II (red dots). The yellow lines indicate the position of the seismic sections (S-1 and S-2). The outline of the subsurface model is shown in black; boreholes are indicated by black triangles. Dashed black lines are cross-sections derived from the subsurface model (CS-1 and CS-2). The DEM is based on data from LGL Niedersachsen.

The oldest Pleistocene sediments at the Schöningen site are Elsterian in age (Elsner, 2003). The basal sedimentary succession consists of Elsterian meltwater deposits and till. Urban *et al.* (1988) and Elsner (2003) report the presence of two Elsterian tills. The older till is thin (1-3 m), clast-poor, has a dark green to black matrix of clay and silt and is of limited lateral extent (~150 m), whereas the younger till is up to 14 m thick, clast-rich, has a dark grey matrix of silt and fine-grained sand and a wide lateral extent of several hundreds of meters (Elsner, 2003). The two tills are separated by coarse-grained meltwater deposits (Elsner, 2003). The younger Elsterian till is overlain by an up to 15 m thick succession of silt, sand and gravel, which was deposited during the retreat of the Elsterian ice sheet (Elsner, 2003).

Embedded between the Elsterian and Saalian glacigenic deposits a complex stack of interglacial deposits occurs (Fig. 2), which were subdivided on the base of palynological data (Urban *et al.*, 1988, 1991b; Elsner, 2003). Within these interglacial deposits clusters of artefacts have been discovered in several stratigraphic levels (Mania, 1995; Thieme, 1997, 1999). The depositional environment and age of the Middle Pleistocene interglacial deposits is still controversial. Elsner (1987) proposed the formation of shallow kettle-hole lakes by dead-ice melting. In contrast, Mania (1998, 2006) assumed a combination of fluvial incision and salt solution in the subsurface, leading to the development of broad channels. According to Mania (1995; 2006) three major channels occur within the Middle Pleistocene interglacial succession, displaying a lateral migration towards the salt wall, interpreted as indicating persistent subsidence of the rim syncline. Based

on palynological data Urban, (1995) defined two new interglacials referred to as “Reinsdorf” and “Schöningen”, thought to overlie basal Holsteinian deposits (Fig. 2). In contrast, Litt *et al.* (2007) stated that the “Reinsdorf” forms part of the Holsteinian interglacial. New 230Th/U data from site 13-II (Fig. 1C) support a Holsteinian age of the “Reinsdorf” succession. Age determinations range from 294 +/-10 to 297 +/-12 ka (Sierralta *et al.* 2012) and 280 to 343 ka (Urban *et al.* 2011), correlating with MIS 9. The “Schöningen interglacial” has been only described from the northern field of the mine and correlated with the Dömnitz warm phase (MIS 7; Fig. 2; Urban *et al.*, 1991b; Litt *et al.*, 2007). This stratigraphic correlation is only based on palynological data and no absolute age determinations are available.

		Litt <i>et al.</i> (2007; 2008)		Urban (2007) Urban <i>et al.</i> (2011)
		Holocene	MIS 1	Holocene
Upper Pleistocene	Weichselian		MIS 2	
	Eemian		MIS 5	Eemian
Middle Pleistocene	Saalian - Complex	Warthe		Schöningen
		Drenthe	MIS 6	
		Dömnitz	MIS 7	
		Fuhne	MIS 8	
	Holsteinian		MIS 9	Reinsdorf Holsteinian
	Elsterian		MIS 10	

Fig. 2: Stratigraphic chart of the Pleistocene succession at Schöningen.

The interglacial succession is unconformably overlain by meltwater deposits and subglacial till of the Saalian Drenthe glaciation (Urban *et al.*, 1991b; Mania, 1995; Lang & Winsemann, 2012). In contrast to the Elsterian deposits the Saalian glacial successions and the underlying interglacial deposits are intensely deformed by glaciectonic processes (Urban *et al.*, 1991b; Elsner, 2003; Lang & Winsemann, 2012). The Saalian glacial deposits are unconformably overlain by Eemian interglacial deposits, which are up to 7 m thick and consist of travertine and peat (Urban *et al.*, 1988; 1991a). Weichselian deposits are probably represented by up to 6 m of loess and gelifluction deposits (Behrend, 1927; Urban *et al.*, 1988, 1991a; Wagner, 2011; Lang & Winsemann, 2012). Within the loess several phases of deposition, erosion and soil formation can be reconstructed (Brosche & Walther, 1978). During the Holocene fluvial deposition, peat accumulation and soil formation took place (Urban *et al.*, 1988, 1991a; Mania, 1995).

Methods and database

Sedimentology

Field work was carried out at different locations within the Schöningen open-cast mine (Fig. 1C). The outcrops were characterised from vertical measured sections and two-dimensional photo panels of the outcrop walls (Figs. 3 and 4). In total 14 sediment logs were measured at the scale of individual beds, noting grain size, bed thickness, bed contacts, bed geometry and internal sedimentary structures. The larger-scale facies architecture is exemplified on one photo panel. Photos illustrate details of the sedimentary facies and deformation structures (Figs. 5 and 6). Soft sediment deformation structures were measured in the field and are plotted in stereographic projection (lower hemisphere equal area projection; Fig. 4B). Palaeoflow directions were obtained from cross-bedding and have been corrected for deformed sections (Fig. 7).

Shear-wave seismic acquisition

To determine the larger-scale architecture of the Schöningen deposits, two shear-wave seismic reflection profiles have been acquired and interpreted (Figs. 8 and 9). A northwest-southeast trending, 1000 m long section (S-1) was measured along the present margin of the open-cast mine and thus close to excavation plateau 13-II. A shorter section (S-2) with a length of 540 m was measured approximately 400 m apart from line S-1.

Acquisition of shallow reflection seismic data was carried out in a SH-SH (source and receivers both horizontally polarised) shear-wave configuration parameterised to a maximum target depth of 50 m. For a high-resolution and fast data acquisition, a Land Streamer unit of 120 SH geophones in 1 m intervals was combined with a small, electro-dynamically driven SH shaker source system mounted on a wheelbarrow unit (Polom, 2006; Polom *et al.*, 2011). We utilised the shear-wave vibroseis method (Crawford *et al.*, 1960; Ghose *et al.*, 1996) with a 30-240 Hz (line S-2: 30-180 Hz) linear frequency

modulated sinusoidal sweep of 10 s duration as a seismic source signal. Owing to the broad bandwidth of three octaves (line S-2: 2.5 octaves) of the source signal combined with the relatively small receiver intervals, the low velocity of shear waves (~ 300 m/s), and assuming a mean wavelength down to 5 m, this set-up results in a vertical resolution of ~ 0.5 m and a lateral resolution starting at 0.5 m close to the surface, decreasing to ~ 1.5 m vertically and ~ 12 m horizontally at 50 m depth prior to the migration process. Seismic data processing was mainly focused on shear-wave velocity analysis after pre-processing of the raw data. Elevation static corrections were applied relative to 107 m a.s.l. elevation datum at the peak of the profile. Time-to-depth conversion was carried out by a carefully smoothed velocity field derived from stacking velocities.

3D subsurface modelling

To analyse the regional distribution of the Pleistocene deposits, outcrop data, geophysical data and 744 borehole data were integrated into a 3D geological model (GOCAD®). The outline of the modelled area is determined by the availability of borehole data. The model area runs parallel to the salt wall and the open-cast mine (Fig. 1C). From outcrop observations and borehole logs seven stratigraphic markers were defined, which represent the base of the Pleistocene succession and the tops of six depositional units. Each stratigraphic surface was triangulated individually from 3D point data and subsequently used to define the thickness of each depositional unit. The geometry of the stratigraphic surfaces and thickness of depositional units are visualised on maps (Fig. 10) and 2D cross-sections (Fig. 11).

Sedimentary facies and architectural elements defined from outcrop sections

An analysis of the sedimentary facies of the Middle Pleistocene deposits has been previously published by Lang & Winsemann (2012). The main facies associations are summarised in Fig. 3. In this paper the emphasis is placed on the larger-scale depositional architecture and the correlation of seismic facies with boreholes and outcrop data. The Palaeogene deposits of the rim syncline are unconformably overlain by Pleistocene deposits that are up to 35 m thick (Fig. 3). It should be emphasised that the age assignments for the Elsterian and Saalian deposits are merely based on lithostratigraphy (Urban, 1995, 2007; Mania, 1995, 1998; Elsner, 2003; Lang & Winsemann, 2012). Numerical dates do only exist for parts of the Middle Pleistocene interglacial deposits, which are correlated with the Holsteinian and MIS 9 (Urban *et al.*, 2011; Sierralta *et al.*, 2012).

Elsterian deposits

The Elsterian meltwater deposits consist of thick-bedded planar or trough cross-stratified pebbly sand and gravel, interpreted as deposited from high-energy tractional flows (Fig. 5A). Up to 0.5 m thick and 6 m wide lenses of clast-supported, massive, normally or inversely graded gravel are commonly inter-

calated and are interpreted as shallow channels, infilled with deposits of non-cohesive debris flows (Mulder & Alexander, 2001; Gani, 2004). Abundant quartz pebbles, armoured mud clasts and lignite clasts bear evidence of the intense erosion of the underlying Paleogene deposits. The Elsterian meltwater deposits form the basal part of the glacial successions, have an overall lenticular geometry and are up to 9 m thick (Fig. 3). The palaeoflows were approximately from the north. The meltwater deposits are unconformably overlain by very thick-bedded dark grey diamicton, which is up to 10 m thick and has an overall lenticular geometry (Fig. 5B, C and D). The diamicton is interpreted as representing Elsterian subglacial till.

The uppermost part of the Elsterian succession consists of thin- to medium-bedded planar-parallel, ripple cross-laminated or massive silt and sand, which are interpreted to result from low-energy turbulent flows and suspension fall-out (Allen, 1984; Mulder & Alexander, 2001). In the lower part of this succession medium- to thick-bedded massive, clast-supported gravel is intercalated, which is interpreted as deposit of non-cohesive debris flows (Mulder & Alexander, 2001; Gani, 2004), which form

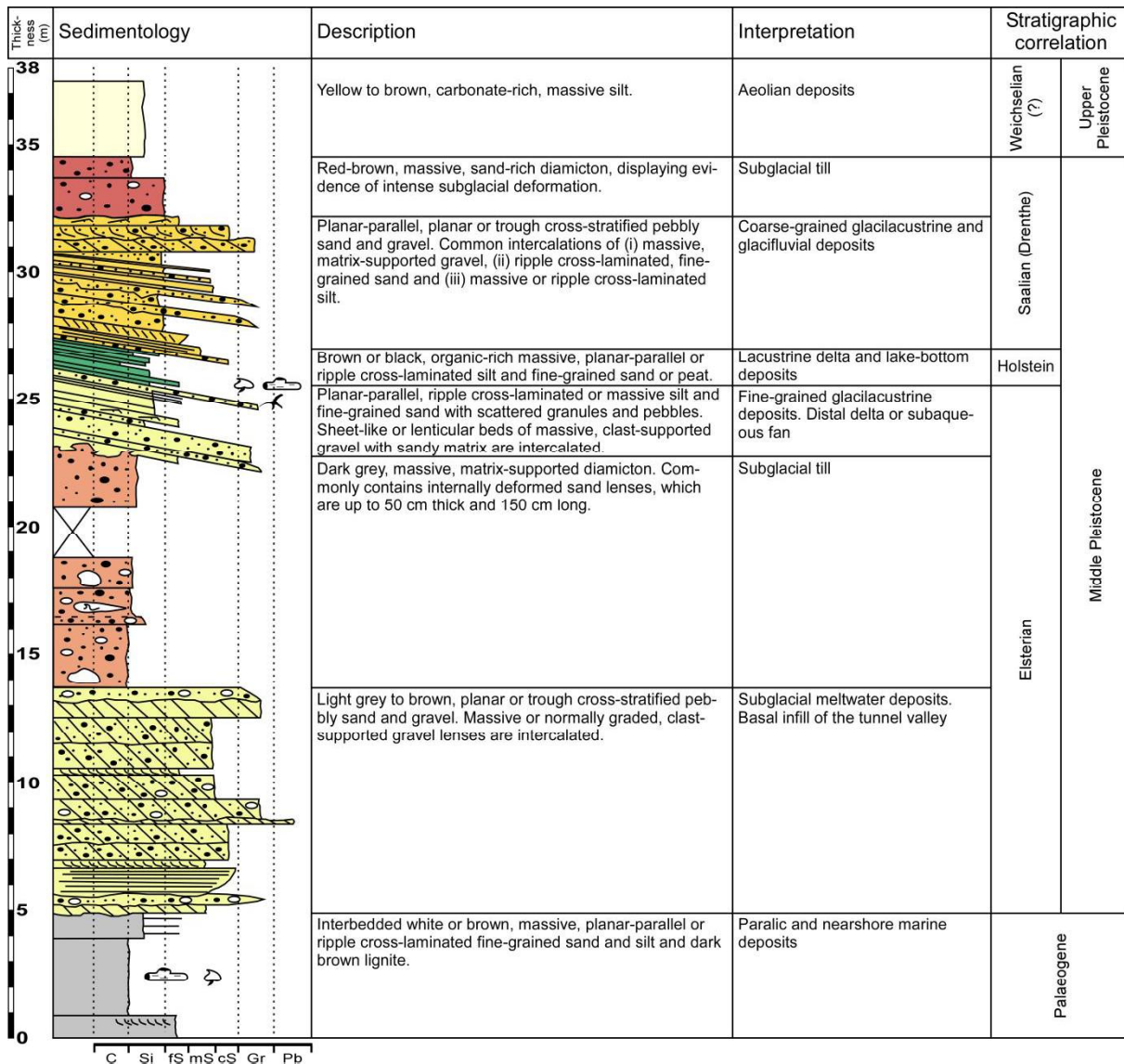


Fig. 3: Interpreted sedimentological log measured at site 12-II. For location see Fig. 1C.

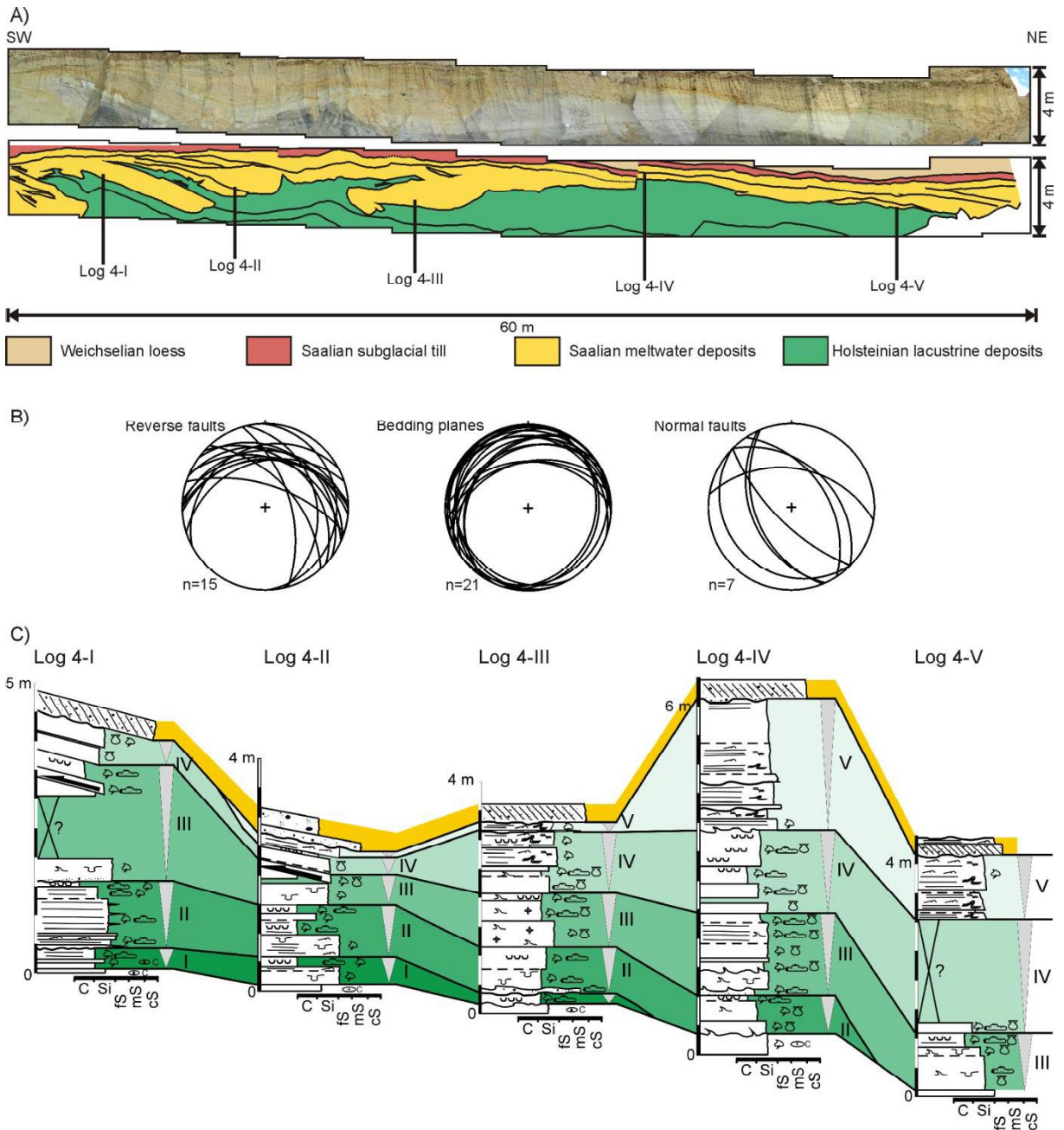


Figure 4: **A)** Photo panel of the outcrop section at excavation site 12-II (Plateau 4). The deposits are intensely deformed by the intrusion of mud diapirs (arrows indicate sense of movement). **B)** Stereographic projection showing the orientation of reverse faults, bedding planes and normal faults within the Saalian meltwater deposits (lower hemisphere equal area projection). **C)** Correlation of the logs displayed in Fig. 7 A. Within the interglacial deposits five shallowing-upwards successions can be correlated, which are interpreted as parasequences.

gently (8-16°) southeast dipping clinofolds and are 1 to 4 m thick (Fig. 5E, F). The palaeoflows were from the north. The uppermost Elsterian deposits are interpreted as glacial lacustrine sediments.

Middle Pleistocene interglacial deposits

The Middle Pleistocene interglacial deposits consist of peat and organic-rich silt and fine-grained sand (Figs. 4 and 6), which were deposited under warm interglacial climatic conditions (Urban *et al.*, 2011)

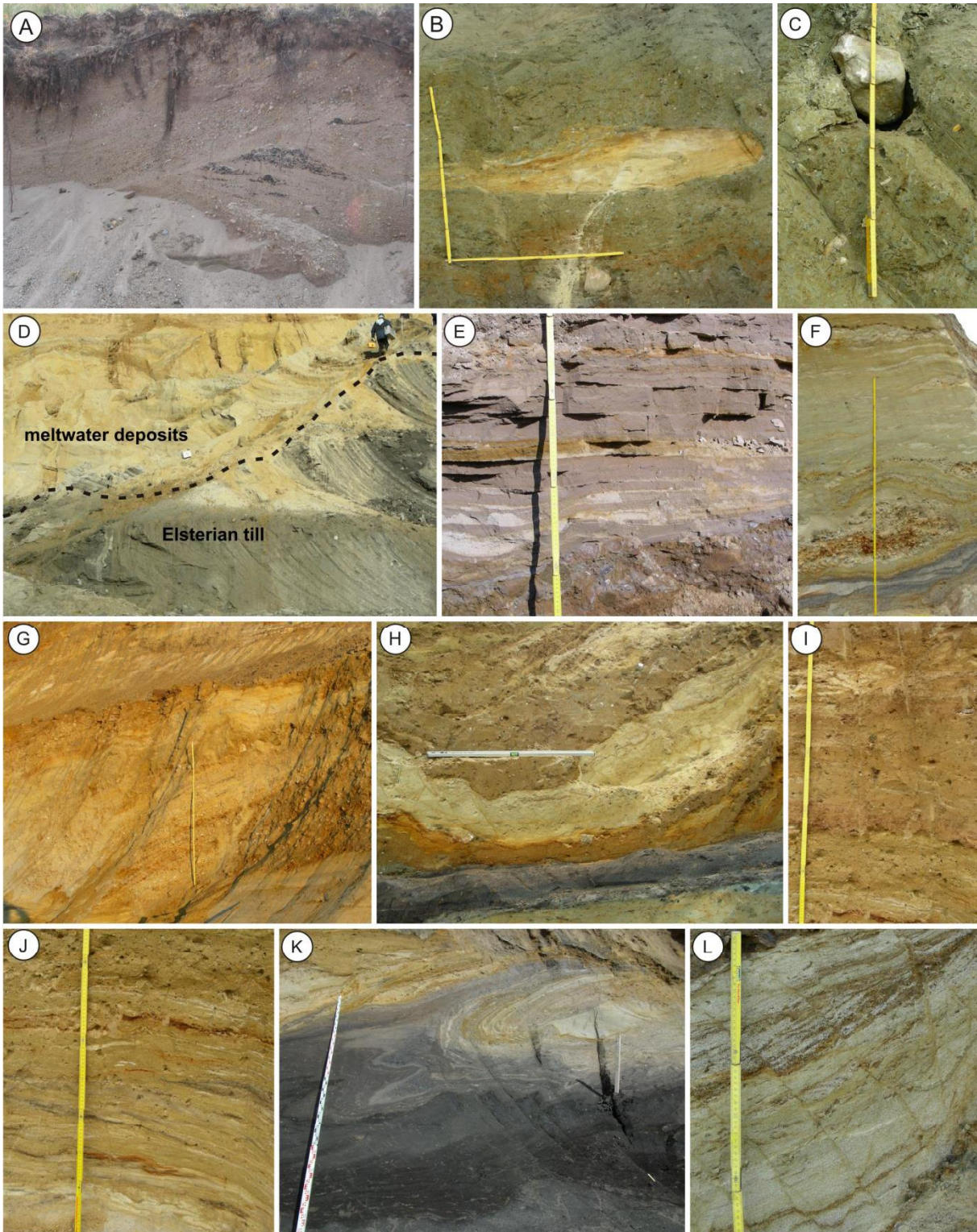


Fig. 5: **A)** Elsterian meltwater deposits. **B)** Fine-grained sheared sand lens within Elsterian subglacial till. **C)** Dark-grey, massive, matrix-supported diamicton, representing the typical facies of the Elsterian subglacial till. **D)** Steep-walled incision into the top of the Elsterian till (black line). **E)** Fine-grained Elsterian glacialacustrine deposits. **F)** Fine-grained Elsterian glacialacustrine deposits, containing lens-shaped gravel, which is interpreted as deposits of non-cohesive debris flows. **G)** Glacialacustrine delta foreset deposits (Saalian). **H)** Intensely deformed Saalian meltwater deposits. **I)** Red-brown, massive, matrix-supported diamicton interpreted as Saalian subglacial till. **J)** Intensely sheared Saalian deposits interpreted as glacitectorite. **K)** Mud diapir, comprising Holsteinian organic-rich silt. The overlying Saalian meltwater deposits are deformed by the intruding diapir, causing faulting and folding. **L)** Fine-grained Saalian glacialacustrine deposits, containing densely spaced normal faults.

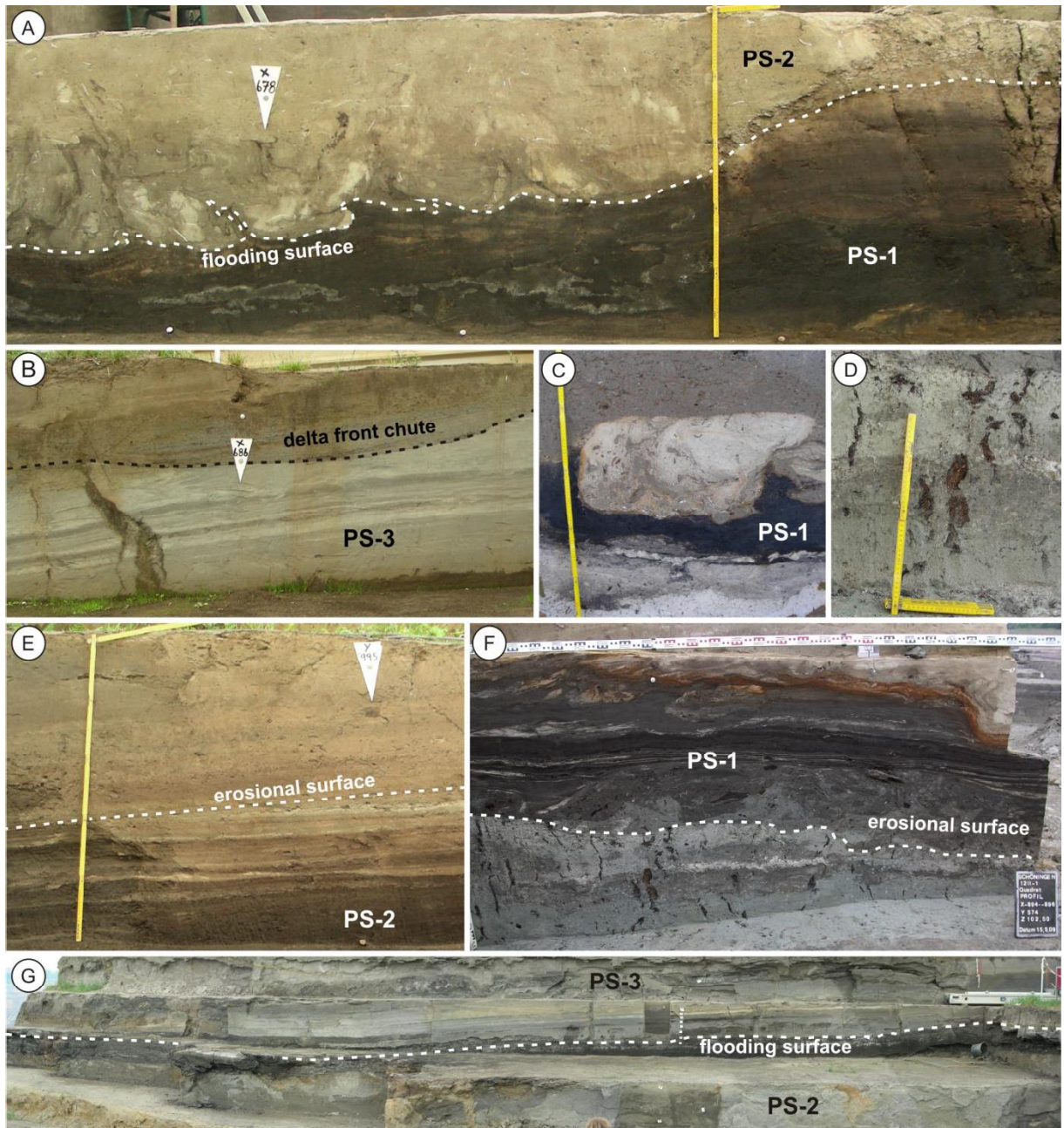


Fig. 6: **A)** Peat layer on top of parasequence PS-1. The top of the peat is eroded and has a steep erosional bench. The peat is overlain by lake-bottom deposits containing abundant bivalve shells. The contact is deformed by flame structures. **B)** Laminated silt and fine-grained sand of the delta front (parasequence PS-3). In the upper part a shallow chute is incised into the delta front (dashed line). The dip is towards the ESE. **C)** Distributary channel of the delta plain, incised into the peat of parasequence PS-1. The channel-fill and the peat display intense deformation by loading and dewatering. **D)** Thick roots below the base of parasequence PS-1. **E)** Erosional surface within delta front deposits (parasequence PS-2) **F)** Thick roots within lake-bottom deposits truncated by an erosional surface at the base of parasequence PS-1. The roots indicate an emersion surface formed during lake-level lowstand. **G)** Photo panel showing the eastwards dipping boundary between parasequences PS-2 and PS-3. The outcrop is 3 m high; the view is towards the south.

within a lake environment (Lang & Winsemann, 2012). The organic-rich interglacial deposits pass upwards into silt and fine-grained sand with rare plant debris, indicating a deteriorating climate with less vegetation and higher rates of erosion near the end of the interglacial. The interglacial deposits are

1 to 6 m thick and form gently (4-10°) northeast- to southeastwards dipping clinoforms, interpreted to represent delta foresets. The palaeoflows were approximately from the northwest. Clinoformal geometries of the Middle Pleistocene interglacial deposits have been described from former outcrops in the northern field of the Schöningen open-cast mine (Elsner, 1987; Hartmann, 1988; Lenhard, 1989; Tschee, 1991; Urban *et al.*, 1988, 1991b). The interglacial deposits at sites 12-II and 13-II form five vertically stacked shallowing-upwards successions (“levels 1 to 5”, cf. Urban, 2007), which prograde eastwards (Fig. 4C). Each shallowing-upwards succession has an erosive base (Fig. 6A, D, F), which is overlain by thin- to medium-bedded planar-parallel or ripple cross-laminated silt or fine-grained sand (Fig. 6B, E). Lag deposits, consisting of few granules or pebbles, occasionally overlie the basal erosional surface. Upwards the successions pass into thin- to thick-bedded massive or planar-parallel laminated silt (Fig. 6B, E). Each succession is topped by a bed of peat or peaty silt (Fig. 6A, C and G). The thickness of the shallowing-upwards successions varies between 0.2 to 3 m and is typically about 0.8 m. The lower four shallowing-upwards successions consist of organic-rich silt and fine-grained sand, while the fifth succession consists of silt and fine-grained sand with sparse organic content. The shallowing-upwards successions are interpreted as parasequences (cf. Van Wagoner *et al.*, 1990), deposited during overall lake-level rise (Fig. 13A).

Saalian deposits

The basal part of the late Saalian Drenthe deposits comprise medium- to thick-bedded planar-parallel or cross-stratified gravel and pebbly sand, deposited by high-energy tractional meltwater flows (Fig. 5G). Massive, clast- or matrix-supported gravel is interpreted as deposit of non-cohesive respectively cohesive debris flows (Fig. 6H; Mulder & Alexander, 2001; Gani, 2004). Thin-bedded massive, planar-parallel or ripple-cross laminated silt and fine-grained sand commonly infill concave-up elements (up to 7 m wide, 1.5 m thick) and are interpreted as deposits from suspension settling or low-energy flows infilling shallow pools (Mulder & Alexander, 2001). The meltwater deposits are 2 to 5 m thick and commonly form southwest-dipping (5-25°) clinoforms in their lower part (Fig. 5 G). In the upper part the deposits are sheet-like with common 1-5 m wide and 1 m deep channels. The

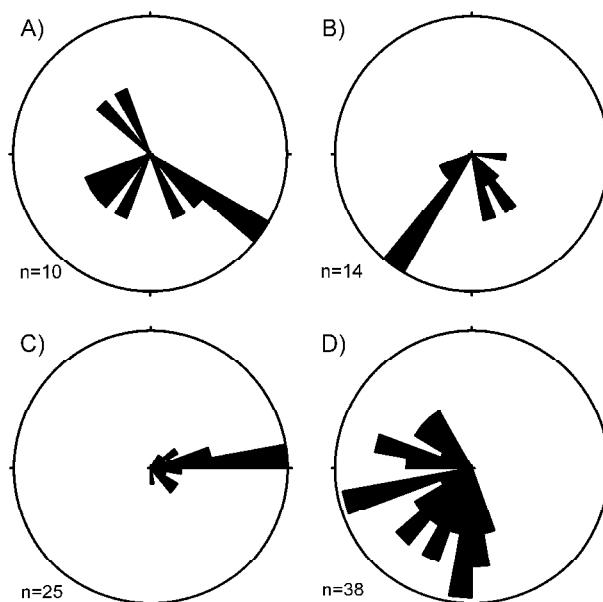


Fig. 7: Rose diagrams displaying measured palaeoflow directions. The petal length indicates the number of data points falling into the respective sector. **A)** Elsterian meltwater deposits (site 12-II). **B)** Elsterian glacial-lacustrine deposits (site 12-II). **C)** Holsteinian deposits (sites 12-II and 13-II). **D)** Saalian meltwater deposits (site 12-II).

palaeoflows were approximately from the northeast. The sedimentary facies and depositional architecture of the Saalian meltwater deposits point to a shallow-water glaciallacustrine delta (Postma, 1990).

The meltwater sediments are unconformably overlain by thick-bedded red-brown sand-rich diamicton, which displays intense simple shear deformation (Fig. 5I, J). The diamicton is interpreted as subglacial till, which is largely developed as a glacitectorite (Evans *et al.*, 2006). The Saalian Drenthe till is up to 2.5 m thick and sheet-like. Locally the till is overlain by up to 0.5 m thick red-brown massive clay-rich silt, which is interpreted as distal glaciallacustrine deposit of the glacial retreat. Ice-proximal deposits of the glacial retreat occur in the northern part of the study area and consist of planar-parallel and cross-stratified sand, pebbly sand and gravel (c.f. chapter 6). The Middle Pleistocene succession is draped by 2 to 5 m thick loess of probably Weichselian age (Urban *et al.*, 1991a; Wagner, 2011).

Soft-sediment deformation structures

The Middle Pleistocene succession is intensely deformed. The soft sediment deformation includes diapirs, flame structures, dish-structures, ball- and pillow-structures, load casts, normal faults, reverse faults, fault propagation folds, recumbent folds and boudinage. As already observed by Elsner (2003) the Saalian deposits are more intensely deformed than the Elsterian deposits. Diapirs are the largest structures in the exposed section (Figs. 4A and 5K) and are up to 8 m wide and 4 m high. Mud of the underlying interglacial deposits is intruded into coarse-grained Saalian meltwater deposits, which display deformation by bending, reverse faulting and brecciation (Figs 4A, B and 5K). The formation of diapirs is caused by density inversion, occurring when water-saturated mud is buried beneath coarser-grained denser sediment, leading to an upward displacement of the overburdened sediment (Mills, 1983; Aber & Ber, 2007). This process may be amplified by the additional load and increased pore pressure provided by an advancing glacier (McCarroll & Rijdsdijk, 2003; Aber & Ber, 2007). The sheared upper parts of the diapirs and the development of reverse faults are an indicator of ice-marginal contractional deformation by ice-thrusting (McCarroll & Rijdsdijk, 2003). Sheared tops of diapirs and reverse faults dip to the northeast and are southwest vergent (Fig. 4B), pointing to an ice advance from the northeast. The intrusion of diapirs also caused bending, normal faulting and crestal collapse above the diapir crests (Figs. 4B and 5K, L) as can be seen in experiments of Rodrigues *et al.* (2009). Dish-structures, flame structures, ball- and pillow-structures and load casts (Fig. 6A, C) are interpreted as dewatering structures, either caused by depositional loading (Lowe 1975) or glacial loading (McCarroll & Rijdsdijk, 2003). Ductile deformation includes recumbent folds, boudinage and deformed flame structures (Fig. 5J). These structures are indicative for subglacial deformation due to intense shearing (McCarroll & Rijdsdijk, 2003) and are characteristic of the Saalian glacitectorite.

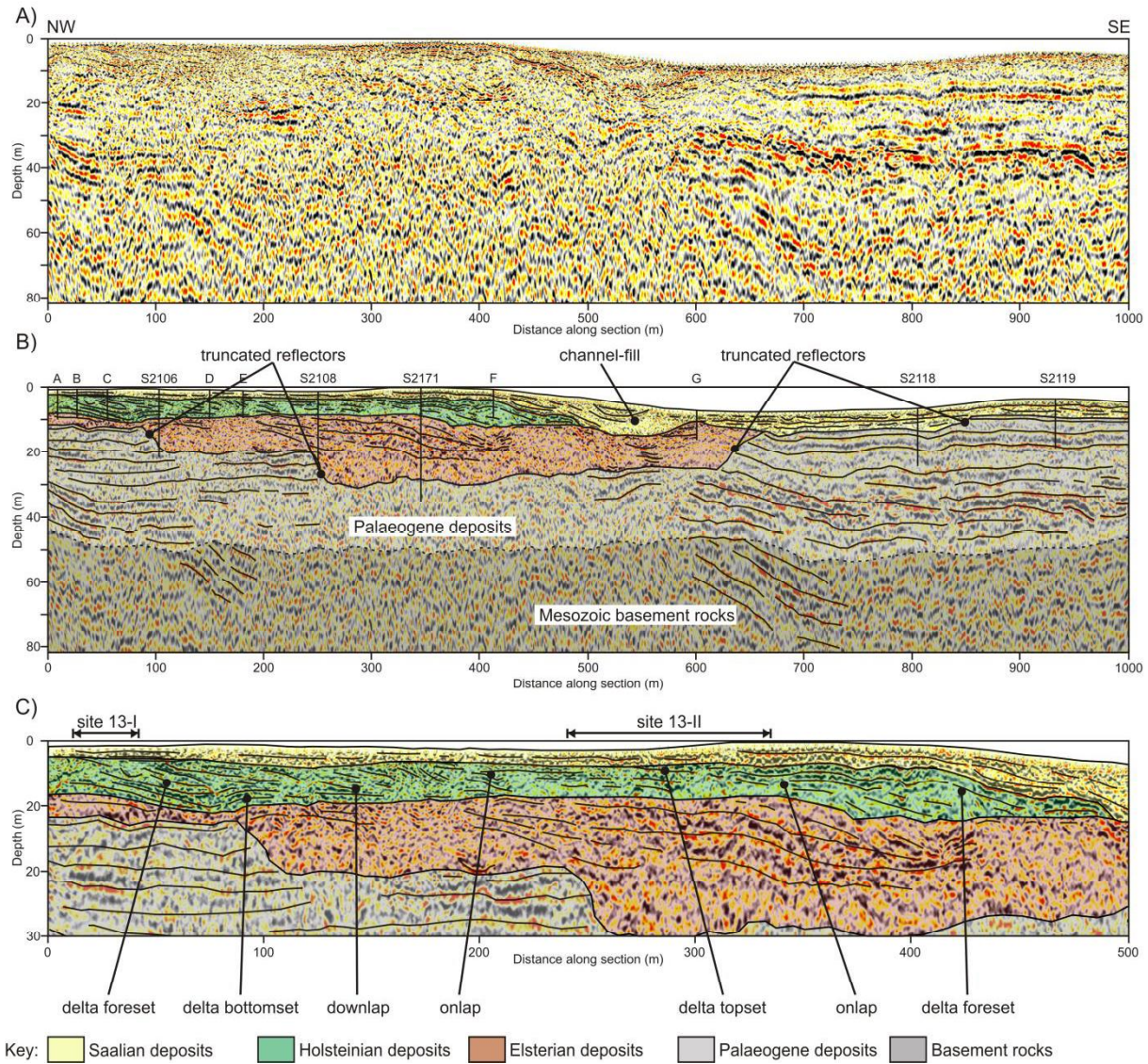


Fig. 8: **A)** Shear-wave seismic depth section (line S-1). **B)** Interpretation of the seismic section. The positions of boreholes and outcrops (A-G) used for the correlation are indicated at the top. **C)** Zoom-in of the northwestern part of the seismic section, which contains the Holsteinian interglacial deposits. For location see Fig. 1C.

Seismic interpretation

Two shear-wave seismic sections (line S-1 and S-2) have been acquired and interpreted to reconstruct the larger-scale stratigraphic architecture. A detailed interpretation of seismic line S-1 is shown in Fig. 8.

From the seismic line six individual seismic facies types were defined (SF-1 to SF-6, Fig. 9). Based on the scheme by Mitchum *et al.* (1977) each seismic facies is defined by external geometry, internal reflector configuration and seismic facies parameters. Seismic facies parameters include amplitude, continuity and density of reflections (Mitchum *et al.*, 1977). The interpretation of the seismic facies was supported by lithologic control provided by outcrops and boreholes.

Seismic facies

Seismic facies SF-1

Seismic facies SF-1 is characterised by parallel, continuous, high amplitude reflectors. Reflectors have a lateral extent of several tens of meters. The density of the reflectors is low; the spacing is 5 to 7 m. Reflectors are parallel and hummocky. Reflectors in SF-1 are gently ($5-10^\circ$) dipping to the southeast. SF-1 forms the lower half of the seismic line and is truncated at a depth of 40-50 m by a subhorizontal, hummocky surface.

Interpretation

Seismic facies SF-1 is interpreted as representing basement rocks. The lithology of the basement rocks is known from boreholes as comprising mostly mudstone. Triassic basement rocks, comprising claystone and limestone of the Upper Muschelkalk (Warburg Fm.) and Lower Keuper (Erfurt Fm.) are cropping out in an abandoned clay pit ~2 km from the seismic line (Duphorn *et al.*, 1974; FEMO, 2008). These basement rocks form part of the Elm anticline and dip $\sim 8^\circ$ to the southeast (FEMO, 2008).

Seismic facies SF-2

Seismic facies SF-2 is characterised by subhorizontal, sheet-like, continuous reflectors. Reflectors form thick (>10 m) packages of interbedded high and low amplitude reflections. Reflectors have a wide lateral extent of several hundred of meters. The density of the reflectors is low; the spacing is 3 to 5 m. Reflectors of SF-2 are truncated at the top.

Interpretation

Seismic facies SF-2 is interpreted as the Palaeogene infill of the rim syncline. Lithology and depth of Palaeogene deposits are known from outcrops and boreholes. The high amplitudes in SF-2 are probably caused by the high impedance contrast between clastic deposits and lignite. Thick packages of high and low amplitude reflectors therefore probably represent interbedded lignite seams and clastic beds. The Paleogene deposits in the Schöningen open-cast mine dip gently ($6-8^\circ$) to the northeast, which means that the seismic line was acquired approximately along strike direction, causing an apparently horizontal reflector pattern.

Seismic facies SF-3

Seismic facies SF-3 is characterised by low amplitude, non-continuous reflections, causing an almost transparent seismic image. Internally SF-3 is diffuse and highly chaotic without clear reflector pattern. In the lower part of SF-3, rare 10-15 m wide, concave-up, medium amplitude reflections occur. SF-3 contains several diffraction hyperbolas.

Interpretation

The almost transparent, chaotic seismic facies SF-3 is interpreted as consisting of gravel, pebbly sand or diamicton. Such coarse-grained deposits tend to scatter the seismic signal and thus produce an almost transparent seismic facies (Pugin *et al.*, 2004; Winsemann *et al.*, 2011a). Diffraction hyperbolas are caused by larger boulders (Pugin *et al.*, 2004). The correlation with borehole logs also indicates the presence of coarse-grained sand, gravel and diamicton. SF-3 is therefore interpreted as representing either coarse-grained meltwater deposits or subglacial till. Although diamicton appears homogenous in boreholes and outcrops, internal reflections may be caused by subtle lithological changes (e.g. sand-clay-ratio) or levels of differential compaction, which affect the propagation of seismic waves (Carr *et al.*, 1998; Fiore *et al.*, 2011). Concave-up reflections are interpreted as channel structures within the meltwater deposits, which have been observed in similar size in outcrop.

Seismic facies SF-4

Seismic facies SF-4 consists of low continuity, high amplitude reflectors. The density of the reflector is low; the spacing is 3 to 5 m. Reflectors are subparallel, hummocky and dip towards the southeast. The external geometry of SF-4 is lens-shaped (250 m wide, 20 m thick).

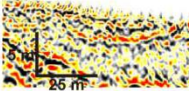
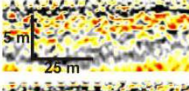
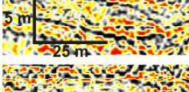
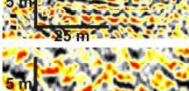
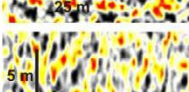
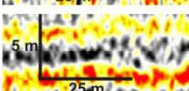
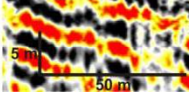

Seismic facies	Seismic facies parameters	Geometry	Interpretation	Sedimentary facies	Example
SF-6b	Medium to low amplitude, continuous to discontinuous reflectors	Concentric trough-fill	Meltwater deposits, channel-fill	Pebbly sand and gravel	
SF-6a	Medium amplitude, continuous to discontinuous reflectors	Parallel to subparallel	Meltwater deposits	Pebbly sand and gravel	
SF-5b	High to medium amplitude, continuous reflectors	Parallel, inclined	Delta foresets	Thin-bedded silt and fine-grained sand	
SF-5a	High to medium amplitude, continuous reflectors	Parallel, sheet-like	Delta topsets	Thin-bedded silt and fine-grained sand	
SF-4	High amplitude, low continuity reflectors	Oblique, hummocky	Fine-grained meltwater deposits	Thick-bedded sand	
SF-3	Transparent, low amplitude, discontinuous reflectors	Parallel, hummocky	Coarse-grained meltwater deposits and till	Pebbly sand, gravel and diamicton	
SF-2	Medium or high amplitude, continuous reflectors	Parallel	Palaeogene marginal marine deposits	Interbedded sand, silt, clay and lignite	
SF-1	High amplitude, continuous reflectors	Parallel, inclined	Mesozoic basement rocks	Mudstone and limestone	

Fig. 9: Description and interpretation of the seismic facies.

Interpretation

The low continuity and wide spacing of the reflectors in SF-4 indicate thick-bedded lithologies with relatively low impedance contrasts. Correlation with borehole logs points to thick-bedded fine- to medium-grained sand. SF-4 is interpreted as the seismic expression of the fine- to medium-grained sand, which forms the uppermost parts of the Elsterian meltwater deposits.

Seismic facies SF-5a and SF-5b

Seismic facies SF-5 is characterised by continuous, high to medium amplitude reflectors. The density of the reflectors is high; the spacing is ~1m. Reflectors of SF-5a are parallel and sheet-like and can laterally be traced for up to 70 m. SF-5b displays an oblique geometry, with clinofolds dipping gently (2-6°) to the southeast. Clinofolds can laterally be traced for up to 50 m. Internally, the seismic facies displays onlapping and toplapping contacts between sheet-like SF-5a reflectors and oblique SF-5b reflectors.

Interpretation

The internal geometry of SF-5 is indicative for deltaic deposition, in which sheet-like reflectors represent topsets and oblique reflectors represent foresets (Mitchum *et al.*, 1977; Wood, 1994). The progradational clinofolds of SF-5a are the most indicative features for deltaic deposition (Vail *et al.*, 1977; Wood, 1994). The apparent dip (2-6°) of the clinofolds corresponds to the typical dip of prodelta mud facies in modern lacustrine fine-grained deltaic systems (Wood, 1994). Internal onlapping contacts indicate repeated base level changes (Vail *et al.*, 1977). Correlation with borehole logs indicates that SF-5 consists of organic-rich silt and fine-grained sand.

Seismic facies SF-6a and SF-6b

Seismic facies SF-6 is characterised by continuous to slightly discontinuous, medium to high amplitude reflectors. The density of the reflectors is high; the spacing is 1 to 2 m. Internally SF-6a displays parallel, sheet-like reflector pattern. Reflectors of SF-6 locally appear slightly blurred. Locally, up to 5 m wide lens-shaped elements occur. SF-6b forms a concave-up, concentric trough, which is approximately 200 m wide and 12 m deep. Reflection amplitude in the basal part is lower than in the upper part of the trough-fill.

Interpretation

Medium to high amplitude reflectors points to a high impedance contrast between these different lithologies. SF-6 is probably the seismic expression of interbedded thin- to medium-bedded silt, sand, gravel and diamicton. The lower amplitude in parts of SF 6 and the blurred appearance of some reflectors points to the presence of coarser-grained deposits, scattering the seismic signal (Pugin *et al.*, 2004). Lens-shaped elements are interpreted as coarse-grained infill of small-scale channels, which

have been observed in outcrop in similar dimension. The concentric geometry of SF-6b points to deposition as infill of a larger-scale channel (Mitchum *et al.*, 1977).

Stacking pattern and seismic stratigraphy

The seismic facies were grouped into packages, which are referred to as seismic-stratigraphic units, in order to build a seismic-stratigraphic framework (Brown & Fisher, 1977). Seismic-stratigraphic units are enveloped by bounding reflectors or unconformities, which are defined by reflector terminations (Brown & Fisher, 1977). Within the seismic line four major bounding surfaces were identified, which separate five seismic-stratigraphic units.

Unit I forms the basal part of the seismic line and consists entirely of SF-1, which represents Mesozoic basement rocks. The southeast-ward dipping reflectors of Unit I are truncated and unconformably overlain by Unit II, which comprises the subhorizontal reflectors of SF-2 and is interpreted as the Palaeogene infill of the rim syncline. The top of Unit II is truncated by a high-relief unconformity, which is overlain by seismic-stratigraphic Units III, IV and V. These units are interpreted as representing the Pleistocene succession and were therefore analysed in more detail (Fig. 8B, C).

The base of Unit III forms a steep walled, flat based trough (Fig. 8B). The trough has a total width of 550 m and a depth of at least 20 m, with the deepest part in the southeast, which is up to 35 m deep and 400 m wide. The basal trough-fill consists of seismic facies SF-3, which displays a chaotic to transparent pattern. Seismic facies SF-4 overlies SF-3 within the deepest part of the trough over a lateral extent of ~220 m with a thickness of ~10 m. In the central part of the line, a second occurrence of SF-3 overlies SF-4. Both seismic facies (SF-3 and SF-4) in Unit III have low continuity reflectors; therefore the bounding surfaces between seismic facies in Unit III are poorly defined. From outcrop and borehole correlation Unit III is interpreted as representing Elsterian meltwater deposits and subglacial till.

Unit IV consists of the more continuous reflectors of SF-5 and displays a notable transition from lower amplitude seismic facies to higher amplitude facies. Oblique reflectors of SF-5b downlap onto the basal boundary of Unit IV (Fig. 8C). In the northwestern part of the seismic line the oblique, up to 6° southeast dipping reflectors of SF-5b dominate the seismic image of Unit IV, while towards the centre of the line the sheet-like reflectors of SF-5a become more common. Within Unit IV onlap and top lap between the clinofolds of SF-5a and the sheet-like reflectors of SF-5b can be observed, which define three unconformities within Unit IV. Based on these unconformities, Unit IV can be subdivided into the subunits IVa, IVb IVc and IVd. From outcrop and borehole correlation Unit IV is interpreted as representing Middle Pleistocene interglacial deposits.

Unit V forms the uppermost part of the seismic line and comprises seismic facies SF-6. In the northwestern part of the line, sheet-like reflectors of SF-6a top lap and probably truncate the underlying reflectors of Unit IV. The central part of the line is characterised by a 200 m wide, up to 12 m deep trough (Fig. 8B). The trough has an asymmetrical shape, with the deepest part and a steep flank to the

southeast and a gentler flank at the northwest. Reflectors of the underlying Units III and IV are truncated by the base of this trough. The infill of the trough comprises concentric reflectors of seismic facies SF-6b, in the uppermost part of the trough reflectors onlap the margin of the trough. The southeastern part of the line consists of sheet-like reflectors of SF-6a, which conformably overlie reflectors of Unit II (Fig. 8B). From outcrop and borehole correlation Unit V is interpreted as representing Saalian meltwater deposits.

3D subsurface model

Distribution and thickness of depositional units

From the 3D subsurface model depth maps, thickness maps and 2D cross-sections were extracted to illustrate the large-scale depositional architecture of the studied succession.

Base of the Pleistocene (Fig. 10A)

The base of the Pleistocene succession is defined by an unconformity, separating the Pleistocene deposits from the underlying Palaeogene deposits or Mesozoic basement rocks. The base of the Pleistocene has an elevation between 68 and 157 m a.s.l. The highest elevations are located in the north and the west of the modelled area. In the southern portion of the modelled area the base of the Pleistocene displays a trough-shaped, 3.5 km long depression. The width of the trough typically is 300-400 m, but may range between 250 and 850 m. The bottom of the trough has an elevation between 68 and 100 m a.s.l. and is thus up to 40 m deeper than the surrounding area. The deepest parts of the trough are separated by up to 15 m high sills. The trough trends NNW-SSE in the northern part, then bends towards the SSW and leaves the modelled area on the southwestern margin. At the southeastern margin of the modelled area probably parts of a second trough are cut by the model.

Elsterian meltwater deposits (Fig. 10B)

The Elsterian meltwater deposits comprise light gray or brown gravel, pebbly sand or sand, which contains abundant lignite fragments. The Elsterian meltwater deposits are restricted to the trough formed by the base of the Pleistocene, usually at an elevation below 100 m a.s.l. High thickness of Elsterian meltwater deposits correspond to the deepest parts of the trough. The maximum thickness is 24 m.

Elsterian till (Fig. 10C)

The Elsterian till comprises dark gray diamicton, commonly containing pebbles and cobbles. The Elsterian till is restricted to the trough formed by the base of the Pleistocene, usually at an elevation below 100-110 m a.s.l. The maximum thickness of the Elsterian till is 15 m.

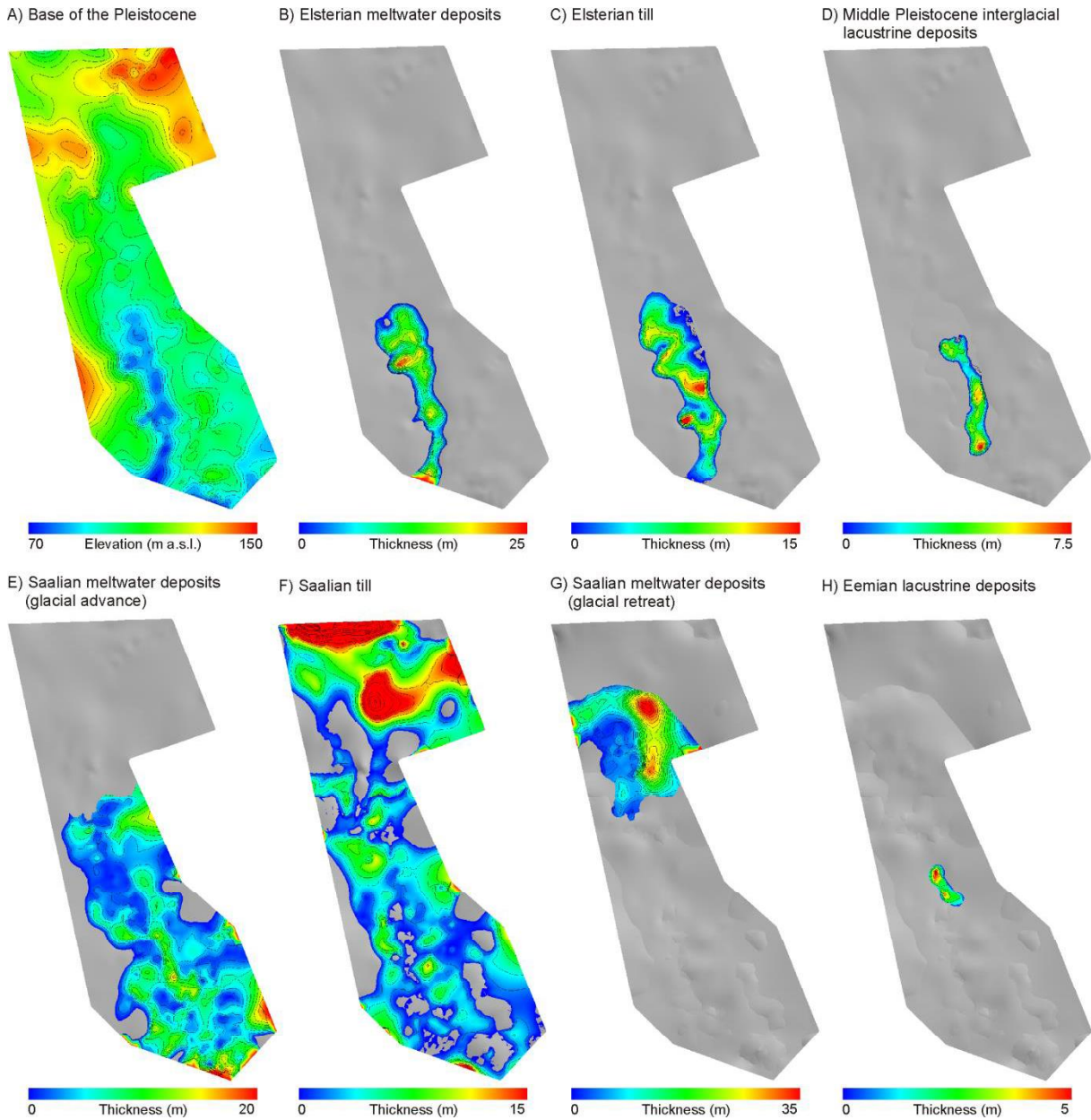


Fig. 10: Depth and thickness maps derived from 3D subsurface modelling (GOCAD). **A)** Geometry of the base of the Pleistocene (5 m contours). **B)** Distribution and thickness of the Elsterian meltwater deposits (2 m contours). **C)** Distribution and thickness of the Elsterian till (2 m contours) **D)** Distribution and thickness of the Holsteinian deposits (1 m contours). **E)** Distribution and thickness of the Saalian meltwater deposits of the glacial advance (2 m contours). **F)** Distribution and thickness of Saalian till (2 m contours). **G)** Distribution and thickness of the Saalian meltwater deposits of the glacial retreat (2 m contours). **H)** Distribution and thickness of the Eemian deposits (1 m contours).

Middle Pleistocene interglacial deposits (Fig. 10D)

The interglacial deposits comprise black or brown fine-grained sand, silt and peat, commonly containing plant debris and shell fragments. Middle Pleistocene interglacial deposits overlie the Elsterian deposits and infill the lowest elevations on top of the Elsterian deposits. The Middle Pleistocene interglacial deposits form an elongate NNW-SSE trending body, which is 2500 m long, 200-400 m wide and covers an area of ~ 1 km². The maximum thickness is 7.5 m.

Saalian meltwater deposits of the glacial advance (Fig. 10E)

The meltwater deposits comprise yellow, orange or red gravel, pebbly sand or sand. Thin beds of silt may be intercalated. The meltwater deposits cover the southern part of the modelled area. The thickness is relatively consistent between 2 and 5 m. Two elongate, NNW-SSE trending thickness maxima (up to 18 m) are observed in the central southern area.

Saalian till (Fig. 10F)

The Saalian till comprises yellow, orange or red, sand-rich diamicton. The Saalian till occurs in the complete modelled area. The maximum thickness of the Saalian till is 25 m in northwest-southeast trending ridges in the northern part of the modelled area. In the southern part of the modelled area the till has a patchy appearance with thicknesses typically ranging 1-3 m with local maxima of up to 8 m.

Saalian meltwater deposits of the glacial retreat (Fig. 10G)

The meltwater deposits comprise yellow or orange pebbly sand or sand. The meltwater deposits of the glacial retreat occur only in the northern part of the modelled area, where they form a ~2 km long, north-south trending, up to 35 m thick sedimentary body. This body has a very steep margin towards the north and thins rapidly towards the south.

Eemian deposits (Fig. 10H)

The Eemian deposits comprise black or brown silt or peat, commonly containing plant debris and shell fragments. Eemian deposits form an elongate, NNW-SSE trending body, which is 1000 m long, 300 m wide and covers an area of ~0.3 km². The maximum thickness is 5 m.

Extracted 2D sections

Two 2D cross-sections have been extracted from the subsurface model (Fig. 11A, B). Cross-section CS-1 runs parallel to the basin axis and cross-section CS-2 perpendicular to the basin axis. Both cross-sections show the deep incision of the base of the Pleistocene into the underlying tilted Palaeogene strata. In cross-section CS-1 the undulating bottom profile of the Pleistocene succession becomes obvious (Fig. 11A). Cross-section CS-2 demonstrates the occurrence of the Pleistocene incision at the boundary between Mesozoic bedrock and unconsolidated Palaeogene deposits (Fig. 11B). Both cross-sections indicate the restriction of Elsterian and Middle Pleistocene interglacial deposits to the deep erosional trough. Due to the curved shape of the Pleistocene depocentre the Middle Pleistocene interglacial deposits are cut twice by line CS-1 (Fig. 11A). The upper part of the sedimentary succession consists of Saalian meltwater deposits and till. In the northern part of cross-section CS-1 the Saalian till reaches the maximum thickness and is unconformably overlain by Saalian meltwater deposits of the glacial retreat.

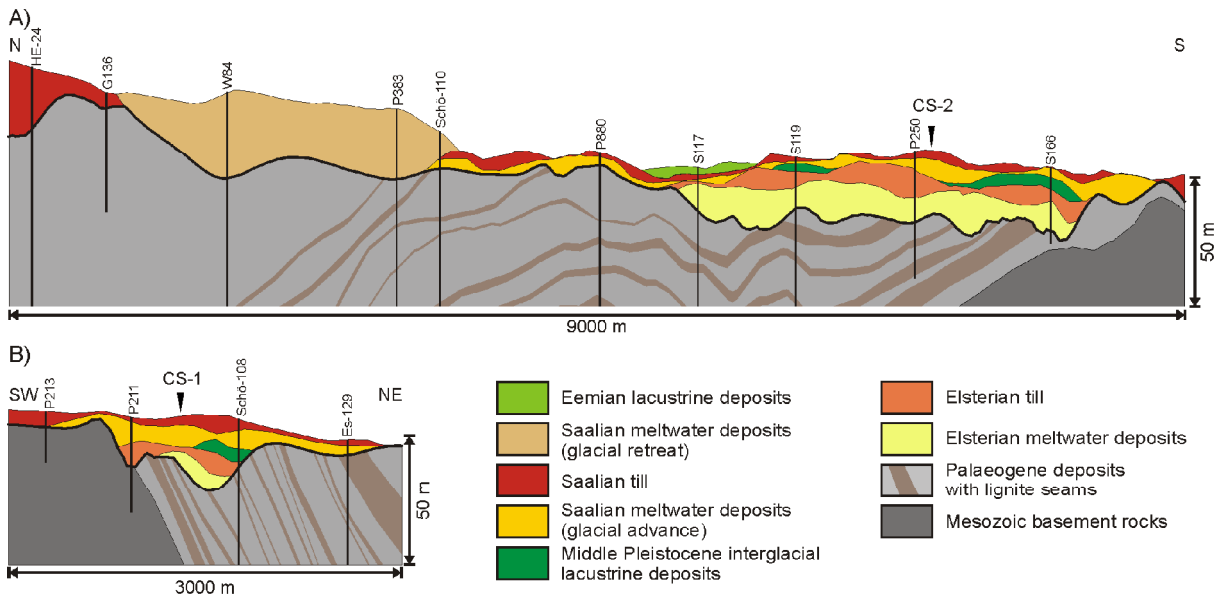


Fig. 11: Extracted 2D cross-sections of the 3D subsurface model (for location see Fig. 1C). **A)** Cross-section CS-1, aligned parallel to the basin axis. **B)** Cross-section CS-2, aligned perpendicular to the basin axis. The cross-section approximately runs along the former divide between the northern and southern fields of the open-cast mine (The positions of boreholes along the lines are indicated).

Depositional model

The Middle Pleistocene succession of Schöningen is interpreted as infill of a 300-400 m wide and up to 40 m deep subglacial tunnel valley that was incised during the Elsterian glaciation (Fig. 12A; s. chapter 8.1). Evidence is given by the erosive base of the Pleistocene succession deeply incising into tilted Palaeogene sediments and Mesozoic basement rocks (Figs. 8B, 10A and 11B). The Elsterian deposits consist of meltwater deposits, subglacial till and glacial lacustrine deposits, which are restricted to the tunnel valley (Fig. 10B, C). The position of the Elsterian meltwater deposits within the tunnel valley indicates deposition by high-energy subglacial meltwater flow. The relatively fine-grained meltwater deposits indicate that deposition probably occurred as backfill coevally with the incision of the tunnel valley during phases of decreased discharge (Piotrowski *et al.*, 1999; Praeg, 2003; Russell *et al.*, 2003). The till was deposited into the tunnel valley by squeezing, lateral flow and melt-out during an advanced stage of ice decay (Piotrowski *et al.*, 1999; Jørgensen & Sandersen, 2006). Elongated, lens-shaped sand or silt intraclasts within the till (Fig. 5B) are interpreted as indicating lateral flow of till into the subglacial depression. At one location, a 25 m wide, 6 m deep very steep-walled incision into the top of the Elsterian till could be observed in outcrop (Fig. 5D), which was filled mostly by medium-bedded planar-parallel stratified pebbly sand. This incision is interpreted as a small-scale subglacial channel, which was probably incised during a local, small-scale re-advance of the ice sheet (Piotrowski *et al.*, 1999; Jørgensen & Sandersen, 2006). Urban *et al.* (1988) and Elsner (2003) reported the presence of a second, older Elsterian till, which is locally occurring, embedded between meltwater deposits. The presence of the older till might indicate incision during oscillations of the ice

front (Elsner, 2003), but might also represent lateral influx of till during reduced meltwater discharge (Piotrowski *et al.*, 1999). The uppermost Elsterian deposits, overlying the till, are interpreted as distal deposits of a glaciallacustrine delta or subaqueous fan (c.f. Postma, 1990; Eyles & Eyles, 1992; Lønne, 1995), deposited in the tunnel valley during the glacial retreat (Lang & Winsemann, 2012).

After deglaciation the tunnel valley remained underfilled and provided accommodation space for interglacial deposition (Figs. 10D and 12B). Organic-rich silt, fine-grained sand and peat, which unconformably overlie the glaciallacustrine deposits, were deposited within an interglacial lake. The maximum extent of the interglacial lake can be estimated from the subsurface model, where the interglacial deposits are 2500 m long, 200-400 m wide and cover an area of ~1 km² (Fig. 10D). The depth of the lake can be estimated from the height of the delta foresets, which has to be corrected for compaction (Wood, 1994). Based on a compaction of 20-30 % in silt and peat successions (Wood, 1994; Van Asselen, 2010), a maximum palaeo-depth of the lake of 6 to 7.5 m can be estimated, corresponding to an elevation of the water table of ~106 m a.s.l. for the interglacial lake-level maximum.

Both outcrop and seismic data sets display the asymmetrical fill of the interglacial Holsteinian lake basin. In outcrop (12-II and 13-II) the lacustrine delta deposits form prograding clinoforms, gently dipping to the northeast and southeast (Figs. 4B, 6G and 8C; s. chapter 8.2). Seismic-stratigraphic Unit IV, which corresponds to the interglacial succession, is interpreted as the seismic image of the fine-grained delta system, getting younger towards the southeast (Fig. 8C). Three unconformities can be identified in the interglacial deposits, interpreted to have been formed during major lake-level falls (Fig. 13A). The oldest part of the interglacial deposits (IV a) comprises delta foresets and bottomsets, which display an aggradational stacking pattern and is therefore interpreted to represent deposits of the lake-level highstand (Catuneanu, 2006). Subunit IV b mainly consists of prograding foresets, which downlap onto the underlying unconformity. This delta progradation is interpreted to represent a normal regression, which was probably triggered by increased sediment supply (Zecchin, 2007). This unit is bounded by an unconformity and overlapped by subunit IV c, indicating a lake-level fall in the range of 4-6 m, followed by an overall lake-level rise of the same range. The magnitude in lake-level change was estimated from the elevation difference between the lowest and the highest reflectors. Subunit IV c again is bounded by an unconformity and overlapped by subunit IVd with a retrogradationally stacking pattern, indicating a lake-level fall followed by overall lake-level rise (Catuneanu, 2006). The reflectors of subunit IV c are correlated with parasequences PS-1 to PS-4 of the interglacial deposits at site 13-II (Fig. 13A). In outcrop, the basal boundary of subunit IV c is characterised by thick roots (Fig. 6F), indicating the growth of terrestrial plants (probably small trees) on the delta plain during subaerial exposure. The exposed interglacial deposits comprise five parasequences. Each parasequence begins with an erosional transgressive surface, where the peat of the underlying parasequence was partly eroded during lake-level rise (Figs. 6A). The basal part of each parasequence comprises silt or fine-grained sand, which were deposited in a prodelta or delta front setting by low-energy turbulent flows and suspension fall-out (Fig. 6A, B and E; Rajchl *et al.*, 2008). Upwards, the succession passes into

more organic-rich silt, deposited on the delta plain (Treese & Wilkinson, 1982; Rajchl *et al.*, 2008). Small (0.5-1 m wide, 0.1-0.2 m deep), sand-filled channels within organic-rich silt (Fig. 6C) are interpreted as distributary channels of the delta plain (Treese & Wilkinson, 1982; Rajchl *et al.*, 2008). The top of each parasequence consists of peat or peaty silt, comprising plant debris accumulated in the swampy environment of the delta plain (Treese & Wilkinson, 1982; Rajchl *et al.*, 2008). In parasequence PS-5 the peat layer is only a few centimetres thick. The deposits of PS-5 are distinct from the underlying parasequences by a considerably lower content of organic debris and are interpreted as correlating with the basal reflector of subunit IV d.

Peat accumulation is controlled by the height of the groundwater table, which is usually directly connected to lake-level changes (Bannerjee *et al.*, 1996; Holz *et al.*, 2002). During the onset of a transgression the increasing accommodation rate allows for the accumulation of thick and laterally extensive peat (Holz *et al.*, 2002). Continued lake-level rise leads to a rapid drowning of the delta plain and enables the preservation of the peat (Holz *et al.*, 2002). Through-out the individual parasequences the assemblages of aquatic and terrestrial plants indicate a shallowing-upwards trend by increasing proportions of terrestrial plants (Urban, 2007; Urban *et al.*, 2011). A substantial amount of palaeoecological data has been collected at Schöningen, especially at site 13-II, but yet no comprehensive model for the complete succession exists. Generally, the number of species in floral and faunal associations decreases upwards through-out parasequence PS-1 to PS-5, indicating climate deterioration (Jechorek, 2000; Mania, 2007; Urban, 2007). The climatic optimum of the Middle Pleistocene interglacial occurred during the deposition of parasequence PS-1 (“level-1”, c.f. Jechorek, 2000; Urban, 2007). The lake-marginal assemblage of large plant remains for PS-1 indicates azonal vegetation dominated by *Alnus glutinosa* sp., reed beds and thermophilous subaqueous plants (Jechorek, 2000). Subaqueous plants were adapted to standing water and high-frequency lake-level changes (Jechorek, 2000). According to Böhme (2000) the faunal assemblages of fishes partly resemble those of hydrologically open modern lakes. The lowermost parasequence PS-1 only contains a low diversity fish fauna (Böhme, 2007) corresponding to the reconstructed low lake-level (Fig. 13A). The ecological optimum of the lake was attained during the deposition of PS-2 with the highest diversity of fish, reptile and amphibian species, abundant vegetation and increasing eutrophy (Böhme, 2000, 2007), corresponding to the observed lake transgression (Fig. 13 A). The presence of halophytic plants within PS-1 and PS-2 indicates slightly saline conditions (Urban *et al.*, 2011). The salt was probably derived from Mesozoic salt-bearing deposits occurring in the shallow subsurface (Behrend, 1927). During the subsequent lake level rise and highstand (parasequences PS-3 to PS-4; Fig. 13 A) the diversity of faunal and floral assemblages decreased, which is attributed to a climatic deterioration (Böhme, 2007; Mania 2007; Urban 2007).

During the Saalian glaciation the older deposits became partly eroded and intensely deformed by glacitectonics (Fig. 4A). The Saalian meltwater deposits are interpreted as proglacial deposit, infilling the remnants of the interglacial lake basin (Fig. 12C, Lang & Winsemann, 2012). A delta prograded

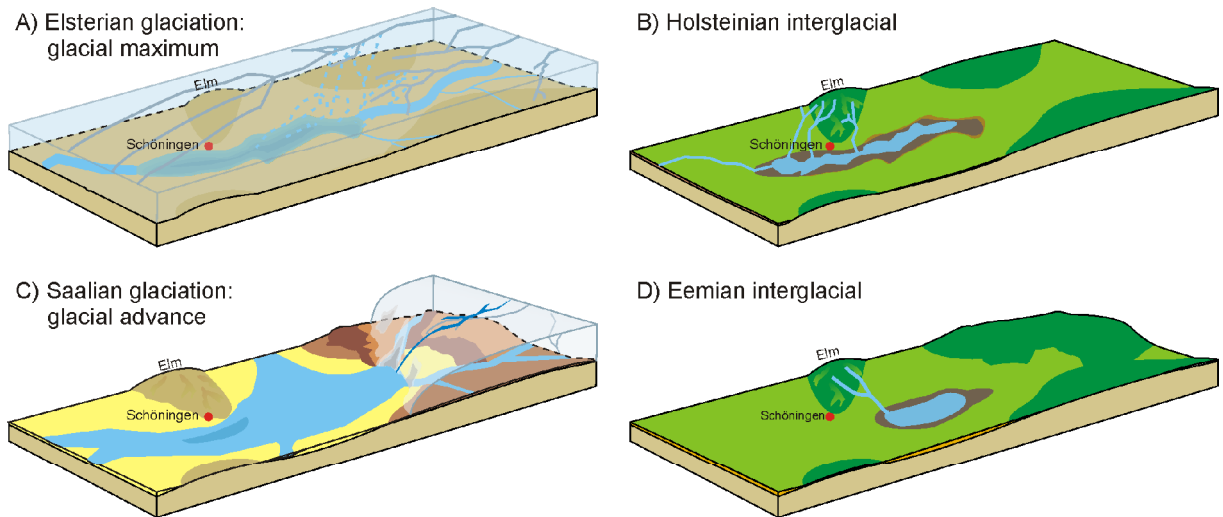


Fig. 12: Palaeogeographic reconstruction of the Schöningen area (figures are not to scale). **A)** Formation of a tunnel valley during the Elsterian glaciation. **B)** Formation of a lake in the remnant tunnel valley during the Holsteinian interglacial. **C)** Formation of a shallow glacialacustrine lake during the Saalian Drenthe ice advance. **D)** Formation of a lake during the Eemian interglacial.

into the shallow lake and was subsequently overlain by laterally more extensive glacial deposits (Zielinski & Van Loon, 2003; Salamon, 2009). From the seismic section, a ~200 m wide, 12 m deep trough can be observed, which is concentrically infilled with meltwater deposits (Fig. 8B). This structure is interpreted as a proglacial infill of the very last remnant of the Elsterian tunnel valley, which probably represents the last phase of reactivation. The Saalian subglacial till is sand-rich and consists in large parts of a glactectonite, derived from the underlying Saalian meltwater deposits. The deformation structures indicate a glacial advance from the northeast. The differential deformation of the Saalian and the Elsterian glacial successions is probably related to differences in palaeotopography, hydrology and the substratum of the glacier. The preserved Elsterian deposits are located deep within the tunnel valley and were thus relatively sheltered from glactectonic deformation, while the area-wide occurring Saalian deposits were more exposed to deformation. Additionally, the more sand-prone Saalian till may also have promoted the drainage of basal meltwater and thus increased ice-bed coupling, allowing for more intense glactectonic deformation (Passchier *et al.*, 2010).

Meltwater deposits of the Saalian glacial retreat are represented by a ~35 m thick, elongate sediment body in the north of the modelled area (Figs. 10G and 11A). These deposits are interpreted as a subaqueous fan. The eroded till below the subaqueous fan deposits (Fig. 11A) points to high-energy jet-flows (Winsemann *et al.*, 2009).

Eemian deposits were not observed during the fieldwork conducted for this study. However, up to 7 m thick Eemian lacustrine deposits have been documented in the former northern field of the open-cast mine (Urban *et al.*, 1988, 1991a, b). The subsurface model indicates the occurrence of Eemian deposits in a shallow, elongated basin (Figs. 10H, 11A and 12D), which is incised into Saalian till. The formation of this basin is attributed to proglacial meltwater erosion during deglaciation.

Discussion

Formation of an Elsterian tunnel valley

The integration of all available data sets indicates that an Elsterian tunnel valley provided the accommodation space for the Middle Pleistocene succession. Our subsurface model shows that the base of the Pleistocene is characterised by a steep-walled, NNW-SSE-trending trough (Fig. 10A). This ~40 m deep trough begins abruptly and displays undulating bottom topography, where up to 15 m high sills separate the deeper parts. In outcrop the base of the Pleistocene is characterised by a steep-walled incision into the underlying deposits. The morphological features of the trough are all indicative for subglacial tunnel valleys, which are typical features of the Elsterian glaciation in northern central Europe (e.g. Eissmann, 1967; Kuster & Meyer, 1979; Ehlers *et al.*, 1984; Huuse & Lykke-Andersen, 2000; Kluiving *et al.*, 2003; Jørgensen & Sandersen, 2006; Stackebrandt, 2009). In the seismic section the steep walls of the trough truncate the basement reflectors, while the bottom of the trough in the seismic section is relatively flat (Fig. 8B), which is typical for subglacial tunnel valleys (Huuse & Lykke-Andersen, 2000; Kluiving *et al.*, 2003; Praeg, 2003; Jørgensen & Sandersen, 2006).

Tunnel valleys form anastomosing subglacial drainage networks, which are incised by subglacial meltwater drainage under high hydrostatic pressure (Ó Cofaigh, 1996; Huuse & Lykke-Andersen, 2000; Stackebrandt, 2009). Repeated, catastrophic discharge events, which are triggered by the tapping of en- or subglacial meltwater reservoirs, significantly enhance the incision of tunnel valleys (Russell *et al.*, 2003; Jørgensen & Sandersen, 2006; Hooke & Jennings, 2006). The incision of tunnel valleys generally occurs close to the ice margin (10's of km) when the glacier is already in a recessional state (Huuse & Lykke-Andersen, 2000; Praeg, 2003).

The dimensions and the infill of the tunnel valley correspond well to those of other tunnel valley systems known from the Pleistocene of northern central Europe (Eissmann, 1967; 2002; Piotrowski *et al.*, 1999; Stackebrandt, 2009) and North America (Hooke & Jennings, 2006) as well as from the Late Ordovician glaciation of North Africa (Le Heron *et al.*, 2004). However, the tunnel valley at Schöningen does not reach the extreme depths of the tunnel valleys known from beneath northern Germany (Ehlers *et al.*, 1984; Ehlers & Linke, 1989; Schwab & Ludwig, 1996) and the North Sea (Wingfield, 1990; Huuse & Lykke-Andersen, 2000; Lutz *et al.*, 2009). These extremely deep tunnel valleys are all located within the Central European Subsidence Zone, where thick, unconsolidated and thus easily erodible Palaeogene and Neogene deposits subcrop the Pleistocene deposits (Stackebrandt, 2009). The rim-synclines of the Helmstedt-Staßfurt-saltwall probably provided a preferential path for the ice and meltwater flow, a phenomenon that has been documented from similar settings (Ehlers *et al.*, 1984; Piotrowski, 1994). The unconsolidated Palaeogene deposits in the rim-syncline provided an easily erodible substratum for tunnel valley incision (Huuse & Lykke-Andersen, 2000; Hooke & Jennings, 2006; Stackebrandt, 2009). The higher permeability of the unconsolidated Palaeogene deposits compared to the Mesozoic basement rocks probably contributed to the preferential pathways of meltwater flow and thus the location of the incision (Hooke & Jennings, 2006). Pressurised groundwater from

the permeable Palaeogene deposits was drawn into the subglacial meltwater channel, promoting liquefaction of the sediment and thus further enhancing the erosion (Boulton *et al.*, 2007). Similar deep incisions into the Palaeogene deposits have been reported from the same rim-syncline ~35 km to the southeast (Ziegenhardt & Kramer, 1968).

Underfilled tunnel valleys, providing accommodation space for post-glacial deposition are a well-documented phenomenon from other tunnel valley systems. Late Elsterian glacial-lacustrine deposits as the Lauenburg Clay Formation and Holsteinian interglacial lacustrine or marine successions, which are infilling underfilled tunnel valleys, are for example known from northern Germany (Kuster & Meyer, 1979; Ehlers & Linke, 1989; Piotrowski, 1994), eastern Germany (Eissmann, 2002), Denmark (Jørgensen & Sandersen, 2006), the Netherlands (Kluiving *et al.*, 2003) and England (Turner, 1970).

Middle Pleistocene interglacial environments

Our study clearly indicates the existence of a long-lived interglacial lake, which formed in the under-filled depression of an Elsterian tunnel valley. The lake was laterally infilled by fine-grained delta systems shed from the Elm ridge in the west. Mania (1995, 1998, 2006) interpreted the interglacial deposits as infill of abandoned fluvial channels, which were extended to lake basins by salt solution in the subsurface. However, the sedimentary facies, depositional architecture and the extent of the interglacial deposits clearly indicate deposition within an elongated lake basin, which formed in the remnant Elsterian tunnel valley. Furthermore, the catchment areas and resulting discharge of all adjacent streams are far too small to cause major fluvial incision. The unconformities, reconstructed from 3D subsurface modeling and shear-wave seismic sections, may resemble fluvial erosional surfaces if poorly exposed and thus may have led to a mis-interpretation as fluvial channels. This effect can be well observed in cross-sections CS-1 and CS-2 (Fig. 11).

The period between the Elsterian and Saalian glaciations is characterised by several climatic oscillations, of which the Holsteinian interglacial represents the climatic optimum (Litt *et al.*, 2007; Ehlers *et al.*, 2011). New numerical U/Th data from site 13-II, level 2, (Urban *et al.*, 2011; Sierralta *et al.*, 2012) range from 343 to 280 ka, thus indicating that the Middle Pleistocene interglacial deposits of Schöningen can be correlated with the Holsteinian interglacial and MIS 9. The palynologically defined “Reinsdorf” interglacial (Urban, 1995) must therefore be regarded as part of the Holsteinian interglacial, as proposed earlier by Litt *et al.* (2007, 2008).

Our reconstructed lake-level curve also bears evidence of climatic oscillations during the Holsteinian (MIS 9) interglacial (Fig. 13A). Lake-level changes are discernible at two orders of magnitude. Higher-magnitude (4-6 m) low-frequency lake-level falls led to the formation of major unconformities within the interglacial deltaic complex (Figs. 8C and 13A). These high-magnitude lake-level changes are interpreted as representing major climatic shifts corresponding to Holsteinian intra-interglacial cooling events (supported by palaeoecological data e.g. Kühl & Litt, 2007; Litt *et al.*, 2007; Koutsodendris *et al.*, 2010; Szymarek, 2011) and sea-level changes (Roe & Preece, 2011). The parasequences

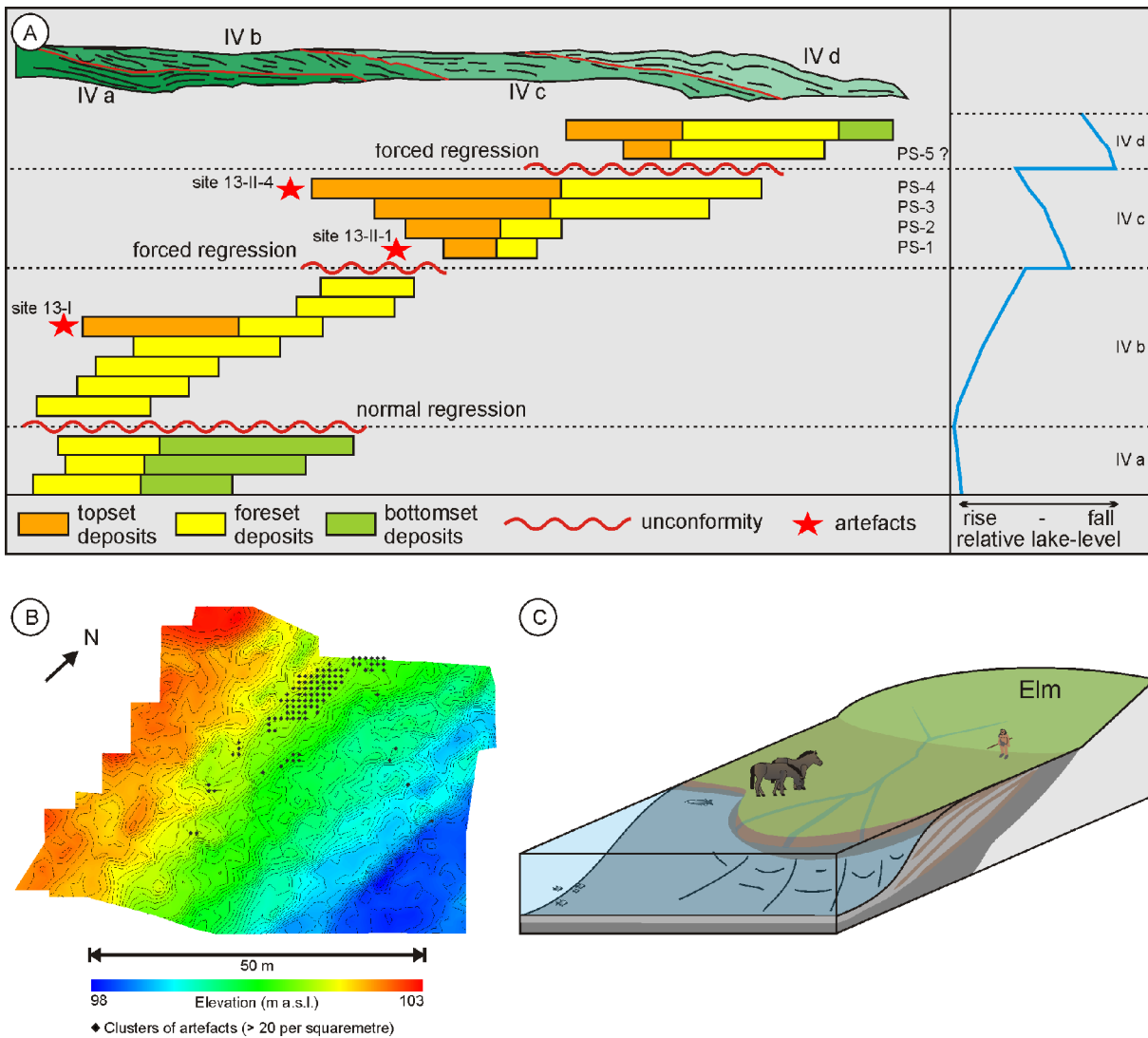


Fig. 13: **A)** Reconstructed lake-level curve for the Holsteinian interglacial succession, based on delta foreset-topset-transitions. The occurrence of the main archaeological findings is indicated by red stars. **B)** Reconstruction of the top of parasequence 4 at site 13-II and the distribution of artefacts, indicating embedding of artefacts parallel to the former shoreline. **C)** Schematic reconstruction of the depositional environment during the Holsteinian interglacial, when early human inhabitants occupied the delta plain and left some of their spears (figure is not to scale).

are interpreted to represent lower-magnitude (1-3 m), high-frequency lake-level changes. Based on palynological interpretation, Urban (2007) related the formation of these shallowing-upward successions (“levels 1 to 5”) to changing climatic conditions. Parasequences PS-1 to PS-5 are characterised by a “Reinsdorf” pollen successions (Urban, 1995, 2007) and may therefore represent the uppermost Holsteinian deposits (Urban *et al.*, 2011). The lowest parasequence (PS-1) represents the phase of the climatic optimum, characterized by relatively dry conditions (Urban 2007), which correlates with the reconstructed lake level lowstand (Fig. 13 A). During the subsequent climate deterioration the interglacial climate oscillated from interstadial to stadial climatic conditions (Urban, 2007). The increasing abundance of wetland and aquatic plants (Urban *et al.*, 2011) in the upper parasequences PS-3 and PS-4 is in accordance with the reconstructed overall lake transgression (Fig. 13A). We suggest that variations in precipitation and surface run-off led to lake-level fluctuations, which controlled the deposition

and stacking pattern of the interglacial succession. Palaeoecological data indicate an at least temporary open hydrological system (Böhme, 2000; Mania, 2007; Urban, 2007). An outlet towards the south probably formed during periods of high lake-levels (above ~103 m a.s.l.) and became closed during lake-level lowstands.

Probably younger middle Pleistocene interglacial deposits have been observed in the northern field of the open-cast mine and were tentatively attributed to MIS 7, based on palynological data (Urban *et al.*, 1991b; Urban, 1995, 2007). However, no absolute age determinations are available and deposits have been completely excavated. Our subsurface model includes possible MIS 7 deposits as a part of the Middle Pleistocene interglacial deposits. The geometry of these sediments (Urban *et al.*, 1991b) also indicates lacustrine deltaic systems, probably deposited farther basinwards. With the final termination of the interglacial the deposition of organic-rich deposits ceased and glacialacustrine sediments of the Saalian glaciation were deposited, which infilled the very last remnant of the tunnel valley.

Implications for archaeology

The long-lived lake attracted animals as well as early human hunters (Fig. 13C). The distribution of artefacts in delta plain deposits at sites 13-I, 13-II and 12-II provides snap-shots of the human presence (Fig. 13A, B). Between sites 12-II and 13-II several other findings have been made (Serangeli & Böhner, 2012). Numerous artefacts were found in different stratigraphic levels throughout the interglacial deposits, indicating the recurring presence of early human inhabitants (Thieme, 1997, 1999). The artefacts at site 13-II are aligned parallel to the former lake margin, where humans occupied a narrow strip on the shoreline, and were preserved due to a subsequent, transgression, leading to a rapid drowning of the delta plain (Fig. 13 B). The correlation between the palaeo-topography, thickness of the organic-rich deposits and clusters of artefacts is conspicuous. However, the archaeological record is in situ, as the complete preservation of the spears indicates. The excavation site 13-II was only affected by very small-scale glacitectonic deformation; in contrast, site 12-II was intensely deformed.

Based on our sequence stratigraphic analysis it is most likely that (i) site 13-I comprises the oldest archaeological findings and (ii) findings of sites 12-II and 13-II are contemporaneous in time. This is also indicated by the pollen record (Urban *et al.*, 2011) and was previously assumed by Thieme (2007).

Conclusions

- The Middle Pleistocene succession of Schöningen was deposited within an Elsterian tunnel valley. This tunnel valley is up to 850 m wide and 40 m deep. It was incised into the unconsolidated Palaeogene deposits of the Helmstedt-Staßfurt rim syncline, providing the accommodation space for subsequent glacial and interglacial deposition.

- The Holsteinian interglacial deposits (MIS 9) of Schöningen have been deposited in an elongated lake, which formed in the remnant Elsterian tunnel valley. The interglacial deposition was affected by repeated climatically controlled lake-level fluctuations in the range of 4-6 m, leading to the formation of laterally stacked delta systems, fed by small streams from the Elm ridge.
- The long-lived interglacial lake attracted animals and early humans ambushing them. Artefacts were embedded on the delta plain and became preserved during lake-level rise.
- Based on the sequence stratigraphic analysis it is most likely that archaeological findings of sites 12-II and 13-II are contemporaneous in time.
- During the Saalian Drenthe glaciation the remnant tunnel valley was completely filled by meltwater deposits and the Middle Pleistocene successions became deformed by the over-riding glacier.

Acknowledgements

Financial support by the Niedersächsisches Ministerium für Wissenschaft und Kultur (MWK) is gratefully acknowledged (Project No. 51420035 and PRO Niedersachsen Project No. 11.2-76202-17-3/09). Constructive comments by two anonymous reviewers are highly appreciated and helped to improve the manuscript. We would like to thank the owner of the Schöningen open-cast mine, E.ON-Kraftwerke GmbH, for the permission to work on their property. Borehole data were generously provided by E.ON-Kraftwerke and the Niedersächsisches Landesamt für Bergbau, Energie und Geologie (LBEG). W. Berkemer, N. Haycock, B. Köhler, M. Kursch, W. Mertens and J. Neumann-Giesen are thanked for technical assistance and support in the field. M. Bagge, S. Cramm, E. Großmann and W. Rode helped with the acquisition and processing of the seismic sections. Many thanks also to N. Conard, L. Eissmann, P. Gibbard, J. Lehmann, T. Van Kolfschoten, K.-D. Meyer, F. Turner and B. Urban for discussion.

References

- Aber, J.S., Ber, A., 2007: Glaciotectonism. *Developments in Quaternary Science* 6. 1-246.
- Allen, J.R.L., 1984: Sedimentary structures: their character and physical basis. *Developments in Sedimentology* 30, 1-663.
- Bannerjee I., Kalkreuth, W., Davies, E.H., 1996: Coal seam splits and transgressive-regressive coal couplets: A key to stratigraphy of high-frequency sequences. *Geology* 24, 1001-1004.
- Behrend, F., 1927: Erläuterungen zur geologischen Karte von Preußen und benachbarten deutschen Ländern 1:25.000, Blatt Schöningen. Preußische geologische Landesanstalt, Berlin, 40 pp.
- Böhme, G., 2000: Reste von Fischen, Amphibien und Reptilien aus der Fundstelle Schöningen 12 bei Helmstedt (Niedersachsen) – Erste Ergebnisse. *Praehistoria Thuringica* 4, 18-27.

- Böhme, G., 2007: Fisch-, Amphibien- und Reptilien-Reste aus der Schichtenfolge des Reinsdorf-Interglazials von Schöningen. *In*: Thieme, H. (Ed.): Die Schöninger Speere – Mensch und Jagd vor 400 000 Jahren. Theiss, Stuttgart, pp. 13-16.
- Boulton, G.S., Lunn, R., Vidstrand, P., Zatzepin, S., 2007: Subglacial drainage by groundwater-channel coupling, and the origin of esker systems: Part 1 – glaciological observations. *Quaternary Science Reviews* 26, 1067-1090.
- Brandes, C., Pollok, L., Schmidt, C., Wilde, V., Winsemann, J., 2012: Basin modelling of a lignite-bearing salt rim syncline: insights into rim syncline evolution and salt diapirism in NW Germany. *Basin Research* 24, 699-716.
- Brosche, K.-U., Walther, M., 1978. Die jungpleistozänen Löß-Deckschichten der Braunkohlentagebaue der Braunschweigischen Kohlenbergwerke (BKB) zwischen Helmstedt und Schöningen. *Eiszeitalter und Gegenwart* 28, 51-67.
- Brown, L.F., Fisher, W.L., 1977: Seismic-stratigraphic interpretation of depositional systems: examples from Brazilian rift and pull-apart basins. *In*: Payton, C.E. (Ed.): *Seismic Stratigraphy – applications to hydrocarbon exploration*. AAPG Memoir 26, pp. 117-133.
- Busschers, F.S., Van Balen, R.T., Cohen, K.M., Kasse, C., Weerts, H.J.T., Wallinga, J., Bunnik, F.P.M., 2008: Response of the Rhine-Meuse fluvial system to Saalian ice-sheet dynamics. *Boreas* 37, 329-468.
- Carr, B.J., Hajnal, Z., Prugger, A., 1998. Shear-wave studies in glacial till. *Geophysics* 63, 1273-1284.
- Cataneanu, O., 2006: *Principles of Sequence Stratigraphy*. Elsevier, Amsterdam, 375 pp.
- Crawford, J.M., Doty, W., Lee, M.R., 1960: Continuous signal seismograph. *Geophysics*, 25, 95-105.
- Duphorn, K., Lang, H.D., Look, E.R., Mengeling, H., Meyer, K.-D., Schneekloth, H., Vinken, R., 1974. CC3926 Braunschweig. Geologische Übersichtskarte 1: 200.000, Bundesanstalt für Geowissenschaften und Rohstoffe.
- Ehlers, J., Meyer, K.-D., Stephan, H.-J., 1984: The pre-Weichselian glaciations of north-west Europe. *Quaternary Science Reviews* 3, 1-40.
- Ehlers, J., Linke, G., 1989: The origin of deep buried channels of Elsterian age in northwest Germany. *Journal of Quaternary Science* 4, 255-265.
- Ehlers, J., Eissmann, L., Lippstreu, L., Stephan, H.-J., Wansa, S., 2004: Pleistocene glaciations of North Germany. *In*: Ehlers, J., Gibbard, P.L. (Eds.): *Quaternary Glaciations. Extent and Chronology Part I, Europe*. *Developments in Quaternary Science* 2, pp. 135-146.
- Ehlers, J., Grube, A., Stephan, H.-J., Wansa, S., 2011: Pleistocene Glaciations of North Germany – New Results. *In*: Ehlers, J., Gibbard, P.L., Hughes, P.D. (eds.): *Quaternary Glaciations – Extent and Chronology – A Closer Look*. *Developments in Quaternary Science* 15, pp. 149-162.
- Eissmann, L., 1967: Glaziäre Destruktionszonen (Rinnen, Becken) im Altmoränengebiet des Norddeutschen Tieflandes. *Geologie* 16, 804-833.

- Eissmann, L., 2002: Quaternary geology of eastern Germany (Saxony, Saxon-Anhalt, South Brandenburg, Thuringia), type area of the Elsterian and Saalian Stages in Europe. *Quaternary Science Reviews* 21, 1275-1346.
- Elsner, H., 1987: Das Quartär im Tagebau Schöningen der Braunschweigischen Kohlenbergwerke AG, Helmstedt. University of Hannover, unpublished diploma thesis, 126 pp.
- Elsner, H., 2003: Verbreitung und Ausbildung Elster-zeitlicher Ablagerungen zwischen Elm und Flechtinger Höhenzug. *Eiszeitalter und Gegenwart* 52, 91-116.
- Evans, D.J.A., Philipps, E.R., Hiemstra, J.F., Auton, C.A., 2006: Suglacial till: Formation, sedimentary characteristics and classification. *Earth Science Reviews* 78, 115-176.
- Eyles, N., Eyles, C.H., 1992: Glacial Depositional Systems; *In: Walker, R.G., James, N.P. (eds.): Facies Models: Response to Sea Level Change; Geological Association of Canada*, pp. 73-100.
- FEMO, 2008: Geotope im Spannungsfeld zwischen Schutz und Nutzung: Naturschutz und Besucherlenkung in ausgewählten Geotopen des Nationalen Geoparks Harz, Braunschweiger Land, Ostfalen. Final Report, 101 pp.
- Fiore, J., Girardclos, S., Pugin, A., Gorin, G., Wildi, W., 2011: Würmian deglaciation of western Lake Geneva (Switzerland) based on seismic stratigraphy. *Quaternary Science Reviews* 30, 377-393.
- Gani, M.R. 2004: From Turbid to Lucid: A Straightforward Approach to Sediment Gravity Flows and Their Deposits. *The Sedimentary Record* 3, 4-8.
- Geyh, M.A., Müller H., 2005: Numerical $^{230}\text{Th}/\text{U}$ dating and a palynological review of the Holsteinian/Hoxnian Interglacial. *Quaternary Science Reviews* 24, 1861-1872.
- Ghose, R., Brouwer, J., Nijhof, V., 1996: A portable S-wave vibrator for high resolution imaging of the shallow subsurface. Extended Abstract, 59th EAGE Conference and Technical Exhibition, Amsterdam.
- Hartmann, T., 1988: Elster- bis Saale-zeitliche Sedimente im Tagebau Schöningen der Braunschweigischen Kohlen-Bergwerke AG, Helmstedt. University of Hannover, unpublished diploma thesis, 153 pp.
- Holz, M., Kalkreuth, W., Banerjee, I., 2002: Sequence stratigraphy of paralic coal-bearing strata: an overview. *International Journal of Coal Geology* 48, 147-179.
- Hooke, R.L., Jennings, C.E., 2006: On the formation of the tunnel valleys of the southern Laurentide ice-sheet. *Quaternary Science Reviews* 25, 1364-1372.
- Huuse, M., Lykke-Andersen, H., 2000: Overdeepened Quaternary valleys in the eastern Danish North Sea: morphology and origin. *Quaternary Science Reviews* 19, 1233-1253.
- Jechorek, H., 2000: Die fossile Flora des Reinsdorf-Interglazial. Paläokarpologische Untersuchungen an mittelpleistozänen Ablagerungen im Braunkohlentagebau Schöningen. *Præhistoria Thuringica* 4, 7-17.
- Jørgensen, F., Sandersen, P.B.E., 2006: Buried and open tunnel valleys in Denmark - erosion beneath multiple ice sheets. *Quaternary Science Reviews* 25, 1339-1363.

- Kluiwing, S.J., Aleid Bosch, J.H., Ebbing, J.H.J., Mesdag, C.S., Westerhoff, R.S., 2003: Onshore and offshore seismic and lithostratigraphic analysis of a deeply incised Quaternary buried valley-system in the Northern Netherlands. *Journal of Applied Geophysics* 53, 249-271.
- Koutsodendris, A. Müller, U.C., Pross, J., Brauer, A., Kotthoff, U., Lotter, A.F., 2010: Vegetation dynamics and climate variability during the Holsteinian interglacial based on a pollen record from Dethlingen (northern Germany). *Quaternary Science Reviews* 29, 3298-3307.
- Krbetschek, M.R., Degering, G., Alexowsky, W., 2008: Infrarot-Radiofluoreszenz-Alter (IR-RF) unter-saalezeitlicher Sedimente Mittel- und Ostdeutschlands. *Zeitschrift der Deutschen Gesellschaft für Geowissenschaften* 159, 133-140.
- Kühl, N., Litt, T., 2007: Quantitative Time-Series Reconstructions of Holsteinian and Eemian Temperatures Using Botanical Data. *In: Sirocko, F., Claussen, M., Goni, M.F.S., Litt, T. (Eds.): The Climate of Past Interglacials; Developments in Quaternary Science* 7, pp. 418-444.
- Kuster, H., Meyer, K.-D., 1979: Glaziäre Rinnen im mittleren und nordöstlichen Niedersachsen. *Eis-zeitalter und Gegenwart* 29, 135-156.
- Lang, J., Winsemann, J., 2012: The 12II DB outcrop Section at Schöningen: Sedimentary Facies and Depositional Architecture. *In: Behre, K.-E. (Ed.), Forschungen zur Urgeschichte im Tagebau von Schöningen* 1, pp. 39-59.
- Le Heron, D.P., Sutcliffe, O., Bourgig, K., Craig, J., Visentin, C., Whittington, R., 2004: Sedimentary architecture of Upper Ordovician tunnel valleys, Gargaf Arch, Libya: Implications for the genesis of a hydrocarbon reservoir. *GeoArabia* 9, 137-160.
- Lenhard, R., 1989: Schichtlagerung und Zusammensetzung Elster- bis Saale-zeitlicher Sedimente im Baufeld Esbeck, Tagebau Schöningen, der Braunschweigischen Kohlen-Bergwerke AG, Helmstedt. Universität Hannover, unpublished diploma thesis, 125 pp.
- Lee, J.R., Busschers, F.S., Sejrup, H.P., 2010: Pre-Weichselian Quaternary glaciations of the British Isles, The Netherlands, Norway and adjacent marine areas south of 68°N: implications for long-term ice sheet development in northern Europe. *Quaternary Science Reviews* 44, 213-228.
- Litt, T., Behre, K.-E., Meyer, K.-D., Stephan, H.-J., Wansa, S., 2007: Stratigraphische Begriffe für das Quartär des norddeutschen Vereisungsgebietes. *Eiszeitalter und Gegenwart* 56, 7-65.
- Litt, T., Schmincke, H.-U., Frechen, M., Schlüchter, C., 2008: Quaternary. *In: McCann, T. (Ed.): The Geology of Central Europe, Vol. 2: Mesozoic and Cenozoic.* pp. 1287-1340.
- Lønne, I. 1995: Sedimentary facies and depositional architecture of ice-contact glaciomarine systems. *Sedimentary Geology* 98, 13-43.
- Look, E., 1984: Geologie und Bergbau im Braunschweiger Land. *Geologisches Jahrbuch A* 78, 1-467.
- Lowe, D.R. 1975: Water-escape structures in coarse-grained sediments. *Sedimentology* 22, 157-204.
- Lutz, R., Kalka, S., Gaedicke, C., Reinhardt, L., Winsemann, J., 2009: Pleistocene tunnel valleys in the German North Sea: spatial distribution and morphology. *Zeitschrift der Deutschen Gesellschaft für Geowissenschaften* 60, 225-235.

- McCarroll, D., Rijdsdijk, K.F., 2003: Deformation styles as a key for interpreting glacial depositional environments. *Journal of Quaternary Science* 18, 473-489.
- Manger, G., 1952. Der Zusammenhang von Salztektonik und Braunkohlenbildung bei der Entstehung der Helmstedter Braunkohlenlagerstätten. *Mitteilungen geologisches Staatsinstitut Hamburg* 21, 7-45.
- Mania, D. 1995: Die geologischen Verhältnisse im Gebiet von Schöningen. *In*: Thieme, H., Maier, R. (Eds.): *Archäologische Ausgrabungen im Braunkohlentagebau Schöningen*. Hannover, pp. 33-43.
- Mania, D. 1998: Zum Ablauf der Klimazyklen seit der Elstervereisung im Elbe-Saalegebiet. *Praehistoria Thuringica* 2, 5-21.
- Mania, D., 2006: Stratigraphie, Klima- und Umweltentwicklung der letzten 400 000 Jahre im Saalegebiet und Harzvorland (Forschungsstand 2006). *Hercynia N.F.* 39, 155-194.
- Mania, D., 2007: Die fossilen Weichtiere (Mollusken) aus den Beckensedimenten des Zyklus Schöningen II (Reinsdorf-Warmzeit). *In*: Hartmut Thieme (Ed.): *Die Schöninger Speere – Mensch und Jagd vor 400 000 Jahren*. Theiss, Stuttgart, pp. 99-104.
- Mills, P.C., 1983: Genesis and diagnostic value of soft-sediment deformation structures – a review. *Sedimentary Geology* 35, 83-104.
- Mitchum, R.M., Vail, P.R., Sangree, J.B., 1977. Seismic stratigraphy and global changes of sea-level, Part 6: stratigraphic interpretation of seismic reflection patterns in depositional sequences. *In*: Payton, C.E. (Ed.): *Seismic Stratigraphy – applications to hydrocarbon exploration*. AAPG Memoir 26, pp. 117-133.
- Mulder, T., Alexander, J., 2001: The physical character of subaqueous sedimentary density flows and their deposits. *Sedimentology* 48, 269-299.
- Ó Cofaigh, C., 1996: Tunnel valley genesis. *Progress in Physical Geography* 20, 1-19.
- Passchier, S., Laban, C., Mesdag, C.S., Rijdsdijk, K.F., 2010: Subglacial bed conditions during Late Pleistocene glaciations and their impact on ice dynamics in the southern North Sea. *Boreas* 39, 633-647.
- Piotrowski, J., 1994: Tunnel-valley formation in northwest Germany – geology, mechanisms of formation and subglacial bed conditions for the Bornhöved tunnel valley. *Sedimentary Geology* 89, 107-141.
- Piotrowski, J., Geletneky, J., Vater, R., 1999: Soft-bedded subglacial meltwater channel from the Welzow-Süd open-cast lignite mine, Lower Lusatia, eastern Germany. *Boreas* 28, 363-374.
- Polom, U., 2006: Vibration generator for seismic applications. United States Patent No. US 7, 136, 325 B2.
- Polom, U., Druivenga, G., Grossmann, E., Grueneberg, S., Rode, W. 2011: Transportabler Scherwellenvibrator. German Patent No. DE 103 27 757 B4.

- Postma, G., 1990: Depositional architecture and facies of river and fan deltas: a synthesis. *In*: Colella, A., Prior, B.D. (Eds.): Coarse-Grained Deltas. Special Publication of the International Association of Sedimentologists 10, pp. 13-27.
- Praeg, D., 2003: Seismic imaging of mid-Pleistocene tunnel-valleys in the North Sea Basin – high resolution from low frequencies. *Journal of Applied Geophysics* 53, 273-298.
- Pugin, A.J.M., Larson, T.H., Sargent, S.L., McBride, J.H., Bexfield, C.E., 2004: Near- surface mapping using SH-wave and P-wave seismic land streamer data acquisition in Illinois, U.S. *The Leading Edge* 23, 677-682.
- Rajchl, M., Uličný, D., Mach, K., 2008: Interplay between tectonics and compaction in a rift-margin, lacustrine delta system: Miocene of the Eger Graben, Czech Republic. *Sedimentology* 55, 1419-1447.
- Rodrigues, N., Cobbold, P.R., Løseth, H. 2009: Physical modeling of sand injectites. *Tectonophysics* 474, 610-632.
- Roe, H.M., Preece, R.C., 2011: Incised palaeo-channels of the late Middle Pleistocene Thames: age, origins and implications for fluvial palaeogeography and sea-level reconstruction in the southern North Sea basin. *Quaternary Science Reviews* 30, 2498-2519.
- Russell H.A.J., Arnott, R.W.C., Sharpe, D.R., 2003: Evidence for rapid sedimentation in a tunnel channel, Oak Ridges Moraine, southern Ontario, Canada. *Sedimentary Geology* 160, 33-55.
- Salamon, T., 2009: Origin of Pleistocene outwash plains in various topographic settings, southern Poland. *Boreas* 38, 362-378.
- Schwab, G., Ludwig, A.O., 1996: Zum Relief der Quartärbasis in Norddeutschland. Bemerkungen zu einer neuen Karte. *Zeitschrift für Geologische Wissenschaften* 24, 343-349.
- Serangeli, J., Böhner, U., 2012: Die pleistozänen Fundstellen in Schöningen. Eine Einführung. *In*: Behre, K.-E. (Ed.), *Forschungen zur Urgeschichte im Tagebau von Schöningen* 1, 23-37.
- Sierralta, M., Frechen, M., Urban, B., 2012: ²³⁰Th/U dating results from opencast mine Schöningen. *In*: Behre, K.-E. (Ed.), *Forschungen zur Urgeschichte im Tagebau von Schöningen* 1, 134-154.
- Stackebrandt, W., 2009: Subglacial channels of Northern Germany – a brief review. *Zeitschrift der Deutschen Gesellschaft für Geowissenschaften* 60, 203-210.
- Szymarek, M., 2011: Climate oscillations of the Holsteinian (Mazovian) Interglacial recorded in shell morphometry of *Viviparus diluvianus* (Kunth, 1865) from eastern Poland. *Quaternary International* 241, 143-159.
- Thieme, H., 1997: Lower Palaeolithic hunting spears from Germany. *Nature* 385, 307-310.
- Thieme, H., 1999: Altpaläolithische Holzgeräte aus Schöningen, Lkr. Helmstedt. Bedeutsame Funde zur Kulturentwicklung des frühen Menschen. *Germania* 77, 451–487.
- Thieme, H., 2007: Die ältesten Speere der Menschheit: Funde von Weltrang. *In*: Thieme, H. (Ed.): *Die Schöninger Speere – Mensch und Jagd vor 400 000 Jahren*. Theiss, Stuttgart, pp. 13-16.

- Toucanne, S., Zaragosi, S., Bourillet, J.F., Cremer, M., Eynaud, F., Van Vliet-Lanoë, B., Penaud, A., Fontanier, C., Turon, J.L., Cortijo, E., Gibbard, P.L., 2009: Timing of massive 'Fleuve Manche' discharges over the last 350 kyr: insights into the European ice-sheet oscillations and the European drainage network from MIS 10 to 2. *Quaternary Science Reviews* 28, 1238–1256.
- Treese, K.L., Wilkinson, B.H., 1982: Peat-marl deposition in a Holocene paludal-lacustrine basin – Sucker Lake, Michigan. *Sedimentology* 29, 375-390.
- Tschie, W., 1991: Die pleistozäne Schichtfolge im Tagebau Schöningen, Baufeld Esbeck der Braunschweigischen Kohlen-Bergwerke AG. Universität Hannover, unpublished diploma thesis, 75 pp.
- Turner, C., 1970: The Middle Pleistocene deposits at Marks Tey, Essex. *Philosophical Transactions of the Royal Society of London. Series B, Biological Sciences* 257, 373-437.
- Urban, B., 1995: Palynological evidence of younger Middle Pleistocene Interglacials (Holsteinian, Reinsdorf, Schöningen) in the Schöningen open cast lignite mine (eastern Lower Saxony, Germany). *Mededelingen Rijks Geologische Dienst* 52, 175-186.
- Urban, B., 2007: Interglacial Pollen Records from Schöningen, North Germany. *In: Sirocko, F., Clausen, M., Goni, M.F.S., Litt, T. (Eds.): The Climate of Past Interglacials; Developments in Quaternary Science* 7, pp. 418-444.
- Urban, B., Thieme, H., Elsner, H., 1988: Biostratigraphische, quartärgeologische und und urgeschichtliche Befunde aus dem Tagebau „Schöningen“, Ldkr. Helmstedt. *Zeitschrift der deutschen geologischen Gesellschaft* 139, 123-154.
- Urban, B., Elsner, H., Hölzer, A., Mania, D., Albrecht, B., 1991a: Eine eem- und frühweichselzeitliche Abfolge im Tagebau Schöningen, Landkreis Helmstedt. *Eiszeitalter und Gegenwart* 41, 85-99.
- Urban, B., Lenhard, R., Mania, D., Albrecht, B., 1991b: Mittelpleistozän im Tagebau Schöningen, Ldkr. Helmstedt. *Zeitschrift der deutschen geologischen Gesellschaft* 142, 351-372.
- Urban, B., Sierralta, M., Frechen, M., 2011: New evidence for vegetation development and timing of Upper Middle Pleistocene interglacials in Northern Germany and tentative correlations. *Quaternary International* 241, 125-142.
- Vail, P.R., Mitchum, R.M., Thompson, S., 1977: Seismic stratigraphy and global changes of sea level, Part 3: relative changes of sea level from coastal onlap. *In: Payton, C.E. (Ed.): Seismic Stratigraphy – applications to hydrocarbon exploration. AAPG Memoir* 26, pp. 63-81.
- Van Asselen, S., 2010: The contribution of peat compaction to total basin subsidence: implications for the provision of accommodation space in organic-rich deltas. *Basin Research* 23, 239-255.
- Van Kolfschoten, T., 1995: Faunenreste des altpaläolithischen Fundplatzes Schöningen 12 (Reinsdorf-Interglazial). *In: Thieme, H., Maier, R. (Eds.): Archäologische Ausgrabungen im Braunkohlentagebau Schöningen. Hannover*, pp. 85-94.
- Van Kolfschoten, T. 2007: Die Kleinsäugerreste aus dem Reinsdorf-Interglazial von Schöningen. *In: Hartmut Thieme (Ed.): Die Schöninger Speere – Mensch und Jagd vor 400 000 Jahren. Theiss, Stuttgart*, pp. 112–117.

- Van Wagoner, J.C., Mitchum, R.M., Campion, K.M., Rahmanian, V.D., 1990: Siliciclastic Sequence Stratigraphy in Well Logs, Cores, and Outcrops: Concepts for High-Resolution Correlation of Time and Facies. AAPG Methods in Exploration Series, No. 7.
- Wagner, B., 2011: Spatial analysis of loess and loess-like sediments in the Weser-Aller catchment (Lower Saxony and Northern Hesse, NW Germany). *E&G Quaternary Science Journal* 60, 27-46.
- Walter, R., 2007: *Geologie von Mitteleuropa*. Schweizerbart'sche Verlagsbuchhandlung, Stuttgart, 511 pp.
- Wingfield, R., 1990: The origin of major incisions within the Pleistocene deposits of the North Sea. *Marine Geology* 91, 31-52.
- Winsemann, J., Hornung, J.J., Meinsen, J., Asprion, U., Polom, U., Brandes, C., Bußmann, M., Weber, C., 2009: Anatomy of a subaqueous ice-contact fan and delta complex, Middle Pleistocene, North-west Germany. *Sedimentology* 56, 1041–1076.
- Winsemann, J., Brandes, C., Polom, U., 2011a: Response of a proglacial delta to rapid high-amplitude lake-level change: an integration of outcrop data and high-resolution shear wave seismic. *Basin Research* 23, 22-52.
- Winsemann, J., Brandes, C., Polom, U., Weber, C., 2011b: Depositional architecture and palaeogeographic significance of Middle Pleistocene glaciolacustrine ice marginal deposits in north-western Germany: a synoptic overview. *E&G Quaternary Science Journal* 60, 212-235.
- Wood, S.H., 1994: Seismic expression and geological significance of a lacustrine delta in Neogene deposits of the western Snake River plain, Idaho. *AAPG Bulletin* 78, 102-121.
- Ziegenhardt, W., Kramer, H.-J., 1968: Der känozoische Sedimentationsablauf in der Egelner Südmulde - Ein Beitrag zur Kinematik und Dynamik halokinetisch angelegter Randsenken. *Geologie* 19, 902-919.
- Zielinski, T., Van Loon, A., 2003: Pleistocene Sandur deposits represent braidplains, not alluvial fans. *Boreas* 32, 590-611.
- Zecchin, M., 2007: The architectural variability of small-scale cycles in shelf and ramp clastic systems: The controlling factors. *Earth-Science Reviews* 84, 21-55.

This chapter has been submitted to *Journal of Human Evolution*

The Middle Pleistocene tunnel valley at Schöningen as a Palaeolithic archive

Jörg Lang¹⁾, Jutta Winsemann¹⁾, Ulrich Polom²⁾, Utz Böhner³⁾ & Jordi Serangeli⁴⁾

- 1) Institut für Geologie, Leibniz Universität Hannover, Callinstraße 30, 30167 Hannover, Germany
- 2) Leibniz Institut für Angewandte Geophysik (LIAG), Stilleweg 2, 30655 Hannover, Germany
- 3) Niedersächsisches Landesamt für Denkmalpflege, Scharnhorststraße 1, 30175 Hannover, Germany
- 4) Institut für Ur- und Frühgeschichte, Eberhard Karls Universität Tübingen, Burgsteige 11, 72070 Tübingen, Germany

Abstract

Schöningen represents one of the key sites for Lower Palaeolithic archaeology in central Europe, where a Middle to Late Pleistocene succession, locally up to 45 m thick, has been preserved in an Elsterian tunnel valley. After deglaciation the tunnel valley remained underfilled and provided the accommodation space for interglacial deposition and also kept the artefact-bearing strata below base level for subsequent erosion. The Holsteinian interglacial (MIS 9) succession consists of laterally and vertically stacked lacustrine delta systems, which were controlled by repeated lake-level changes. In the face of changing climatic and environmental conditions the long-lived interglacial lake provided an attractive site for animals and early humans. Artefacts were deposited on the delta plain and became embedded during lake-level rise. Although the area was considerably affected by erosion and glaciectonic deformation during the subsequent late Saalian glaciation (MIS 6), the artefact-bearing Holsteinian strata were preserved in the deeper part of the tunnel valley.

Tunnel valleys should be regarded as potential archives for interglacial deposits, which may contain important Palaeolithic sites. Interglacial lakes situated within underfilled tunnel valleys represent attractive sites for animals and early human hunter-gatherers. Tunnel valleys may provide a high accommodation space and therefore also have a high preservation potential.

Introduction

Schöningen represents an outstanding geological and archaeological archive, where unique artefacts from the Lower Palaeolithic have been recovered from Middle Pleistocene interglacial deposits. The Middle Pleistocene interglacial succession at Schöningen provides a very well preserved, long-lasting

archive for the period between the Elsterian and the Saalian glaciations. As well as the archaeological findings, there exists an extensive biostratigraphic data base, which includes palynological data (Urban, 1995, 2007; Urban & Sierralta, 2012; Urban *et al.*, 1988, 1991, 2011) and analyses of plant remains (Jechorek, 2000), molluscs (Mania, 2007), mammals (Van Kolfshoten, 1995, 2007), fish, reptiles and amphibians (Böhme, 2000, 2007). However, the interpretation of this important environmental archive has long been controversial. Previous geological models (Mania, 1998, 2006) interpreted the interglacial deposits as infills of abandoned fluvial channels. However, new geophysical and geological data clearly show that the interglacial succession was deposited within a long-lived lake, which formed in an underfilled Elsterian tunnel valley (Lang *et al.*, 2012; Lang & Winsemann, 2012). The distribution of the interglacial deposits and the archaeological sites is related to lake-level fluctuations of the interglacial lake (Lang *et al.*, 2012). The lake-level fluctuations have previously been recognised in the palaeo-ecological analysis of floral (Jechorek, 2000; Urban, 2007; Urban *et al.*, 2011) and faunal associations (Böhme, 2000, 2007). The aim of this paper is to provide a synoptic overview of the depositional environment and stratigraphic framework of the Schöningen sites and to stress the importance of the geological setting, where the deposition within an overdeepened tunnel valley allowed for the preservation of this unique site.

Introduction to tunnel valleys

The erosion by glaciers and glacial meltwater has the potential of providing accommodation space for glacial and inter- or post-glacial deposition, especially in settings where accommodation space is generally low. Tunnel valleys are elongated subglacial incisions, which are eroded by meltwater under high hydrostatic pressure and form anastomosing subglacial drainage networks (Ó Cofaigh, 1996; Huuse & Lykke-Andersen, 2000; Kehew *et al.*, 2012; Van der Vegt *et al.*, 2012). Buried tunnel valleys are a typical feature of the Middle Pleistocene Elsterian glaciation across northern central Europe (Ehlers *et al.*, 1984; Huuse & Lykke-Andersen, 2000; Kluiving *et al.*, 2003; Praeg, 2003; Lutz *et al.*, 2009; Stackebrandt, 2009). Tunnel valley fills may typically be subdivided into a primary glacial fill and a secondary non-glacial fill (e.g. Van der Vegt *et al.*, 2012). Syn-glacial tunnel valley fills include glacial fluvial and glacial lacustrine deposits and till, which are deposited both subglacially and proglacially during deglaciation. Interglacial infills of tunnel valley commonly comprise lacustrine deposits or, if the setting is at the interglacial coastline, paralic or marine deposits (Kuster & Meyer, 1979; Piotrowski, 1994; Janszen *et al.*, 2012a; Kehew *et al.*, 2012; Lang *et al.*, 2012; Van der Vegt *et al.*, 2012).

Setting

The Schöningen open-cast mine (Fig. 1) is located within the southwestern rim syncline of the northwest-southeast-trending Helmstedt-Staßfurt salt wall. Towards the west the rim syncline is

bounded by the Elm anticline (up to 323 m a.s.l.), which comprises mostly Triassic limestones. The main infill of the rim syncline consists of an up to 366 m thick marginal marine lignite-bearing Palaeogene succession (Brandes *et al.*, 2012; Osman *et al.*, *in press*), which is unconformably overlain by up to 45 m thick Middle to Upper Pleistocene deposits (Elsner, 2003; Lang *et al.*, 2012; Lang & Winsemann, 2012). The Pleistocene succession comprises Elsterian and Saalian glacifluvial, glaciallacustrine and subglacial deposits, Holsteinian and Eemian lacustrine deposits and Weichselian loess and solifluidal deposits (Mania, 1998, 2006; Urban *et al.*, 1988, 1991; Elsner, 2003; Lang *et al.*, 2012; Lang & Winsemann, 2012). Deposits of the Elsterian glaciation and the subsequent Holsteinian interglacial (MIS 9) have been deposited in an Elsterian tunnel valley (Lang *et al.*, 2012). The remnant tunnel valley was completely filled by glaciallacustrine deposits and overlain by subglacial till during the Saalian Drenthe glaciation (MIS 6).

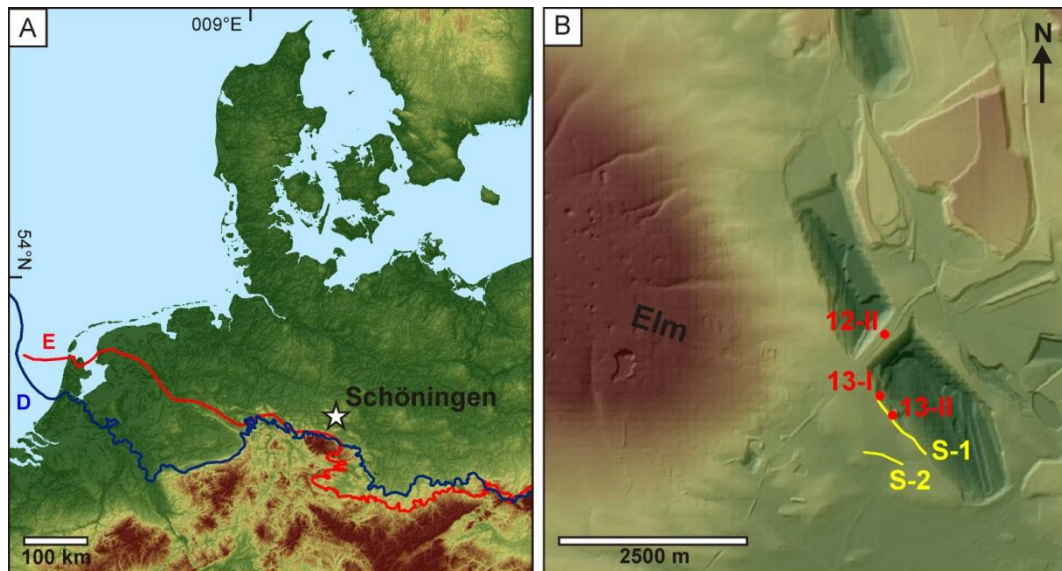


Fig. 1: **A)** Location of the study area and maximum extent of the Middle Pleistocene Fennoscandian ice sheets (E: Elsterian, D: Saalian Drenthe; modified after Ehlers *et al.*, 2011). **B)** Hill-shaded relief model of the study area, showing the locations of the excavation sites 13-I, 12-II and 13-II (red dots). The yellow lines indicate the position of the measured seismic profiles (S-1 and S-2). The digital elevation model (DEM) is based on data from the Landesamt für Geoinformation und Landentwicklung Niedersachsen (LGLN).

Interglacial deposits and archaeological sites

At Schöningen the deposits of the Elsterian and Saalian glaciations are separated by an up to 7.5 m thick interglacial lacustrine succession. This succession was deposited by east- to southwards prograding delta systems into a lake, which formed within the remnant tunnel valley and was affected by repeated lake-level changes (Lang *et al.*, 2012). These lake-level changes are attributed to climatic shifts between stadial and interstadial phases during the interglacial period (Urban, 2007; Urban *et al.*, 2011; Lang *et al.*, 2012).

Within the interglacial deposits several Palaeolithic archaeological sites were discovered, each containing several archaeological horizons. The main archaeological sites are referred to as sites 13-I, 12-II and 13-II (Fig. 1B; cf. Serangeli *et al.*, 2012). Numerous other Middle Pleistocene open-air sites in Schöningen bear fewer remains, but the evidence for human presence is unambiguous. At site 13-I several flint artefacts have been discovered, which were associated with bones of large mammals (Thieme, 1999). The site Schöningen 13-II, level 4, may be considered as the most important site for the discovery of eight spears, the remains of twenty butchered horses and ~1500 flint artefacts (Thieme, 1997, 1999, 2007). From the site Schöningen 12 II, level 1, several possible wooden shafts, more than 1000 bones of large mammals, numerous fragments of wood and several flint tools were recovered (Thieme, 1999, 2007; Serangeli and Böhner, 2012). Based on the stratigraphic relationships site 13-I is considered older than sites 12-II and 13-II, which are probably of the same age (Mania, 1998, 2006; Lang *et al.*, 2012). The numerical age of site 13-II was determined based on $^{230}\text{Th}/\text{U}$ data to range from 280-350 ka (Sierralta *et al.*, 2012) and 280 to 343 ka (Urban *et al.*, 2011), thus correlating with MIS 9 (Holsteinian). The palynological data also point to a Holsteinian age. The late Holsteinian succession is referred to as Reinsdorf (Urban, 1995, 2007; Urban *et al.*, 2011).

The artefacts recovered at the Schöningen sites include flint tools, possible wooden shafts and the spears as well as numerous animal bones with cut- and impact-marks. These artefacts provide evidence for repeated hunting and butchering activities, requiring complex planning and traditions. Altogether, the Schöningen sites represent a milestone in the evolution of human culture. In this context, a robust understanding of the geological and environmental context is fundamental for the research of the settlement dynamics amongst Lower Palaeolithic humans in northern central Europe.

Reconstruction of the depositional environment

The new depositional model for the Pleistocene succession of Schöningen is based on the interpretation of outcrop sections, 744 borehole logs and two high-resolution 2D shear-wave seismic reflection lines. All sedimentological and geophysical data sets were integrated into a high-resolution 3D geological subsurface model (GOCAD[®]) to reconstruct the spatial distribution of facies associations and the large-scale depositional architecture.

Formation of a tunnel valley beneath the Elsterian ice sheet

The Elsterian tunnel valley at Schöningen displays the typical dimensions (up to 850 m wide, 40 m deep), undulating basal profile and abrupt beginning of subglacial tunnel valleys (Fig. 2A; Lang *et al.*, 2012). The tunnel valley trends NNW to SSE in the northern part and bends to the southwest when leaving the rim syncline (Fig. 2A, B). The seismic sections and the subsurface model show that the tunnel valley is broader, shallower and flat-bottomed in the north, where it is incised into unconsolidated marginal marine Paleogene deposits, and narrower, deeper and V-shaped in the south, where it is

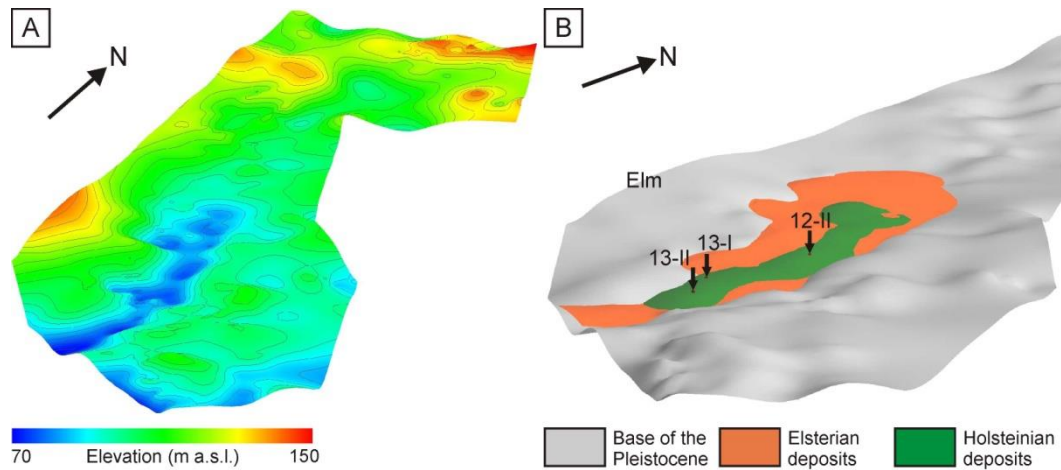


Fig. 2: Perspective views into the 3D subsurface model (5x vertical exaggeration). View is from the southeast. **A)** Geometry of the Elsterian tunnel valley. Contour lines are in 5 m intervals. **B)** Distribution of Elsterian and Holsteinian deposits within the tunnel valley. The three main archaeological sites (13-I, 12-II and 13-II) are indicated.

incised into Triassic mud- and limestones (Fig. 3). The incision of tunnel valleys is favoured by easily erodible substrates (Huuse & Lykke-Andersen, 2000; Stackebrandt, 2009; Janszen *et al.*, 2012b) such as the unconsolidated Paleogene infill of the rim syncline. Within fine-grained sediments with low permeabilities high pressure gradients between the meltwater channel and the substratum may trigger liquefaction and thus further enhance the erosion (Hooke & Jennings, 2006; Boulton *et al.*, 2007; Janszen *et al.*, 2012b). The differences in geometry along the tunnel valley match examples for tunnel valleys incised into substrates with different erodibilities (Janszen *et al.*, 2012b; Moreau *et al.*, 2012). The unconsolidated Paleogene rim-syncline infill allowed for a broad, flat-bottomed incision, while the Triassic bedrock shows a narrow, V-shaped geometry (Fig. 3).

The basal infill of the Schöningen tunnel valley consists of cross-stratified pebbly sand and gravel, which is interpreted as meltwater deposit. These deposits are unconformably overlain by massive diamicton, representing subglacial till (Fig. 2B). During the retreat of the Elsterian ice sheet fine-grained glacial lacustrine deposits were shed into the tunnel valley from northerly directions (Fig. 4A; Lang *et al.*, 2012).

Formation of an interglacial lake during the Holsteinian (MIS 9)

After final deglaciation the tunnel valley remained underfilled and an interglacial lake formed within the basin. The interglacial deposits comprise organic-rich silt or fine-grained sand and peat and are interpreted as representing topsets, foresets and bottomsets of fine-grained lacustrine delta systems (Fig. 5). The delta systems formed on the western shore of the interglacial lake, while deposits from the eastern shore are absent. Several small streams were probably fed from springs on the eastern flank of the Elm ridge, similar to the modern situation. The springs along the Elm ridge are located at elevations of 170-200 m a.s.l. Their locations are controlled by differences in rock permeabilities between Triassic limestones and mudstones and faults (Behrend, 1927; Look, 1984). The water from the

springs is very rich in calcium carbonate derived from the Triassic limestones (Huckriede, 1965). Sequence stratigraphic analysis of the interglacial lacustrine succession relates the lateral and vertical stacking pattern of the delta systems to repeated lake-level changes in the order of 4-6 m (Lang *et al.*, 2012), which can probably be correlated with the climatic fluctuations reconstructed from palynological data by Urban (1995, 2007). Within seismic line S-1 (Fig. 3), which connects the archaeological sites 13-I and 13-II, four unconformity-bound seismic-stratigraphic units were defined by Lang *et al.* (2012). The unconformities represent lake-level falls in the order of 4-6 m, each followed by a transgression (Fig. 5). During the life-span of the interglacial lake early humans repeatedly inhabited the shoreline and left artefacts on the delta plains.

In outcrop, sites 12-II and 13-II both display an internal stack of five shallowing-upwards successions (parasequences, PS), which are interpreted as representing high-frequency lake-level changes with magnitudes of 1-3 m (Lang *et al.*, 2012). Each shallowing-upwards succession is bounded by flooding

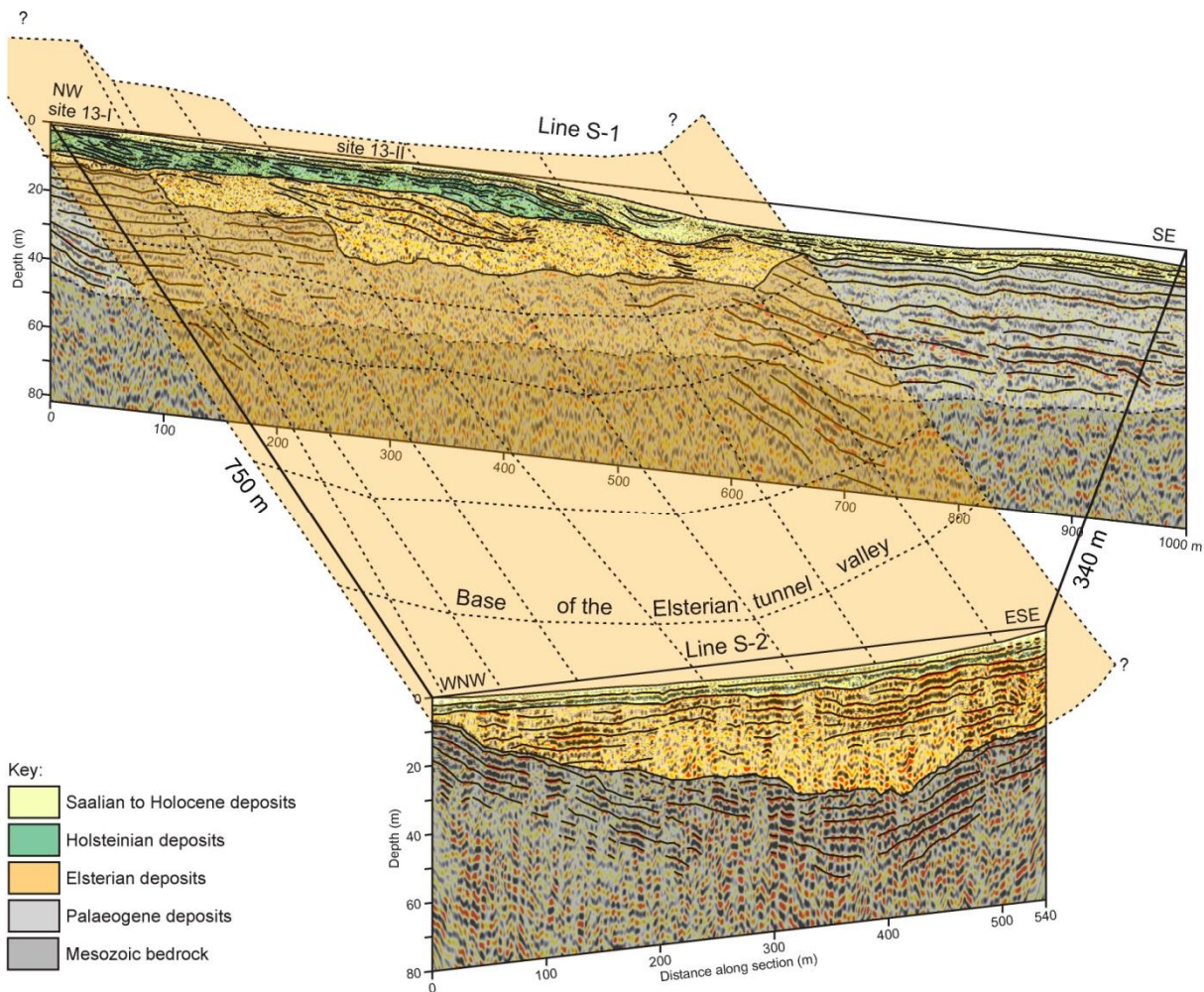


Fig. 3: Perspective view of the two shear-wave seismic lines. View is from the southwest. The base of the tunnel valley is broad and flat in line S-1, and V-shaped in line S-2. The differences in geometry are probably caused by the different erodibility of the unconsolidated Palaeogene sediments (line S-1) and the Mesozoic bedrock (line S-2). A more detailed interpretation of the seismic facies is provided by Lang *et al.* (2012). For location see Fig. 1B.

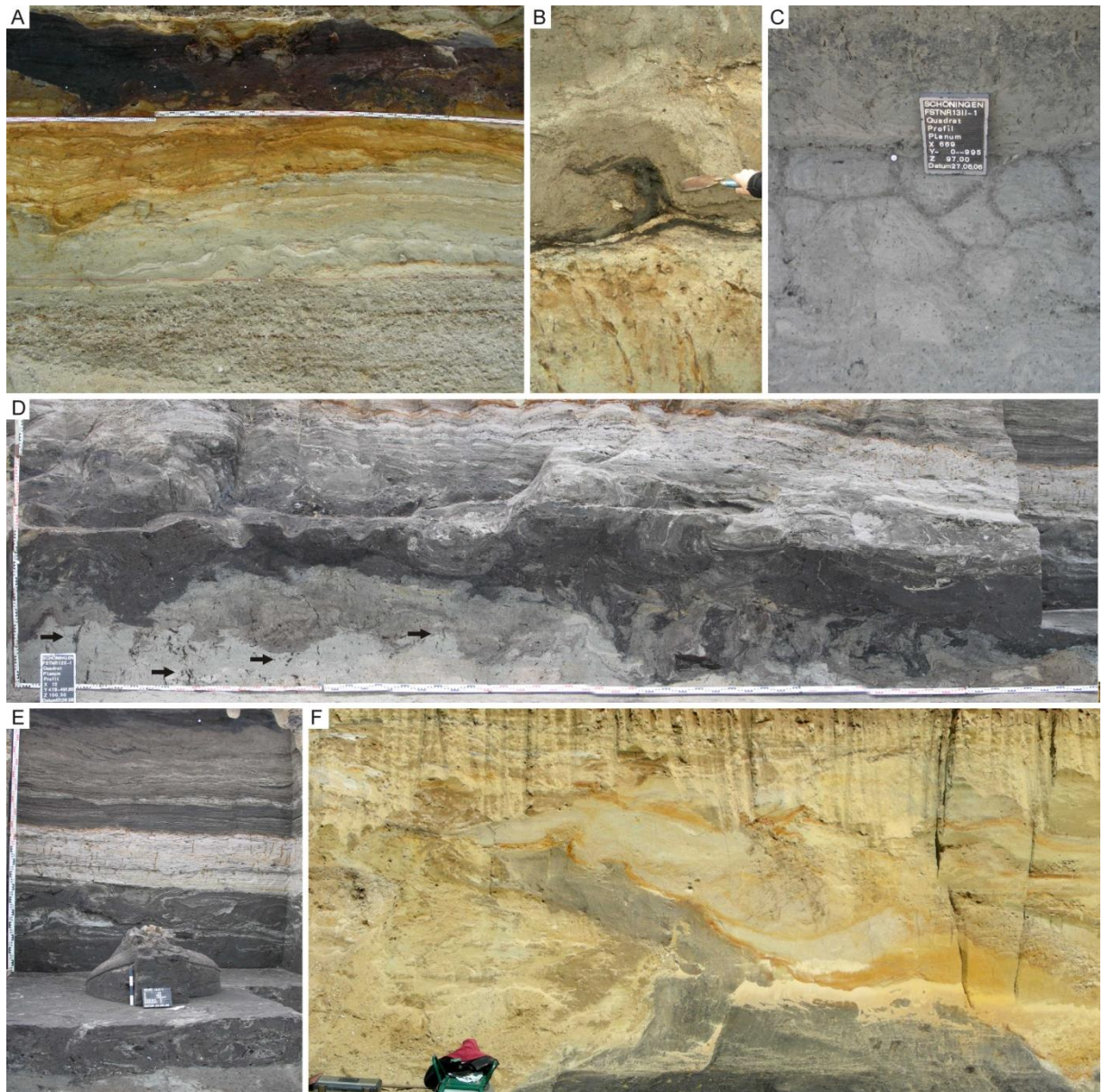


Fig. 4: **A)** Fining-upwards succession of coarse- and fine-grained glacial-lacustrine deposits (Elsterian), unconformably overlain by organic-rich lacustrine deposits (Holsteinian; site 12-II). **B)** Massive silt of the prodelta is unconformably overlying thin peat-rich delta plain deposits. A flame structure comprising delta plain deposits intruded into the overlying prodelta deposits, probably caused by ice loading (site 13-II, level 2). **C)** Polygonal pattern of mud cracks in lacustrine silt of the early interglacial, indicating subaerial exposure during lake-level lowstand. The deposits are overlain by organic-rich lacustrine deposits, pointing to subsequent transgression. The mud cracks can probably be correlated with the unconformity separating the deposits of sites 13-I and 13-II. **D)** Light grey lake-bottom deposits of the early Holsteinian are unconformably overlain by more organic-rich delta front and delta plain deposits of parasequence PS-1 (site 12-II, level 1). Roots within the lake-bottom deposits (arrow) are truncated and indicate emersion during lake-level lowstand. The unconformity displays intense deformation by loading and dewatering. **E)** Bovine skull (cf., *bubalus*) recovered from the base of parasequence PS-1 (site 12-II, level 1). **F)** Interglacial lacustrine deposits intruding as mud diapirs into overlying Saalian meltwater deposits. The vergence of the mud diapir and related thrust faults is towards the southeast, indicating proglacial deformation during the Saalian glacial advance.

surfaces and comprises deposits of the prodelta or delta front in the lower parts, overlain by deposits of the delta plain (Fig. 4B, C, D, E). Archaeological findings mostly occur in deposits of the delta plain, indicating activities of early humans at the lake margin. During transgressions artefacts became embedded and thus preserved (Lang *et al.*, 2012). The occurrence of these small-scale shallowing-upward successions was previously observed by Urban (2007) and related to climatic fluctuations between stadial and interstadial conditions. Within the individual shallowing-upwards successions the assemblages of plants indicate increasing terrestrialisation (Urban, 2007; Urban *et al.*, 2011). The diversity of fish, amphibian and reptile species also indicates changing ecological and hydrological conditions (Böhme, 2000), which correlate well with the reconstructed high-frequency lake-level fluctuations. The maximum extent of the interglacial lake at Schöningen (Fig. 6A) has been reconstructed from the delta topset-foreset-transitions assuming a maximum lake level of 105 m a.s.l. However, the continuation of the lake towards the south remains uncertain due to post-Holsteinian erosion. Figure 6B shows the progradation of delta systems into the lake during the formation of sites 12-II and 13-II, level 4 (PS-4). Fluctuations of the lake level in a magnitude of 5-10 m and changes of the trophic state or a similar Holsteinian lake in northern Germany have been reconstructed by Koutsodendris *et al.* (2013) based on the diatom record. These fluctuations were caused by short-term climatic variability and changes in the vegetation cover of the catchment area (Koutsodendris *et al.*, 2013).

Saalian glaciation

During the Saalian Drenthe glaciation (MIS 6) the study area was again transgressed by the Scandinavian ice sheet. Coarse-grained glacial lacustrine deposits infilled the last remnant of the Elsterian tunnel valley, before laterally more extensive glacial fluvial deposits and subglacial till covered larger parts of the study area (Lang *et al.*, 2012). Glacitectonic deformation affected large parts of the deposits at Schöningen (Urban *et al.*, 1991; Elsner, 2003; Lang *et al.*, 2012; Lang & Winsemann, 2012). Parts of the artefact-bearing strata, especially at site 12-II, have been heavily deformed by glacitectonic processes (Fig. 4F) while other sites (13-II) were hardly affected. The Holsteinian deposits in the tunnel valley remained well below base level and were thus preserved.

Discussion

The Middle Pleistocene succession of Schöningen was deposited within an Elsterian tunnel valley, which provided the accommodation space and protected the deposits from subsequent erosion. Tunnel valleys commonly represent the depocentres for glacial and interglacial deposition (e.g. Stackebrandt, 2009; Krohn *et al.*, 2009; Janszen *et al.*, 2012a, Van der Vegt *et al.*, 2012). Since the incision of tunnel valleys is one of the deepest-reaching erosional processes they provide sites with a high preservation potential, especially in areas affected by multiple glaciations. The preservation of post-Elsterian interglacial successions in tunnel valleys, which mostly comprise lacustrine successions, is

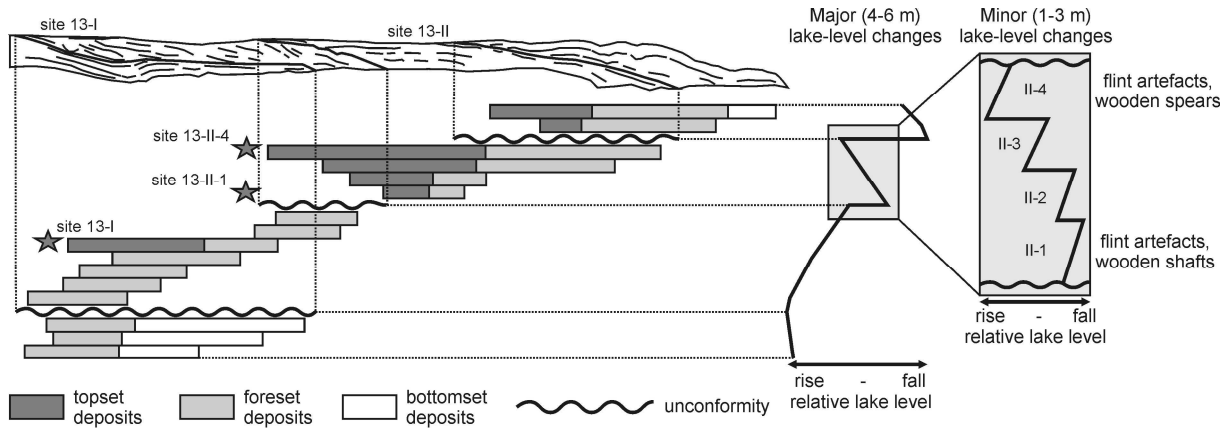


Fig. 5: Reconstructed lake-level curve for the Holsteinian interglacial succession, based on delta foreset-topset-transitions in the seismic section S-1 (modified after Lang *et al.*, 2012). The reconstruction of the minor lake-level fluctuations, which controlled the formation of sites 12-II and 13-II, is based on the shallowing-upwards successions observed in the outcrops. The positions of the main archaeological horizons are indicated.

for example well documented in Germany (Kuster & Meyer, 1979; Piotrowski, 1994, Eissmann, 2002; Stephan *et al.*, 2011; Janszen *et al.*, 2012a), the Netherlands (Kluiwing *et al.*, 2003), Denmark (Jørgensen & Sandersen, 2006) and England (Turner, 1970; Preece *et al.*, 2006). There are several examples of archaeological sites associated with lacustrine tunnel valley fills. Lower Palaeolithic artefacts have been recovered from the infill of a Middle Pleistocene Anglian (Elsterian) tunnel valley in eastern England (Preece *et al.*, 2006, 2007), Upper Palaeolithic and Mesolithic sites occur within Late Pleistocene Weichselian tunnel valleys in northern Germany (Bratlund, 1996) and Denmark (Larson, 1990; Rømer *et al.*, 2006).

The formation and preservation of Palaeolithic sites depends largely on the depositional environments and accommodation space. However, the formation of an archaeological site like Schöningen, where prolonged human presence is evident, requires an environment suitable for early human inhabitation. Especially for Lower Palaeolithic sites it is commonly ambiguous if the sites represent environments favoured by the early humans or with favourable preservation potential (Hijma *et al.*, 2012). Most Palaeolithic open-air sites are associated with either fluvial or lacustrine environments (Ashton *et al.*, 2006; Bridgland *et al.*, 2006; Preece *et al.*, 2006; Ashley *et al.*, 2010). Ashton *et al.* (2006) suggested that early humans favoured fluvial environments due to a greater variety of resources (plants, animals, lithic raw material) compared to lacustrine settings. However, in a delta plain setting the benefits from both fluvial and lacustrine environments may exist. Lacustrine environments are characterised by low-energy depositional processes and therefore have a higher potential to preserve artefacts *in situ*. The interglacial succession at Schöningen contains several pronounced unconformities due to fluctuating lake levels (Lang *et al.*, 2012) but the artefact-bearing strata were never completely reworked. The unconformities are related lake-level falls and subaerial exposure during lake-level lowstand (Fig. 4C, D). Subsequent transgressions led to a rapid embedding of artefacts, which had probably been left on

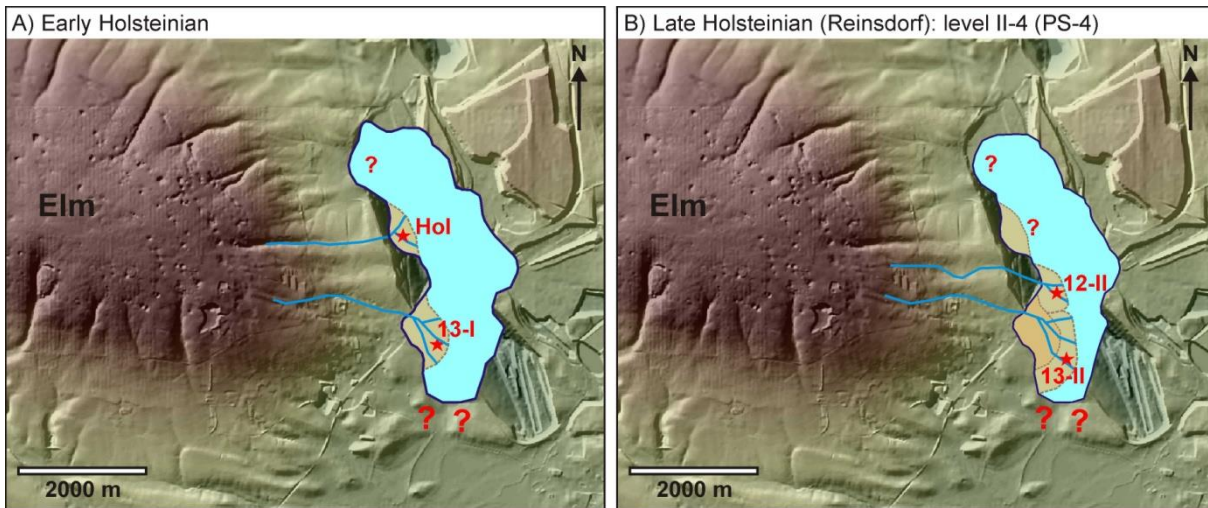


Fig. 6: Palaeogeographic reconstructions of the Holsteinian interglacial lake. The delta systems were shed by surface run-off from the Elm, probably fed by springs. The eastern part of the Elm has an elevation of up to 290 m a.s.l. The lake extent is outlined on the hill-shaded relief model (DEM data by LGLN). Note that the modern landscape east of the Elm is heavily modified by mining activity. **A)** Reconstruction of the maximum lake extent during the early Holsteinian when site 13-I formed. δ Holö in the northern part of the lake indicates the location of Holsteinian lake-marginal deposits previously described by Urban *et al.* (1988, 1991) **B)** The late Holsteinian (δ Reinsdorfö, c.f. Urban, 1995) delta systems 12-II and 13-II unconformably overlie the early Holsteinian deltas. The unconformity developed during a major lake-level fall. Subsequently the lake level rose again and deltas 12-II and 13-II were deposited.

the exposed delta plain surface. After embedding the artefacts remained under the groundwater level, allowing for the excellent preservation of organic material.

The archaeological sites and their internal horizons document occupation by early humans in spite of changing environmental conditions (Thieme, 1999; Urban, 2007). Site 12-II, level 1, and site 13-II, level 1, are attributed to the interglacial optimum phase. In contrast, sites 13-I, level 1, is attributed to boreal conditions of an early interglacial phase and site 13-II, level 4, is attributed to boreal conditions at the end of an interglacial (Thieme, 1999). The broad range of climatic conditions indicates that the lake margin provided an attractive site for animals and early humans ambushing them, particularly under meliorating environmental conditions. The delta systems were fed by springs and surface run-off from the Elm ridge, which provided a constant source of water and probably prevented a complete drying up of the interglacial lake. Additionally the high calcium carbonate content of the water favoured the preservation of bones. Especially during the rather dry and cold early and late phases of the interglacials the wetland of the delta plains probably represented a flourishing ecosystem within a rather dry and hostile environment (cf., Oviatt *et al.*, 2006; Preece *et al.*, 2006; Yansa, 2007; Ashley *et al.*, 2008, 2010). Even the shores of proglacial lakes have been recognised as inhabitable sites for early hunter-gatherers (Overstreet & Kolb, 2003; Hill, 2007).

Conclusions

Schöningen provides an excellent site for the preservation of early human artefacts in several ways. During the Elsterian glaciation a tunnel valley was incised into the unconsolidated Paleogene deposits of the rim syncline. This overdeepened elongated basin provided the necessary accommodation space for subsequent glacialacustrine and lacustrine deposition. A lake formed within the remnant tunnel valley and persisted through-out the Middle Pleistocene Holsteinian interglacial (MIS 9). The Holsteinian interglacial succession consists of laterally and vertically stacked lacustrine delta systems, which were affected by repeated lake-level fluctuations. The margin of the interglacial lake provided an attractive site for animals and early humans ambushing them, especially during the climatic melioration phase towards the termination of the interglacial. The very last remnant of the tunnel valley was only filled during the advance of the late Saalian Drenthe (MIS 6) ice sheet. Although the morphology of the area was considerably modified by erosion and glacitectonic deformation during the subsequent Saalian glaciation, the artefact-bearing Holsteinian strata remained sheltered in the overdeepened tunnel valley.

Therefore tunnel valleys should be regarded as potential archives for interglacial deposits, which may contain important Palaeolithic sites. Interglacial lakes within underfilled tunnel valleys represent attractive sites for animals and early human hunter-gatherers. Tunnel valleys also provide accommodation space and have a high preservation potential.

Acknowledgements

Financial support by the Niedersächsisches Ministerium für Wissenschaft und Kultur (MWK) is gratefully acknowledged (Project No. 51420035 and PRO Niedersachsen Project No. 11.2-76202-17-3/09). We would like to thank E.ON-Kraftwerke GmbH for the permission to work on their property. Borehole data were generously provided by E.ON-Kraftwerke and the Niedersächsisches Landesamt für Bergbau, Energie und Geologie (LBEG). Fugro N.V. provided GeODin software for data management. W. Berkemer, N. Haycock, B. Köhler, M. Kursch, J. Lehmann, W. Mertens and J. Neumann-Giesen are thanked for technical assistance and support in the field. M. Bagge, S. Cramm, E. Großmann and W. Rode carried out the acquisition and processing of the seismic sections. F. Busch is thanked for GIS work. Many thanks are also due to N. Conard, C. Brandes, D. Steinmetz and B. Urban for discussion.

References

- Ashley, G.M., Tactikos, J.C., Owen, R.B., 2008: Hominin use of springs and wetlands: Paleoclimate and archaeological records from Olduvai Gorge (~1.7961.74 Ma). *Palaeogeography, Palaeoclimatology, Palaeoecology* 272, 1-16.

- Ashley, G.M., Dominguez-Rodrigo, M., Bunn, H.T., Mabulla, A.Z.P., Baquedano, E., 2010: Sedimentary geology and human origins: a fresh look at Olduvai Gorge, Tanzania. *Journal of Sedimentary Research* 80, 703-709.
- Ashton, N., Lewis, G.L., Parfitt, S., White, M., 2006: Riparian landscapes and human habitat preferences during the Hoxnian (MIS 11) Interglacial. *Journal of Quaternary Science* 21, 497-505.
- Behrend, F., 1927: Erläuterungen zur geologischen Karte von Preußen und benachbarten deutschen Ländern 1:25.000, Blatt Schöningen. Preußische Geologische Landesanstalt, Berlin, 40 pp.
- Böhme, G., 2000: Reste von Fischen, Amphibien und Reptilien aus der Fundstelle Schöningen 12 bei Helmstedt (Niedersachsen) ó Erste Ergebnisse. *Praehistoria Thuringica* 4, 18-27.
- Böhme, G., 2007: Fisch-, Amphibien- und Reptilien-Reste aus der Schichtenfolge des Reinsdorf-Interglazials von Schöningen. *In*: Thieme, H. (Ed.), *Die Schöninger Speere ó Mensch und Jagd vor 400 000 Jahren*. Theiss, Stuttgart, pp. 13-16.
- Boulton, G.S., Lunn, R., Vidstrand, P., Zatsepin, S., 2007: Subglacial drainage by groundwater-channel coupling, and the origin of esker systems: Part 1 ó glaciological observations. *Quaternary Science Reviews* 26, 1067-1090.
- Brandes, C., Pollok, L., Schmidt, C., Wilde, V., Winsemann, J., 2012: Basin modelling of a lignite-bearing salt rim syncline: insights into rim syncline evolution and salt diapirism in NW Germany. *Basin Research* 24, 699-716.
- Bratlund, B., 1996: Hunting Strategies in the Late Glacial of Northern Europe: A Survey of the Faunal Evidence. *Journal of World Prehistory* 10, 1-48.
- Bridgland, D.R., Antoine, P., Limondin-Lozourt, N., Santisteban, J.I., Westaway, R., White, M.J., 2006: The Palaeolithic occupation of Europe as revealed by evidence from the rivers: data from IGCP 449. *Journal of Quaternary Science* 21, 437-455.
- Ehlers, J., Meyer, K.-D., Stephan, H.-J., 1984: The pre-Weichselian glaciations of north-west Europe. *Quaternary Science Reviews* 3, 1-40.
- Ehlers, J., Grube, A., Stephan, H.-J., Wansa, S., 2011: Pleistocene Glaciations of North Germany ó New Results. *In*: Ehlers, J., Gibbard, P.L., Hughes, P.D. (Eds.): *Quaternary Glaciations ó Extent and Chronology ó A Closer Look*. *Developments in Quaternary Science* 15, pp. 149-162.
- Eissmann, L., 2002: Quaternary geology of eastern Germany (Saxony, Saxon-Anhalt, South Brandenburg, Thuringia), type area of the Elsterian and Saalian Stages in Europe. *Quaternary Science Reviews* 21, 1275-1346.
- Elsner, H., 2003: Verbreitung und Ausbildung Elster-zeitlicher Ablagerungen zwischen Elm und Flechtinger Höhenzug. *Eiszeitalter und Gegenwart* 52, 91-116.
- Hijma, M.P., Cohen, K.M., Roebroeks, W., Westerhoff, W.E., Busschers, F.S., 2012: Pleistocene RhineóThames landscapes: geological background for hominin occupation of the southern North Sea region. *Journal of Quaternary Science* 27, 17-39.

- Hill, C.L., 2007: Geoarchaeology and Late Glacial Landscapes in the Western Lake Superior Region, Central North America. *Geoarchaeology* 22, 15-47.
- Hooke, R.L., Jennings, C.E., 2006. On the formation of the tunnel valleys of the southern Laurentide ice-sheet. *Quaternary Science Reviews* 25, 1364-1372.
- Huckriede, R., 1967: Neues zur Geologie des Elms (Niedersachsen). *Geologica et Palaeontologica* 1, 87-95.
- Huuse, M., Lykke-Andersen, H., 2000: Overdeepened Quaternary valleys in the eastern Danish North Sea: morphology and origin. *Quaternary Science Reviews* 19, 1233-1253.
- Janszen, A., Moreau, J., Moscariello, A., Ehlers, J., Kröger, J., 2012a: Time-transgressive tunnel-valley infill revealed by a three-dimensional sedimentary model, Hamburg, north-west Germany. *Sedimentology* 60, 693-719.
- Janszen, A., Spaak, M., Moscariello, A., 2012b: Effects of the substratum on the formation of glacial tunnel valleys: an example from the Middle Pleistocene of the southern North Sea. *Boreas* 41, 629-643.
- Jechorek, H., 2000: Die fossile Flora des Reinsdorf-Interglazial. Paläokarpologische Untersuchungen an mittelpleistozänen Ablagerungen im Braunkohlentagebau Schöningen. *Praehistoria Thuringica* 4, 7-17.
- Kehew, A.E., Piotrowski, J.A., Jørgensen, F., 2012: Tunnel valleys: Concepts and controversies ó A review. *Earth-Science Reviews* 113, 33-58.
- Kluiwing, S.J., Aleid Bosch, J.H., Ebbing, J.H.J., Mesdag, C.S., Westerhoff, R.S., 2003: Onshore and offshore seismic and lithostratigraphic analysis of a deeply incised Quaternary buried valley-system in the Northern Netherlands. *Journal of Applied Geophysics* 53, 249-271.
- Koutsodendris, A., Lotter, A.F., Kirilova, E., Verhagen, F.T.M., Brauer, A., Pross, J., 2013: Evolution of a Holsteinian (MIS 11c) palaeolake based on a 12-ka-long diatom record from Dethlingen (northern Germany). *Boreas* 42, 714-728.
- Krohn, C.F., Larsen, N.K., Kronborg, C., Nielsen, O.B., Knudsen, K.L., 2009: Litho- and chronostratigraphy of the Late Weichselian in Vendsyssel, northern Denmark, with special emphasis on tunnel-valley infill in relation to a receding ice margin. *Boreas* 38, 811-833.
- Kuster, H., Meyer, K.-D., 1979: Glaziäre Rinnen im mittleren und nordöstlichen Niedersachsen. *Eiszeitalter und Gegenwart* 29, 135-156.
- Lang, J., Winsemann, J., Steinmetz, D., Polom, U., Pollok, L., Böhner, U., Serangeli, J., Brandes, C., Hampel, A., Winghart, S., 2012: The Pleistocene of Schöningen, Germany: a complex tunnel valley fill revealed from 3D subsurface modelling and shear wave seismics. *Quaternary Science Reviews* 39, 86-105.
- Lang, J., Winsemann, J., 2012: The outcrop section at Schöningen 12II DB, Plateau 4 and 5: sedimentary facies and depositional architecture. *In: K. Behre (Ed.), Die chronologische Einordnung der*

paläolithischen Fundstellen von Schöningen. Forschungen zur Urgeschichte im Tagebau von Schöningen 1, 39-59.

Larson, L., 1990: The Mesolithic of Southern Scandinavia. *Journal of World Prehistory* 4, 257-309.

Look, E., 1984: Geologie und Bergbau im Braunschweiger Land. *Geologisches Jahrbuch A* 78, 1-467.

Lutz, R., Kalka, S., Gaedicke, C., Reinhardt, L., Winsemann, J., 2009: Pleistocene tunnel valleys in the German North Sea: spatial distribution and morphology. *Zeitschrift der Deutschen Gesellschaft für Geowissenschaften* 60, 225-235.

Mania, D., 1998: Zum Ablauf der Klimazyklen seit der Elstervereisung im Elbe-Saalegebiet. *Praehistoria Thuringica* 2, 5-21.

Mania, D., 2006: Stratigraphie, Klima- und Umweltentwicklung der letzten 400 000 Jahre im Saalegebiet und Harzvorland (Forschungsstand 2006). *Hercynia N.F.* 39, 155-194.

Mania, D., 2007: Die fossilen Weichtiere (Mollusken) aus den Beckensedimenten des Zyklus Schöningen II (Reinsdorf-Warmzeit). *In: H. Thieme (Ed.), Die Schöninger Speere ó Mensch und Jagd vor 400 000 Jahren.* Theiss, Stuttgart, pp. 99-104.

Moreau, J., Huuse, M., Janszen, A., van der Vegt, P., Gibbard, P.L., Moscariello, A., 2012: The glaciogenic unconformity of the southern North Sea. *In: Huuse, M., Redfern, J., Le Heron, D.P., Dixon, R.J., A. Moscariello, A., Craig, J. (Eds.), Glaciogenic reservoirs.* Geological Society of London Special Publication 368, pp. 99-110.

Ó Cofaigh, C., 1996: Tunnel valley genesis. *Progress in Physical Geography* 20, 1-19.

Osman, A., Pollok, L., Brandes, C., Winsemann, J., *in press.* Sequence stratigraphy of a Paleogene coal bearing rim syncline: interplay of salt dynamics and sea-level changes, Schöningen, Germany. *Basin Research*, doi: 10.1111/bre.12021.

Overstreet, D.F., Kolb, M.F., 2003: Geoarchaeological Contexts for Late Pleistocene Archaeological Sites with Human-Modified Woolly Mammoth Remains in Southeastern Wisconsin, U.S.A. *Geoarchaeology* 18, 91-114.

Oviatt, C.G., Madsen, D.B., Schmitt, D.N., 2003: Late Pleistocene and early Holocene rivers and wetlands in the Bonneville basin of western North America. *Quaternary Research* 60, 200-210.

Piotrowski, J., 1994: Tunnel-valley formation in northwest Germany ó geology, mechanisms of formation and subglacial bed conditions for the Bornhöved tunnel valley. *Sedimentary Geology* 89, 107-141.

Praeg, D., 2003: Seismic imaging of mid-Pleistocene tunnel-valleys in the North Sea Basin ó high resolution from low frequencies. *Journal of Applied Geophysics* 53, 273-298.

Preece, R.C., Gowlett, J.A.J., Parfitt, S.A., Bridgland, D.R., Lewis, S.G., 2006: Humans in the Hoxnian: habitat, context and fire use at Beeches Pit, West Stow, Suffolk, UK. *Journal of Quaternary Science* 21, 485-496.

Preece, R.C., Parfitt, S.A., Bridgland, D.R., Lewis, S.G., Rowe, P.J., Atkinson, T.C., Candy, I., Debenham, N.C., Penkman K.E.H., Rhodes, E.J., Schwenninger, J.-L., Griffiths, H.I., Whittaker,

- J.E., Glead-Owen, C., 2007: Terrestrial environments during MIS 11: evidence from the Palaeolithic site at West Stow, Suffolk, UK. *Quaternary Science Reviews* 26, 1236-1300.
- Rømer, S., Breuning-Madsen, H., Balstrøm, T., Jensen, A.-E., 2006: Short Contribution: Mapping Quaternary Deposits as a Method for Explaining the Distribution of Mesolithic Sites in Reclaimed Landscapes: An Example from Vålse Vig, Southeast Denmark. *Geoarchaeology* 21, 113-124.
- Serangeli, J., Böhner, U., 2012: Die Artefakte von Schöningen und ihre zeitliche Einordnung. *In*: K. Behre (Ed.), Die chronologische Einordnung der paläolithischen Fundstellen von Schöningen. *Forschungen zur Urgeschichte im Tagebau von Schöningen* 1, 23-37.
- Serangeli, J., Böhner, U., Conard, N.J., Haßmann, H., 2012: Die pleistozänen Fundstellen in Schöningen ó eine Einführung. *In*: K. Behre (Ed.), Die chronologische Einordnung der paläolithischen Fundstellen von Schöningen. *Forschungen zur Urgeschichte im Tagebau von Schöningen* 1, 23-37.
- Sierralta, M., Frechen, M., Urban, B., 2012: $^{230}\text{Th}/\text{U}$ dating results from opencast mine Schöningen *In*: K. Behre (Ed.), Die chronologische Einordnung der paläolithischen Fundstellen von Schöningen. *Forschungen zur Urgeschichte im Tagebau von Schöningen* 1, 143-154.
- Stackebrandt, W., 2009: Subglacial channels of Northern Germany ó a brief review. *Zeitschrift der Deutschen Gesellschaft für Geowissenschaften* 60, 203-210.
- Stephan, H.-J., Urban, B., Lüttig, G., Menke, B., Sierralta, M., 2011: Palynologische, petrographische und geochronologische Untersuchungen an Ablagerungen der Leck-Warmzeit (spätes Mittelpleistozän) und begleitender Sedimente. *Geologisches Jahrbuch A* 160, 1-80.
- Thieme, H., 1997: Lower Palaeolithic hunting spears from Germany. *Nature* 385, 307-310.
- Thieme, H., 1999: Altpaläolithische Holzgeräte aus Schöningen, Ldkr. Helmstedt. *Bedeutsame Funde zur Kulturentwicklung des frühen Menschen. Germania* 77, 451-487.
- Thieme, H., 2007: Die ältesten Speere der Menschheit: Funde von Weltrang. *In*: Thieme, H. (Ed.), Die Schöninger Speere ó Mensch und Jagd vor 400 000 Jahren. Theiss, Stuttgart, pp. 13-16.
- Turner, C., 1970: The Middle Pleistocene deposits at Marks Tey, Essex. *Philosophical Transactions of the Royal Society of London. Series B, Biological Sciences* 257, 373-437.
- Urban, B., 1995: Palynological evidence of younger Middle Pleistocene interglacials (Holsteinian, Reinsdorf, Schöningen) in the Schöningen open cast lignite mine (eastern Lower Saxony, Germany). *Mededelingen Rijks Geologische Dienst* 52, 175-186.
- Urban, B., 2007: Interglacial Pollen Records from Schöningen, North Germany. *In*: Sirocko, F., Claussen, M., Goni, M.F.S., Litt, T. (Eds.), *The Climate of Past Interglacials; Developments in Quaternary Science* 7, pp. 418-444.
- Urban, B., Sierralta, M., 2012: New palynological evidence and correlation of Early Palaeolithic sites in Schöningen 12 B and 13 II, Schöningen open lignite mine. *In*: K. Behre (Ed.), Die chronologi-

sche Einordnung der paläolithischen Fundstellen von Schöningen. Forschungen zur Urgeschichte im Tagebau von Schöningen 1, 77-96.

- Urban, B., Thieme, H., Elsner, H., 1988: Biostratigraphische, quartärgeologische und urgeschichtliche Befunde aus dem Tagebau Schöningen, Ldkr. Helmstedt. Zeitschrift der Deutschen Geologischen Gesellschaft 139, 123-154.
- Urban, B., Lenhard, R., Mania, D., Albrecht, B., 1991: Mittelpleistozän im Tagebau Schöningen, Ldkr. Helmstedt. Zeitschrift der Deutschen Geologischen Gesellschaft 142, 351-372.
- Urban, B., Sierralta, M., Frechen, M., 2011: New evidence for vegetation development and timing of Upper Middle Pleistocene interglacials in Northern Germany and tentative correlations. Quaternary International 241, 125-142.
- Van der Vegt, P., Janszen, A., Moscariello, A., 2012: Tunnel valleys: current knowledge and future perspectives. *In:* Huuse, M., Redfern, J., Le Heron, D.P., Dixon, R.J., Moscariello, A., Craig, J. (Eds.), Glaciogenic reservoirs. Geological Society of London Special Publication 368, pp. 75-97.
- Van Kolfschoten, T., 1995: Faunenreste des altpaläolithischen Fundplatzes Schöningen 12 (Reinsdorf-Interglazial). *In:* Thieme, H., Maier, R. (Eds.), Archäologische Ausgrabungen im Braunkohlentagebau Schöningen. Hannover, pp. 85-94.
- Van Kolfschoten, T. 2007. Die Kleinsäugerreste aus dem Reinsdorf-Interglazial von Schöningen. *In:* Hartmut Thieme (Ed.), Die Schöninger Speere ó Mensch und Jagd vor 400 000 Jahren. Theiss, Stuttgart, pp. 112-117.
- Wagner, B., 2011: Spatial analysis of loess and loess-like sediments in the Weser-Aller catchment (Lower Saxony and Northern Hesse, NW Germany). E&G Quaternary Science Journal 60, 27-46.
- Yansa, C.H., 2007: Lake Records of Northern Plains Paleindian and Early Archaic Environments: The Park Oasis Hypothesis. Plains Anthropology 52, 109-144.

This chapter has been published as: Lang & Winsemann, 2013, *Sedimentary Geology* 296, 36-54, doi: 10.1016/j.sedgeo.2013.08.005 and can be found at:
<http://www.sciencedirect.com/science/article/pii/S0037073813001474>

Lateral and vertical facies relationships of bedforms deposited by aggrading supercritical flows: from cyclic steps to humpback dunes

Jörg Lang¹⁾ & Jutta Winsemann¹⁾

1) Institut für Geologie, Leibniz Universität Hannover, Callinstraße 30, 30167 Hannover, Germany

Abstract

The preservation of bedforms related to supercritical flows and hydraulic jumps is commonly considered to be rare in the geologic record, although these bedforms are known from a variety of depositional environments. This field-based study presents a detailed analysis of the sedimentary facies and stacking pattern of deposits of cyclic steps, chutes-and-pools, antidunes and humpback dunes from three-dimensional outcrops. The well exposed Middle Pleistocene successions from northern Germany comprise glaciallacustrine ice-contact subaqueous fan and glacial lake-outburst flood deposits. The studied successions give new insights into the depositional architectures of bedforms related to supercritical flows and may serve as an analogue for other high-energy depositional environments such as fluvial settings, coarse-grained deltas or turbidite systems.

Deposits of cyclic steps occur within the glacial lake-outburst flood succession and are characterised by lenticular scours infilled by gently to steeply dipping backsets. Cyclic steps formed due to acceleration and flow thinning when the glacial lake-outburst flood spilled over a push-moraine ridge. These bedforms are commonly laterally and vertically truncated and alternate with deposits of chutes-and-pools and antidunes. The subaqueous fan successions are dominated by laterally extensive sinusoidal waveforms, which are interpreted as deposits of aggrading stationary antidunes, which require quasi-steady flows at the lower limit of the supercritical flow stage and high rates of sedimentation. Humpback dunes are characterised by downflow divergent cross-stratification, displaying differentiation into topsets, foresets and bottomsets, and are interpreted as deposited at the transition from subcritical to supercritical flow conditions or vice versa. Gradual lateral and vertical transitions between humpback dunes and antidune deposits are very common.

The absence of planar-parallel stratification in all studied successions suggests that the formative of these bedforms is suppressed in flows characterised by hydraulic jumps and highly aggradational conditions. The large-scale lateral and vertical successions of bedforms are interpreted as representing the

temporal and spatial evolution of the initial supercritical flows, which was strongly affected by the occurrence of hydraulic jumps. Small-scale facies changes and the formation of individual bedforms are interpreted as controlled by fluctuating discharge, bed topography and pulsating unstable flows.

Introduction

Field examples of deposits related to supercritical flows and hydraulic jumps are known from a variety of depositional environments, for example alluvial fans (Blair, 1999), beaches (Broome & Komar, 1979), deltas (Massari, 1996), fluvial and glacial systems (Langford and Bracken, 1987; Alexander & Fielding, 1997; Fralick, 1999; Kjær *et al.*, 2004; Fielding, 2006), ice-marginal subaqueous fans and deltas (Gorrell & Shaw, 1991; Brennand, 1994; Russell & Arnott, 2003; Johnsen & Brennand, 2004, 2006; Russell *et al.*, 2007; Ghiene *et al.*, 2010; Winsemann *et al.*, 2009, 2011; Girard *et al.*, 2012a, b; Hirst, 2012; Lang *et al.*, 2012a), glacial lake-outburst flood deposits (Duller *et al.*, 2008; Carling *et al.*, 2009; Marren *et al.*, 2009), subglacial lakes and cavities (Russell *et al.*, 2003; Clerc *et al.*, 2012), submarine fans (Walker, 1967; Hand *et al.*, 1972; Weirich, 1988; Kostic & Parker, 2006; Postma *et al.*, 2009; Cartigny *et al.*, 2011) and volcanoclastic deposits (Schmincke *et al.*, 1973). However, for most examples of supercritical flow deposits no further distinction has been drawn between the various depositional processes, which include the formation of antidunes, chutes-and-pools and cyclic steps. The preservation of supercritical flow deposits is commonly attributed to rapidly decelerating flows under highly aggradational bed conditions (Russell & Arnott, 2003; Fielding, 2006; Duller *et al.*, 2008; Winsemann *et al.*, 2009, 2011). Processes related to supercritical flows and hydraulic jumps constitute an important aspect of sedimentation in glacial settings, as well as in proximal reaches of deltas and submarine fans. The occurrence of these deposits in glacial settings, including subaqueous ice-contact fans and glacial deltas, indicates that these bedforms might be considered as a characteristic feature of such depositional systems. Glacial supercritical flow deposits are commonly interpreted as pointing to major meltwater drainage events related to the outburst of sub- and proglacial lakes (Russell & Arnott, 2003; Duller *et al.*, 2008; Winsemann *et al.*, 2009, 2011; Girard *et al.*, 2012b).

Well exposed Middle Pleistocene ice-marginal deposits in northern Germany provide the opportunity to study the facies architecture of successions comprising cyclic steps, chutes-and-pools and antidunes in three-dimensional outcrops. Four field examples from subaqueous ice-contact fan and glacial lake-outburst flood deposits will be presented in detail. The main objective of this study is to explore systematic lateral and vertical facies changes of deposits interpreted as representing deposition by rapidly decelerating supercritical flow. The criteria for the recognition of the various bedforms will be specified and field evidence for supercritical flows will be discussed and linked to flow conditions.

Deposits of supercritical flows in glacial settings are frequently related to high-discharge events in ice-proximal settings and their recognition is therefore relevant for the reconstruction of depositional

processes and palaeo-flows near the palaeo-ice margins. The well exposed Pleistocene subaqueous ice-contact fans may further serve as an analogue for comparable Palaeozoic deposits forming important hydrocarbon reservoirs across North Africa (e.g., Hirst *et al.*, 2002; Le Heron *et al.*, 2009; Hirst, 2012; Lang *et al.*, 2012a) and South America (e.g., Potter *et al.*, 1995; Henry *et al.*, 2010).

Deposition by supercritical flows

Supercritical to transcritical flows and hydraulic jumps produce a variety of bedforms, including cyclic steps, chutes-and-pools and antidunes. The stability fields of the different bedforms are controlled by a variety of factors, including flow velocity, flow depth, sediment load, grain size, bed roughness, slope and dynamic viscosity (Southard & Boguchwal, 1990; Van den Berg & Van Gelder, 1993, 1998; Van den Berg & Nio, 2010). Flume studies by Cartigny *et al.* (*in press*) indicate that the formation of upper stage plane beds and antidunes depends strongly on the Froude number, which is a function of flow velocity and flow depth, while chutes-and-pools and cyclic steps are more dependent on flow-sediment interactions expressed by the dimensionless mobility parameter, which is a function of flow velocity, density of fluid and grains, grain-size and bed roughness.

Antidune deposits are generally characterised by gently upflow-dipping backsets, which are deposited beneath in-phase wave trains at Froude numbers between 0.8 and 1.8 (Gilbert, 1914; Kennedy, 1963; Allen, 1984; Carling & Shvidchenko, 2002). Antidune wave breaking may occur after a threshold of the wave steepness is reached (Kennedy, 1963) and causes repeated aggradation and degradation of antidune bedforms (Middleton, 1965; Alexander *et al.*, 2001). Chutes-and-pools form in the troughs scoured upflow of hydraulic jumps and are characterised by troughs filled with steeply upflow-dipping laminae (Middleton, 1965; Alexander *et al.*, 2001). The formation of chutes-and-pools requires higher Froude numbers than those for antidunes (1.6-2.1; Alexander *et al.*, 2001; Cartigny *et al.*, *in press*). Cyclic steps are characterised by a train of slowly upslope migrating hydraulic jumps spaced at regular intervals, which cause erosion at the upflow-sides and deposition on the downflow-sides of each hydraulic jump (Winterwerp *et al.*, 1992; Taki & Parker, 2005; Kostic *et al.* 2010; Cartigny *et al.*, 2011). The wavelength of one cyclic step is defined by the distance between the two bounding hydraulic jumps. Flume experiments on the formation of cyclic steps indicate mean values of the Froude number of ~2.2 with peaks of up to 25 (Muto *et al.*, 2012; Cartigny *et al.*, *in press*). Cyclic steps are characterised by the regular spaced migrating hydraulic jumps, while hydraulic jumps associated with chutes-and-pools occur more irregularly spaced due to their spontaneous occurrence. The occurrence of cyclic step deposits is mainly known from deep sea environments (seafloor topography and turbidite systems), where wavelengths have magnitudes of hundreds of metres to kilometre-scale and amplitudes of tens of metres (Kostic & Parker, 2006; Lamb *et al.*, 2008; Spinewine *et al.*, 2009; Cartigny *et al.*, 2011; Armitage *et al.*, 2012). Up to now, the only described outcrop example of cyclic step deposits was provided by Cartigny *et al.* (2012) from deposits of high-density turbidity currents. These deposits

comprise (i) crudely low-angle stratified or massive conglomeratic scour-fills, (ii) conglomeratic scour-fills with backsets and (iii) flat lens-shaped sandy beds displaying internal low-angle truncations.

Study area

During the Pleistocene, northern Germany was affected by three major glaciations of the Elsterian, Saalian and Weichselian glacial periods (Fig. 1A). From the Saalian glaciation two major ice advances, the Drenthe and Warthe are known (Ehlers *et al.*, 2004, 2011). Saalian ice-marginal deposits have been studied at four sites in northern Germany (Fig. 1A), where large ice-dammed lakes formed at the southwestern margin of the Scandinavian ice sheet due to the blockage of river drainage pathways to the north (Thome, 1983; Klostermann, 1992a; Van der Wateren, 1994; Eissmann, 2002; Winsemann *et al.*, 2009, 2011). Ice-marginal glaciallacustrine deposits consist of coarse-grained deltas and subaqueous fans, which bear evidence of fluctuating lake-levels (e.g., Winsemann *et al.*, 2009, 2011). During deglaciation the lakes catastrophically drained due to the opening of lake outlets, which caused high-magnitude outburst floods (Winsemann *et al.*, 2011). The drainage pathway of the glacial lake-outburst floods has been reconstructed by Meinsen *et al.* (2011). In the most proximal areas the drainage pathway is characterised by the occurrence of deep plunge pools, channels, streamlined hills and large V-shaped megaflutes. In the Lower Rhine Embayment highly dissected push moraines indicate the flood pathway towards the west into the North Sea.

Subaqueous ice-contact fan deposits

Subaqueous ice-contact fans (also known as grounding line fans) are deposited where sediment-laden meltwater is released as an efflux jet from en- or subglacial conduits into a standing water body, and are known from both glacialmarine (Powell, 1990) and glaciallacustrine (Russell & Arnott, 2003; Russell *et al.*, 2007; Hornung *et al.*, 2007; Winsemann *et al.*, 2009) environments. Depositional processes by meltwater flows released at the grounding line of the glacier can be explained with the plane-wall jet flow model, with the basin floor acting as the basal boundary of the flow (Powell, 1990; Gorrell & Shaw, 1991; Russell & Arnott, 2003; Russell *et al.*, 2007). Typically, jet flows and their deposits can be subdivided into three zones: (i) zone of flow establishment (ZFE), (ii) zone of flow transition (ZFT) and (iii) zone of established flow (ZEF; Bates, 1953; Powell, 1990; Russell & Arnott, 2003). Within initially supercritical jets, a hydraulic jump associated with rapid deceleration occurs in the ZFT, while entrainment of ambient water will be highest within the supercritical jet region (Rajaratnam & Subramanyam, 1986; Russell & Arnott, 2003).

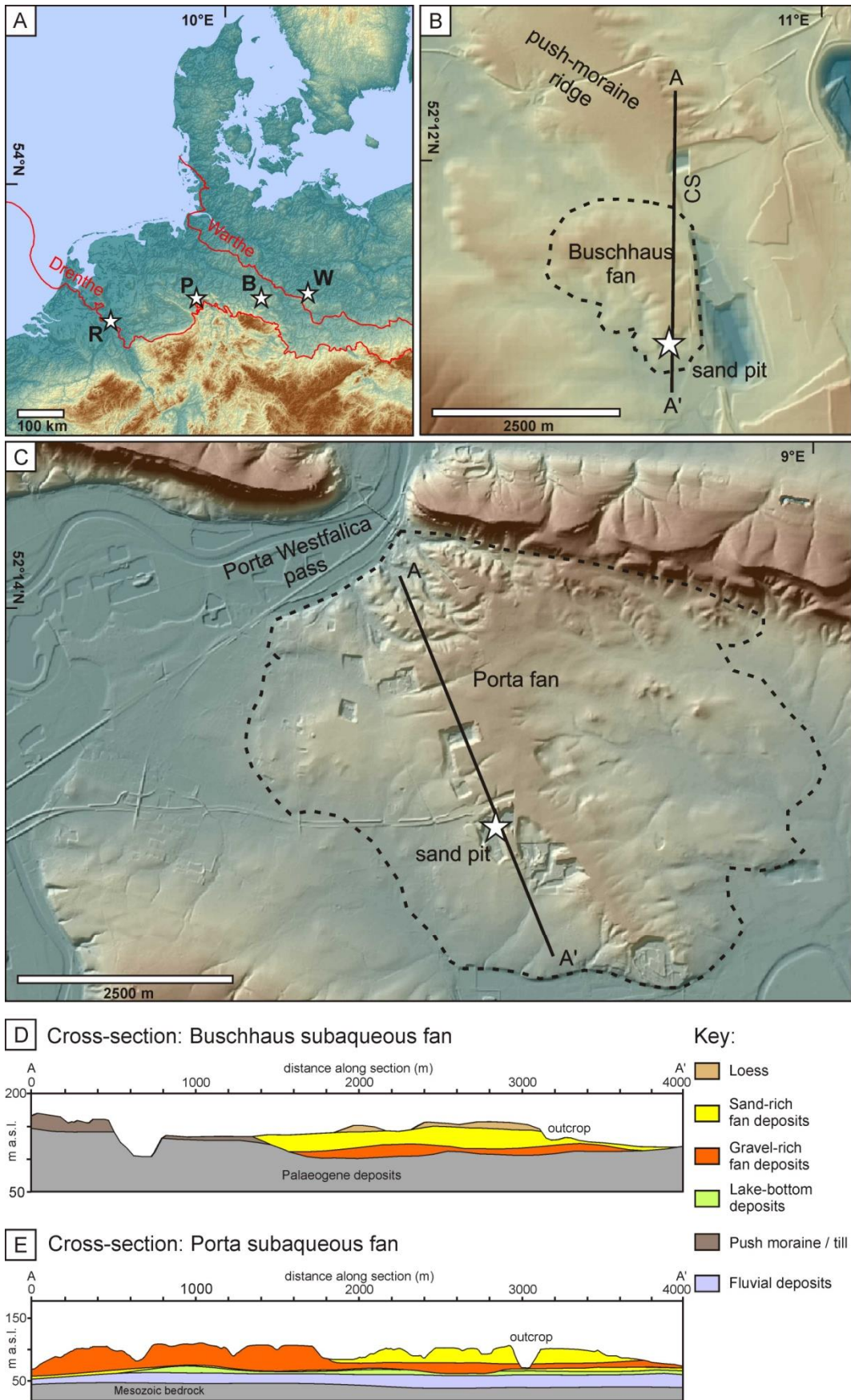


Fig. 1 (previous page): **A**) Overview map of the study area, showing the maximum extent of the Older Saalian Drenthe and Younger Saalian Warthe ice advances (modified after Ehlers *et al.*, 2011). White stars indicate the locations of the studied outcrops (**B**: Buschhaus; **P**: Porta; **R**: Reichswald; **W**: Wollin). **B**) Hill-shaded relief model of the Buschhaus fan (dashed black line), showing the location of the outcrop. The digital elevation model (DEM) is based on data from the Landesamt für Geoinformation und Landentwicklung Niedersachsen (LGLN). **C**) Hill-shaded relief model of the Porta fan (dashed black line), showing the location of the outcrop. The DEM is based on data from the Bezirksregierung Köln. **D**) 2D cross-section of the Buschhaus fan. Palaeoflow is to the SSW. For location see Fig. 1B (A-A \emptyset). **E**) 2D cross-section of the Porta fan complex. Palaeoflow is approximately to the south (Winsemann *et al.*, 2009). For location see Fig. 1C (A-A \emptyset). The cross-sections are extracted from 3D subsurface models of the subaqueous fans, which are based on the available borehole data.

Porta subaqueous fan

The Porta subaqueous fan and delta complex (Fig. 1A, C) was deposited on a flat lake-bottom surface at the margin of the retreating Saalian Drenthe ice sheet. The 600 m wide Porta Westfalica pass at the northwestern margin of the fan acted as a bedrock feeder channel (Winsemann *et al.*, 2009). The northernmost fan complex is up to 55 m thick and has a radial shape with a diameter of approximately 6.5 km. The sedimentary facies and large-scale architecture of the fan complex have been studied in detail by Hornung *et al.* (2007) and Winsemann *et al.* (2009) and interpreted as deposited by subcritical and supercritical meltwater jets. Gravel-rich incipient fan deposits are unconformably overlying lake-bottom deposits and are overlain by sand-rich fan deposits (Fig. 1E). New outcrop walls in sand pits (Fig. 1C) provide a three-dimensional, but non-continuous, exposure of the jet-efflux deposits with a length of ~300 m approximately parallel to the main palaeoflow direction and ~350 m across the main palaeoflow direction, which was towards the SSW. The stacking pattern displays a rapid downflow evolution from highly scoured and planar cross-stratified gravel to low-angle cross-stratified sand to trough cross-stratified and climbing-ripple cross-laminated sand.

Buschhaus subaqueous fan

The Buschhaus subaqueous fan (Fig. 1A, B) was deposited in front of a morainal ridge during the glacial retreat of the Saalian Drenthe ice sheet (Duphorn *et al.*, 1974; Look, 1984; Lang *et al.*, 2012b). The fan has a radial diameter of approximately 2.3 km and is up to 50 m thick. Borehole data indicate that gravel-rich deposits of the incipient fan are unconformably overlain by sand-rich fan deposits (Fig. 1D). The subaqueous fan deposits were studied in a sand pit, where a ~25 m thick succession is exposed. The upper ~12 m of the exposed succession display a vertically and laterally highly variable stack of bedforms, including low-angle cross-stratification, inclined-parallel stratification, planar, trough and sigmoidal cross-stratification and climbing-ripple cross-lamination. Beds dip very gently (1-5°) to the south and unconformably overlie large-scale trough cross-stratified gravel of the basal fan deposits. The outcrop walls provide a three-dimensional exposure of the upper section, with walls of ~80 m length parallel to the main palaeoflow direction and ~60 m across the main palaeoflow direction, which was towards the SSW.

Wollin subaqueous fan

The Wollin subaqueous fan was deposited in an ice-marginal setting during the retreat of the Saalian Warthe ice sheet (Ziermann, 1987; Lippstreu, 1995). The sand-rich subaqueous fan deposits have a total thickness of ~35 m and are interbedded with fine-grained glacialacustrine deposits (Ziermann, 1987). The subaqueous fan deposits were studied in a sand pit near Wollin (Fig. 1A), where ~10 m thick deposits are exposed, overlain by a glacialacustrine delta and till. The exposed subaqueous fan deposits consist mainly of sinusoidal stratified, well-sorted, fine-grained sand with intercalated low-angle cross-stratified and trough cross-stratified sand. The outcrop wall provided a ~60 m long section oblique to the main palaeoflow direction, which was towards the SSW.

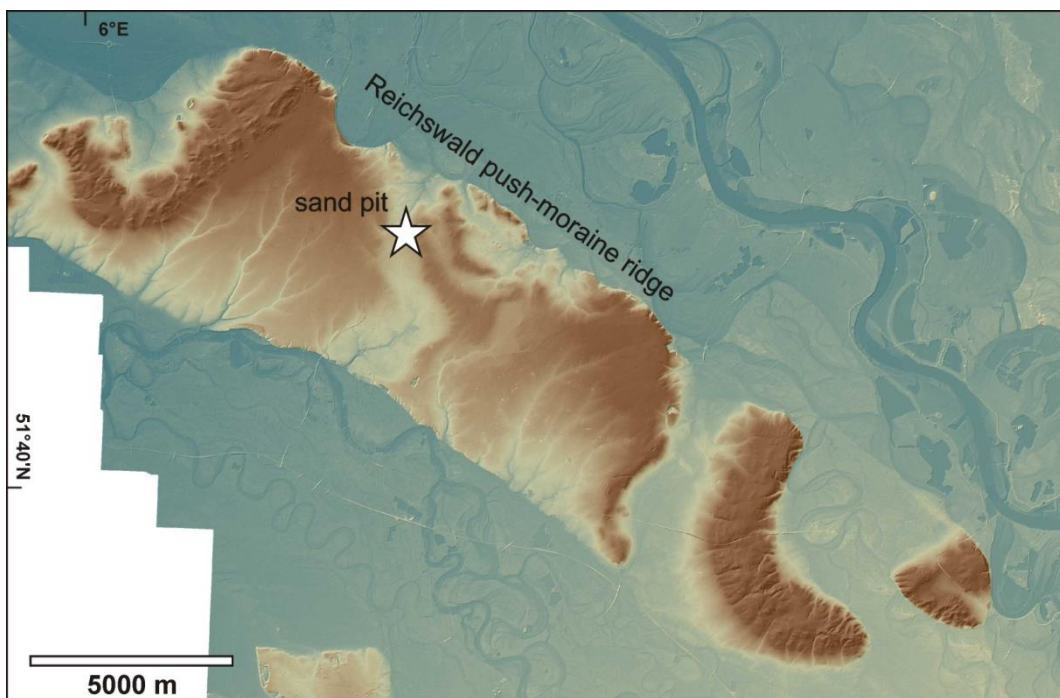


Fig. 2: Hill-shaded relief model of the Reichswald push-moraine ridge, showing the location of the outcrop. The DEM is based on data from the Bezirksregierung Köln.

Glacial lake-outburst flood deposits

Glacial lake-outburst flood deposits were studied at the Reichswald push-moraine ridge, which forms part of a large northwest-southeast trending system of push moraines in the Lower Rhine Embayment and the Netherlands (Klostermann, 1992a, b; Busschers *et al.*, 2008; Skupin & Zandstra, 2010; Figs. 1A, 2). The push-moraine complex of the Lower Rhine Embayment was probably dissected by Middle Pleistocene (Saalian Drenthe) glacial lake-outburst floods (Meinsen *et al.*, 2011; Fig. 2). In the lee of the Reichswald push moraine ridge sand- and gravel-rich sediments, which were partly deposited by the glacial lake-outburst floods, form a gently southwestward dipping ramp. Superimposed dry channels on top and in the lee of the push-moraine ridge can still be observed in the modern topography.

The studied outcrop section is located within one of these large dry channels (Fig. 2). The channel is slightly sinuous and widens downflow from 1 km in the north to 2.8 km in the southwest. The channel floor lies 10-15 m deeper than the surrounding surface. The studied ~ 15 m thick succession is exposed in a sand pit, which is located at the inner side of a channel bend (Fig. 2). The outcrop walls provided discontinuous sections oblique to main the palaeoflow direction, which was towards the southwest.

Sedimentary facies and depositional geometries

Bedform geometries and lateral and vertical facies transitions have been mapped in detail from four outcrops, exposing subaqueous fan deposits (Buschhaus, Porta and Wollin) and glacial lake-outburst flood deposits (Reichswald). The bed geometries, sedimentary structures and dimensions of the individual sedimentary facies are summarised in Table 1 and illustrated in Figs. 3-8. The deposits include lenticular and sheet-like bedforms and are characterised by thin- to thick-bedded, low-angle cross-stratified, sigmoidal cross-stratified and subhorizontally stratified gravel, pebbly sand and fine- to coarse-grained sand. Individual laminae are 0.2 to 1 cm thick and normally graded or, less common, inversely graded. Dip directions are multidirectional, both foresets and backsets occur. Internal contacts commonly display low-angle truncations ($<10^\circ$). Basal bed contacts are mostly erosional. Internally, the facies can be subdivided based on the external geometry of the beds and the internal stratification pattern (Table 1; Figs. 3-5). A noteworthy observation is the absence of planar-parallel stratification in all studied outcrop sections.

Discrimination between the various geometries observed in the studied successions is in general based on sections oriented approximately parallel to the main palaeoflow direction. In all studied successions the main palaeoflow direction could be determined from the dip directions of the foresets of dunes and ripples. The determination of the main palaeoflow direction allows foresets and backsets to be distinguished.

The stacking pattern of the studied successions is interpreted in terms of spatial and temporal changes of the flow conditions. The terminology for the changing flow conditions is adopted from Kneller (1995).

Subaqueous fan deposits

Description

Deposits of upflow migrating (Facies 2.1; Fig. 3I, J) and stationary antidunes (Facies 2.2; Fig. 4) form laterally extensive sheet-like undulating beds, which dominate the large-scale architecture of the mid-fan successions. The exposed up to 15 m thick deposits display 1-4 m thick thinning-upwards pack-

Table 1: Description and interpretation of the sedimentary facies.

Lenticular bedforms

Facies 1.1 Gently dipping concave backsets

Description (in flow geometry)	Across flow geometry	Dimensions	Interpretation
Shallow troughs infilled by gently dipping concave-up backsets. Backsets are downflow divergent. The backset dip steepens downflow. The basal bed contact is erosional. A thin (1-10 cm) base-concordant massive layer, containing the coarser-grained clasts, may cover the base of the trough.	Subhorizontal stratification with low-angle truncations and wide concave-up trough-fills.	Lateral extent (l): 2-13 m Thickness (D): 0.1-0.4 m Dip: 5-10° (backsets) Aspect ratio D/l: 0.04	Deposition by cyclic steps (Kostic & Parker, 2006; Spinewine <i>et al.</i> , 2009; Cartigny <i>et al.</i> , 2011, <i>in press</i> ; Muto <i>et al.</i> , 2012). The troughs are scoured just upflow of steadily upflow migrating hydraulic jumps (Kostic & Parker, 2006; Cartigny <i>et al.</i> , 2011). The gently dipping backsets are deposited downflow of a hydraulic jump (Cartigny <i>et al.</i> , <i>in press</i>). Supercritical flow is re-established by rapid aggradation lowering the flow depth (Cartigny <i>et al.</i> , <i>in press</i>). Massive basal layers are deposited by liquefied flows or slumps derived from erosion at the upflow end of the trough (Cartigny <i>et al.</i> , <i>in press</i>) or by rapid tractionless sediment fall-out beneath a hydraulic jump (Postma <i>et al.</i> , 2009).

Fig. 8A, B

Facies 1.2 Steeply dipping backsets

Description (in flow geometry)	Across flow geometry	Dimensions	Interpretation
Deep troughs infilled by steeply dipping backsets. Backsets are concave-up or planar and strongly downflow divergent. The basal bed contact is erosional. A thin (1-5 cm) base-concordant massive layer, containing the coarser-grained clasts, may cover the base of the trough.	Concave-up concentric trough-fills.	Lateral extent (l): 0.4-0.8 m Depth (D): 0.2-0.3 m Dip: 10-20° (backsets) Aspect ratio D/l: 0.4	Deposits of chutes-and-pools (Schmincke <i>et al.</i> , 1973; Fralick, 1999; Fielding, 2006; Duller <i>et al.</i> , 2008) or highly aggradational cyclic steps (Cartigny <i>et al.</i> , <i>in press</i>). The deep troughs are scoured just upflow of temporarily stationary hydraulic jumps; backsets are subsequently deposited on the stoss-slope of the trough (Alexander <i>et al.</i> , 2001; Duller <i>et al.</i> , 2008). The coarse-grained basal layers within the troughs point to rapid suspension fall-out downflow of the hydraulic jump (Alexander <i>et al.</i> , 2001).

Fig. 3C

Facies 1.3 Gently dipping concave- to convex-up foresets and concentric trough-fills

Description (in flow geometry)	Across flow geometry	Dimensions	Interpretation
Troughs infilled by convex-up or concave-up foresets or by concave-up concentric base-parallel laminae. Downflow transitions from concave-up into convex-up foreset geometries are common. The basal bed contact is erosional. Downflow dipping, convex-up foresets may resemble sigmoidal foresets but can be distinguished by the more gentle dip.	Concave-up concentric trough-fills.	Lateral extent (l): 0.5-4 m Depth (D): 0.3-1.2 m Dip: 10-15° (foresets) Aspect ratio D/l: 0.5	Deposition by chutes-and-pools and breaking, unstable antidunes (Schmincke, 1973; Fielding, 2006; Duller <i>et al.</i> , 2008; Cartigny <i>et al.</i> , <i>in press</i>). Troughs are scoured upflow of the hydraulic jump of chutes-and-pools or by the breaking antidune wave (Alexander <i>et al.</i> , 2001; Duller <i>et al.</i> , 2008). Deposition occurs in the central portion of the trough immediately behind the hydraulic jump or after antidune wave breaking, respectively (Alexander <i>et al.</i> , 2001; Duller <i>et al.</i> , 2008; Cartigny <i>et al.</i> , <i>in press</i>).

Fig. 3D, E, F

Sheet-like bedforms

Facies 2.1 Gently dipping foresets or backsets

Description (in flow geometry)	Across flow geometry	Dimensions	Interpretation
Gently upflow or downflow dipping foresets and backsets. Internal laminae are upflow divergent, which is commonly associated with an upflow increase in bed thickness. Individual laminae display planar, concave-up or convex-up geometries. The basal bed contact is erosional and planar. Internal low-angle (<10°) truncations are common.	Wide concave-up lens-fills.	Lateral extent (l): 0.5-2 m Thickness (D): 0.3-1 m Dip: 5-15° (foresets / backsets)	Deposition by breaking and upflow migrating antidunes (Fielding, 2006; Duller <i>et al.</i> , 2008). Backsets represent deposition on the stoss-side of the antidune, while foresets represent settling on the lee-side of the next downflow antidune (Cartigny <i>et al.</i> , <i>in press</i>). The lee-side deposits are commonly eroded during upflow migration and wave-breaking (Kennedy, 1963; Alexander <i>et al.</i> , 2001).

Fig. 3G, H, I, J

Table 1 (continued)

Facies 2.2 Sinusoidal-stratified waveforms

Description (in flow geometry)	Across flow geometry	Dimensions	Interpretation
<p>Symmetrical low amplitude sinusoidal-stratified waveforms, which can be traced along outcrops for up to 40 m. Laterally, the thickness pinches and swells slightly due to converging and diverging stratification. Internal low-angle truncations are common. The basal bed contacts are erosional or sharp and planar. The wavelength and amplitude commonly decrease downflow. Vertically, the crests of the waveforms are symmetrically in-phase stacked.</p> <p>Commonly occurring parallel to flow concave- or convex-up bedforms (1.2-8 m wide) most probably represent remnants of eroded waveforms. Locally, divergent stratification was observed at the lee-side of the waveforms.</p>	<p>Wide (3-13 m) concave-up or convex-up lenticular and subhorizontal undulating sheet like geometries.</p>	<p>Lateral extent (l): 7-40 m</p> <p>Thickness (D): 0.5-1.2 m</p> <p>Wavelength (L): 1.2-12 m</p> <p>Amplitude (y): 0.1-0.7 m</p> <p>Wave steepness (y/L): 0.05</p>	<p>Deposition by aggrading stationary antidunes, requiring quasi-steady supercritical flows, which allowed for the preservation of both stoss- and lee-sides of the in-phase waves (Cheel, 1990; Brennand, 1994; Russell & Arnett, 2003; Ito & Saito, 2006; Duller <i>et al.</i>, 2008; Ito, 2010). The in-phase relationship between flow and bedforms is caused by the variation of the boundary shear stress in the flow, which is highest beneath the wave crests and lowest beneath the wave troughs (Chanson, 2000). A prolonged period of high rates of aggradation is required (Middleton, 1965; Allen, 1984), although aggradation is non-continuous, as indicated by internal erosional contacts (Duller <i>et al.</i>, 2008). Downflow divergent stratification points to a transition towards downflow migrating antidunes (Ito, 2010).</p>

Fig. 4A, B, C, D

Facies 2.3 Sigmoidal foresets

Description (in flow geometry)	Across flow geometry	Dimensions	Interpretation
<p>Sigmoidal downflow divergent cross-sets, which display differentiation into topset, foreset and bottomset laminae. Topset laminae are thin (<0.2 m), relatively fine-grained and subhorizontal. The coarsest grains are located just below the brink separating topsets and foresets or above the foreset-bottomset-transition. The foresets are either parallel or divergent and may be planar, concave- or convex-up. The transition between topsets and foresets displays variable brink trajectories. Climbing brink trajectories are usually associated with strongly divergent foresets, while horizontal or falling brink trajectories are associated with rather parallel foresets. The bottomset laminae are parallel and relatively fine-grained. The contact of the bottomsets with the basal bed boundary is tangential. The basal contact is sharp or erosional. Sigmoidal cross-sets in-filling troughs tend to have falling brink trajectories.</p>	<p>Subhorizontal to concave-up sheet-like or lenticular geometries.</p>	<p>Lateral extent (l): 0.5-25 m</p> <p>Thickness (D): 0.1-2 m</p> <p>Dip: 15-35° (foresets)</p>	<p>Deposition by humpback dunes, representing transitional bedforms between lower and upper flow-regime conditions, occurs when the Froude number is close to unity and rates of deposition are high (Saunderson & Lockett, 1983; Chakraborty & Bose, 1992; Fielding & Webb, 1996; Fielding, 2006). Different trajectories of the topset-foreset-transition point to different rates of deposition. Climbing or horizontal brink trajectories indicate the highest rates of deposition, forming geometries comparable to climbing dunes or ripples. Falling brink trajectories are commonly related to the filling of troughs.</p>

Fig. 5A, B, C, D, E, F

ages comprising aggrading antidune deposits, which can be traced for up to 60 m in flow direction, corresponding to the total width of the outcrop sections (Figs. 6, 7). Within the antidune packages individual beds have erosional contacts, causing internal low-angle truncations, which may be laterally discontinuous (e.g., Fig. 7D). Perpendicular to the palaeoflow direction, the antidune packages have more lenticular geometries and the lateral extent is typically limited to 3-15 m (Fig. 6B). The stationary antidune packages are separated by erosionally based sheet-like or lenticular beds. Sheet-like beds

comprise deposits of humpback dunes (Facies 2.3; Fig. 5), are up to 2 m thick and can be laterally traced for up to 25 m (Figs. 6A, 7A). Deposits of humpback dunes are typically restricted to single beds that are enclosed between deposits of stationary antidunes. Gradual facies transitions were observed between deposits of stationary antidunes and humpback dunes (Figs. 5-7). Humpback dunes commonly flatten-out upwards and evolve into sinusoidal stratified deposits of aggrading antidunes. The same transition occurs in downflow direction, where convex-up cores of antidunes were observed to form 1-2 m downflow of the foreset-bottomset-transition of humpback dunes (Fig. 5F). Locally, extremely steeply dipping (70-90°) humpback dune foresets and (recumbent) folding of the foresets were observed (Fig. 5C).

Erosionally based lenticular beds are infilled by deposits of chutes-and-pools and breaking antidunes (Facies 1.2, 1.3) or by deposits of 3D dunes, depending on the position within the succession (Fig. 7). Troughs infilled with deposits of chutes-and-pools and breaking antidunes are more common in more proximal and stratigraphically lower parts of the successions (Fig. 7A), while 3D dunes are more common in distal settings and the upper parts of the succession (Fig. 7). Individual troughs are 0.15-0.75 m deep and up to 4 m wide. Troughs infilled by deposits of chutes-and-pools and breaking antidunes usually form isolated features. Troughs infilled by deposits of 3D dunes may occur as isolated features or form multi-laterally offset stacked nested successions that are up to 3 m deep and up to 15 m wide. Vertical alternation between deposits of stationary antidunes and 3D dunes may be very rapid and occurs also on the scale of individual beds (Figs. 9, 10D, E). The subaqueous fan successions typically display an increasing proportion of deposits of 3D dunes towards the tops of the successions (Fig. 10F). Climbing ripple cross-laminated sand was observed as infill of up to 4 m wide and 2.5 m deep troughs or as up to 0.75 m thick sheets, draping remnant topographies, within the subaqueous fan successions (Fig. 10G).

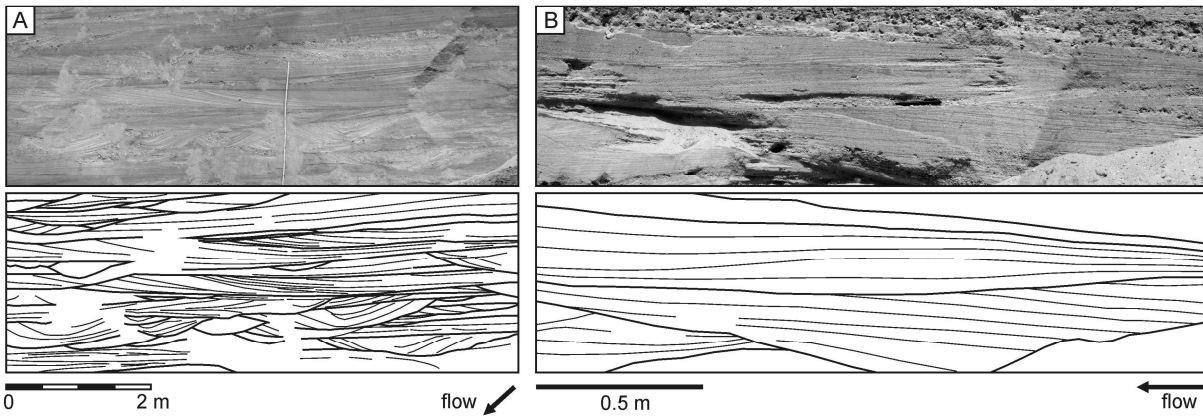
At the Porta and Buschhaus fans the studied sandy bedforms unconformably overly highly scoured massive, planar cross-stratified and subhorizontally stratified gravel (Fig. 10A, B). At the Porta fan a lateral transition from sandy into gravelly bedforms can be observed approximately 200-300 m upflow of the studied outcrops (Fig. 10C).

Interpretation

The stacking pattern of the subaqueous fan successions is controlled by the large-scale downflow evolution (Fig. 11A) and small-scale spatial and temporal fluctuations of the flow conditions (Fig. 11B). The vertical trends observed at the Porta and Buschhaus fans indicate a transition from gravelly incipient fan deposits of the proximal zone of flow transition to sandy deposits of the distal zone of flow transition, pointing to deposition by overall waning flows. The large-scale lateral trend observed at the Porta fan is interpreted as representing deposition by depletive flows. Depletive flow conditions were caused by the rapid expansion and deceleration of the meltwater jet flows downflow of the meltwater conduits.

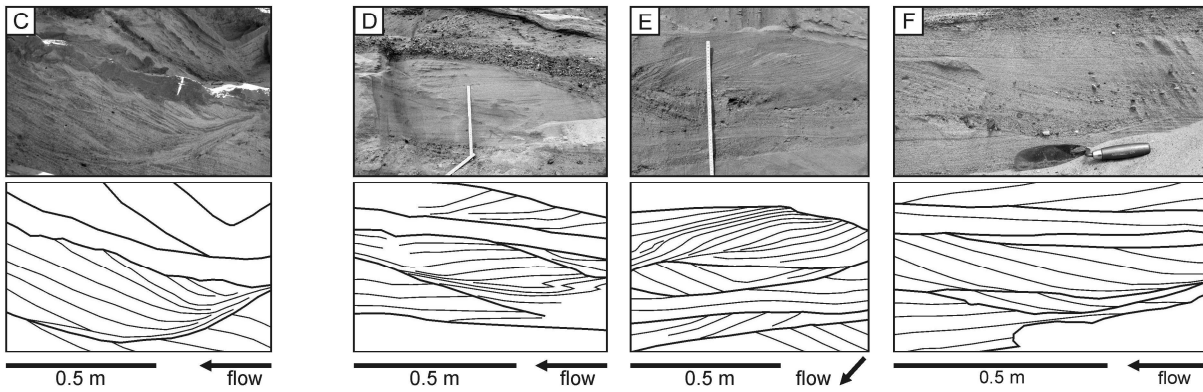
1. Lenticular bedforms

Facies 1.1 Gently dipping backsets:
deposits of cyclic steps with lower aggradation rates



Facies 1.2 Steeply dipping backsets:
deposits of chutes-and-pools
or highly aggradational cyclic steps

Facies 1.3 Gently dipping concave-up to convex-up foresets / concentric trough-fills:
deposits of chutes-and-pools and breaking antidunes



2. Sheet-like bedforms

Facies 2.1 Gently dipping foresets and backsets:
deposits of breaking and upflow migrating antidunes

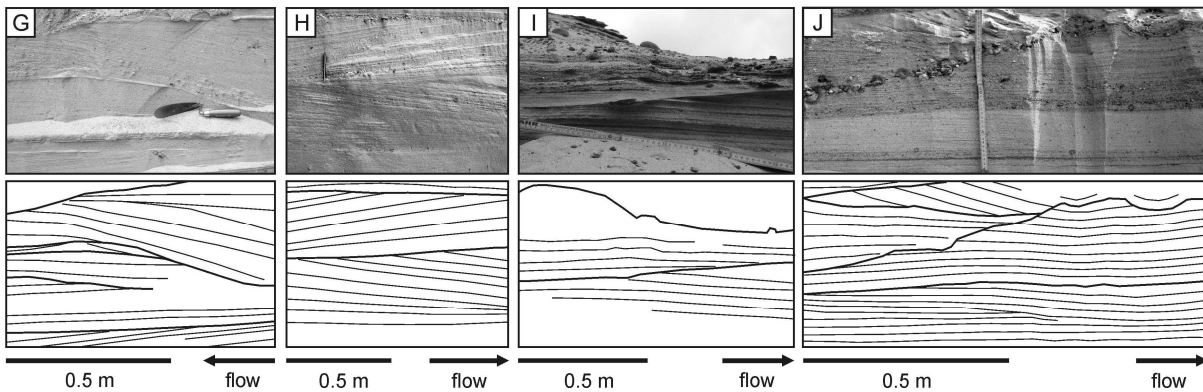


Fig. 3: Photos and line drawings illustrating the internal geometries of the sedimentary facies. **A)** Wide lenticular scour-fills (4 sets) infilled with gently dipping backsets interpreted as cyclic step deposits, overlying chute-and-pool deposits (Reichswald). **B)** Cyclic step deposits characterised by gently dipping backsets infilling lenticular scours (Reichswald). **C)** Steeply dipping backsets, interpreted as chute-and-pool deposit (Porta fan). **D)** Lens-fills with gently dipping concave- to convex-up foresets are interpreted as chute-and-pool deposit incised into deposits of stationary antidunes (Buschhaus fan). **E)** Gently dipping concave- to convex-up foresets interpreted as chute-and-pool deposit, overlying concentric trough-fills of breaking antidunes (Buschhaus fan). **F)** Concentric trough-fill, unconformably overlain by gently dipping concave-up backsets interpreted as breaking antidune deposit (Buschhaus fan). **G)** Gently dipping planar fore- and backsets interpreted as deposits of breaking antidunes. Internal truncations indicate repeated wave breaking (Buschhaus fan). **H)** Gently dipping fore- and backsets interpreted as breaking antidune deposits (Reichswald). **I)** Erosional truncation between antidune sets (Porta fan). **J)** Pebble-gravel covered erosional truncation between antidune sets, interpreted as drop-out armour (Buschhaus fan). The clasts represent the coarsest grain-sizes that can be transported as bedload (Foley, 1977).

2. Sheet-like beds (continued)

Facies 2.2 Sinusoidal waveforms:
deposits of aggrading stationary antidunes

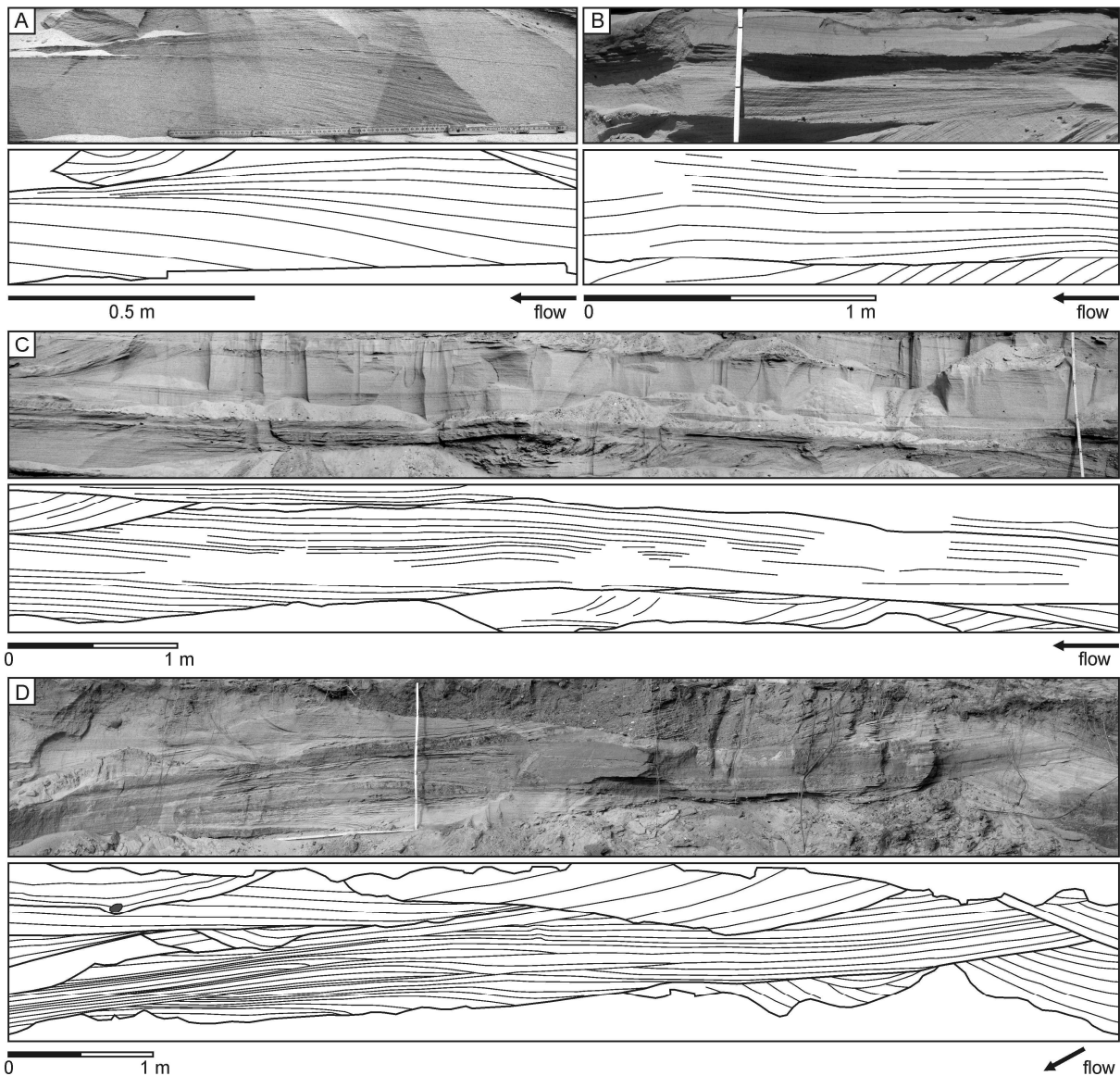


Fig. 4: Photos and line drawings illustrating the internal geometries of the sedimentary facies. **A)** Upflow divergent stratification, interpreted as aggrading antidune deposit (Buschhaus fan). **B)** Downflow divergent stratification, interpreted as aggrading antidune deposit (Buschhaus fan). **C)** Aggrading antidune deposits consisting of fine- to medium-grained sand, unconformably overlying trough cross-stratified pebbly sand (Buschhaus fan). The wavelength is ~ 3 m; the amplitude is 0.1 m. **D)** Aggrading antidune deposits with a wavelength of ~ 5.6 m and amplitude of 0.1 m. The left part of the waveform displays increasingly downflow divergent lamination, which is interpreted as representing downflow migration of the bedform. The antidune deposits are overlain by remnants of another aggrading antidune (upper left) and 3D dunes (Porta fan).

The laterally extensive stationary antidune deposits (Table 1) represent phases of sustained quasi-steady flows under highly aggradational conditions. However, aggradation was non-continuous, because internal erosional contacts point to recurring phases of erosion and deposition during bedform aggradation. The lower across flow extent of the stationary antidune deposits is interpreted as related to the three-dimensional geometry of antidune waves and their deposits (Spinewine *et al.*, 2009; Yokokawa *et al.*, 2010) or may be caused by the channelization of flows into topographically lower areas.

2. Sheet-like beds (continued)

Facies 2.3 Sigmoidal foresets:
deposits of humpback dunes

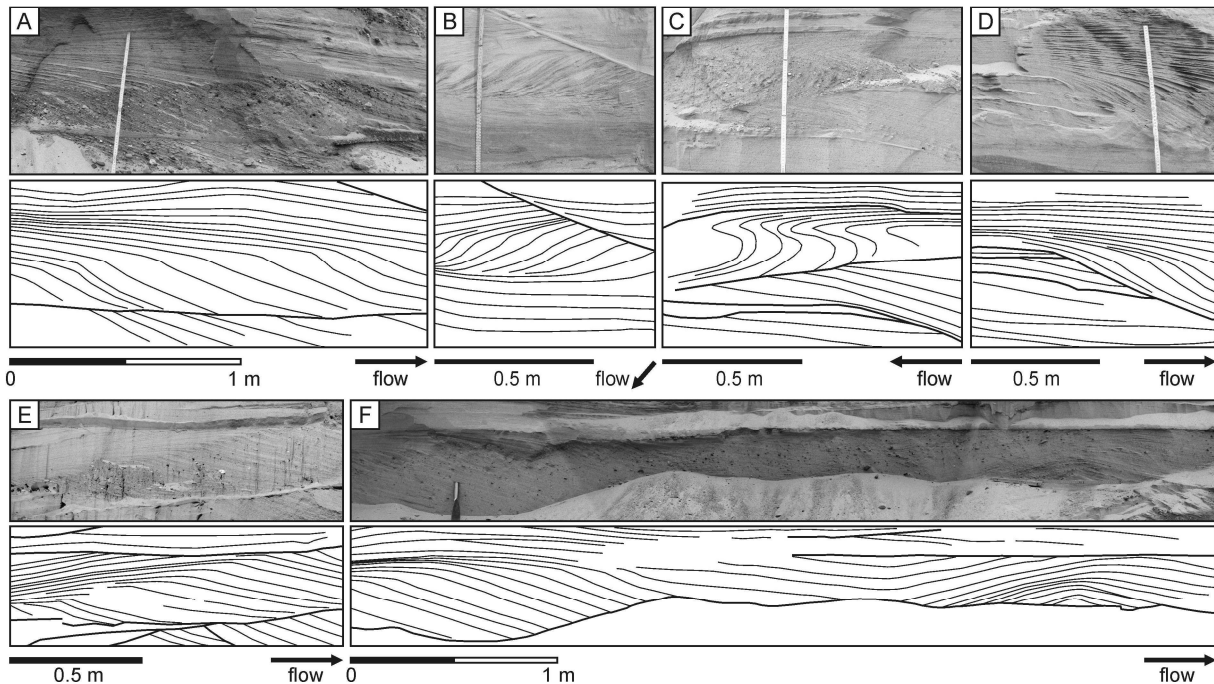


Fig. 5: Photos and line drawings illustrating internal geometries of the sedimentary facies. **A)** Humpback dune with downflow dipping topsets and subhorizontal brink trajectory (Porta fan). Upwards, the humpback dune evolves into aggrading antidune deposits with a wavelength of ~ 0.8 m. **B)** Transition from low-angle cross-stratification (antidune deposit) into a humpback dune, evolving upwards into antidune low-angle cross-stratification (Buschhaus fan). **C)** Humpback dune with foresets displaying recumbent folding due to liquefaction and current drag (Buschhaus fan). **D)** Humpback dune with horizontal topsets and falling brink trajectory infilling an erosional trough (Buschhaus fan). **E)** Humpback dune with upflow dipping topsets and climbing brink geometry (Porta fan). **F)** Transition from humpback dune geometry into convex-up geometry, interpreted as initial growth of an antidune (Porta fan). The humpback dune displays upflow dipping topsets and subhorizontal brink trajectory. The humpback dune is overlain by aggrading antidune deposits with a wavelength of ~ 1 m.

The aggrading stationary antidunes are separated by deposits of either higher-energy supercritical flows, as chutes-and-pools and breaking antidunes, or lower-energy subcritical flows, as humpback dunes, 3D dunes and climbing ripples (Table 1). Both types of flows tend to rework the stationary antidune deposits. Isolated intercalations of chute-and-pool and breaking antidune deposits point to phases of fluctuating flow conditions. The formation of chutes-and-pools and breaking antidunes is interpreted as related to waxing flow conditions due to fluctuating discharge. Waxing flow conditions will allow for antidune wave breaking or the occurrence of localised hydraulic jumps by raising the Froude number and causing the flow to become unstable, resulting in the formation of breaking antidunes and chutes-and-pools (Alexander *et al.*, 2001; Cartigny *et al.*, *in press*). Subsequent waning flow conditions will re-establish flow conditions in the range conducive to the formation of stationary antidunes (Fig. 13B).

The close association of laterally extensive stationary antidune deposits and humpback dunes seems to be a typical feature of the zone of flow transition of subaqueous ice-contact fan deposits. The upward flattening and gradual transition of humpback dunes into upper stage plane beds or antidunes is con-

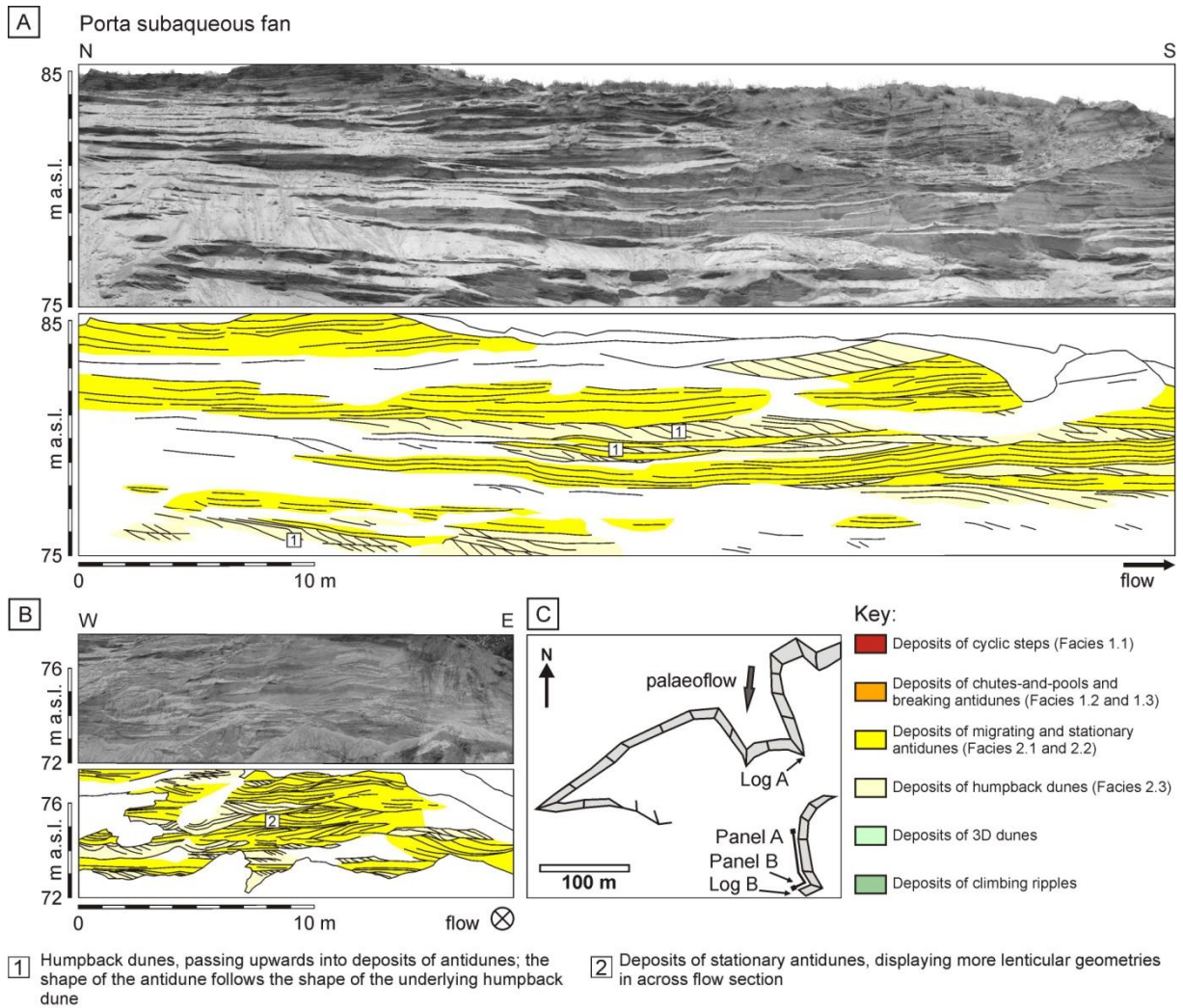


Fig. 6: Photo panels of the Porta fan. The arrows indicate the mean palaeoflow direction towards SSW. Both panels are separated by a ~5 m gap due to outcrop conditions. **A)** Section in flow direction. **B)** Across flow section. **C)** Sketch of the outcrop section, indicating the locations of the logs and panels.

sidered a characteristic feature of humpback dunes deposited by waxing flows attaining supercritical flow conditions (Røe, 1987; Chakraborty & Bose, 1992; Fielding, 2006; Ghienne *et al.*, 2010; Hirst, 2012). The observed oversteepened foresets and recumbent folds in the studied outcrops are interpreted to represent deformation caused by liquefaction (Lowe, 1975; Owen, 1996) and current drag applied over the surface of humpback dunes (Røe & Hermansen, 2006). Liquefaction is facilitated by the differential turbulence pattern and pressure fluctuations in flows approaching supercritical conditions (Røe & Hermansen, 2006).

Migrating 3D dunes are deposited by subcritical flows that rework any underlying deposits as is indicated by the erosional bed contacts. Climbing ripple successions represent lower flow stages and high rates of sedimentation from suspension during phases of reduced discharge.

The coarse-grained deposits of the proximal zone of flow transition have previously been interpreted as large scour-fills (Hornung *et al.*, 2007; Winsemann *et al.*, 2009). However, new outcrop sections in

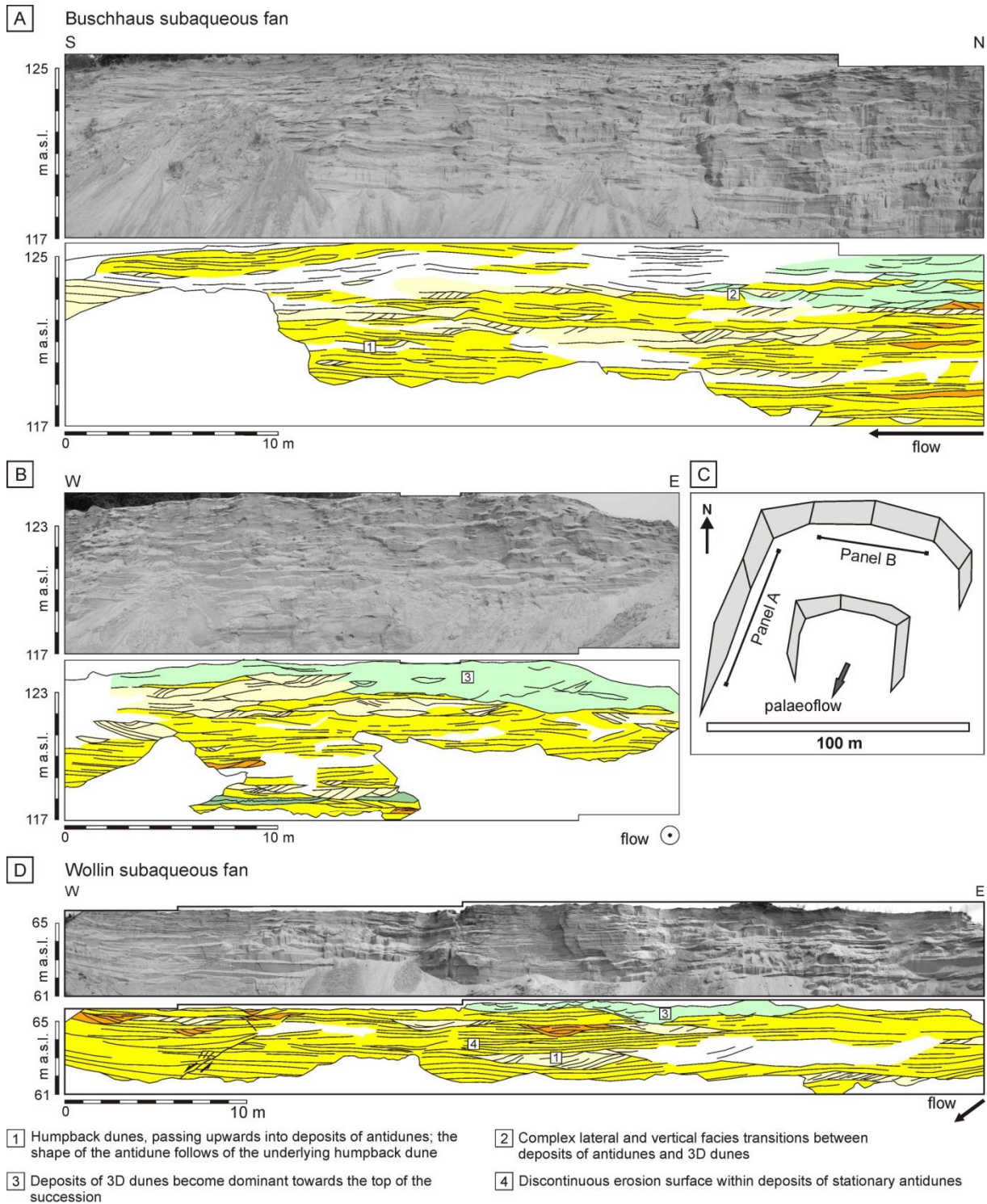


Fig. 7: Photo panels of the Buschhaus and Wollin fans. The arrows indicate the main palaeoflow direction towards SSW. The key for the colour code of the sedimentary facies is given in Fig. 6. **A)** Section of the Buschhaus fan in flow direction. **B)** Across flow section of the Buschhaus fan. Both panels are separated by a ~8 m gap due to outcrop conditions. **C)** Sketch of the outcrop section, indicating the locations of the panels. **D)** Photo panel of the Wollin fan.

the Porta fan indicate that low-angle stratified gravel and lenticular scour-fills (Fig. 10A-C) actually may represent gravel antidunes (cf., Alexander & Fielding, 1997; Duller *et al.*, 2008), which pass downflow into sandy supercritical bedforms (Fig. 11A). The coarse-grained scour-fills with planar and

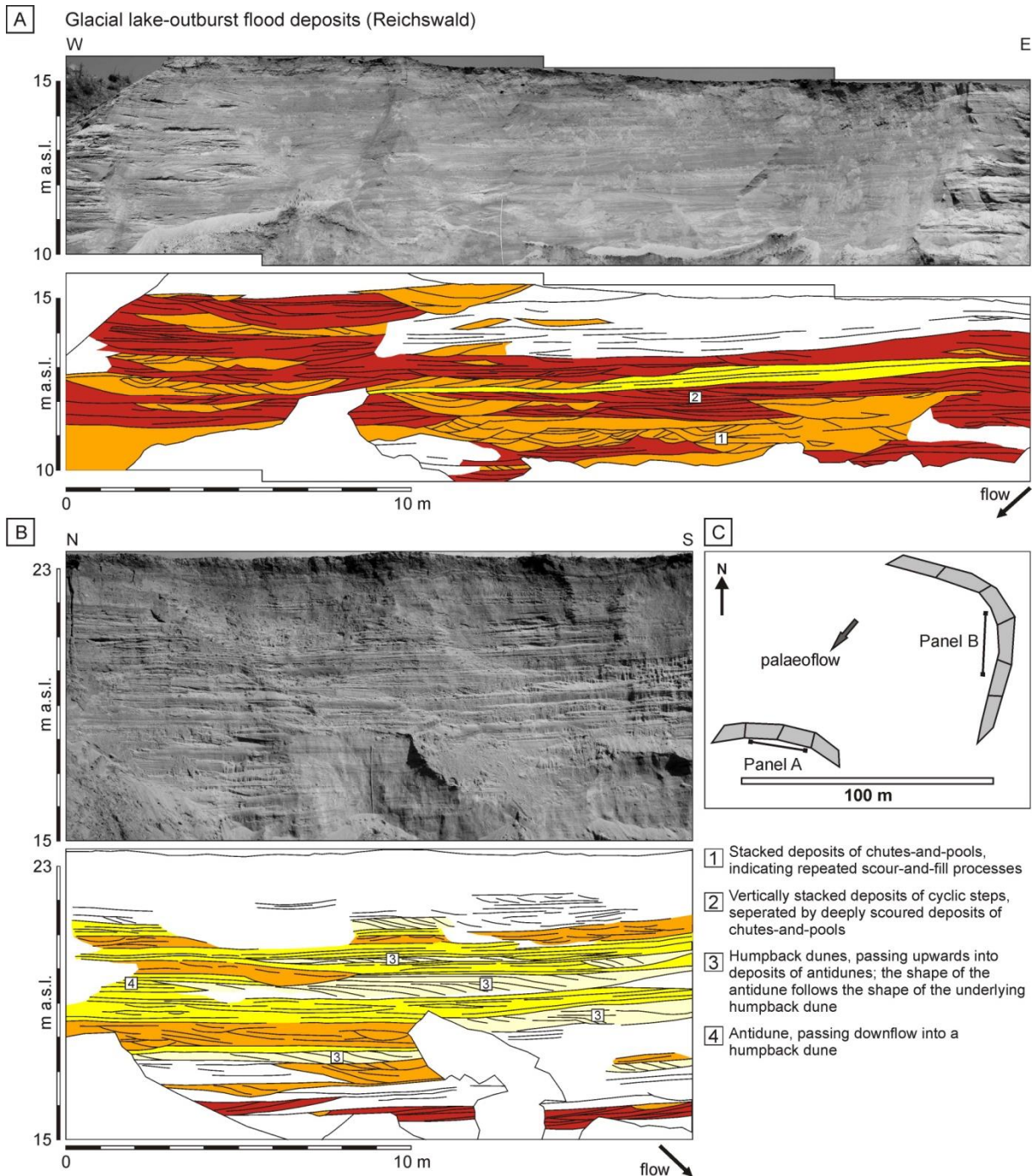


Fig. 8: Photo panels of the glacial lake-outburst flood deposits in the lee of the Reichswald push-moraine ridge. The arrows indicate the mean palaeoflow direction towards the southwest. The key for the colour code of the sedimentary facies is given in Fig. 6. **A)** The lower part of the succession comprises mainly vertically stacked cyclic step and chute-and-pool deposits. **B)** The upper part of the succession comprises deposits of chutes-and-pools, antidunes and hummock dunes. **C)** Sketch of the outcrop section, indicating the locations of the panels.

sigmoidal foresets may be interpreted as a product of downstream migrating antidunes (cf., Duller *et al.*, 2008). The upflow facies transition from sandy stationary antidunes to gravel antidunes would match results from flume experiments (Cartigny *et al.*, *in press*), where the formation of antidunes in coarser-grained sediments requires higher flow velocities.

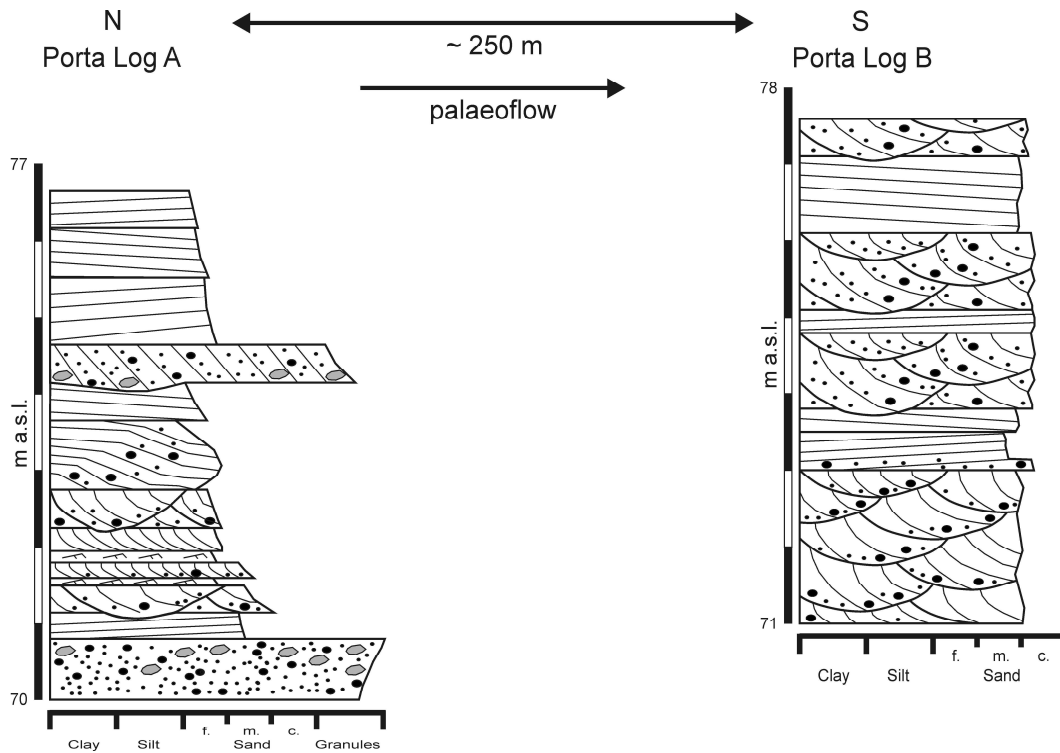


Fig. 9: Rapid vertical and lateral facies changes in the distal zone of flow transition (Porta subaqueous fan). The logs are aligned approximately along the main palaeoflow direction. For locations see Fig. 6C.

Glacial lake-outburst flood deposits

Description

In the lower part of the glacial lake-outburst flood succession deposits of cyclic steps (Facies 1.1; Fig. 3A, B) form up to 13 m wide lenticular beds that truncate each other laterally and vertically (Fig. 8A). The cyclic step deposits are laterally and vertically truncated and unconformably overlain by deposits of chutes-and-pools (Facies 1.2; Fig. 3C) and breaking antidunes (Facies 1.3; Fig. 3D-F). They form wide (>20 m) and thick (~2 m) sets of multi-laterally offset stacked nested erosional troughs (Fig. 8A). In the upper part of the glacial lake-outburst flood succession deposits of chutes-and-pools and breaking antidunes form laterally extensive up to 2.5 m thick bedsets (Fig. 8B), which become thinner and less extensive towards the top of the succession. These deposits are interbedded with deposits of up-flow migrating antidunes (Facies 2.1; Fig. 3G, H), humpback dunes (Facies 2.3; Fig. 5) and 3D dunes in up to 2 m thick sheet-like bedsets. Antidune, humpback dune and 3D dune deposits become more frequent up-section. The deposits of antidunes and humpback dunes commonly display gradual lateral and vertical facies changes (Fig. 8B).

Interpretation

Within the glacial lake-outburst flood deposits the lower part of the succession is dominated by deposits of cyclic steps, which represent the highest-energy deposits being preserved (Table 1). The wide lens-shaped deposits of cyclic steps probably only represent the preserved lower part of the bedforms

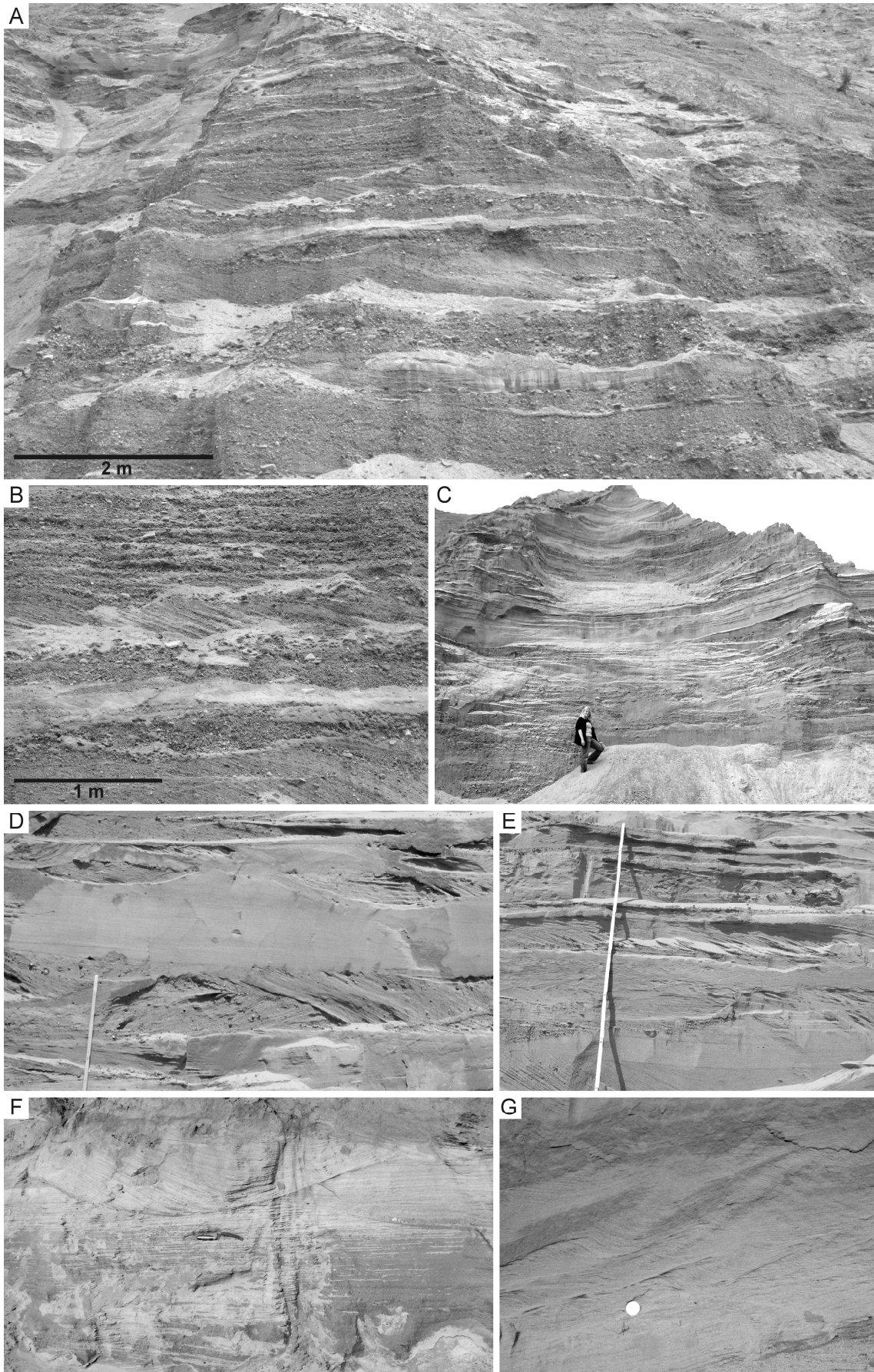


Fig. 10 (previous page): Sedimentary facies and small-scale facies changes of the subaqueous fan successions. **A)** Intensely scoured pebble to cobble gravel, unconformably overlain by planar cross-stratified and low-angle cross-stratified granule to pebble gravel (Porta fan). The lowermost deposits are interpreted as large-scale scour-fills. The overlying planar cross-stratified and low-angle cross-stratified granule to pebble gravel is interpreted as representing gravel antidune deposits. Palaeoflow is towards the left. The outcrop is located approximately 200 m upflow of the studied sandy bedforms. **B)** Low-angle cross-stratified granule to pebble gravel with common low-angle internal truncations, which are interpreted as deposits of gravel antidunes (Porta fan). The gravel antidunes are unconformably overlying planar and trough cross-stratified gravel and pebbly sand interpreted as scour-fills and 3D dunes. Palaeoflow is towards the left. (Photo by B. Garlt) **C)** Low-angle cross-stratified granule to pebble gravel, which is interpreted as a gravelly antidune deposit, passing upwards into low-angle, cross-stratified, pebbly sand deposited by stationary antidunes (Porta fan). The outcrop is located approximately 200-300 m upflow of the studied sandy bedforms. Palaeoflow is towards the left. Person for scale is ~160 cm. **D)** Repeated vertical facies changes between deposits of stationary antidunes and 3D dunes, indicating fluctuating flow conditions (Buschhaus fan). Palaeoflow is towards the observer. **E)** Small-scale vertical facies transition indicating waxing flow conditions (Buschhaus fan). A climbing ripple cross-laminated succession is unconformably overlain by humpback dune deposits, which pass vertically into deposits of stationary antidunes. The antidune deposits are unconformably overlain by small-scale chute-and-pool deposits. Palaeoflow is towards the observer. **F)** Deposits of stationary antidunes are unconformably overlain by 3D dunes, indicating reworking by subcritical flow (Porta fan; trowel for scale is 28 cm). **G)** Thick succession of climbing ripples indicating low flow stages (Porta fan; coin for scale is 26 mm in diameter).

because erosive contacts with overlying deposits indicate partial reworking of the cyclic step deposits. Deposits of chutes-and-pools and breaking antidunes (Table 1) interbedded with the cyclic step deposits point to temporally rapidly changing flow conditions. The nested erosional troughs of the chute-and-pool and antidune deposits point to repeated scour-and-fill processes during their deposition. The dominance of deposits of chutes-and-pools, antidunes, humpback dunes and 3D dunes in the upper part of the glacial lake-outburst flood deposits indicates overall waning flow conditions. The studied succession of glacial lake-outburst flood deposits is thus interpreted as representing one single high-magnitude flood event, which incised the channel into the push-moraine ridge and subsequently deposited a vertical succession related to waning flows (Fig. 12).

Discussion

The sedimentary facies and depositional geometries within the studied outcrop sections point to deposition by aggradational supercritical flows, characterised by rapid flow expansion and deceleration. The observed complex lateral and vertical stacking patterns are interpreted as representing (i) overall waning or depletive flows on a larger scale superimposed by (ii) internal variations of the flow conditions related to pulsating flow due to unstable flow conditions, bed topography and fluctuating discharge.

Cyclic steps

Deposits of cyclic steps were observed in the basal part of the glacial lake-outburst flood succession. Depositional cyclic steps have so far mainly been observed in bathymetric and high-resolution seismic

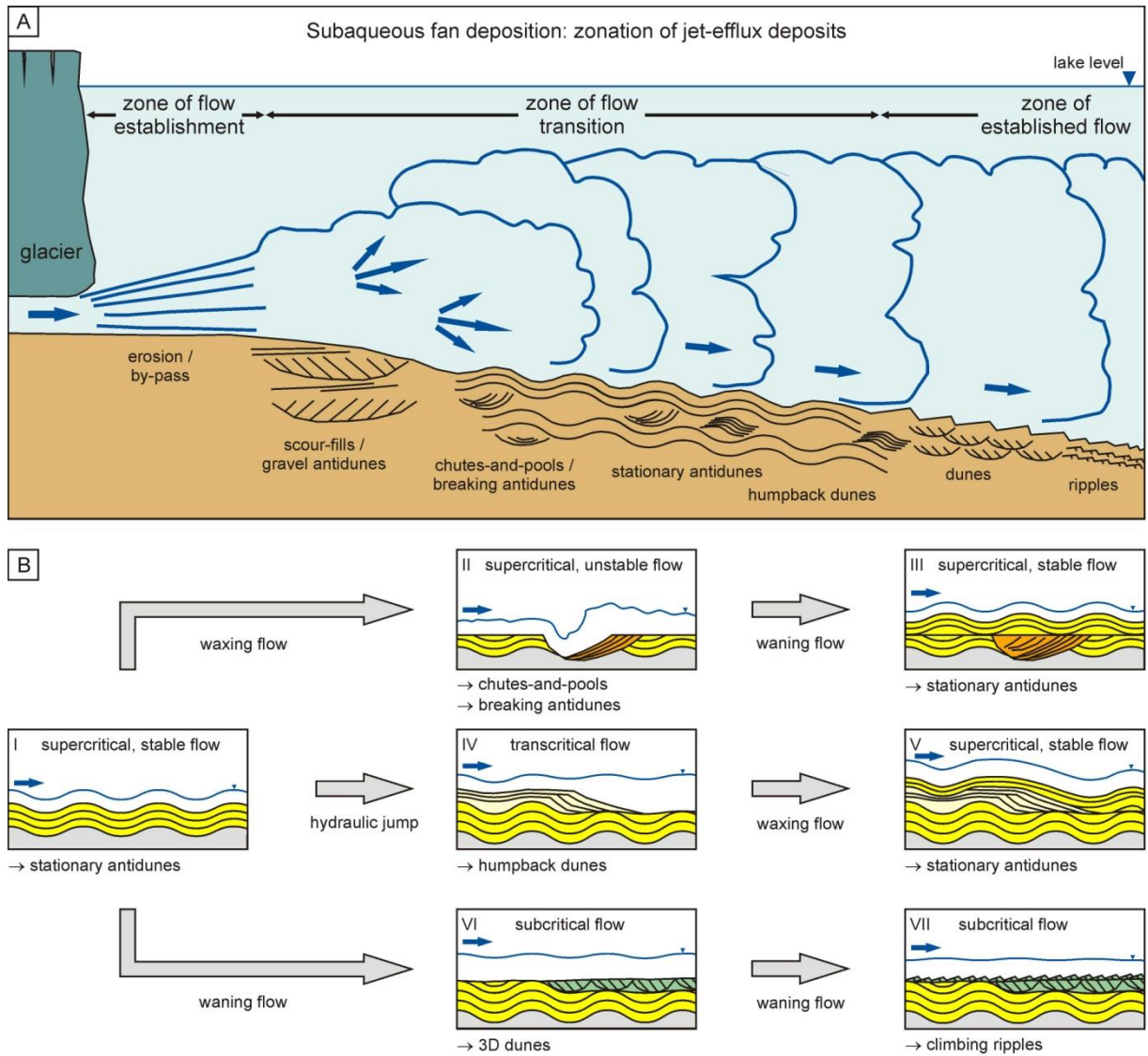


Fig. 11: A) Zonation of the jet-efflux deposits. The figure is not to scale. Coarse-grained scour-fills and gravel antidunes form in the proximal zone of flow transition, passing downflow into chute-and-pools, breaking antidunes and aggrading stationary antidunes. Intercalated deposits of aggrading stationary antidunes and humpback dunes represent deposition by flows fluctuating between super- and transcritical conditions. Dunes and ripples are deposited by subcritical flows in the zone of established flow. **B)** Scheme of possible successions of bedforms within the zone of flow transition of a subaqueous fan. The figures are not to scale. A supercritical relatively stable flow, depositing aggrading stationary antidunes is here considered as the initial flow state (I). Waxing flow conditions will create a more unstable flow, forming breaking antidunes and chutes-and-pools. Waning flows will re-establish aggrading stationary antidunes (II-III). A local hydraulic jump causes the deposition of humpback dunes in the lee of an antidune bedwave. Waxing flow conditions or flow thinning and acceleration will lead to a gradual transition to aggrading stationary antidunes (IV-V). Flow waning leads to reworking of the antidune deposits and deposition of 3D dunes by subcritical flows. Further flow waning causes deposition of climbing ripples (VI-VII). Waning and waxing flow stages are related to fluctuating discharge.

data from deepwater environments such as canyon floors and turbidite systems (Fildani *et al.*, 2006; Lamb *et al.*, 2008; Heiniö & Davies, 2009; Cartigny *et al.*, 2011; Kostic, 2011; Armitage *et al.*, 2012). Field examples of the internal structure of cyclic step deposits are yet only described from deposits of coarse-grained high-density turbidites (Cartigny *et al.*, 2012). The distinction between cyclic steps and

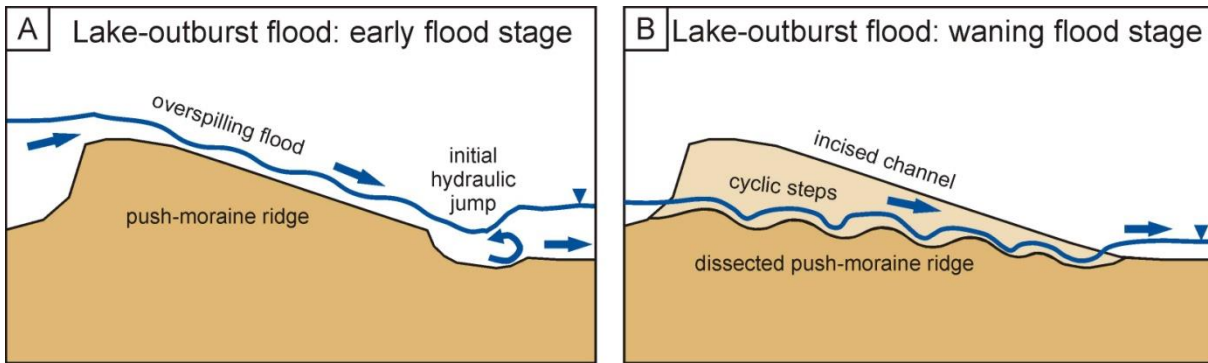


Fig. 12: Dissection of the push-moraine ridge and formation of cyclic steps during the glacial lake-outburst flood. The figures are not to scale. **A)** During the early stage of the outburst flood the flood waters spill completely over the lower reaches of the push moraine ridge. At the lee-side slope break a hydraulic jump occurs and commences to migrate upflow due to lee-side erosion. **B)** During the waning flood stage the hydraulic jump has evolved into a train of cyclic steps. The waning flood waters drain through the incised channel.

chutes-and-pools may be ambiguous because the formative flow conditions and the depositional process are very similar (Taki & Parker, 2005; Kostic *et al.*, 2010; Kostic, 2011; Cartigny *et al.*, *in press*). The aspect ratio of the scour and the backset dip of cyclic steps and chutes-and-pools also depend on the aggradation rate: higher aggradation rates will produce scours with higher aspect ratios and steeper backsets (Cartigny *et al.*, *in press*). Therefore, chutes-and-pools and cyclic steps might be difficult to distinguish in the field. The observed bedforms in the glacial lake outburst-flood succession might either represent deposits of cyclic steps or chutes-and-pools. We distinguished deposits of cyclic steps (Facies 1.1) from those of chutes-and-pools (Facies 1.2, 1.3) on the basis of their lower aspect ratios and less steeply dipping backsets (Table 1), while deposits of chutes-and-pools comprise troughs with higher aspect ratios infilled by steeply dipping backsets, commonly associated with concentric trough-fills and gently dipping convex-up foresets. The main argument is that an increase in the aggradation rate would probably be caused by a decrease in flow velocity and the mobility parameter, leading to the preferred formation of chutes-and-pools.

The flow conditions necessary for the formation of cyclic steps were established when the glacial lake-outburst flood spilled over the push-moraine ridge, resulting in acceleration and thinning of the flow (Fig. 12A). Flow thinning when spilling over topographic obstacles and associated acceleration on the lee-side is a process known for the initiation of cyclic steps by raising the Froude number (Fildani *et al.*, 2006; Spinewine *et al.*, 2009). Cyclic steps developed from hydraulic jumps triggered at the slope-break at the base of the push-moraine ridge and began to incise into the ridge. Flume studies indicate that cyclic steps are initiated by a hydraulic jump at the downflow break of the slope and migrate upslope until they reach the upper slope break, where they vanish and a new hydraulic jump forms at the downslope termination (Taki & Parker, 2005; Spinewine *et al.*, 2009; Muto *et al.*, 2012). Upslope migration of the cyclic steps led to the incision of a channel (Fig. 12B) similar to the process previously described from incised valley formation (Strong & Paola, 2008; Winsemann *et al.*, 2011; Muto *et al.*, 2012) and channel initiation on submarine fans (Fildani *et al.*, 2006; Lamb *et al.*, 2008; Armitage *et*

al., 2012). During later waning flow stages the channel was broadened and the initial topography of the cyclic steps smoothed. Chutes-and-pools and antidunes became dominant during the waning flood stage and partly reworked the underlying cyclic step deposits. The studied glacial lake-outburst flood succession was preserved at the inner side of a channel bend, where the subsequent flows did not re-work it.

Deposits of cyclic steps were not observed in the subaqueous fan successions, although estimates for the Froude number during incipient fan deposition ($Fr_0 > 5$; Winsemann *et al.*, 2009) are well within the range of cyclic step formation. However, the assumption of the Froude number may considerably be overestimated because it was calculated only on the basis of the large-scale geometry of the fan deposits. Alternatively, assuming that the Froude number was very high, the formation of cyclic steps may have been suppressed due to the very coarse grain-sizes and high sediment loads during initial fan formation. A high ratio of the sediment settling velocity to the flow velocity may suppress the formation of hydraulic jumps and thus the establishment of cyclic steps due to too rapid sedimentation from supercritical flows (Kostic & Parker, 2006; Kostic, 2011). Similarly, high basal sediment concentrations change the threshold for the formation of supercritical bedforms (Kostic, 2011; Cartigny *et al.*, 2012). The initiation of cyclic steps is further related to high slope angles, which allow for the formation of submerged hydraulic jumps (Cartigny *et al.*, *in press*). The slope angle and associated break of slope on the lee-side of the push-moraine ridge ($1.7\text{--}5^\circ$) were adequate to produce cyclic steps, while the subaqueous fans were deposited on nearly flat basin floors.

Aggrading stationary antidunes and humpback dunes

Long wavelength low amplitude waveforms, which are interpreted as deposits of stationary aggrading antidunes, are known from a variety of settings and occur at several orders of magnitude. Waveforms with wavelengths of several metres to decametres and amplitudes lower than 0.25 m were observed in ice-contact subaqueous fan deposits (Brennand, 1994; Hornung *et al.*, 2007; Winsemann *et al.*, 2009) and turbiditic successions (Hirst *et al.*, 2002; Ito, 2010; Mukti & Ito, 2010; Hirst, 2012). Within successions related to glacial lake-outburst floods waveforms were observed with wavelengths of 20–230 m and amplitudes of up to 5 m (Johnsen & Brennand, 2004; Duller *et al.*, 2008; Carling *et al.*, 2009; Winsemann *et al.*, 2011; Girard *et al.*, 2012a, b).

The stationary wave trains, which were responsible for the deposition of thick aggrading antidune waveforms, may have formed downflow of an undular hydraulic jump. Undular hydraulic jumps represent the weakest type of hydraulic jumps and trigger the formation of a stationary wave train, which comprises several (generally 3–12) downflow diminishing wavelets (Broome & Komar, 1979; Allen, 1984; Chanson, 2001). The Froude number downflow of an undular hydraulic jump is just below unity and thus sufficient for the formation of stationary antidunes and the wave steepness of the wave trains matches the wave steepness of antidune waves (Allen, 1984; Cheel, 1990; Chanson, 2000, 2001). The formation of stationary waves and antidunes downflow of hydraulic jumps has been described from

various settings (Jopling, 1965; Broome & Komar, 1979; Russell & Arnott, 2003; Alexander *et al.*, 2008; Duller *et al.*, 2008, Winsemann *et al.*, 2009, 2011). Aggrading stationary antidunes are thus interpreted as representing deposition by steady flows at the lower limit of the supercritical flow stage, where a hydraulic jump establishes the necessary highly aggradational conditions. The hydraulic jump may occur directly in front of the meltwater conduit (Russell & Arnott, 2003) or at the mouth of a large-scale distributary channel (Winsemann *et al.*, 2009).

Humpback dunes are generally interpreted as representing bedforms of the transition between subcritical and supercritical flows (Saunderson & Lockett, 1983; Chakraborty & Bose, 1992; Fielding, 2006). The geometry of humpback dunes resembles geometries known from climbing-dune cross-stratification (Gorrell & Shaw, 1991; Fielding, 2006; Russell *et al.*, 2007; Ghienne *et al.*, 2010) and so-called hydraulic jump unit bars (Macdonald *et al.*, 2009, 2013). Depositional architectures similar to humpback dunes have been described from delta mouth-bars (Chough & Hwang, 1997) and delta bottomsets (Winsemann *et al.*, 2011). All these deposits have been attributed to deposition downflow of hydraulic jumps and rapid flow expansion, causing dumping of the sediment load. Humpback dunes are distinguished from climbing dunes by the internal downflow divergent sigmoidal cross-stratification and distinct partitioning into dune topsets, foresets and bottomsets. In contrast, climbing dune cross-stratification resembles the geometries known from climbing-ripple cross-lamination, including stoss-erosional and stoss-depositional planar and trough climbing cross-strata (Russell *et al.*, 2007; Ghienne *et al.*, 2010).

Humpback dunes are commonly associated with aggrading stationary antidunes, pointing to deposition downflow of local hydraulic jumps formed on the lee-side of antidune bedwaves. The gradual transition of humpback dunes into antidune deposits indicates re-establishment of supercritical flow conditions. Flume experiments on hydraulic jump unit bar formation by Macdonald *et al.* (2013) indicate that bar growth is self-limiting due to flow thinning and acceleration above the aggrading bar. Fielding (2006) interpreted the transition to bedforms of the upper flow stage as pointing to a transition to supercritical flow conditions. Small-scale transitions between humpback dunes and antidunes may thus be controlled by bed topography, while larger-scale transitions probably require waxing flows.

The mapped facies architecture of the subaqueous fans indicates that depositional processes were strongly affected by hydraulic jumps. Local hydraulic jumps, which control the facies changes within the successions, are controlled by minor fluctuations of the flow and changes of the bed topography due to erosion and deposition (Fig. 11B). The distinctive proximal to distal succession of sedimentary facies within glacial jet-flow deposits is commonly attributed to the occurrence of hydraulic jumps in initially supercritical flows (Powell, 1990; Gorrell & Shaw, 1991; Russell & Arnott, 2003; Hornung *et al.*, 2007; Russell *et al.*, 2007; Winsemann *et al.*, 2009; Fig. 11A). This apparent difference in scale of the hydraulic jumps points to density stratification within the sediment-laden jet-flows (cf., Section 5.3)

Depth and velocity of the flows

At the Porta and Buschhaus subaqueous fan outcrop sections the wavelength and amplitudes of the aggrading antidune bedforms were measured. The wavelengths and amplitudes of in-phase antidune bedforms scale with the depth and velocity of the flow responsible for their deposition (Kennedy, 1963; Hand, 1969). The relation between antidune wavelength (L) and flow depth (d) is $d = L \cdot \frac{\rho_1}{2 \cdot (\rho_1 + \rho_2)}$ for a submerged flow, where the density of the flow (ρ_2) is larger than the density of the ambient fluid (ρ_1) (Allen, 1984). The density of the ambient lake water is assumed to be 1000 kg/m³, while hyperconcentrated flood conditions with densities between 1300 and 1800 kg/m³ can be assumed for the meltwater flow (Brennand, 1994). Applying this equation on the wavelengths measured in the subaqueous fan successions provides estimates of the flow depths, which range between 0.1 and 0.8 m for the measured wavelengths (Table 2). These values fit well with estimates made for similar sized antidunes in ice-contact fan deposits (Brennand, 1994; Hornung *et al.*, 2007). The low flow depths indicate that supercritical bedforms deposited from jet flows behave independently of the water depth of the basin. The calculated flow depths do not correspond to the entire flow depths, but to the flow depth responsible for deposition in a stratified flow. Flow stratification is mainly caused by vertical density contrasts between denser lower and less dense upper parts of the flow (Hand *et al.*, 1972). Stationary waves, which are responsible for the deposition of in-phase bedwaves, form as Kelvin-Helmholtz instabilities at internal boundaries of stratified flows (Prave & Duke, 1990; Mulder *et al.*, 2009; Ito, 2010).

The flow velocity (U) for antidune deposition can be estimated by applying $U = \zeta \cdot (g \cdot d \cdot (\rho_1 - \rho_2) / \rho_1)$ (Hand *et al.*, 1972; Allen, 1984). The resulting mean velocity for the meltwater jet is 1 ms⁻¹, with values ranging from 0.5 to 1.6 ms⁻¹ (Table 2). These results fit well with estimations for the formation of antidunes in other jet flows (Brennand, 1994), but is considerably lower than estimated flow velocities of 5-7 ms⁻¹ in the more proximal zone of flow establishment (Powell, 1990; Gorrell & Shaw, 1991).

Comparison of the observed bedforms with flume studies

Flume experiments indicate that a downflow succession may exist that comprises (1) cyclic steps, (2) chutes-and-pools, (3) breaking and upflow migrating antidunes, (4) stationary antidunes, (5) downflow migrating antidunes, (6) humpback dunes and (7) dunes and ripples (Kennedy, 1963; Saunderson and Lockett, 1983; Allen, 1984; Cheel, 1990; Alexander *et al.*, 2001; Cartigny *et al.*, *in press*). The transitions between the different bedform stability fields mainly depend on flow velocity, flow depth, sediment load, grain size, bed roughness and slope (Van den Berg & Van Gelder, 1993, 1998; Van den Berg & Nio, 2010; Cartigny *et al.*, *in press*). The grain-size in the studied outcrop sections is very similar, thus diminishing the effect of grain-size on bedform stability. Sediment load and fluid density during the deposition of the studied subaqueous fan and glacial lake-outburst flood deposits were quite similar, because both settings are characterised by highly aggradational conditions, requiring highly

Table 2: Wavelength, wave amplitude and wave steepness of aggrading antidunes measured at the Porta and Buschhaus outcrop sections and comparison with examples from the literature. The flow depth and flow velocity were calculated based on the antidune wavelength.

Wavelength	Amplitude	Wave steepness	Flow depth	Flow velocity	Depositional setting and age	Source
L (m)	y (m)	y/L	d (m)	U (ms ⁻¹)		
Porta subaqueous fan						
3.0	0.25	0.08	0.2*	0.8*	Subaqueous ice-contact fan, Pleistocene	This study
5.6	0.08	0.01	0.4*	1.1*	Subaqueous ice-contact fan, Pleistocene	This study
9.6	0.40	0.04	0.6*	1.4*	Subaqueous ice-contact fan, Pleistocene	This study
10.8	0.50	0.04	0.7*	1.5*	Subaqueous ice-contact fan, Pleistocene	This study
12.0	0.40	0.03	0.8*	1.6*	Subaqueous ice-contact fan, Pleistocene	This study
Buschhaus subaqueous fan						
1.2	0.10	0.08	0.1*	0.5*	Subaqueous ice-contact fan, Pleistocene	This study
2.6	0.20	0.08	0.2*	0.7*	Subaqueous ice-contact fan, Pleistocene	This study
2.7	0.15	0.05	0.2*	0.7*	Subaqueous ice-contact fan, Pleistocene	This study
2.8	0.07	0.02	0.2*	0.8*	Subaqueous ice-contact fan, Pleistocene	This study
4.0	0.35	0.09	0.3*	0.9*	Subaqueous ice-contact fan, Pleistocene	This study
6.0	0.20	0.03	0.4*	1.1*	Subaqueous ice-contact fan, Pleistocene	This study
Examples from the literature						
1.5 - 3.5	0.1 - 0.25	~ 0.06	-	-	Glacimarine turbidites, Ordovician	Hirst, 2012
3 - 20	0.06 - 0.2	~ 0.02	-	-	Turbidites, Miocene	Mukti & Ito, 2010
5 - 20	0.25 - 1.25	~ 0.04	0.4 - 1.8*	1 - 3*	Subaqueous ice-contact fan, Pleistocene	Brennand, 1994
7 - 63	0.4 - 2.2	~ 0.05	~ 3.8	-	Marine turbidites, Pleistocene	Ito, 2010
24 - 96	0.3 - 1.3	~ 0.01	5 - 19	6 - 12	Glacial lake-outburst flood deposits, Holocene	Duller <i>et al.</i> , 2008
40	2	~ 0.05	-	-	Glacial lake-outburst flood deposits, Ordovician	Girard <i>et al.</i> , 2012
60 - 90	~ 5	~ 0.07	9 - 14	10 - 12	Glacial lake-outburst flood deposits, Pleistocene	Winsemann <i>et al.</i> , 2011
100 - 230	1.5 - 3.5	~ 0.02	16 - 36	13 - 19	Glacial lake-outburst flood deposits, Pleistocene	Carling <i>et al.</i> , 2009

* average value for fluid densities ranging from 1300 to 1800 kg/m³

sediment-laden flows. Bed topography generally varies rapidly on a small scale and is permanently modified due to erosion and deposition.

In general, the observed succession of bedforms in the field sites is in good accordance with the results from various flume experiments (Cheel, 1990; Alexander *et al.*, 2001; Cartigny *et al.*, *in press*). As can be expected, the transitions between the various bedforms in fluctuating natural flows are more rapid

and complex than within controlled flume experiments. Aggrading stationary antidunes are essentially absent in flume experiments, although they are theoretically predicted (Kennedy, 1963; Middleton, 1965; Cheel, 1990). This might be an effect of the relatively low sediment loads in most flume studies compared to sediment-laden flows, as glacial jets (Brennand, 1994; Russell & Arnott, 2003, Winsemann *et al.*, 2009), turbidity currents (Mulder *et al.*, 2009; Ito, 2010; Mukti & Ito, 2010; Hirst, 2012) and glacial lake-outburst floods (Johnsen & Brennand, 2004; Winsemann *et al.*, 2011; Girard *et al.*, 2012a, b).

Both field and flume studies of transcritical to supercritical flow deposits observe the deposition of upper flow stage planar-parallel stratified beds by flows with a Froude number of ~ 1 (Saunderson & Lockett, 1983; Allen, 1984; Cheel, 1990; Nnadi & Wilson, 1995; Kjær *et al.*, 2004; Fielding, 2006). The absence of planar-parallel stratification in all studied successions suggests that the deposition of upper stage plane beds is inhibited. The Froude number of any supercritical flow is conjugated to the Froude number of the subcritical flow after undergoing a hydraulic jump (Chow, 1959; Chanson, 2000; Cartigny *et al.*, *in press*). Therefore, when supercritical flows undergo hydraulic jumps the formation of planar-parallel stratification may be prevented. Alternatively, Jopling (1965) suggested that stationary waves should be considered equivalent to upper stage plane beds because of their similar range of Froude numbers. Both field and flume studies of upper stage plane beds indicate a low lateral continuity of the laminae, the presence internal low-angle discontinuities, slight thinning and thickening of individual laminae and a transition to low-angle cross-stratification and convex-up bedforms (Allen, 1984; Paola *et al.*, 1989; Best & Bridge, 1992; Fielding, 2006), indicating flow conditions fluctuating to the antidune stability field (Fielding, 2006). Under high rates of aggradation these features will become more pronounced, causing the absence of apparently planar-parallel stratified beds, again demonstrating the major influence of the aggradation rate on bedforms related to supercritical flows (cf., Cartigny *et al.*, *in press*).

Conclusions

The studied successions provide new insights into the anatomy of bedforms related to highly aggradational supercritical flows and hydraulic jumps. These bedforms are characteristic for subaqueous ice-contact fan and glacial lake-outburst flood deposits and may also occur in other high-energy settings such as glacial settings, fluvial environments, coarse-grained deltas or turbidite systems.

Bedforms include cyclic steps, chutes-and-pools, breaking antidunes, aggrading stationary antidunes and humpback dunes. Deposits of cyclic steps are characterised by broad lenticular scours infilled by gently dipping backsets. These bedforms are interbedded with deposits of chutes-and-pools and breaking antidunes, pointing to deposition under supercritical and rapidly changing unstable flow conditions. Deposits of chutes-and-pools and breaking antidunes comprise a variety of geometries, including steeply dipping backsets, gently dipping concave-convex foresets and concentric lens-fills.

Interbedded deposits of aggrading stationary antidunes and humpback dunes represent characteristic bedforms of the zone of flow transition of glaciallacustrine ice-contact subaqueous fans. Deposits of aggrading stationary antidunes are characterised by sheet-like sinusoidal stratified beds. Humpback dunes comprise downflow divergent sigmoidal foresets and are interpreted as deposited at the transition from subcritical to supercritical flow conditions or vice versa.

The lateral and vertical successions of supercritical bedforms are interpreted as representing both (i) the temporal and spatial evolution of the initial supercritical flows on a large scale, which are in general characterised by waning flow conditions, and (ii) internal short-term temporal and spatial variations of the flow conditions. Small-scale lateral and vertical facies changes are interpreted as controlled by fluctuating discharge, bed topography and pulsating unstable flows.

Acknowledgements

Financial support by the Niedersächsisches Ministerium für Wissenschaft und Kultur (MWK) is gratefully acknowledged (PRO Niedersachsen Project No. 11.2-76202-17-3/09). We would like to thank the owners of the sand pits for the permission to work on their property. Borehole data were generously provided by E.ON-Kraftwerke GmbH, Niedersächsisches Landesamt für Bergbau, Energie und Geologie, Brinkmeyer Kieswerk GmbH & Co. KG., E.ON Westfalen Weser AG and Geologischer Dienst NRW (Krefeld). C. Brandes, J. Meinsen, L. Pollok, K. Skupin and D. Steinmetz are thanked for discussion and help with field work. Critical comments by P. Carling and J. Venditti on an earlier version of this manuscript helped to sharpen our ideas. Constructive reviews by M. Cartigny, P. Fralick and editor J. Knight are highly appreciated and helped to improve our manuscript.

References

- Alexander, J., Fielding, C., 1997: Gravel antidunes in the tropical Burdekin River, Queensland, Australia. *Sedimentology* 44, 327-337.
- Alexander, J., Bridge, J.S., Cheel, R.J., Leclair, S.F., 2001: Bedforms and associated sedimentary structures formed under supercritical water flows over aggrading sand beds. *Sedimentology* 48, 133-152.
- Alexander, J., McLelland, S.J., Gray, T.E., Vincent, C.E., Leeder, M.R., Ellett, S., 2008: Laboratory sustained turbidity currents form elongate ridges at channel mouths. *Sedimentology* 55, 845-868.
- Allen, J.R.L., 1984: Sedimentary structures: their character and physical basis. *Developments in Sedimentology* 30, 1-663.
- Armitage, D.A., McHargue, T., Fildani, A., Graham, S.A., 2012: Postavulsion channel evolution: Niger Delta continental slope. *AAPG Bulletin* 96, 823-843.
- Bates, C.C., 1953: Rational theory of delta formation. *AAPG Bulletin* 37, 2119-2162.

- Best, J., Bridge, J., 1992: The morphology and dynamics of low amplitude bedwaves upon upper stage plane beds and the preservation of planar laminae. *Sedimentology* 39, 737-752.
- Blair, T.C., 1999: Sedimentary processes and facies of the waterlaid Anvil Spring Canyon alluvial fan, Death Valley, California. *Sedimentology* 46, 913-940.
- Brennand, T.A., 1994. Macroforms, large bedforms and rhythmic sedimentary sequences in subglacial eskers, south-central Ontario: implications for esker genesis and meltwater regime. *Sedimentary Geology* 91, 9-55.
- Broome, R., Komar, P.D., 1979: Undular hydraulic jumps and the formation of backlash ripples on beaches. *Sedimentology* 26, 543-559.
- Busschers, F.S., Van Balen, R.T., Cohen, K.M., Kasse, C., Weerts, H.J.T., Wallinga, J., Bunnik, F.P.M., 2008: Response of the Rhine-Meuse fluvial system to Saalian ice-sheet dynamics. *Boreas* 37, 329-468.
- Carling, P.A., Shvidchenko, A.B., 2002: A consideration of the dune-antidune transition in fine gravel. *Sedimentology* 49, 1269-1282.
- Carling, P.A., Burr, D.M., Johnsen, T.F., Brennand, T.A., 2009: A review of open-channel megaflood depositional landforms on Earth and Mars. *In: Burr, D.M., Carling, P.A., Baker, V.R. (Eds.), Megaflooding on Earth and Mars. Cambridge University Press, Cambridge, pp. 33-49.*
- Cartigny, M.J.B., Postma, G., van den Berg, J.H., Mastbergen, D., 2011: A Comparative study of sediment waves and cyclic steps based on geometries, internal structures and numerical modelling. *Marine Geology* 280, 40-56.
- Cartigny, M.J.B., Postma, G., Kleverlaan, K., Ventra, D., van den Berg, J., 2012: Experimental studies of supercritical bedforms applied to coarse-grained turbidite deposits of the Tabernas intermontane Basin (SE Spain, late Miocene). *In: Cartigny, M.J.B. (Ed.), Morphodynamics of supercritical high-density turbidity currents. Utrecht Studies in Earth Sciences* 10, pp. 105-132.
- Cartigny, M.J.B., Ventra, D., Postma, G. and van den Berg, J.H., *in press*: Morphodynamics and sedimentary structures of bedforms under supercritical-flow conditions: new insights from flume experiments. *Sedimentology*, doi: 10.1111/sed.12076.
- Chakraborty, C., Bose, P.K., 1992: Ripple/dune to upper stage plane bed transition: some observations from the ancient record. *Geological Journal* 27, 349-359.
- Chanson, H., 2000: Boundary shear stress measurements in undular flows: Application to standing wave bed forms. *Water Resources Research* 36, 3063-3076.
- Chanson, H., 2001: Current knowledge in hydraulic jumps and related phenomena. A survey of experimental results. *European Journal of Mechanics B/Fluids* 28, 191-210.
- Cheel, R.J., 1990: Horizontal lamination and the sequence of bed phases and stratification under upper-flow-regime conditions. *Sedimentology* 37, 517-529.
- Chough, S.K., Hwang, I.G., 1997: The Duksung fan delta, SE Korea: Growth of delta lobes on a Gilbert-type topset in response to relative sea-level rise. *Journal of Sedimentary Research* 67, 725-739.

- Chow, V.T., 1959: Open-channel hydraulics. McGraw-Hill Book Company, New York, 679 pp.
- Clerk, S., Buonchristiani, J.-F., Guiraud, M., Desaubliaux, G., Portier, E., 2012: Depositional model in subglacial cavities, Killiney Bay, Ireland. Interactions between sedimentation, deformation and glacial dynamics. *Quaternary Science Reviews* 33, 142-164.
- Duller, R.A., Mountney, N.P., Russell, A.J., Cassidy, N.C., 2008: Architectural analysis of a volcaniclastic jökulhlaup deposit, southern Iceland: sedimentary evidence for supercritical flow. *Sedimentology* 55, 939-964.
- Duphorn, K., Lang, H.D., Look, E.R., Mengeling, H., Meyer, K.-D., Schneekloth, H., Vinken, R., 1974: CC3926 Braunschweig. Geologische Übersichtskarte 1: 200.000, Bundesanstalt für Geowissenschaften und Rohstoffe, Hannover.
- Ehlers, J., Eissmann, L., Lippstreu, L., Stephan, H.-J., Wansa, S., 2004: Pleistocene glaciations of North Germany. *In*: Ehlers, J., Gibbard, P.L. (Eds.), *Quaternary Glaciations. Extent and Chronology Part I, Europe. Developments in Quaternary Science* 2, pp. 135-146.
- Ehlers, J., Grube, A., Stephan, H.-J., Wansa, S., 2011. Pleistocene Glaciations of North Germany ó New Results. *In*: Ehlers, J., Gibbard, P.L., Hughes, P.D. (Eds.), *Quaternary Glaciations ó Extent and Chronology ó A Closer Look. Developments in Quaternary Science* 15, pp. 149-162.
- Eissmann, L., 2002: Quaternary geology of eastern Germany (Saxony, Saxon-Anhalt, South Brandenburg, Thuringia), type area of the Elsterian and Saalian Stages in Europe. *Quaternary Science Reviews* 21, 1275-1346.
- Fielding, C.R., 2006: Upper flow regime sheets, lenses and scour fills: Extending the range of architectural elements for fluvial sediment bodies. *Sedimentary Geology* 190, 227-240.
- Fielding, C.R., Webb, J.A., 1996: Facies and cyclicity of the Late Permian Bainmedart Coal Measures in the Northern Prince Charles Mountains, MacRobertson Land, Antarctica. *Sedimentology* 43, 295-322.
- Fildani, A., Normark, W.R., Kostic, S., Parker, G., 2006: Channel formation by flow stripping: large-scale scour features along the Monterey East Channel and their relation to sediment waves. *Sedimentology* 53, 1265-1287.
- Foley, M.G., 1977: Gravel-lens formation in antidune-regime flow ó a quantitative hydrodynamic indicator, *Journal of Sedimentary Petrology* 47, 738-746.
- Fralick, P., 1999: Paleohydraulics of chute-and-pool structures in a Paleoproterozoic fluvial sandstone. *Sedimentary Geology* 125, 129-134.
- Ghienne, J.-F., Girard, F., Moreau, J., Rubino, J.-L., 2010: Late Ordovician climbing-dune cross-stratification: a signature of outburst floods in proglacial outwash environments? *Sedimentology* 57, 1175-1198.
- Gilbert, G.K., 1914: The transportation of debris by running water. US Geological Survey Professional Paper 86, 1-263.

- Girard, F., Ghienne, J.-F., Rubino, J.-L., 2012a: Channelized sandstone bodies (cordons) in the Tassili n'Ajjer (Algeria & Libya): snapshots of a Late Ordovician proglacial outwash plain. *In*: Huuse, M., Redfern, J., Le Heron, D.P., Dixon, R.J., Moscariello, A., Craig, J. (Eds.), *Glaciogenic Reservoirs*. Geological Society of London Special Publication 368, pp. 355-379.
- Girard, F., Ghienne, J.-F., Rubino, J.-L., 2012b: Occurrence of hyperpycnal flows and hybrid event beds related to glacial outburst events in a Late Ordovician proglacial delta (Murzuq Basin, SW Libya). *Journal of Sedimentary Research* 82, 688-708.
- Gorrell, G., Shaw, J., 1991: Deposition in an esker, bead and fan complex, Lanark, Ontario, Canada. *Sedimentary Geology* 72, 285-314.
- Hand, B.M., 1969: Antidunes as trochoidal waves. *Journal of Sedimentary Petrology* 39, 1302-1309.
- Hand, B.M., Middleton, G.V., Skipper, K., 1972: Antidune cross-stratification in a turbidite sequence, Cloridorme Formation, Gaspé, Quebec. *Sedimentology* 18, 135-138.
- Heiniö, P., Davies, R.J., 2009: Trails of depressions and sediment waves along submarine channels on the continental margin of Espirito Santo Basin, Brazil. *GSA Bulletin* 121, 698-711.
- Henry, L.C., Isbell, J.L., Limarino, C.O., McHenry, L.J., Fraiser, M.L., 2010: Mid-Carboniferous deglaciation of the Protoprecordillera, Argentina recorded in the Agua de Jagüel palaeovalley. *Palaeogeography, Palaeoclimatology, Palaeoecology* 298, 112-129.
- Hirst, J.P.P., 2012: Ordovician proglacial sediments in Algeria: insights into the controls on hydrocarbon reservoirs in the In Amenas field, Illizi Basin. *In*: Huuse, M., Redfern, J., Le Heron, D.P., Dixon, R.J., Moscariello, A., Craig, J. (Eds.), *Glaciogenic Reservoirs*. Geological Society of London Special Publication 368, pp. 319-353.
- Hirst, J.P.P., Benbakir, A., Payne, D.F., Westlake, I.R., 2002: Tunnel valleys and density flow processes in the Upper Ordovician glacial succession, Illizi Basin, Algeria: influence on reservoir quality. *Journal of Petroleum Geology* 25, 297-324.
- Hornung, J.J., Aspiron, U., Winsemann, J., 2007: Jet-efflux deposits of a subaqueous ice-contact fan, glacial Lake Rinteln, northwestern Germany. *Sedimentary Geology* 193, 167-192.
- Ito, M., 2010: Are coarse-grained sediment waves formed as downstream-migrating antidunes? Insights from an early Pleistocene submarine canyon on the Boso Peninsula, Japan. *Sedimentary Geology* 226, 1-8.
- Ito, M., Saito, T., 2006: Gravel waves in an ancient canyon: analogous features and formative processes of coarse-grained bedforms in a submarine-fan system, the Lower Pleistocene of the Boso Peninsula, Japan. *Journal of Sedimentary Research* 76, 1274-1283.
- Johnsen, T.F., Brennand, T.A., 2004: Late-glacial lakes in the Thompson Basin, British Columbia: paleogeography and evolution. *Canadian Journal of Earth Sciences* 41, 1367-1383.
- Johnsen, T.F., Brennand, T.A., 2006: The environment in and around ice-dammed lakes in the moderately high relief setting of the southern Canadian Cordillera. *Boreas* 35, 106-125.

- Jopling, A.V., 1965: Hydraulic factors controlling the shape of laminae in laboratory deltas. *Journal of Sedimentary Petrology* 35, 777-791.
- Kennedy, J.F., 1963: The mechanics of dunes and antidunes in erodible-bed channels. *Journal of Fluid Mechanics* 16, 521-544.
- Kjær, K.H., Sultan, L., Krüger, J., Schomacker, A., 2004: Architecture and sedimentation of outwash fans in front of the Mýrdalsjökull ice cap, Iceland. *Sedimentary Geology* 172, 139-163.
- Klostermann, J., 1992a: Das Quartär der Niederrheinischen Bucht ó Ablagerungen der letzten Eiszeit am Niederrhein. Geologisches Landesamt Nordrhein-Westfalen, Krefeld, 200 pp.
- Klostermann, J., 1992b: Erläuterungen zu Blatt 4303 Uedem. Geologisches Landesamt Nordrhein-Westfalen, Krefeld, 130 pp.
- Kneller, B., 1995: Beyond the turbidite paradigm: physical models for deposition of turbidites and their implications for reservoir prediction. *In: Hartley, A.J., Prosser, D.J. (Eds.), Characterization of Deep Marine Clastic Systems. Geological Society of London Special Publication 94*, pp. 31-49.
- Kostic, S., 2011: Modeling of submarine cyclic steps: controls on their formation, migration, and architecture. *Geosphere* 7, 294-304.
- Kostic, S., Parker, G., 2006: The response of turbidity currents to a canyonófan transition: internal hydraulic jumps and depositional signatures. *Journal of Hydraulic Research* 44, 631-653.
- Kostic, S., Sequeiros, O., Spinewine, B., Parker, G., 2010: Cyclic steps: A phenomenon of supercritical shallow flow from the high mountains to the bottom of the ocean. *Journal of Hydro-environment Research* 3, 167-172.
- Lamb, M.P., Parsons, J.D., Mullenbach, B.L., Finlayson, D.P., Orange, D.L., Nitttrouer, C.A., 2008: Evidence for superelevation, channel incision, and formation of cyclic steps by turbidity currents in Eel Canyon, California. *GSA Bulletin* 120, 463-475.
- Lang, J., Dixon, R.J., Le Heron, D.P., Winsemann, J., 2012a: Depositional architecture and sequence stratigraphic correlation of Upper Ordovician glaciogenic deposits, Illizi Basin, Algeria. *In: Huuse, M., Redfern, J., Le Heron, D.P., Dixon, R.J., Moscariello, A., Craig, J. (Eds.), Glaciogenic Reservoirs. Geological Society of London Special Publication 368*, pp. 293-317.
- Lang, J., Winsemann, J., Steinmetz, D., Polom, U., Pollok, L., Böhner, U., Serangeli, J., Brandes, C., Hampel, A., Winghart, S., 2012b: The Pleistocene of Schöningen, Germany: a complex tunnel valley fill revealed from 3D subsurface modelling and shear wave seismics. *Quaternary Science Reviews* 39, 86-105.
- Langford, R., Bracken, B., 1987: Medano Creek, Colorado, a model for upper-flow-regime fluvial deposition. *Journal of Sedimentary Petrology* 57, 863-870.
- Le Heron, D.P., Craig, J., Etienne, J.L., 2009: Ancient glaciations and hydrocarbon accumulations in North Africa and the Middle East. *Earth-Science Reviews* 93, 47-76.
- Lippstreu, L., 1995: VI. Brandenburg. *In: Benda, L. (Ed.), Das Quartär Deutschlands. Borntraeger, Berlin*, pp. 117-147.

- Look, E.-R., 1984: Geologie und Bergbau im Braunschweiger Land. *Geologisches Jahrbuch A* 78, 1-467.
- Lowe, R.L., 1975: Water escape structures in coarse-grained sediments. *Sedimentology* 22, 157-204.
- Macdonald, R.G., Alexander, J., Bacon, J.C., Cooker, M.J., 2009: Flow patterns, sedimentation and deposit architecture under a hydraulic jump on a non-eroding bed: defining hydraulic-jump unit bars. *Sedimentology* 56, 1346-1367.
- Macdonald, R.G., Alexander, J., Bacon, J.C., Cooker, M.J., 2013: Variations in the architecture of hydraulic-jump bar complexes on non-eroding beds. *Sedimentology* 60, 1291-1312.
- Marren, P.M., Russell, A.J., Rushmer, E.L., 2009: Sedimentology of a sandur formed by multiple jökulhlaups, Kverkfjöll, Iceland. *Sedimentary Geology* 213, 77-88.
- Massari, F., 1996: Upper-flow-regime stratification types on steep-face, coarse-grained, Gilbert-type progradational wedges (Pleistocene, southern Italy). *Journal of Sedimentary Research* 66, 364-375.
- Meinsen, J., Winsemann, J., Weitkamp, A., Landmeyer, N., Lenz, A., Dölling, M., 2011: Middle Pleistocene (Saalian) lake outburst floods in the Münsterland Embayment (NW Germany): impacts and magnitudes. *Quaternary Science Reviews* 30, 2597-2625.
- Middleton, G.V., 1965: Antidune cross-bedding in a large flume. *Journal of Sedimentary Petrology* 35, 922-927.
- Mukti, M.M., Ito, M., 2010: Discovery of outcrop-scale fine-grained sediment waves in the lower Halang Formation, an upper Miocene submarine-fan succession in West Java. *Sedimentary Geology* 231, 55-62.
- Mulder, T., Razin, P., Faugeres, J.-C., 2009: Hummocky cross-stratification-like structures in deep-sea turbidites: Upper Cretaceous Basque basins (Western Pyrenees, France). *Sedimentology* 56, 997-1015.
- Muto, T., Yamagishi, C., Sekiguchi, T., Yokokawa, M., Parker, G., 2012: The hydraulic autogenesis of distinct cyclicity in delta foreset bedding: flume experiments. *Journal of Sedimentary Research* 82, 545-558.
- Nnadi, F.N., Wilson, K.C., 1995: Bed-load motion at high shear stress: dune washout and plane-bed flow. *Journal of Hydraulic Engineering* 121, 267-273.
- Owen, G., 1996: Experimental soft-sediment deformation: structures formed by the liquefaction of unconsolidated sands and some ancient examples. *Sedimentology* 43, 279-293.
- Paola, C., Wiele, S.M., Reinhart, M.A., 1989: Upper-regime parallel lamination as the result of turbulent sediment transport and low-amplitude bed forms. *Sedimentology* 36, 47-59.
- Postma, G., Cartigny, M., Kleverlaan, K., 2009: Structureless, coarse-tail graded Bouma Ta formed by internal hydraulic jump of the turbidity current? *Sedimentary Geology* 219, 1-6.
- Potter, P.E., Franca, A.B., Spencer, C.W., Caputo, M.V., 1995: Petroleum in glacially-related sandstones of Gondwana: a review. *Journal of Petroleum Geology* 18, 397-420.

- Powell, R.D., 1990: Glacimarine processes at grounding-line fans and their growth to ice-contact deltas. *In: Dowdeswell, J.A., Scourse, J.D. (Eds.), Glacimarine Environments: Processes and Sediments. Geological Society of London Special Publication 53*, pp. 53-73.
- Prave, A.R., Duke, W.L., 1990: Small-scale hummocky cross-stratification in turbidites: a form of antidune stratification? *Sedimentology* 37, 531-539.
- Rajaratnam, N., Subramanyam, S., 1986: Plane turbulent denser wall jets and jumps. *Journal of Hydraulic Research* 24, 281-296.
- Røe, S.-L., 1987: Cross-strata and bedforms of probable transitional dune to upper-stage plane-bed origin from a Late Precambrian fluvial sandstone, northern Norway. *Sedimentology* 34, 89-101.
- Røe, S.-L., Hermansen, M., 2006: New aspects of deformed cross-strata in fluvial sandstones: examples from Neoproterozoic formations in northern Norway. *Sedimentary Geology* 186, 283-293.
- Russell, H.A.J., Arnott, R.W.C., 2003: Hydraulic jump and hyperconcentrated-flow deposits of a glacial subaqueous fan: Oak Ridges Moraine, Southern Ontario, Canada. *Journal of Sedimentary Research* 73, 887-905.
- Russell, H.A.J., Arnott, R.W.C., Sharpe, D.R., 2003: Evidence for rapid sedimentation in a tunnel channel, Oak Ridges Moraine, southern Ontario, Canada. *Sedimentary Geology* 160, 33-55.
- Russell, H.A.J., Sharpe, D.R., Bajk, A.F., 2007: Sedimentary signatures of the Waterloo Moraine, Ontario, Canada. *In: Hambrey, M., Christoffersen, P., Glasser, N., Hubbard, B. (Eds.), Glacial Processes and Products. International Association of Sedimentologists Special Publication 39*, pp. 85-108.
- Saunderson, H.C., Lockett, F.P.J., 1983: Flume experiments on bedforms and structures at the dune-plane bed transition. *In: Collinson, J.D., Lewin, L. (Eds.), Modern and ancient fluvial systems. International Association of Sedimentologists Special Publication 6*, pp. 49-58.
- Schmincke, H.-U., Fisher, R.V., Water, A.C., 1973: Antidune and chute and pool structures in the base surge deposits of the Laacher See area, Germany. *Sedimentology* 20, 553-574.
- Skupin, K., Zandstra, J.G., 2010: Gletscher der Saale-Kaltzeit am Niederrhein. *Geologischer Dienst Nordrhein-Westfalen, Krefeld*, 116 pp.
- Southard, J.B., Boguchwal, L.A., 1990: Bed configurations in steady unidirectional water flows. Part 3. Effects of temperature and gravity. *Journal of Sedimentary Petrology* 60, 680-686.
- Spinewine, B., Sequeiros, O.E., Garcia, M.H., Beaubouef, R.T., Sun, T., Savoye, B., Parker, G., 2009: Experiments on wedge-shaped deep sea sedimentary deposits in minibasins and/or on channel levees emplaced by turbidity currents. Part II. Morphodynamics of the wedge and of the associated bedforms. *Journal of Sedimentary Research* 79, 608-628.
- Strong, N., Paola, C., 2008: Valleys that never were: time versus stratigraphic surfaces. *Journal of Sedimentary Research* 78, 579-593.
- Taki, K., Parker, G., 2005: Transportational cyclic steps created by flow over an erodible bed. Part 1. Experiments. *Journal of Hydraulic Research* 43, 488-501.

- Thome, K.N., 1983: Gletscherosion und -akkumulation im Münsterland und angrenzenden Gebieten. *Neues Jahrbuch für Geologie und Paläontologie - Abhandlungen* 166, 116-138.
- Van den Berg, J.H., Van Gelder, A., 1993: A new bedform stability diagram, with emphasis on the transition of ripples to plane bed in flows over fine sand and silt. *In: Marzo, M., Puigdefabregas, C. (Eds.), Alluvial sedimentation. International Association of Sedimentologists Special Publication 17*, pp. 11-21.
- Van den Berg, J.H., Van Gelder, A., 1998: Discussion: Flow and sediment transport over large subaqueous dunes: Fraser River, Canada. *Sedimentology* 45, 217-221.
- Van den Berg, J.H., Nio, S.D., 2010: Sedimentary structures and their relation to bedforms and flow conditions. EAGE Publications, Houten, 138 pp.
- Van der Wateren, F.M., 1994: Proglacial subaqueous outwash fan and delta sediments in push moraines ó indicators of subglacial meltwater activity. *Sedimentary Geology* 91, 145-172.
- Walker, R.G., 1967: Upper flow regime bed forms in turbidites of the Hatch Formation, Devonian of New York State. *Journal of Sedimentary Petrology* 37, 1052-1058.
- Weirich, F.H., 1988: Field evidence for hydraulic jumps in subaqueous sediment gravity flows. *Nature* 332, 626-629.
- Winsemann, J., Hornung, J.J., Meinsen, J., Asprion, U., Polom, U., Brandes, C., Bußmann, M., Weber, C., 2009: Anatomy of a subaqueous ice-contact fan and delta complex, Middle Pleistocene, NW Germany. *Sedimentology* 56, 1041-1076.
- Winsemann, J., Brandes, C., Polom, U., 2011: Response of a proglacial delta to rapid high-amplitude lake-level change: an integration of outcrop data and high-resolution shear wave seismic. *Basin Research* 23, 22-52.
- Winterwerp, J.C., Bakker, W.T., Mastbergen, D.R., Van Rossum, H., 1992: Hyper-concentrated sand-water mixture flows over erodible beds. *Journal of Hydraulic Engineering* 118, 1508-1525.
- Yokokawa, M., Hasegawa, K., Kanbayashi, S., Endo, N., 2010: Formative conditions and sedimentary structures of sandy 3D antidunes: an application of the gravel step-pool model to fine-grained sand in an experimental flume. *Earth Surface Processes and Landforms* 35, 1720-1729.
- Ziermann, H., 1987: Lithofazieskarten Quartär, 1:50000, Blatt 2165 Ziesar. Zentrales Geologisches Institut, Potsdam.

This chapter has been submitted to Quaternary Science Reviews

Do salt structures react to ice-sheet loading? Insights from two-dimensional finite-element modelling

Jörg Lang¹⁾, Andrea Hampel¹⁾, Christian Brandes¹⁾ & Jutta Winsemann¹⁾

1) Institut für Geologie, Leibniz Universität Hannover, Callinstraße 30, 30167 Hannover, Germany

Abstract

During the past decades the effect of glacio-isostatic adjustments has received much attention. However, the reaction of salt structures to ice-sheet loading and unloading is yet poorly understood. Our study aims to test conceptual models of the interaction between ice-sheet loading and salt structures by finite-element modelling (ABAQUSTM). Our models consist of 2D cross-sections, which represent simplified geological cross-sections from the Central European Basin System. The model layers represent (i) sedimentary rocks of elastoplastic rheology, (ii) a viscoelastic diapir and layer of salt and (iii) an elastic basement. The geometry and rheology of the model layers and the magnitude, spatial distribution and timing of ice-sheet loading were systematically varied to detect the controlling factors. On top of the model, a temporarily variable pressure represents the ice advance and retreat. The durations of the individual loading phases were defined to resemble the durations of the Pleistocene ice advances in northern central Europe. All simulations indicate that salt structures respond to ice-sheet loading. An ice advance towards the diapir causes flow of salt from the source layer below the ice sheet towards the diapir, resulting in an uplift of up to +3.8 m. The diapir continues to rise as long as the load is applied to the source layer but not to the crest of the diapir. When the diapir is transgressed by the ice sheet the diapir is pushed down (up to -36 m) as long as load is applied to the crest of the diapir. During and after ice unloading large parts of the displacement are compensated by a reversal of the salt flow. Plastic deformation of the overburden is restricted to the area immediately above the salt diapir. The displacements after unloading range between -3.1 and +2.7 m. Larger displacements are observed in models with deep-rooted diapirs, higher thickness of the ice sheet, longer duration of the loading phase, higher thickness of the salt source layer and lower viscosity of the salt. The rise or fall of diapirs triggered or amplified by ice-sheet loading will probably affect glacial erosion and deposition above the diapir and within the rim synclines, although the resulting displacements in the range of a few decimetres to a few metres are probably too low to have a marked effect on the advance or retreat pattern of the ice sheets.

Introduction

A correlation between subsurface structures, as faults zones and salt structures, and Pleistocene glacial features, as ice-marginal valleys, terminal moraines, tunnel valleys and river courses, has been recognised along the margins of the Fennoscandian ice sheets in the Central European Basin System (Gripp, 1952; Liszkowski, 1993; Pedersen, 2000; Schirrmeister, 1999; Sirocko *et al.*, 2002, 2008; Kurzawa, 2003; Reicherter *et al.*, 2005; Aber & Ber, 2007; Ber, 2009), but also from the margins of the Laurentide ice sheets in the Michigan Basin in the northeastern USA (White, 1992; Aber & Ber, 2007). These correlations are interpreted as pointing to an interaction between the ice-sheets and the subsurface structures (cf., Sirocko *et al.*, 2008). The correlation between ice-sheet loading-unloading and tectonic processes has received much attention since the concept of glacio-isostasy was first introduced in the 19th century (Stewart *et al.*, 2000). During glacial cycles the stress field in the lithosphere is strongly affected by the stress applied by ice sheet loading. The interactions between ice sheets and crustal deformation are complex and depend on the magnitude of the ice sheet, the distance to the centre of the ice sheet and the pre-existing stress field (Johnston, 1987; Johnston *et al.*, 1998; Wu *et al.*, 1999; Stewart *et al.*, 2000; Hampel & Hetzel, 2006; Hampel *et al.*, 2009).

Geological models of processes related to the glacio-isostatic rebound need to take into account that deformation will be focussed along pre-defined zones of weakness, such as faults (Liszkowski, 1993; Brandes *et al.*, 2011). This is especially important for areas that have a complex deformation history and experienced repeated reactivation of fault zones, as the Central European Basin System (e.g., Scheck-Wenderoth & Lamarche, 2005; Maystrenko *et al.*, 2008). During the Pleistocene large parts of the Central European Basin System were affected the multiple advances of the Fennoscandian ice sheets (Litt *et al.*, 2008; Lee *et al.*, 2010; Ehlers *et al.*, 2011; Houmark-Nielsen, 2011; Laban & van der Meer, 2011; Marks, 2011). Evidence for seismicity triggered by ice-sheet loading and unloading is known from regions that were beneath the ice sheets (Dehls *et al.*, 2000; Mörner, 2004) as well as proglacial and periglacial regions (Brandes *et al.*, 2011, 2012; Hoffmann & Reicherter, 2012; Brandes & Winsemann, 2013).

Salt structures represent zones of weakness within basin fills that accumulate strain during phases of deformation (Hudec & Jackson, 2007) and perturb the regional stress field (Brandes *et al.*, 2013). Based on field observations conceptual models for the interaction of the load applied by ice sheets and salt diapirs were proposed (Liszkowski, 1993, Stackebrandt, 2005; Lehné & Sirocko, 2007; Sirocko *et al.*, 2008). The load applied by an ice sheet advance towards a salt diapir is interpreted to reactivate or accelerate the rise of the diapir and subsidence of the rim synclines (Lehné & Sirocko, 2007; Sirocko *et al.*, 2008; Fig. 1A). Between the diapir and the ice sheet glacial successions may be deposited, which may be deformed into push-moraines during ongoing ice advance (Sirocko *et al.*, 2008). If the ice sheet transgresses the diapir the load will impede further rise or even force the diapir to subside (Liszkowski, 1993; Fig. 1B). The subsequent removal of the ice load during deglaciation will then

allow the diapir to rise once again (Liszkowski, 1993; Sirocko *et al.*, 2008; Fig. 1C). Faults above the crest of the diapir may be reactivated during the loading and unloading cycle, although the sense of fault slip may switch during the different stages of the process (Liszkowski, 1993; Lehné & Sirocko, 2007; Sirocko *et al.*, 2008).

To evaluate the concept of ice-salt interaction, we apply finite-element models to simulate the reaction of salt structures to ice-sheet loading and unloading. Based on our modelling results we quantify the spatiotemporal evolution of the salt diapir and its host sediments with respect to the vertical and horizontal displacements. The model set-up and input parameters are systematically varied to determine the controlling factors of the interaction. Our results indicate that diapirs will rise up to +2.7 m in front of an ice sheet and will be pushed down up to -36 m below an ice sheet. The reactivation of salt structures by ice-sheet loading will influence the depositional architecture and preservation potential of glacial and interglacial deposits in their vicinity. Also the long-term stability of waste-disposal sites within salt structures and the integrity of structural hydrocarbon reservoirs related to salt structures are likely to be affected by ice-induced salt flow.

Model setup

Model geometry and parameters

To simulate the interaction between subsurface salt structures and the load applied by an ice sheet a 2D finite-element model was built using the commercial software ABAQUS™ (Version 6.12). The model represents a 50 km long and 10 km deep cross-section through the uppermost crust (Fig. 2). The model domain was meshed using triangular plane-strain elements with a maximum edge length of ~50 m.

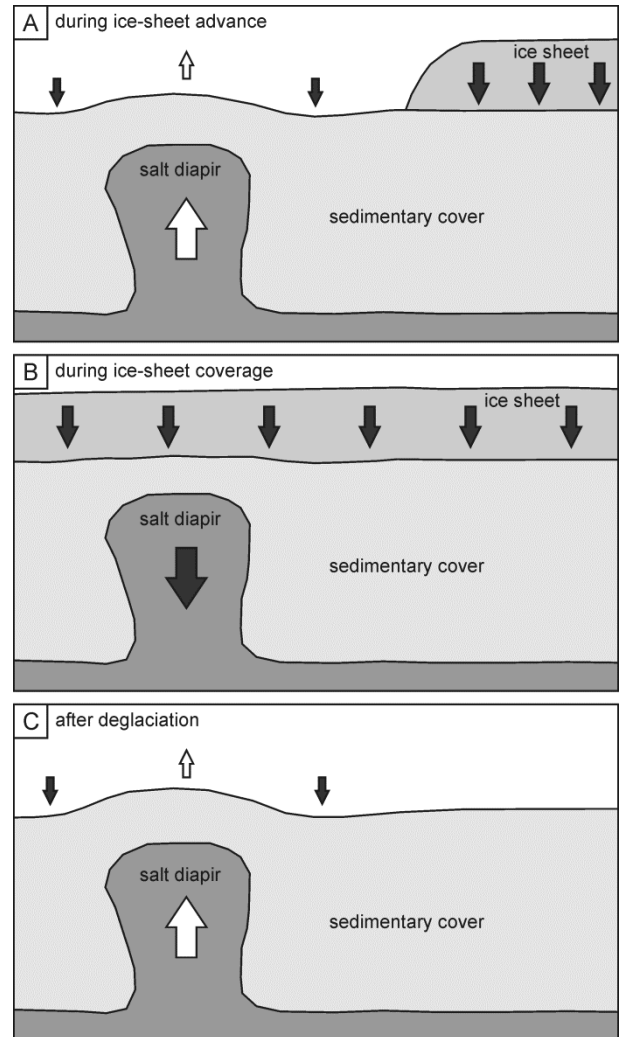


Fig. 1: Conceptual model of the interaction of salt diapirs and ice sheets (compiled from Liszkowski, 1993; Lehné & Sirocko, 2007; Sirocko *et al.*, 2008). **A)** During the ice advance the diapir rises due to the load applied to the salt source layer by the ice sheet. **B)** During ice coverage the diapir is pushed down by the load of the ice sheet applied to the top of the diapir. **C)** After deglaciation the diapir may rise again.

Boundary conditions were defined to fix the bottom of the model in both the horizontal and vertical directions and the two sides of the model in the horizontal direction. The internal geometries of the modelled layers were chosen to resemble the geometries of salt structures and their overburden in intra-continental basins, for example in the Central European Basin System (s. Section 3). The physical parameters (e.g., density, elasticity) of the different materials in the model (Table 1) represent those of typical sedimentary rocks (Kopf, 1967; Lama & Vutukuri, 1978; Gercek, 2007; Bräuer *et al.*, 2011; Riosecco *et al.* 2013). The salt has a linear viscosity of $1 \cdot 10^{17}$ to $1 \cdot 10^{18}$ Pa*s, which reflects the range of natural variations in salt viscosity (Van Keken *et al.*, 1993; Weijermars *et al.*, 1993). Such values have also been applied in several other numerical simulations of salt tectonics (e.g., Gemmer *et al.*, 2004; Ismael-Zadeh *et al.*, 2004; Albertz & Ings, 2012; Allken *et al.*, 2013). However, the viscosity of natural salt will broadly vary depending on salt mineralogy, grain size, water contents and temperature (Van Keken *et al.*, 1993; Weijermars *et al.*, 1993).

To gain insight into the control on the interaction between salt structures and ice-sheet loading, the geometry and rheology of the modelled cross-sections were systematically varied. Also, simulations with different cross-sections were conducted to investigate the effect of model geometry on the response of the salt diapir to ice-sheet loading.

A first series of simulations was run with a cross-section representing an idealised symmetrical salt diapir, overlain by overburden strata forming both primary and secondary rim-synclines (Fig. 2C, D). The base of the salt layer has a depth of 1600 m or 5000 m, respectively. The crest of the salt diapir is covered by ~50 m of overburden. Except for the diapir at the centre of the cross-section, the salt layer is horizontal and has a constant thickness. The thickness of the salt layer was modified in different model runs (125, 250 and 500 m).

A second series of models was run with a geometry based on a northeast-southwest trending regional lithostratigraphic cross-section from the Helmstedt-Staßfurt salt wall in the Subhercynian Basin in northern Germany (Figs. 2E, 3; cf., Chapter 3). The cross-section is centred on an approximately symmetrical salt diapir. The base of the salt has a depth of 1600 m; the crest of the diapir is covered by ~50 m of overburden. Below the northeastern rim syncline the remnant salt layer has a maximum thickness of ~440 m and pinches out ~5 km from the diapir. The remnant salt layer beneath the southwestern rim syncline is thinner (~50 m) and passes laterally into a 10 km wide, ~900 m thick salt pillow. Beyond the salt pillow to the southwest and the salt pinch-out to the northeast strata are horizontal and have constant thicknesses. The lithological units represent the Palaeogene infill of the secondary rim synclines, the Upper Triassic Keuper Group, the Middle Triassic Muschelkalk Group, the Lower Triassic Buntsandstein Group, the salt of the Upper Permian Zechstein Group and the underlying Palaeozoic sedimentary basement rocks (Table 1).

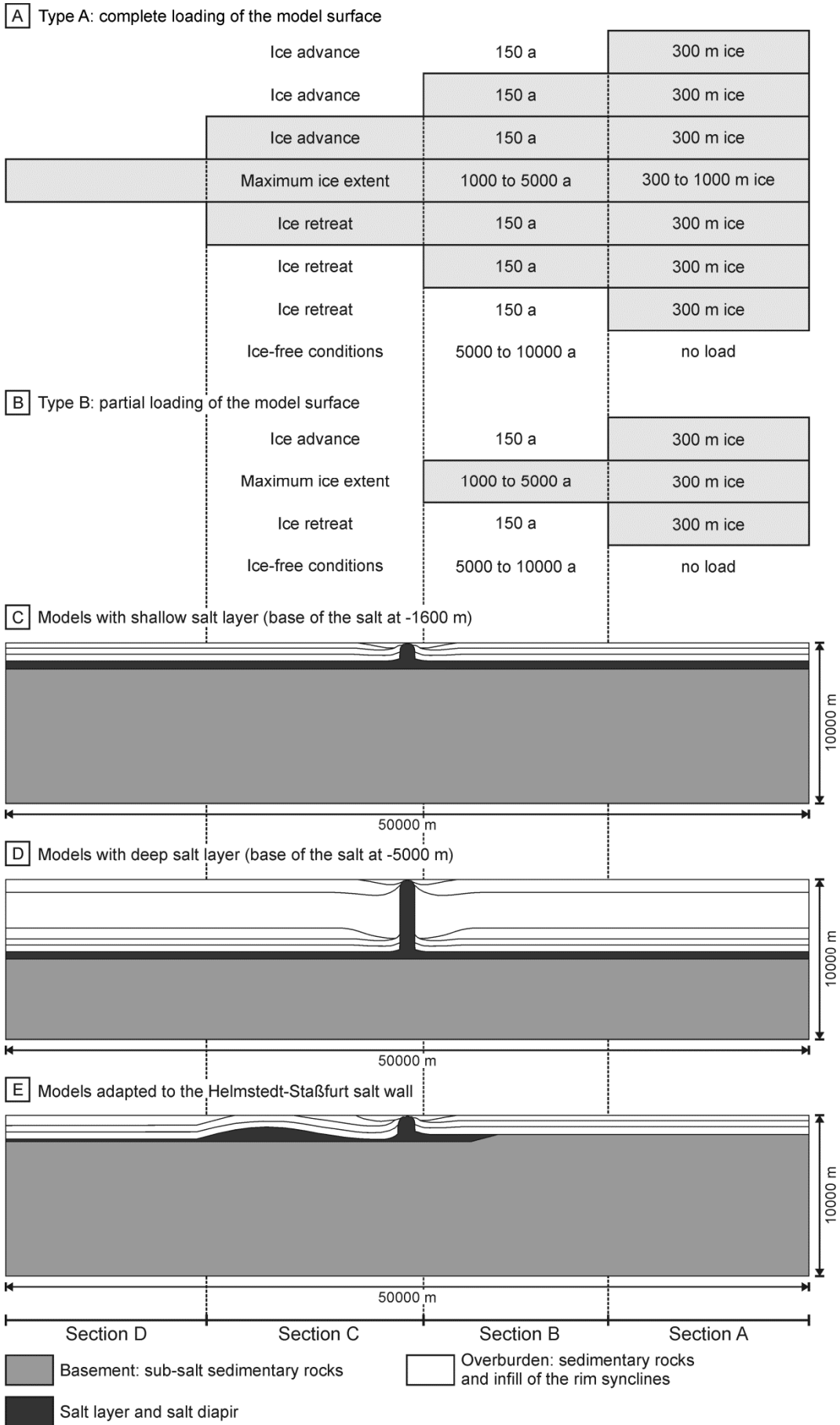


Fig. 2 (previous page): **A)** Scheme for the temporal evolution of ice-sheet loading for an ice advance that transgresses the diapir (δ Type A δ). The shading indicates which sections (dashed lines) are loaded during the respective modelling step. The duration and ice thickness for each step is given. **B)** Scheme for the temporal evolution of ice-sheet loading for an ice advance that terminates in front of the diapir (δ Type B δ). **C)** Geometry of the model with shallow salt layer and small diapir. **D)** Geometry of the model with deep salt layer and large diapir. **E)** Geometry of the model with a cross-section adapted from the geological cross-section of the Helmstedt-Staßfurt salt wall (Fig. 3C).

Simulation of ice-sheet loading

The applied load was adjusted to reflect ice-sheet loading and unloading during the Pleistocene glaciations. To simulate an ice advance from the northeast (right side of the model) to the southwest (left side of the model) the surface of the model was partitioned into four sections (A to D; Fig. 2). The sections were loaded in consecutive steps to simulate the ice advance, beginning with Section A. The ice retreat was simulated by consecutive unloading of the sections in reverse order, beginning with Section D. The boundary between sections B and C was offset 1 km to the right from the centre of the model.

The load was applied as pressure and corresponds to the weight of the ice sheet (ice density: 900 kg/m^3). The thickness of an idealised circular ice sheet with a parabolic profile can be estimated

Table 1: Model units, corresponding stratigraphic units and mechanical parameters used in the simulations.

Model unit	Stratigraphic unit	Lithology ^{a)}	Density ^{b)} (kg/m^3)	Elastic modulus ^{c)} E (GPa)	Poisson ratio ^{d)} P	Viscosity ^{e)} μ (Pa*s)	Yield stress ^{f)} (MPa)	
Overburden strata	Palaeogene	unconsolidated clastics and lignite	2000	5	0.25	-	1	
		clastics and lignite	2100	5	0.25	-	1 - 10	
	Triassic	Jurassic / Cretaceous	limestone and marlstone	2500	40	0.25	-	40
		Keuper	marlstone and sandstone	2500	40	0.25	-	40
		Muschelkalk	limestone and marlstone	2600	50	0.25	-	50
	Buntsandstein	mudstone and sandstone	2600	50	0.25	-	50	
Salt layer	Permian	Zechstein	salt	2200	30	0.25	$1*10^{17}$ - $1*10^{18}$	-
Basement	Palaeozoic	sedimentary rocks	2700	60	0.25	-	300	

a) Look, 1984 b) Kopf, 1967 c) Riosecco *et al.* 2013; Bräuer *et al.*, 2011 d) Gercek, 2007 e) Van Keken *et al.*, 1993 f) Lama & Vutukuri, 1978

based on the distance to the ice margin and basal shear stress of the ice sheet (Nye, 1952; Lambeck *et al.*, 2006; Benn & Hulton, 2010). We estimated ice thicknesses between 300 and 1000 m, assuming that our case study areas were 40 to 200 km distant from the ice margin (cf., Section 3). The last step without load represents the re-adjustment of the modelled section to non-glaciated, unloaded conditions. The durations of the loading and unloading phases were adjusted to represent realistic glacial episodes (Fig. 2A, B). The duration of each modelling step during ice advance and retreat is 150 a, corresponding to a rate of ice advance and retreat of ~110 m/a, which is in the range of estimates for advance rates of the Pleistocene ice sheets (Ehlers, 1990; Lunkka *et al.*, 2001; Clark *et al.*, 2012; Narloch *et al.*, 2013). The durations of the glacial maxima were varied to examine the reactions to different periods of loading. Durations of 1000 to 5000 a can be estimated for stable active ice margins during Pleistocene glacial maxima (Lambeck *et al.*, 2006; Lüthgens *et al.*, 2011).

Two different maximum ice extents were modelled. Type **1** represents a glaciation where the modelled section is completely ice-covered (Fig. 2A). The simulated thickness of the ice sheet was 300 m during ice advance and retreat and 300, 500 and 1000 m, respectively, during the maximum ice extent. The ice thickness was increased during the maximum ice extent to simulate the greater thickness of a large ice sheet at its maximum extent. Type **2** represents an ice advance, where the salt diapir is not transgressed by the ice sheet and the ice advance halts 1000 m in front of the diapir (Fig. 2B). The simulated ice thickness for this configuration was 300 m for all steps.

Model runs with the geometry adapted to the regional lithostratigraphic cross-section of the Helmstedt-Staßfurt salt wall were performed with multiple ice-sheet loading-unloading phases to simulate the different glaciations that affected the study area during the Middle Pleistocene. However, there is no well-established temporal framework for the Middle Pleistocene glaciations, especially for the duration of the maximum ice extents and the temporary halts during ice advance and retreat. Hence, four different simulations were conducted with two and three ice advances, respectively, and variable durations of the glacial maxima. In the study area, the Helmstedt-Staßfurt salt wall is crossed by a terminal moraine, which has been attributed to an ice-marginal position during both ice advance and retreat (Look, 1984). To simulate the effects of a prolonged halt of the ice sheet at this line, a halt of the ice margin of 1000 a at a distance of 1000 m to the diapir, during both the advance and retreat of the ice sheet, was included in one simulation.

Case study

The Central European Basin System

The Central European Basin System (CEBS) contains numerous salt structures and was affected by repeated ice advances during the Pleistocene. It therefore represents a perfect area to study the interaction of ice sheet and salt structures (Fig. 3A). The formation of the CEBS commenced in the latest Carboniferous to Early Permian after the Variscian Orogeny (Betz *et al.*, 1987; Kley *et al.*, 2008). Dur-

ing the Mesozoic changing tectonic regimes led to the formation of various subbasins and increasing basin complexity (Fig. 3A). The evolution and the present day geometries within the CEBS are strongly influenced by rising Permian salt. Salt movement in the CEBS was initially triggered by extensional faulting during the Early Triassic (Kockel, 2003; Mohr *et al.*, 2005; Lohr *et al.*, 2007). Subsequent pulses of extension during the Late Triassic to early Late Cretaceous caused further phases of salt movement (Jaritz, 1973; Mohr *et al.*, 2005; Stollhofen *et al.*, 2008). The Late Cretaceous basin inversion again led to the mobilisation of salt and was commonly accompanied by shortening of salt structures (Kockel, 2003; Mohr *et al.*, 2005; Lohr *et al.*, 2007; Brandes *et al.*, 2013).

The Subhercynian Basin

For a case study we chose the Subhercynian Basin, which is a relatively small subbasin of the CEBS located at its southern margin. The Subhercynian Basin is bounded by the Gifhorn fault zone to the west, by the Harz Mountains to the southwest and the Flechtingen High to the northeast (Stackebrandt, 1986; Fig. 3B). The formation of the Subhercynian Basin is related to the Late Cretaceous phase of basin inversion at the southern margin of the CEBS (Voigt *et al.*, 2006; Brandes *et al.*, 2013). The up

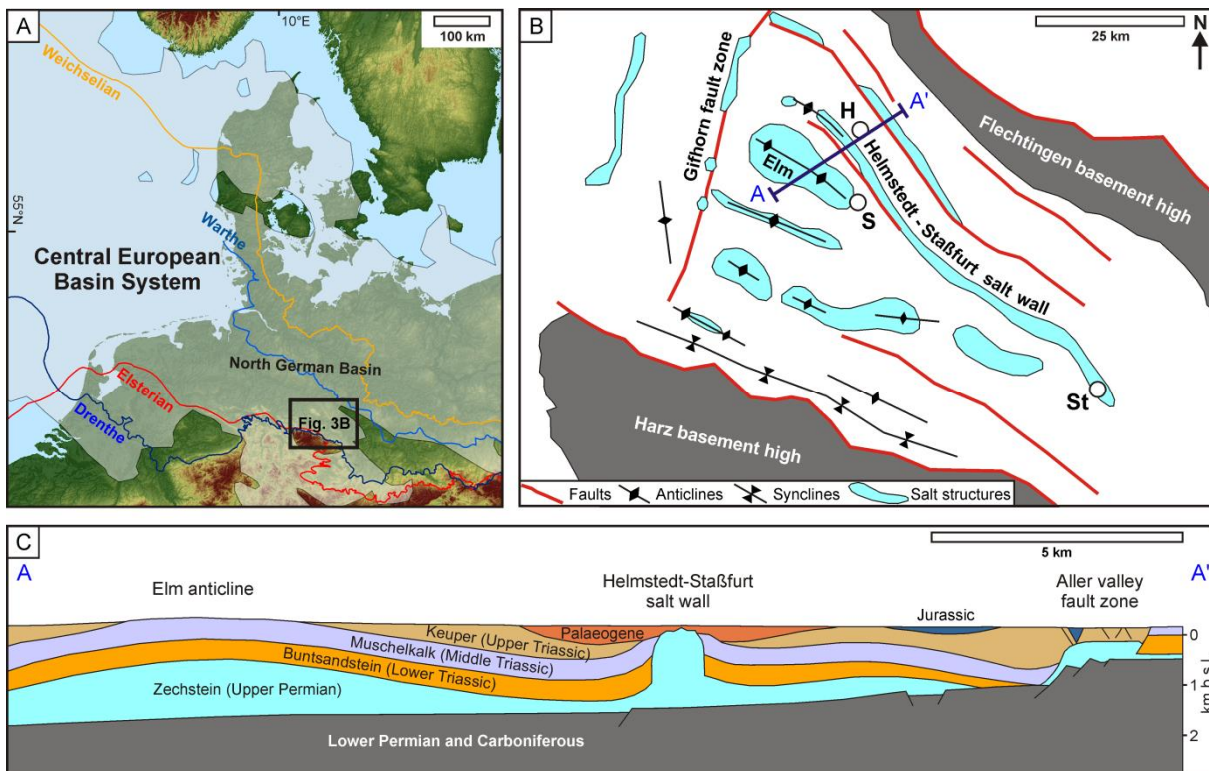


Fig. 3: **A)** Overview map of the Central European Basin System, which is outlined by the present day extent of Permian deposits (shaded area; modified after Maystrenko *et al.*, 2013). The maximum extents of the major Pleistocene ice advances are indicated (modified after Ehlers *et al.*, 2011). The Subhercynian Basin is located within the black box. **B)** Structural map of the Subhercynian Basin (based on Stackebrandt, 1986; modified after Brandes *et al.*, 2012; H: Helmstedt; S: Schöningen; St: Staßfurt). **C)** Cross-section of the Helmstedt-Staßfurt salt wall (modified after Baldschuhn *et al.*, 1996), which provided the base for the model geometries. The location of the cross-section is shown in Fig. 3B (blue line).

to 2-3 km thick basin fill has the highest thickness at the southwestern basin margin and pinches-out towards the northeastern basin margin (DEKORP Basin Research Group, 1999). Diapirs and pillows of salt of the Upper Permian Zechstein Group subdivide the fill of the Subhercynian Basin into several northwest-southeast trending anticlines and synclines (Fig. 3B). The lower basin fill comprises Permian to Cretaceous pre-inversion deposits and is dominated by Triassic rocks (Look, 1984; Baldschuhn *et al.*, 1996; Fig. 3C). Up to 2.5 km thick Upper Cretaceous syn-inversion deposits occur at the southern basin margin (Voigt *et al.*, 2006). Palaeogene deposits are restricted to salt-related minibasins, as the rim synclines of the Helmstedt-Staßfurt salt wall (Look, 1984; Karpe, 1994).

The Helmstedt-Staßfurt salt wall trends northwest-southeast, is ~70 km long and on both sides accompanied by secondary rim synclines (Fig. 3B). The infill of the rim synclines consists of up to 360 m thick unconsolidated Palaeogene coal-bearing marginal marine deposits (Manger, 1952; Brandes *et al.*, 2012; Osman *et al.*, *in press*). A northwest-southeast striking normal fault below the salt wall suggests initial reactive salt rise during Late Triassic extension (Baldschuhn *et al.*, 1996; Brandes *et al.*, 2012). The main phase of salt rise and subsidence in the rim synclines occurred during the Palaeogene and was diachronous along strike (Niebuhr & Ernst, 1991; Karpe, 1994; Brandes *et al.*, 2012). In the model of Brandes *et al.* (2012) the salt wall was initiated by diapirs defining the terminations of the salt wall, which were subsequently connected by the rising salt. This interpretation is supported by deposits getting successively younger along strike towards the centre of the structure (Niebuhr & Ernst, 1991; Karpe, 1994). For the southwestern rim syncline between Helmstedt and Schöningen, Brandes *et al.* (2012) modelled maximum subsidence rates of 76-80 m/Ma for the early stage of basin evolution between 57 and 50 Ma, which subsequently decreased to minimum subsidence rates of 2-20 m/Ma for the terminal stage of basin evolution (~ 34 Ma). The decrease in subsidence rate points to depletion of the salt source layer (Brandes *et al.*, 2012). Although the salt layer has become very thin (>200 m) below the southwestern rim syncline, a salt weld is not developed.

During the Middle Pleistocene the Subhercynian Basin was transgressed by the ice sheets of the Elsterian (MIS 10 and / or 12) and Saalian Drenthe (MIS 6) glaciations, while the subsequent younger Saalian Warthe (MIS 6) and Late Pleistocene Weichselian (MIS 2) ice advances did not reach the study area (Ehlers *et al.*, 2011; Fig. 3A). The Palaeogene fill of the rim synclines of the Helmstedt-Staßfurt salt wall is unconformably overlain by Pleistocene deposits. The Pleistocene deposits attain a maximum thickness of ~45 m in an Elsterian tunnel valley, which is incised into the infill of the southwestern rim syncline of the Helmstedt-Staßfurt salt wall (Lang *et al.*, 2012). The presence of Elsterian and Saalian subglacial tills, which are separated by Holsteinian (MIS 9) interglacial deposits, shows that the study area was at least twice covered by ice sheets (Urban *et al.*, 2011; Lang *et al.* 2012).

Modelling results

All our simulations indicate that salt diapirs respond to the load applied by ice sheets; however, deformation of the overburden is restricted to the area immediately above the salt diapir. An ice advance towards the diapir causes salt flow from the source layer below the ice sheet towards the diapir resulting in diapir uplift. The diapir continues to rise as long as the load is applied to the source layer but not to the crest of the diapir. When the diapir is transgressed by the ice sheet it is pushed downwards as long as load is applied to the crest of the diapir. During and after the removal of the ice load large parts of the displacement are reversed due to the downward salt flow during ice retreat and the elasticity of the modelled materials.

The results of our models vary depending on the pre-defined geometries and parameters. The most distinctive differences in the model responses are related to the type of ice-sheet loading (Type A vs. Type B). The location of the deformation within the salt layer and diapir depends on the style of ice-sheet loading. In all models the deformation is focussed at the top of the diapir and near the base of the diapir, i.e. at the transition into the salt source layer. In the models with complete ice coverage (Type A) the largest deformation of the salt occurs near the top of the diapir. The sense of displacement changes depending on the relative location of the ice margin (Figs. 4, 5). In contrast, in the models with partial ice coverage (Type B) the deformation in the salt is highest near the base of the diapir, where lateral salt flow from the source layer enters the diapir. Most deformation of the overburden occurs immediately above the diapir. Some deformation is also observed in the rim synclines and close to the ice-marginal positions during ice advance and retreat (Figs. 4A, 5A). Plastic deformation of the overburden is restricted to the section immediately above the crest of the diapir. The magnitude of the displacement at the end of the simulations ranges between -3.1 and +2.7 m, depending on the depth to the base of the salt layer, the salt viscosity, the thickness of the salt source layer, the duration of the loading phase and the magnitude of the load (Fig. 6).

Simulations with complete ice coverage (Type A)

In type A models, the diapir is transgressed by the ice sheet and pushed downwards. An ice advance towards the diapir causes flow of salt from the salt layer below the ice sheet towards the diapir, finally resulting in uplift of the diapir crest (Fig. 4A, B). This process commences instantaneously when load is applied onto the model surface underlain by a salt layer. Ice-sheet loading of the salt layer results in expulsion of salt from the salt layer beneath the ice sheet and salt flow into the unloaded part of the salt layer. Even an ice margin at a distance of 12.5 km to the diapir (load restricted to Section A) causes a slight (0.2-0.5 m) rise of the diapir (Fig. 4A). The diapir continues to rise as long as load is applied to the salt layer and the diapir is not transgressed by the ice sheet. As soon as the ice sheet transgresses the diapir, the rise of the diapir terminates and the diapir is pushed down, resulting in a depression of the model surface above the diapir and slight broadening of the diapir, causing horizon-

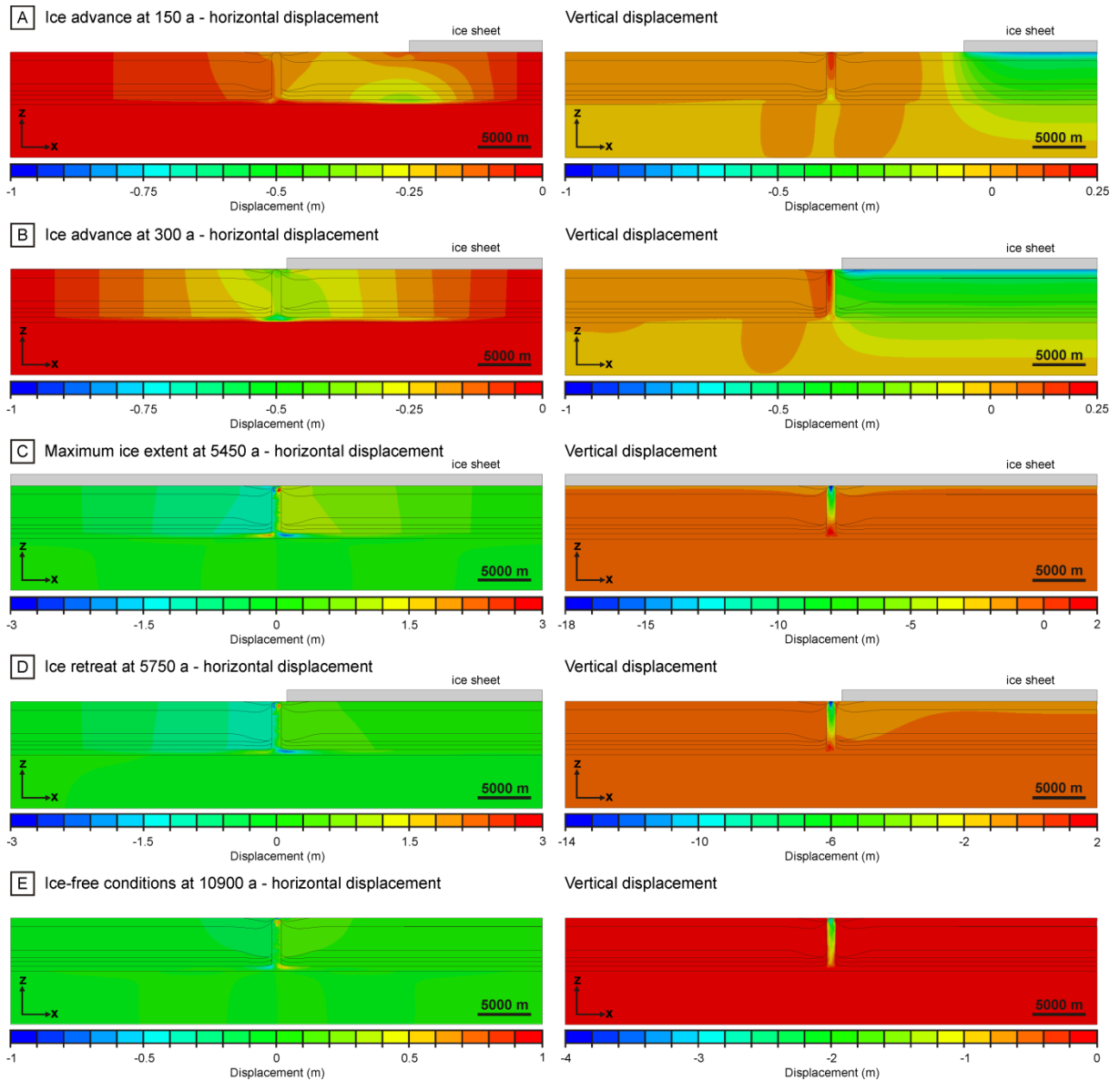


Fig. 4: Horizontal and vertical displacement of the modelled cross-section during an ice loading-unloading cycle with complete ice coverage. The depth to the base of the salt layer is 5000 m; the salt layer is 500 m thick. The grey bar at the model surface represents the extent of the ice sheet. The applied load corresponds to the weight of a 300 m thick ice sheet during ice advance and retreat and a 500 m thick ice sheet during the maximum ice extent. **A)** Ice advance after 150 a model time. **B)** Ice advance after 350 a model time. **C)** End of the maximum ice extent after 5450 a model time. The duration of the maximum ice extent was 5000 a. **D)** Ice retreat after 5750 a model time. **E)** End of the ice-free period after 10900 a model time. The duration of the ice-free period was 10000 a.

tal displacement of the strata onlapping the diapir (Fig. 4C). The initially rapid downward displacement ceases when approaching a certain maximum displacement (Fig. 6A, B). The maximum observed downward displacement was -35.8 m beneath a 1000 m thick ice sheet (light blue curve in Fig. 6B). In the models with a duration of the glacial maximum of 1000 a, the displacement will eventually not reach the maximum (Fig. 6C). The downward displacement ends when the load is removed from the top of the diapir during ice retreat. The load that is applied to the salt layer during ice retreat again causes salt flow into the diapir and thus again reverses the sense of movement of the diapir (Fig. 4D).

During the early ice retreat the diapir rises very rapidly. After the complete removal of the load this upward movement continues due to the elasticity of the modelled materials (Figs. 4E; 6A, B, C). How much of the earlier downward displacement is compensated by the renewed rise and the magnitude of the final surface displacement above the diapir depends on the yield strength of the overburden, the salt viscosity, the thickness of the salt source layer and the magnitude of the load. The maximum residual downward displacement was -3.1 m (light blue line in Fig. 6B). In high viscosity salt models the displacement may even result in uplift of the surface above the diapir during ice retreat (0.6 m of uplift; red curve in Fig. 6A). The maximum observed rates of salt flow during the rise and fall of the diapir were ~20 mm/a. In the simulations with lower salt viscosity ($1 \cdot 10^{17}$ Pa*s) the maximum rate of salt flow was 60 mm/a.

Simulation with partial ice coverage (Type B)

In type B models the maximum ice advance does not transgress the diapir but terminates 1000 m in front of the diapir. Therefore, during the maximum ice extent, only one half of the model is loaded, which results in a steady salt flow from the source layer into the diapir, allowing the diapir to rise as long as load is applied (Fig. 5). The uplift of the crest of the diapir increases with longer duration of the loading phase. The rise is initially rapid and approaches a maximum value where the rate of rise becomes very low (Fig. 6D, E). After the removal of the load, the diapir slightly subsides due to the elastic behaviour of the surrounding layers. The maximum uplift above the diapir was +1.4 m (black curve in Fig. 6E). In one simulation with a deep salt layer and a thick overburden, we lowered the yield stress of the layer representing the Palaeogene deposits by one order of magnitude (1 MPa instead of 10 MPa), which resulted in larger uplift of up to +3.8 m during loading and +2.7 m of residual uplift (blue curve in Fig. 6E). The maximum observed rates of salt flow during the rise of the diapir were ~1 mm/a.

Simulations with a geometry adapted from the Helmstedt-Staßfurt salt wall

The results from the model with a setup adapted from the Helmstedt-Staßfurt salt wall (Fig. 7) are similar to those of the simplified models. The diapir begins to rise as soon as load is applied onto the salt layer. When the diapir is transgressed by the ice sheet, the sense of movement is reversed and the diapir is pushed down by up to -4.7 m until the load is removed again (Fig. 7A). Loading of the salt layer during the glacial retreat causes the diapir to rise again. The net downward displacement of the crest of the diapir and the covering overburden is up to -0.4 m at the end of the model runs (Fig. 7A). The overall amount of rise during ice advance and retreat is lower than in the models with an idealised geometry due to the lateral pinch-out of the salt layer. In the simulation with a stationary ice margin northeast of the diapir, the amount of rise of the diapir is up to +1.3 m during ice advance (Fig. 7D).

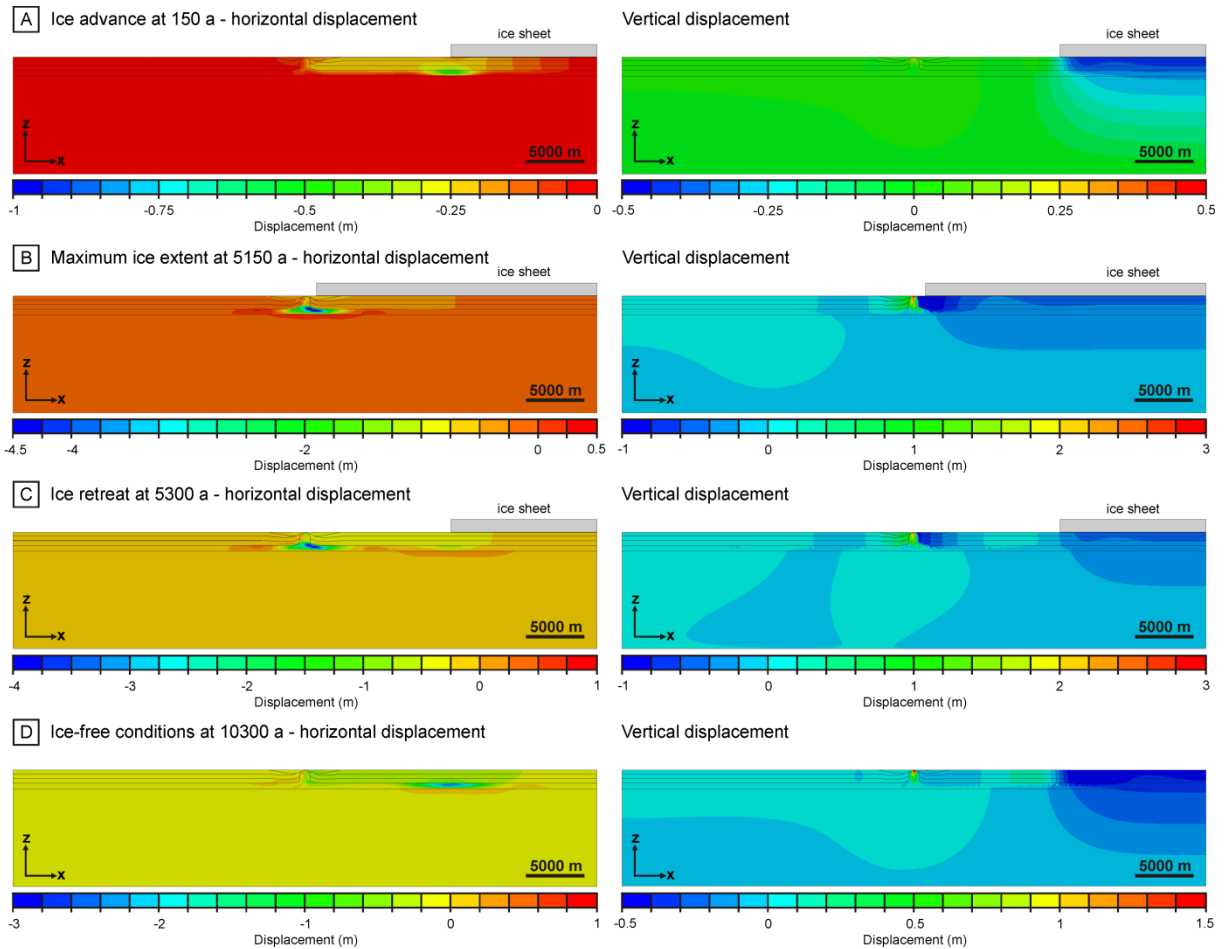


Fig. 5: Horizontal and vertical displacement of the modelled cross-section during an ice loading-unloading cycle with partial ice coverage. The depth to the base of the salt layer is 1600 m; the salt layer is 500 m thick. The grey bar at the model surface represents the extent of the ice sheet. The applied load corresponds to the weight of a 300 m thick ice sheet during all steps. **A)** Ice advance after 150 a model time. **B)** End of the maximum ice extent after 5150 a model time. The duration of the maximum ice extent was 5000 a. **C)** Ice retreat after 5300 a model time. **D)** End of the ice-free period after 10300 a model time. The duration of the ice-free period was 10000 a.

However, the amount of upward vertical displacement is by far exceeded by the downward movement during the maximum ice extent (up to -4.4 m). If the ice sheet remains for a longer time interval in the rim syncline during the retreat, the diapir experiences a longer period of rising, which results in a net uplift of the diapir (up to +0.5 m). The simulations with several ice-sheet loading-unloading cycles show that the difference in displacement between the first and the second or third glaciation is of the order of only several centimetres and hence rather low (Fig. 7A, B, C).

Discussion

Controlling factors for salt diapir response to ice-sheet loading

The style and magnitude of the reaction depends on the location of the ice margin during the maximum ice advance, the thickness of the ice sheet, the duration of the loading phases, the size of the salt

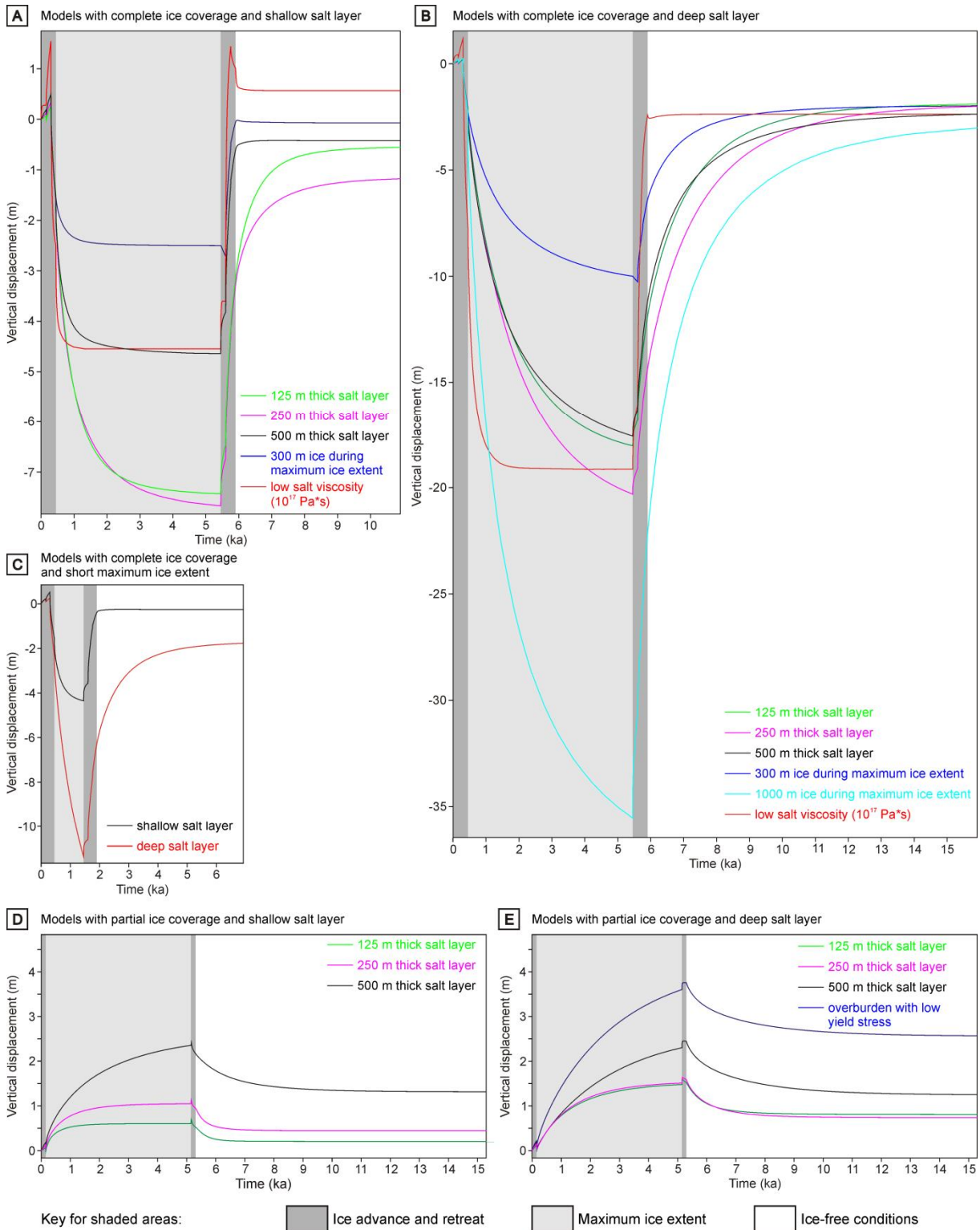


Fig. 6: Vertical displacement at the model surface above the crest of the salt diapir. The grey shading indicates the stage of the ice advance. **A)** Models with complete ice coverage and a shallow salt layer (base of salt at -1600 m). **B)** Models with complete ice coverage and deep salt layer (base of salt at -5000 m). **C)** Models with complete ice coverage and shorter phase of maximum ice extent (1000 a). **D)** Models with partial ice coverage and shallow salt layer (base of salt at -1600 m). **E)** Models with partial ice coverage and deep salt layer (base of salt at -5000 m).

diapir, the viscosity of the salt, the yield stress of the overburden and the thickness of the salt source layer. First order control is exerted by the location of the ice margin relative to the salt diapir. If the diapir is transgressed by the ice sheet, the load applied to the top of the diapir forces the diapir to move downwards, resulting in a slight broadening of the diapir stem. The deformation during complete ice coverage is characterised by the downward displacement of the top of the salt diapir and some flow from the source layer into the diapir (Fig. 4C). The deformation at the base of the diapir is caused by downward displacement of the overburden, which is transferred into the source layer and causes lateral salt flow from the source layer into the diapir. If the diapir is not transgressed by the ice sheet but remains outside the ice margin, the load applied to the source layer causes salt flow into the diapir and rise of the diapir (Fig. 5B). The horizontal displacement due to lateral salt flow into the diapir is larger than the rise of the diapir. Lateral salt flow mainly occurs from the part of the source layer immediately beneath the ice margin.

Duration of ice loading

The magnitude of the displacement is controlled by the duration of ice-sheet loading; longer ice-sheet loading generally results in larger displacement (Fig. 6). The rate of surface displacement above the diapir is initially high (up to 10 mm/a) but ceases rapidly when approaching the maximum displacement. In models with a shallow salt layer the maximum displacement is reached within the first 1000 a of the maximum ice-loading phase in most simulations (Fig. 6A, C, D). Models with a deep salt layer are more inert and take longer to attain the maximum displacement. However, the largest part of the displacement occurs again within the first 1000 a of the maximum ice-loading phase (Fig. 6B, E). An endurance of a stable ice margin of ~1000 a is thus sufficient to allow for significant rise of a diapir at the ice margin. Much longer loading phases may apply if a diapir is transgressed by an ice sheet and thus not affected by fluctuations at the ice margin.

Rates of salt flow and maximum displacement

The rates of salt flow in the models with complete ice coverage were more than one order of magnitude higher than those in the models with partial ice coverage (20 mm/a vs. 1 mm/a). This difference is probably related to the effect of an ice load exerted directly onto the top of a diapir versus the ice load applied onto the source layer via the overburden. The rates of salt flow triggered by the ice load applied onto the source layer are within the range of estimates for long-term flow rates of salt in the Central European Basin System (Zirngast, 1996; Kukla *et al.*, 2008).

All model runs indicate that the movement of the diapir approaches a maximum displacement, where rise or fall of the diapir ceases (Fig. 6). The maximum displacement is controlled by an equilibrium state between ice-sheet loading and the elasticity and compressibility of the overburden. In models with complete ice coverage the downward displacement of the diapir is also counteracted by salt flow from the source layer into the diapir. The magnitude of the maximum displacement and the loading

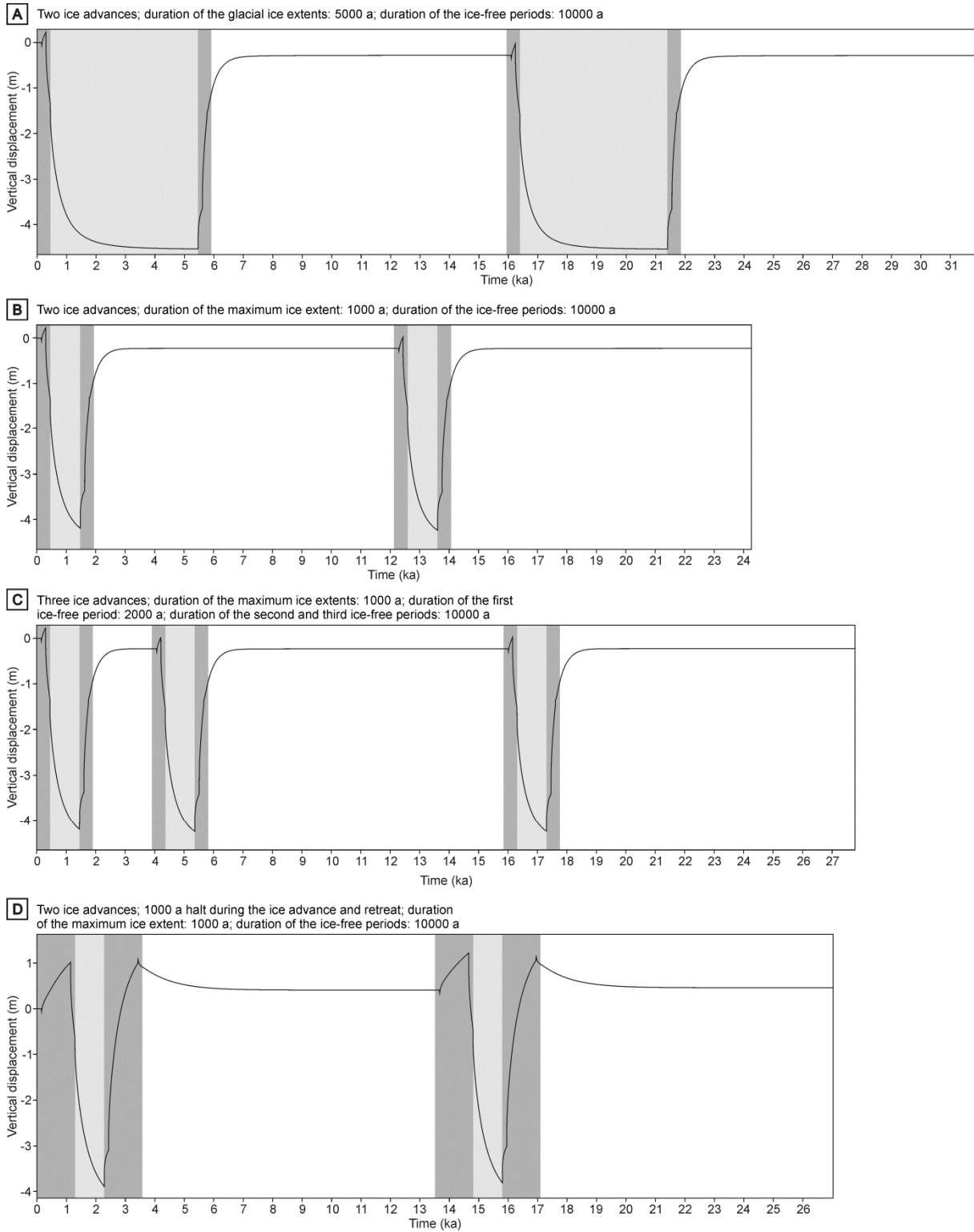


Fig. 7: Vertical displacement at the model surface above the crest of the salt diapir for models adapted from the geometry of the Helmstedt-Staßfurt salt wall and multiple ice advances. The grey shading indicates the stage of the ice advance (key is given in Fig. 6.). The ice thickness is 300 m during ice advance and retreat and 500 m during maximum ice extent. **A)** Two ice advances with maximum ice extent periods lasting 5000 a and ice-free periods lasting 10000 a. **B)** Two ice advances with maximum ice extent periods lasting 1000 a and ice-free periods lasting 10000 a. **C)** Three ice advances with maximum ice extent periods lasting 1000 a. The first ice-free period lasts 2000 a, the second and third ice-free periods last 10000 a. **D)** Two ice advances with maximum ice extent periods lasting 1000 a and ice-free periods lasting 10000 a. During each ice advance and retreat the ice margin halts 1000 a in the northeastern rim syncline.

time until reaching it depends on the magnitude of the load, the size of the diapir, the thickness of the salt source layer and the rheology of the modelled materials.

Size of the diapir and source layer thickness

In the models with complete ice coverage (δType Aö) the size of the diapir exerts a major control on the maximum displacement, both during ice-sheet loading and after the removal of the ice load during ice retreat. The downward displacement during the maximum ice extent is three to four times larger in the models with a 5000 m deep salt layer and a large diapir compared to those with a 1600 m deep salt layer and a small diapir (Fig. 6A, B). These differences are caused by the volume of salt within the modelled section. A larger volume of salt allows for larger magnitudes of deformation. The influence of the diapir size is minor in models with partial ice coverage (δType Bö), where the flow of salt from the source layer into the diapir is the primary processes responsible for deformation (Fig. 6D, E).

The influence of the salt source layer thickness differs in the various models. In the models with partial ice coverage, the displacement is larger in models with thicker source layer, whereas this trend is more distinct in the models with a shallow salt layer than in those with a deep salt layer (Fig. 6). This reaction is interpreted as related to the available amount of salt in the source layer and the higher resistance to flow in a thinner source layer. Salt flow from a thicker source layers is in general much more effective than from a thin source layers due to the lower influence of boundary drag forces (Cohen & Hardy, 1996; Waltham, 1997; Hudec & Jackson, 2007). In the models with complete ice coverage the influence of the source layer thickness is less pronounced, which is probably caused by the predominance of deformation in the upper part of the salt diapir. The largest displacements (up to -21.2 m; pink curve in Fig. 6B) occur in the models with 250 m thick source layers, while the 500 m thick source layer shows the lowest displacement (-18.3 m; black curve in Fig. 6B).

Salt viscosity

The magnitude of the displacement in the models is further controlled by the viscosity of the salt, with lower salt viscosities resulting in higher displacement and higher rates of salt flow (red curves in Fig. 6A, B). This finding is in agreement with other modelling studies, which showed that the salt viscosity exerts a fundamental control on the evolution of salt structures (Cohen & Hardy, 1996; Gemmer *et al.*, 2004; Albertz & Ings, 2012). In our models we assumed a linear viscous behaviour of the salt. However, natural salt flow may also behave power-law viscous, where the dynamic viscosity decreases with increasing rates of shear (Van Keken *et al.*, 1993; Hudec & Jackson, 2007), probably reducing the magnitude of displacement.

The interaction of salt structures and ice sheets

Our modelling results generally support the previously developed conceptual models for the interaction of ice sheets and salt diapirs, although our modelled displacements considerably differ from those

estimated from field observations in the Central European Basin System (e.g., Liszkowski, 1993; Sirocko *et al.*, 2008). Our models imply that the fall of a diapir beneath an ice sheet attains larger magnitudes (up to -36 m) than the rise in front of the advancing ice margin (up to +3.8 m). This is probably owed to the higher mobility of the large salt body of the diapir compared to the relatively thin salt source layer. The lateral flow of salt from the source layer into the diapir during complete ice coverage is much lower than the downward displacement in the upper part of the diapir. However, the largest part of the downward displacement is compensated by the reversal of the salt flow and rise of the diapir during ice retreat. The previous conceptual models assume actively rising salt structures, which are supported or impeded in their rise by ice-sheet loading, while our models start with inactive salt diapirs. Active salt structures will probably undergo more uplift in front of an ice sheet, which causes additional load onto the source layer, while the downwards displacement of a salt structure beneath an ice sheet will be counteracted by ongoing salt rise, resulting in lower magnitudes of displacement.

Subglacial processes

Our models show a strong depression above diapirs beneath ice sheets. Most of the subglacial fall of the diapir is compensated by reversed salt flow during the subsequent ice retreat and interglacial phases, preserving only a shallow depression of the surface above salt diapirs (Fig. 4E). Such depressions might serve as preferential pathways for subglacial meltwater and potentially add to erosion. However, the interaction between salt structures and meltwater erosion may be more complex due to the increased heat-flux above salt structures (e.g., Bayer *et al.*, 1997, Delisle *et al.*, 2007; Grassmann *et al.*, 2010). The primary control on the occurrence of subglacial erosion by ice and meltwater is exerted by the erodibility of the substratum, which is closely coupled to the drainage capacity (Huuse & Lykke-Andersen, 2000; Stackebrandt, 2009; Janszen *et al.*, 2012). Fracture zones above reactivated salt structures will further contribute to the erodibility of the substratum and thus represent zones of preferential incision (Dobracki & Krzyszkowski, 1997; Huuse & Lykke-Andersen, 2000; Grim & Sirocko, 2012). The drainage capacity also strongly affects the coupling between the glacier and the bed and thus the sliding behaviour of an ice sheet (Piotrowski & Tulaczyk, 1999; Narloch *et al.*, 2013). The presence of permafrost considerably lowers the drainage capacity (Narloch *et al.*, 2013). The reduced thickness of permafrost in the proximity of salt structures (Delisle *et al.*, 2007; Grassmann *et al.*, 2010) may increase the drainage capacity, increase the ice-bed coupling and thus influence the regional flow pattern of the ice sheet. Increased ice-bed coupling slows down the sliding ice sheet (Narloch *et al.*, 2013) and favours glacetectonic thrusting at the ice margin (Van der Wateren, 2002; Passchier *et al.*, 2010). The influence of the thermal conditions above salt structures on the behaviour of the ice sheet will probably be larger than the influence of the topography related to rising or falling salt diapirs.

Reaction of the rim synclines

The surface of our models displays some downward displacement above the salt diapir and in the rim synclines during and after ice-sheet loading (Fig. 4C). In models with partial ice coverage the subsidence is restricted to the ice-covered rim syncline, while the other rim syncline is slightly uplifted (Fig. 5C). Subsidence in rim synclines is created by the expulsion of salt from the underlying source layer due to sediment loading (Waldron & Rygel, 2005; Hudec & Jackson, 2007; Brandes *et al.*, 2012). Salt flow from the source layer beneath the ice sheet occurs not only from beneath the rim synclines, but also from more distant parts of the ice-loaded salt source layer. Significant thinning of the source layer beneath the rim synclines is thus prevented. The deformation observed in the rim synclines in our models is rather related to the compaction of their low-strength infills than to the expulsion of underlying salt from the source layer. Salt flow from the source layer is controlled by the thickness of the source layer (Fig. 6D, E; cf. Section 5.1). Uplift observed in the rim syncline that was not covered by ice is caused by the deforming salt diapir, which is displaced away from the ice sheet.

Comparison to other models

Our modelling results can be compared to models where salt movement is triggered by a prograding sediment wedge. In these models salt is expelled basin-wards beneath the prograding sediment wedge. The style of the resulting salt structures and overburden deformation depends strongly on the progradation rate and style (Cohen & Hardy, 1996; Koyi, 1996; Gemmer *et al.*, 2004; Vendeville, 2005; Adam & Krezsek, 2012). The advance of an ice sheet into a salt-bearing basin may cause differential loading comparable to a prograding sediment wedge (Jackson & Talbot, 1986). The rates of ice sheet advance are much faster than the progradation rates in sedimentary systems. The Pleistocene ice sheets advanced at rates of 75-150 m/a (Ehlers, 1990; Lunkka *et al.* 2001; Clark *et al.*, 2012), while sedimentary wedges at passive continental margins typically prograde at rates of several centimetres per year (Carvajal *et al.*, 2009). Although the density of ice is lower ($\sim 900 \text{ kg/m}^3$) than the density of unconsolidated siliciclastic sediments ($\sim 2000 \text{ kg/m}^3$), an advancing ice sheet is able to apply the same load several hundred times faster than a prograding sediment wedge. However, ice-sheet loading is a short-lived and transient phenomenon and the load applied by the weight of an ice sheet is removed with the decay of the ice sheet. Previously inactive salt structures will therefore become only reactivated during ice-sheet loading and unloading, while a permanent reactivation seems unlikely.

Implications for the salt structures in the Central European Basin System

Regional studies of the interaction between salt structures and ice-sheet loading need to take into account the geometry of the salt structure, ice thickness and the distance of the particular study area to the ice margin. Rising salt diapirs in front of an advancing ice sheet may explain local correlations between terminal moraines and salt structures (Gripp, 1952; Schirrmeister, 1999; Sirocko *et al.*, 2008). The northern parts of Central European Basin System experienced more ice advances, thicker ice

sheets and longer durations of ice coverage than areas farther south. The general trend of the Middle and Late Pleistocene advances of the Fennoscandian ice sheets is characterised by successively lesser extents of the younger ice advances (Fig. 3A). The different maximum extents of the ice sheets may have led to complex interactions between ice sheets and salt structures. Salt structures located near the maximum extent of the younger ice advances were thus subject to both subglacial fall during the older ice advances and proglacial rise during the younger ice advances. This pattern is similar to the displacement curve shown in Fig. 7D, where the downward displacement during ice-sheet coverage is compensated and exceeded by the rise of the diapir in front of the ice sheet during a delayed phase of ice retreat.

Field examples

Based on our modelling results it seems unlikely that a few metres of salt rise could represent a significant obstacle to a large advancing ice sheets as assumed in previous conceptual models. The Subhercynian Basin for example, where differences in elevation of more than 200 m occur, was twice completely transgressed by the Middle Pleistocene ice sheets (Look, 1984; Ehlers *et al.*, 2011; Fig. 3A). Nevertheless, a surface uplift of only a few metres will be able to influence the depositional architecture of proglacial deposits, for example by restricting the distribution of ice-proximal deposits to a zone between the glacier and the diapir, and act as buttress for the glacitectonic formation of push-moraines. Kurzawa (2003) observed significant differences in the depositional architectures of Pleistocene glacial deposits due to actively rising salt structures in Poland. Above the crests of rising salt structures the Pleistocene deposits are thin and comprise mostly till. In contrast, thick successions of till, glacialfluvial and glaciallacustrine deposits, which were deposited during multiple glacial advances, are preserved within the adjacent rim synclines (Kurzawa, 2003).

Maps of the salt diapirs, which show indications for Pleistocene to Holocene rise, were published for Germany (Illies, 1955; Hurtig, 1965) and Poland (Liszkowski, 1993). Interestingly, most of the diapirs, which have penetrated the modern surface or are interpreted as actively rising, are located in a zone close to the maximum ice extent of the last, respectively the penultimate glaciation. Therefore, the recent rise of these diapirs has likely been triggered or at least amplified by ice-sheet loading. Sirocko *et al.* (2002) presented an example from the Wedehof diapir in northwestern Germany, which is outlined at the modern surface by a topographic high with a central depression. According to Sirocko *et al.* (2002) the surface topography above the diapir indicates a rise of ~50 m since the Elsterian glaciation, which thus represented a topographic obstacle to the advancing ice sheets. Palaeoflow directions obtained from Saalian meltwater deposits above the diapir indicate that the diapir acted as an obstacle (Sirocko *et al.*, 2002). A similar example was presented by Stackebrandt (2005) from the Sperenberg diapir in eastern Germany, which is interpreted as having risen during the Pleistocene and Holocene due to ice-sheet loading. The cap rock of the diapir has pierced the modern surface, leading to the formation of a low hill that is surrounded by lakes that formed due to subsurface salt dissolution

(Stackebrandt, 2005). Both diapirs are located very close to Pleistocene ice margins and are thus in a setting that should be prone to the amplification of salt rise by ice-sheet loading, corresponding to our model set-up with partial ice coverage. However, compared to our modelling results the estimated magnitudes of uplift in these examples are too high to be caused by ice-sheet loading alone, but require continuous diapiric rise controlled by the regional stress field or sediment-loading in the rim synclines. Field examples also show that diapirs piercing the surface in cold and dry conditions during a glaciation may be affected by a relief reversal, if rates of salt dissolution increase in wetter interglacial climate, leading to the dissolution of the near-surface top of the diapir (cf., Gripp, 1952).

At some salt diapirs brecciation of the cap rock and incorporation of Pleistocene glacial debris into the cap rock breccia is observed (Jaritz, 1994; Caspers *et al.*, 1995; Köthe *et al.*, 2007). This incorporation has been interpreted as representing injection of the glacial debris into the cap rock breccia by the high hydraulic pressure under the ice-sheet (Caspers *et al.*, 1995). Alternatively, the elevated lithostatic pressure during ice-sheet loading and contemporary salt rise may have led to the incorporation of glacial debris into the brecciated cap rock.

For the Schöningen area, the ongoing rise of the salt wall associated with subsidence in the rim synclines has been proposed as a mechanism to explain the formation of Pleistocene and Holocene depocentres (Manger, 1952; Mania, 1998). Although new results clearly show that the Middle Pleistocene sediments have been deposited within an Elsterian tunnel valley (Lang *et al.*, 2012), the formation of thick Holocene peat bog deposits in the inner part of the rim synclines and above the salt wall may point to ongoing salt movement (cf., Manger, 1952), which was probably amplified by ice-sheet loading during the Elsterian and Saalian glaciations.

Conclusions

Our simulations indicate that salt structures respond to surface loading applied by a 300 to 1000 m thick ice sheet. The first order control is exerted by the location of the ice margin relative to the salt diapir. If the diapir is transgressed by the ice sheet, the load applied to the top of the diapir forces the diapir to move downwards, resulting in a slight broadening of the upper parts of the diapir stem. Most of this subglacial downwards displacement is compensated by a reversal of the salt flow, which causes the diapir to rise during the subsequent ice retreat and interglacial phases. If the diapir is not transgressed by the ice sheet but remains outside the ice margin, the load applied to the source layer causes salt flow from the source layer into the diapir and rise of the diapir. Plastic deformation of the overburden is restricted to the area immediately above the salt diapir. Larger displacements are observed in models with larger diapirs, thicker ice sheets, longer loading phases, higher thickness of the salt source layer, lower yield strength of the overburden and lower viscosity of the salt.

Our modelling results support the previous conceptual models of the interaction of ice sheets and salt diapirs (e.g. Liszkowski, 1993; Sirocko *et al.*, 2008), although modelled displacements are much lower

than those estimated from field examples. We therefore assume that ice-induced salt rise will not affect the large-scale advance or retreat pattern of an ice sheet. However, the rise or fall of diapirs triggered or amplified by ice-sheet loading will affect glacial erosion and deposition above the diapir and within the rim synclines. Because glaciations are a relatively short-lived phenomenon, the re-activation of salt structures by ice-sheet loading is restricted to the phases of loading and immediately thereafter. If the maximum extent of ice sheets successively decreases during the course of repeated ice advances, the rise of a diapir in front of an ice sheet during younger, less extensive ice advances will compensate and exceed the fall of a diapir beneath an ice sheet during the older, more extensive ice advance.

Acknowledgements

Financial support by the Niedersächsisches Ministerium für Wissenschaft und Kultur (MWK) is gratefully acknowledged (PRO Niedersachsen Project No. 11.2-76202-17-3/09). T. Li, G. Maniatis and H. Turpeinen are thanked for their help with ABAQUS.

References

- Aber, J.S., Ber, A. 2007: Glaciotectonism. *Developments in Quaternary Science* 6, 1-246.
- Adam, J., Krezsek, C., 2012: Basin-scale salt tectonic processes of the Laurentian Basin, Eastern Canada: insights from integrated regional 2D seismic interpretation and 4D physical experiments. *In: Alsop, G.I., Archer, S.G., Hartley, A.J., Grant, N.T., Hodgkinson, R. (Eds.), Salt tectonics, sediments and prospectivity. Geological Society Special Publications 363*, pp. 331-360.
- Albertz, M., Ings, S.J., 2012: Some consequences of mechanical stratification in basin-scale numerical models of passive-margin salt tectonics. *In: Alsop, G.I., Archer, S.G., Hartley, A.J., Grant, N.T., Hodgkinson, R. (Eds.), Salt tectonics, sediments and prospectivity. Geological Society Special Publications, 363*, pp. 303-330.
- Allken, V., Huismans, R.S., Fossen, H., Thieulot, C., 2013: 3D numerical modelling of graben interaction and linkage: a case study of the Canyonlands grabens, Utah. *Basin Research* 25, 1-14.
- Baldschuhn, R., Binot, F., Fleig, S., Kockel, F., 1996: Geotektonischer Atlas von Nordwest-Deutschland und dem deutschen Nordsee-Sektor. *Geologisches Jahrbuch A* 153, 1-55.
- Bayer, U., Scheck, M., Koehler, M., 1997: Modeling of the 3D thermal field in the northeast German basin. *Geologische Rundschau* 86, 241-251.
- Benn, D.I., Hulton, N.R.J., 2010: An Excel™ spreadsheet program for reconstructing the surface profile of former mountain glaciers and ice caps. *Computers & Geosciences* 36, 605-610.
- Ber, A., 2009: Vertical stress of the Pleistocene continental glaciers and its hypothetical evidence in present relief of northern Europe. *Polish Geological Institute Special Papers* 25, 7-12.

- Betz, D., Führer, F., Greiner, G., Plein, E., 1987: Evolution of the Lower Saxony Basin. *Tectonophysics* 137, 127-170.
- Brandes, C., Winsemann, J., 2013: Soft sediment deformation structures in NW Germany caused by Late Pleistocene seismicity. *International Journal of Earth Sciences* 102, 2255-2274.
- Brandes, C., Polom, U., Winsemann, J., 2011: Reactivation of basement faults: interplay of ice-sheet advance, glacial lake formation and sediment loading. *Basin Research* 23, 53-64.
- Brandes, C., Pollok, L., Schmidt, C., Riegel, W., Wilde, V., Winsemann, J., 2012: Basin modelling of a lignite-bearing salt rim syncline: insights into rim syncline evolution and salt diapirism in NW Germany. *Basin Research* 24, 699-716.
- Brandes, C., Schmidt, C., Tanner, D.C., Winsemann, J., 2013: Paleostress pattern and salt tectonics within a developing foreland basin (northwestern Subhercynian Basin, northern Germany). *International Journal of Earth Sciences* 102, 2239-2254.
- Bräuer, V., Eickemeier, R., Eisenburger, D., Grisseemann, C., Hesser, J., Heusermann, S., Kaiser, D., Nipp, H.-K., Nowak, T., Plischke, I., Schnier, H., Schulze, O., Sönke, J., Weber, J.R., 2011: Description of the Gorleben site Part 4: Geotechnical exploration of the Gorleben salt dome. Schweizerbart, Stuttgart, 184 pp.
- Carvajal, C., Steel, R., Petter, A., 2009: Sediment supply: The main driver of shelf-margin growth. *Earth-Science Reviews* 96, 221-248.
- Caspers, G., Jordan, H., Merkt, J., Meyer, K.-D., Müller, H., Streif, H., 1995: Niedersachsen. *In: Benda, L. (Ed.), Das Quartär Deutschlands*. Borntraeger, Berlin, pp. 23-58.
- Clark, C.D., Hughes, A.L.C., Greenwood, S.L., Jordan, C., Sejrup, H.P., 2012: Pattern and timing of retreat of the last British-Irish Ice Sheet. *Quaternary Science Reviews* 44, 112-146.
- Cohen, H.A., Hardy, S., 1996: Numerical modelling of stratal architectures from differential loading of a mobile substratum. *In: Blundell, G.I., Davison, I. (Eds.), Salt tectonics*. Geological Society Special Publications 100, pp. 265-273.
- Dehls, J.F., Olesen, O., Olsen, L., Harald Blikra, L. 2000: Neotectonic faulting in northern Norway; the Stuuragurra and Nordmannvikdalen postglacial faults. *Quaternary Science Reviews*, 19 1447-1460.
- DEKORP Basin Research Group 1999: The deep structure of the NE German Basin constraints on the controlling mechanisms of intracontinental basin development. *Geology* 27, 55-58.
- Delisle, G., Grassmann, S., Cramer, B., Messner, J., Winsemann, J., 2007: Estimating episodic permafrost development in northern Germany during the Pleistocene. *In: Hambrey, M., Christoffersen, P., Glasser, N., Hubbard, B. (Eds.), Glacial Processes and Products*. International Association of Sedimentologists Special Publications 39, pp. 109-119.
- Dobracki, R., Krzyszkowski, D., 1997: Sedimentation and erosion at the Weichselian ice-marginal zone near Golczewo, northwestern Poland. *Quaternary Science Reviews* 16, 721-740.

- Ehlers, J., 1990: Reconstructing the dynamics of the north-west European Pleistocene ice-sheets. *Quaternary Science Reviews* 9, 71-83.
- Ehlers, J., Grube, A., Stephan, H.-J., Wansa, S., 2011: Pleistocene Glaciations of North Germany ó New Results. *In: Ehlers, J., Gibbard, P.L., Hughes, P.D. (Eds.), Quaternary Glaciations ó Extent and Chronology ó A Closer Look. Developments in Quaternary Science* 15, pp. 149-162.
- Gemmer, L., Ings, S.J., Medvedev, S., Beaumont, C., 2004: Salt tectonics driven by differential sediment loading: stability analysis and finite-element experiments. *Basin Research* 16, 199-218.
- Gercek, H., 2007: Poisson's ratio values for rocks. *International Journal of Rock Mechanics & Mining Sciences* 44, 1-13.
- Grassmann, S., Cramer, B., Delisle, G., Hantschel, T., Messner, J., Winsemann, J., 2010: pT-effects of Pleistocene glacial periods on permafrost, gas hydrate stability zones and reservoir of the Mittelplate oil field, northern Germany. *Marine and Petroleum Geology* 27, 298-306.
- Grim, S., Sirocko, F., 2012: Natural depressions on modern topography in Schleswig-Holstein (Northern Germany) indicators for recent crustal movements or only kettle holes? *Zeitschrift der Deutschen Gesellschaft für Geowissenschaften* 163, 469-481.
- Gripp, K., 1952: Inlandeis und Salzaufstieg. *Geologische Rundschau* 40, 74-81.
- Hampel, A., Hetzel, R., 2006: Response of normal faults to glacial-interglacial fluctuations of ice and water masses on Earth's surface. *Journal of Geophysical Research* 111, B06406, DOI: 10.1029/2005JB004124.
- Hampel, A., Hetzel, R., Maniatis, G., Karow, T., 2009: Three-dimensional numerical modeling of slip rate variations on normal and thrust fault arrays during ice cap growth and melting. *Journal of Geophysical Research* 114, B08406, DOI: 10.1029/2008JB006113.
- Hoffmann, G., Reicherter, K., 2012: Soft-sediment deformation of Late Pleistocene sediments along the southwestern coast of the Baltic Sea (NE Germany). *International Journal of Earth Sciences* 101, 351-363.
- Houmark-Nielsen, M., 2011: Pleistocene Glaciations in Denmark: A closer look at Chronology, Ice Dynamics and Landforms. *In: Ehlers, J., Gibbard, P.L., Hughes, P.D. (Eds.), Quaternary Glaciations ó Extent and Chronology ó A Closer Look. Developments in Quaternary Science* 15, pp. 47-58.
- Hudec, M.R., Jackson, M.P.A., 2007: Terra infirma: Understanding salt tectonics. *Earth-Science Reviews* 82, 1-28.
- Hurtig, E., 1965: Beziehungen zwischen Oberflächenmorphologie und Salzstrukturen. *Geologie & Geophysik* 7, 42-56.
- Huuse, M., Lykke-Andersen, H., 2000: Overdeepened Quaternary valleys in the eastern Danish North Sea: morphology and origin. *Quaternary Science Reviews* 19, 1233-1253.
- Illies, H., 1955: Pleistozäne Salzstockbewegungen in Norddeutschland und ihre regionale Anordnung. *Geologische Rundschau* 43, 70-78.

- Ismael-Zadeh, A., Tsepelev, I., Talbot, C., Korotkii, A., 2004: Three-dimensional forward and backward modelling of diapirism: numerical approach and its applicability to the evolution of salt structures in the Pricaspian basin. *Tectonophysics* 387, 81-103.
- Jackson, M.P.A., Talbot, C.J., 1986: External shapes, strain rates, and dynamics of salt structures. *GSA Bulletin* 97, 305-323.
- Janszen, A., Spaak, M., Moscariello, A., 2012: Effects of the substratum on the formation of glacial tunnel valleys: an example from the Middle Pleistocene of the southern North Sea. *Boreas* 41, 629-643.
- Jaritz, W., 1973: Zur Entstehung der Salzstrukturen Norddeutschlands. *Geologisches Jahrbuch A* 10, 1-77.
- Jaritz, W., 1994: Die Entwicklungsgeschichte des Standortes Gorleben als natürliches Analogon für das Langzeitverhalten eines Barrierensystems. *Zeitschrift der Deutschen Geologischen Gesellschaft* 145, 192-206.
- Johnston, A.C., 1987: Suppression of earthquakes by large continental ice sheets. *Nature*, 330, 467-469.
- Johnston, P., Wu, P., Lambeck, K., 1998: Dependence of horizontal stress magnitude on load dimension in glacial rebound models. *Geophysical Journal International* 132, 41-60.
- Karpe, W., 1994: Zur Dynamik halokinetischer Randsenken auf der Subherzynen Scholle. *Hallesches Jahrbuch für Geowissenschaften* 16, 79-93.
- Kley, J., Franzke, H.J., Jähne, F., Krawczyk, C., Lohr, T., Reicherter, K., Scheck-Wenderoth, M., Sippel, J., Tanner, D., van Gent, H., 2008: Strain and stress. *In: Littke, R., Bayer, U., Gajewski, D., Nelskamp, S. (Eds.), Dynamics of Complex Intracontinental Basins ó The Central European Basin System. Springer, Berlin, pp. 97-124.*
- Kockel, F., 2003: Inversion structures in Central Europe ó Expressions and reasons, an open discussion. *Netherlands Journal of Geosciences* 82, 367-382.
- Kopf, M., 1967: Der Dichteansatz für das Norddeutsch-Polnische Becken unter der besonderen Berücksichtigung des vertikalen Dichtegradienten. *Geologie* 16, 181-199.
- Koyi, H., 1996: Salt flow by aggrading and prograding overburdens. *In: Blundell, G.I., Davison, I. (Eds.), Salt tectonics. Geological Society Special Publications* 100, pp. 243-258.
- Köthe, A., Hoffmann, N., Krull, P., Zirngast, M., Zwirner, R., 2007: Description of the Gorleben site Part 2: Geology of the overburden and adjoining rock of the Gorleben salt dome. *Geologisches Jahrbuch C* 72, 1-201.
- Kukla, P.A., Urai, J.L., Mohr, M., 2008: Dynamics of salt structures. *In: Littke, R., Bayer, U., Gajewski, D., Nelskamp, S. (Eds.), Dynamics of Complex Intracontinental Basins ó The Central European Basin System. Springer, Berlin, pp. 233-245.*
- Kurzawa, M., 2003: The sedimentary record and rates of Quaternary vertical tectonic movements in NW Poland. *Quaternary International* 101-102, 137-148.

- Laban, C., van der Meer, J.J.M., 2011: Pleistocene Glaciation in the Netherlands. *In*: Ehlers, J., Gibbard, P.L., Hughes, P.D. (Eds.), *Quaternary Glaciations – Extent and Chronology – A Closer Look*. *Developments in Quaternary Science* 15, pp. 247-260.
- Lama, R.D., Vutukuri, V.S., 1978: *Handbook on mechanical properties of rocks – testing techniques and results – Volume 2*. *Series on Rock and Soil Mechanics* 3, 1-481.
- Lambeck, K., Purcell, A., Funder, S., Kjaer, K.H., Larsen, E., Möller, P., 2006: Constraints on the Late Saalian to early Middle Weichselian ice sheet of Eurasia from the field data and rebound modelling. *Boreas* 35, 539-575.
- Lang, J., Winsemann, J., Steinmetz, D., Polom, U., Pollok, L., Böhner, U., Serangeli, J., Brandes, C., Hampel, A., Winghart, S., 2012: The Pleistocene of Schöningen, Germany: a complex tunnel valley fill revealed from 3D subsurface modelling and shear wave seismics. *Quaternary Science Reviews* 39, 86-105.
- Lee, J.R., Busschers, F.S., Sejrup, H.P., 2010: Pre-Weichselian Quaternary glaciations of the British Isles, The Netherlands, Norway and adjacent marine areas south of 68°N: implications for long-term ice sheet development in northern Europe. *Quaternary Science Reviews* 44, 213-228.
- Lehné, R., Sirocko, F., 2007: *Rezente Bodenbewegungspotenziale in Schleswig-Holstein (Deutschland) – Ursachen und ihr Einfluss auf die Entwicklung der rezenten Topographie*. *Zeitschrift der deutschen Gesellschaft für Geowissenschaften* 158, 329-347.
- Litt, T., Schmincke, H.-U., Frechen, M., Schlüchter, C., 2008: Quaternary. *In*: McCann, T. (Ed.), *The Geology of Central Europe, Vol. 2: Mesozoic and Cenozoic*. The Geological Society, London, pp. 1287-1340.
- Lohr, T., Krawczyk, C.M., Tanner, D.C., Samiee, R., Endres, H., Oncken, O., Trappe, H., Kukla, P.A., 2007: Strain partitioning due to salt: insights from interpretation of a 3D seismic data set in the NW German Basin. *Basin Research* 19, 579-597.
- Look, E.-R., 1984: *Geologie und Bergbau im Braunschweiger Land*. *Geologisches Jahrbuch A* 78, 1-467.
- Liszkowski, J., 1993: The effects of Pleistocene ice-sheet loading-deloadng cycles on the bedrock structure of Poland. *Folia Quaternaria* 64, 7-23.
- Lunkka, J.P., Saarnisto, M., Gey, V., Demidov, I., Kiselova, V., 2001: Extent and age of the Last Glacial Maximum in the southeastern sector of the Scandinavian Ice Sheet. *Global and Planetary Change* 31, 407-425.
- Lüthgens, C., Böse, M., Preusser, F., 2011: Age of the Pomeranian ice-marginal position in northeastern Germany determined by Optically Stimulated Luminescence (OSL) dating of glaciofluvial sediments. *Boreas* 40, 598-615.
- Manger, G., 1952: *Der Zusammenhang von Salztektunik und Braunkohlenbildung bei der Entstehung der Helmstedter Braunkohlenlagerstätten*. *Mitteilungen geologisches Staatsinstitut Hamburg* 21, 7-45.

- Mania, D., 1998: Zum Ablauf der Klimazyklen seit der Elstervereisung im Elbe-Saalegebiet. *Præhistoria Thuringica* 2, 5-21.
- Marks, L., 2011: Quaternary Glaciations in Poland. *In: Ehlers, J., Gibbard, P.L., Hughes, P.D. (Eds.), Quaternary Glaciations ó Extent and Chronology ó A Closer Look. Developments in Quaternary Science* 15, pp 299-303.
- Maystrenko, Y., Bayer, U., Brink, H.J., Littke, R., 2008: The Central European Basin System ó an Overview. *In: Littke, R., Bayer, U., Gajewski, D., Nelskamp, S. (Eds.), Dynamics of Complex Intracontinental Basins ó The Central European Basin System. Springer, Berlin*, pp. 16-34.
- Maystrenko, Y. P., Bayer, U., Scheck-Wenderoth, M., 2013: Salt as a 3D element in structural modelling ó example from the Central European Basin System. *Tectonophysics* 591, 62-82.
- Mohr, M., Kukla, P.A., Urai, J.L., Bresser, G., 2005: Multiphase salt tectonic evolution in NW Germany: seismic interpretation and retro-deformation. *International Journal of Earth Sciences* 94, 917-940.
- Mörner, N.A., 2004: Active faults and paleoseismicity in Fennoscandia, especially Sweden. Primary structures and secondary effects. *Tectonophysics* 380, 139-157.
- Narloch, W., Wysota, W., Piotrowski, J.A., 2013: Sedimentological record of subglacial conditions and ice sheet dynamics of the Vistula Ice Stream (north-central Poland) during the Last Glaciation. *Sedimentary Geology* 293, 30-44.
- Niebuhr, B., Ernst, G., 1991: Faziesgeschichte und Entwicklungsdynamik von Campan, Maastricht und Eozän im Beienroder Becken (E-Niedersachsen). *Zeitschrift der Deutschen Geologischen Gesellschaft* 142, 251-283.
- Nye, J.F., 1952: The Mechanics of glacier flow. *Journal of Glaciology* 2, 82-93.
- Osman, A., Pollok, L., Brandes, C., Winsemann, J., *in press*: Sequence stratigraphy of a Paleogene coal bearing rim syncline: interplay of salt dynamics and sea-level changes, Schöningen, Germany. *Basin Research*, DOI: 10.1111/bre.12021.
- Passchier, S., Laban, C., Mesdag, C.S., Rijdsdijk, K.F., 2010: Subglacial bed conditions during Late Pleistocene glaciations and their impact on ice dynamics in the southern North Sea. *Boreas* 39, 633-647.
- Pedersen, S.A.S., 2000: Superimposed deformation in glaciotectonics. *Bulletin of the Geological Society of Denmark* 46, 125-144.
- Piotrowski, J.A., Tulaczyk, S., 1999: Subglacial conditions under the last ice sheet in northwest Germany: ice-bed separation and enhanced basal sliding? *Quaternary Science Reviews* 18, 737-751.
- Riosecco, E.M., Löhken, J., Schellschmidt, R., Tischner, T., 2013: 3-D geomechanical modelling of the stress field in the North German Basin: case study GeneSys-Borehole GT-1 in Hannover Groß-Buchholz. *PROCEEDINGS, Thirty-Eighth Workshop on Geothermal Reservoir Engineering. Stanford, USA.*

- Reicherter, K., Kaiser, A., Stackebrandt, W., 2005: The post-glacial landscape evolution of the North German Basin: morphology, neotectonics and crustal deformation. *International Journal of Earth Sciences* 94, 1083-1093.
- Scheck-Wenderoth, M., Lamarche, J., 2005: Crustal memory and basin evolution in the Central European Basin System – new insights from a 3D structural model. *Tectonophysics* 397, 143-165.
- Schirrmeister, L., 1999: Die Positionen weichselzeitlicher Eisrandlagen in Norddeutschland und ihr Bezug zu unterlagernden Salzstrukturen. *Zeitschrift für geologische Wissenschaften* 27, 111-120.
- Sirocko, F., Szeder, T., Seelos, C., Lehné, R., Rein, B., Schneider, W.M., Dimke, M., 2002: Young tectonic and halokinetic movements in the North-German Basin: its effect on formation of modern rivers and surface morphology. *Netherlands Journal of Geosciences* 81, 431-441.
- Sirocko, F., Reicherter, K., Lehné, R., Hübscher, Ch., Winsemann, J., Stackebrandt, W., 2008: Glaciation, salt and the present landscape. *In: Littke, R., Bayer, U., Gajewski, D., Nelskamp, S. (Eds.), Dynamics of Complex Intracontinental Basins – The Central European Basin System*. Springer, Berlin, pp. 233-245.
- Stackebrandt, W., 1986: Beiträge zur tektonischen Analyse ausgewählter Bruchzonen der Subherzynen Senke und angrenzender Gebiete (Aufrichtungszone, Flechtinger Scholle). *Veröffentlichungen des Zentralinstituts für Physik der Erde* 79, 1-81.
- Stackebrandt, W., 2005: Neotektonische Aktivitätsgebiete in Brandenburg (Norddeutschland). *Brandenburger geowissenschaftliche Beiträge* 12, 165-172.
- Stackebrandt, W., 2009: Subglacial channels of Northern Germany – a brief review. *Zeitschrift der deutschen Gesellschaft für Geowissenschaften* 160, 203-210.
- Stewart, I. S., Sauber, J., Rose, J., 2000: Glacio-seismotectonics: ice sheets, crustal deformation and seismicity. *Quaternary Science Reviews* 19, 1367-1389.
- Stollhofen, H., Bachmann, G.H., Barnasch, J., Bayer, U., Beutler, G., Franz, M., Kästner, M., Legler, B., Mutterlose, J., Radies, D., 2008: Upper Rotliegend to Early Cretaceous basin development. *In: Littke, R., Bayer, U., Gajewski, D., Nelskamp, S. (Eds.), Dynamics of Complex Intracontinental Basins – The Central European Basin System*. Springer, Berlin, pp. 181-210.
- Urban, B., Sierralta, M., Frechen, M., 2011: New evidence for vegetation development and timing of Upper Middle Pleistocene interglacials in Northern Germany and tentative correlations. *Quaternary International* 241, 125-142.
- Van der Wateren, F.M., 2002: Processes of glaciotectionism. *In: Menzies, J. (Ed.), Modern and past glacial environments*. Elsevier, Amsterdam, pp. 417-443.
- Van Keken, P.E., Spiers, C.J., van den Berg, A.P., Muyzert, E.J., 1993: The effective viscosity of rock-salt: implementation of steady-state creep laws in numerical models of salt diapirism. *Tectonophysics* 225, 457-476.
- Vendeville, B.C., 2005: Salt tectonics driven by sediment progradation: Part I – Mechanics and kinematics. *AAPG Bulletin* 89, 1071-1079.

- Voigt, T., Wiese, F., von Eynatten, H., Franzke, H. J., Gaupp, R., 2006: Facies evolution of syntectonic Upper Cretaceous deposits in the Subhercynian Cretaceous Basin and adjoining areas (Germany). *Zeitschrift der Deutschen Gesellschaft für Geowissenschaften*, 157, 203-243.
- Waldron, J.W.F., Rygel, M.C., 2005: Role of evaporite withdrawal in the preservation of a unique coal-bearing succession: Pennsylvanian Joggins Formation, Nova Scotia. *Geology* 33, 337-340.
- Waltham, D., 1997: Why does salt start to move? *Tectonophysics* 282, 117-128.
- Weijermars, R., Jackson, M.P.A., Vendeville, B.C., 1993: Rheological and tectonic modeling of salt provinces. *Tectonophysics* 217, 143-174.
- White, W.A., 1992: Displacement of salt by the Laurentide Ice Sheet. *Quaternary Research* 38, 305-315.
- Wu, P., Johnston, P., Lambeck, K., 1999: Postglacial rebound and fault instability in Fennoscandia. *Geophysical Journal International* 139, 657-670.
- Zirngast, M., 1996: The development of the Gorleben salt dome (northwest Germany) based on quantitative analysis of peripheral sinks. *In: Blundell, G.I., Davison, I. (Eds.), Salt tectonics. Geological Society Special Publications* 100, pp. 203-226.

6. Synthesis

6.1 Generation of the accommodation space

The integration of outcrop, borehole and seismic data clearly shows that the accommodation space for the Middle Pleistocene succession at Schöningen was provided by an elongated erosional depression. The undulating basal profile and the elongated shape exclude an origin as a fluvial channel or a glacial basin, but are characteristic of a subglacial tunnel valley (Huuse & Lykke-Andersen, 2000; Kehew *et al.*, 2012; Van der Vegt *et al.*, 2012). The tunnel valley was incised during the Elsterian glaciation and acted as a long-lived depocentre, accommodating Elsterian, Holsteinian and Saalian deposits. After being completely filled the tunnel valley was buried by Saalian subglacial till and Weichselian loess.

Other potential mechanisms for the generation of the accommodation space, as subsidence in the rim syncline, differential compaction or subsurface salt dissolution, can be ruled out. The main phase of subsidence in the rim synclines ceased already in the Eocene due to the depletion of the salt layer. The location of the Pleistocene depocentre at the outer margin of the rim syncline does not match the migration pattern of the main depocentre of the rim synclines towards the salt wall (Brandes *et al.*, 2012; Osman *et al.*, *in press*). Finite-element modelling of the response of salt structures to ice-sheet loading indicates that ice load may trigger the rise or fall of salt structures. However, the location of the Pleistocene depocentre at Schöningen again differs from the subsidence pattern observed in the model (cf., Chapter 6.4). There is also no indication for differential compaction or subsurface salt dissolution. The lignite seams, which may strongly compact during their burial, are either laterally continuous (Brandes *et al.*, 2012) or absent beneath the Pleistocene depocentre (Osman *et al.*, *in press*).

6.1.1 Formation of the tunnel valley

The 3D subsurface model reveals the dimensions and geometry of the tunnel valley (Fig. 1A). The tunnel valley is 300-850 m wide, 40 m deep and has steep walls. The general trend of the tunnel valley is NNW-SSE and slightly arcuate. The length of the tunnel valley could not be measured because the tunnel valley leaves the model area towards the south. The tunnel valley is broader, shallower and flat-bottomed in the north, where it is incised into unconsolidated Palaeogene deposits of the rim syncline, and narrower, deeper and V-shaped in the south, where it is incised into Triassic mudstone and limestone. The unconsolidated deposits provided a preferential pathway for the drainage of subglacial meltwater and an easily erodible substratum for tunnel valley incision (cf., Huuse & Lykke-Andersen, 2000; Janszen *et al.*, 2012b). The incision by subglacial meltwater is strongly controlled by the hydraulic conductivity of the substratum (Janszen *et al.*, 2012b). Permeability contrasts of the substratum cause water-pressure differences that trigger fracturing and fluidisation of the impermeable layer. The fluidised layer then drains towards the area of lower water-pressure, which is usually the ice margin or an evolving subglacial meltwater channel (Hooke & Jennings, 2006; Boulton *et al.*, 2007; Janszen *et al.* 2012b).

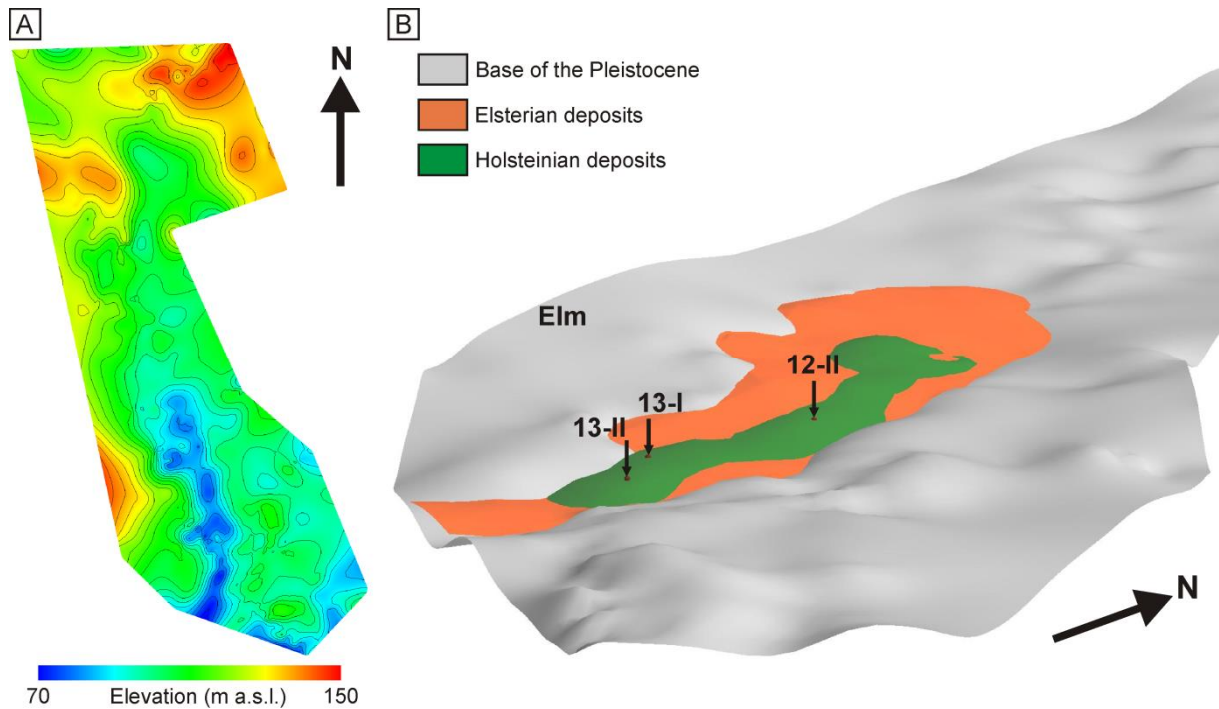


Fig. 1: A) Depth map of the base of the Pleistocene extracted from the 3D subsurface model (5 m contours). The Pleistocene depocentre in the south displays the characteristic features of a tunnel valley. B) Distribution of Elsterian and Holsteinian deposits within the tunnel valley and locations of the main archaeological sites (5x vertical exaggeration). In the southwest the base of the Pleistocene rises towards the Elm ridge.

Subglacial meltwater probably initially incised into the rim-syncline fill and subsequently into the Triassic rocks further south. Similar deep incisions into the Palaeogene deposits, which may also represent tunnel valleys, were reported from the same rim syncline near Egelu ~35 km to the southeast (Ziegenhardt & Kramer, 1968). The majority of the Elsterian tunnel valleys in northern Germany are located in the Central European Subsidence Zone, where the unconsolidated Cenozoic deposits reach their maximum thickness (Stackebrandt, 2009). The infill of the rim synclines of the Helmstedt-Staßfurt salt wall probably provided a comparable, but much smaller, zone that favoured the incision of tunnel valleys.

6.1.2 Infill of the tunnel valley

The Elsterian syn-glacial infill of the tunnel valley comprises meltwater deposits, subglacial till and glaciallacustrine deposits (Fig. 1B). The basal erosional surface incises steeply into the underlying Palaeogene deposits and is overlain by meltwater deposits, which were probably deposited subglacially during the incision of the tunnel valley (cf., Piotrowski *et al.*, 1999; Praeg, 2003; Russell *et al.*, 2003). The meltwater deposits are unconformably overlain by subglacial till, which was deposited in the tunnel valley by squeezing, lateral flow and melt-out during an advanced stage of ice decay (cf., Piotrowski *et al.*, 1999; Jørgensen & Sandersen, 2006). Alternatively, the subglacial till may have been deposited during a re-advance of the ice sheet. The cross-section of the tunnel valley in seismic profile S-1 displays a deep, central incision, which is flanked by a terrace at one margin. Borehole data

indicate that in this position Elsterian till is overlying the Palaeogene deposits. These observations indicate widening of the tunnel valley by direct glacial erosion beneath an (re-) advancing ice sheet (Huuse & Lykke-Andersen, 2000; Stewart *et al.*, 2013). At one location, a small-scale subglacial channel, which was incised into the Elsterian till and infilled by meltwater deposits, was observed. Altogether, the depositional architecture of the basal tunnel-valley fill is interpreted as indicating recurring phases of erosion and deposition during several periods of ice-sheet advance and retreat. However, it is arguable if these phases relate to repeated ice advances during the Elsterian glaciation or to changing ice and meltwater dynamics during a single ice advance.

The subglacial till passes upwards into glacialacustrine deposits, representing distal delta or subaqueous fan deposits. The gradual contact, which is deformed by load casts, suggests a rather gradual transition from subglacial to glacialacustrine environments. Blocking of the tunnel valley by dead ice during deglaciation (cf., Kuster & Meyer, 1979) can therefore probably be ruled out. After the final deglaciation the tunnel valley remained underfilled and acted as a depocentre for a complex lacustrine succession (Fig. 1B), recording a complex interglacial phase between the Elsterian and the Saalian glaciations (cf., Chapter 6.2). During the Saalian glaciation parts of the former tunnel valley were reactivated as a proglacial meltwater channel before the tunnel valley was completely filled and buried by glacialacustrine and glacialfluvial deposits and till. Glacitectonic deformation was intense during the Saalian ice advance and affected both Saalian and pre-Saalian deposits. However, deep-reaching incision did not occur during the Saalian glaciation and the older interglacial succession remained sheltered within the tunnel valley. This general trend of deep incision during the Elsterian and intense glacitectonic deformation during the Saalian has commonly been observed across northern central Europe and is interpreted as indicating warmer temperatures during the Elsterian ice retreat, enhancing the meltwater discharge and thus favouring subglacial incision (Van Dijke & Veldkamp, 1996; Passchier *et al.*, 2010; Kehew *et al.*, 2012). This interpretation is supported by the marine sediment record, which suggests a rather gradual climate change towards the end of MIS 6 (McManus *et al.*, 1999; Toucanne *et al.*, 2009). The maximum insolation during this phase was probably lower than during the terminations of other glaciations (Toucanne *et al.*, 2009), because the precession and tilt cycles were out of phase (Ruddiman, 2006).

6.2 Interglacial depositional environments

After the final retreat of the Elsterian ice sheet the tunnel valley remained underfilled and provided the accommodation space for Holsteinian (MIS 9, cf., Urban *et al.*, 2011) interglacial deposition. The interglacial deposits comprise organic-rich silt or fine-grained sand and peat and are interpreted as representing topsets, foresets and bottomsets of lacustrine delta systems. The delta systems formed on the western shore of the interglacial lake and were fed by springs and surface run-off from the eastern flank of the Elm ridge (Fig. 1B). The vertical and lateral stacking pattern of the delta deposits was controlled by lake-level fluctuations.

6.2.1 Sequence stratigraphic analysis

Indications for fluctuating lake levels have previously been observed from palaeo-ecological data (e.g., Böhme, 2000; Jechorek, 2000, Urban, 2007). Urban (2007) observed five shallowing-upwards successions at site 13-II and related them to climatic changes. Based on the sequence stratigraphic interpretation of the outcrop and seismic data a lake-level curve was reconstructed. The overall trend of the lake-level evolution is characterised by a long-term regression of the relative lake level, probably caused by the successive infill of the basin (Fig. 2). The seismic data reveal three unconformities, which point to lake-level falls with a magnitude of 4-6 m and divide the delta deposits into four subunits (Fig. 2). The three younger subunits each comprise delta foreset and topset deposits that can be correlated with the so-called δSchöningen Cyclesö I, II and III defined by Urban (1995, 2007) and Mania (1998). Within the interglacial deposits at sites 12-II and 13-II five prograding parasequences were observed, which correspond to the shallowing-upwards successions observed by Urban (2007). These parasequences are interpreted as pointing to high-frequency lake-level changes with a magnitude of 1-3 m. The basal part of each parasequence consists of lake-bottom and delta-front deposits, while the upper parts comprise delta-plain deposits. The correlation of both the large-scale and the small-scale lake-level changes with the palaeo-ecological data (cf., Urban, 1995, 2007; Böhme, 2000; Jechorek, 2000; Urban *et al.*, 2011) indicates a climatic control on the lake level. Climatic changes control the lake-level via the interplay of the groundwater table, the surface run-off and the density and type of vegetation coverage (cf., Koutsodendris *et al.*, 2013). The higher-magnitude lake-level changes were probably related to major climatic shifts, which correspond to intra-interglacial cooling events during the Holsteinian interglacial (Desprat *et al.*, 2007; Kühl & Litt, 2007; Litt *et al.*, 2008; Koutsodendris *et al.*, 2010, 2013). The lower-magnitude high-frequency lake-level changes, which are documented by the parasequences, have been attributed to climatic fluctuations between stadial and interstadial conditions (Urban, 2007). The fluctuation between stadial and interstadial conditions is controlled by a millennial-scale climatic cyclicity, which occurs during both glacial and interglacial phases (Dansgaard *et al.*, 1993; Bond *et al.*, 1997, 2001; McManus *et al.*, 1999; Dokken *et al.*, 2013). The amplitude of these cycles is significantly higher during glacial phases (δDansgaard-Oeschger-Cyclesö; McManus *et al.*, 1999; Wolff *et al.*, 2010; Dokken *et al.*, 2013), than during interglacial phases (δBond-Cyclesö; Bond *et al.*, 1997, 2001; Müller *et al.*, 2005). The forcing mechanism of these cycles is probably solar activity (Beer *et al.*, 2000; Bond *et al.*, 2001), which triggers pulse-like changes of the oceanic North Atlantic Current and the atmospheric North Atlantic Oscillation (Broecker, 2003; Dokken *et al.*, 2013). The millennial-scale cycles are characterised by initial rapid warming, followed by a more gradual cooling phase (Wolff *et al.*, 2010; Dokken *et al.*, 2013). Such sudden warming events are likely to increase the advection of warm, moist air to northern central Europe and thus increase precipitation (Wanner *et al.*, 2001; Müller *et al.*, 2005). Increasing precipitation probably triggered the lake-level rises, which are recorded by the basal flooding surfaces of the

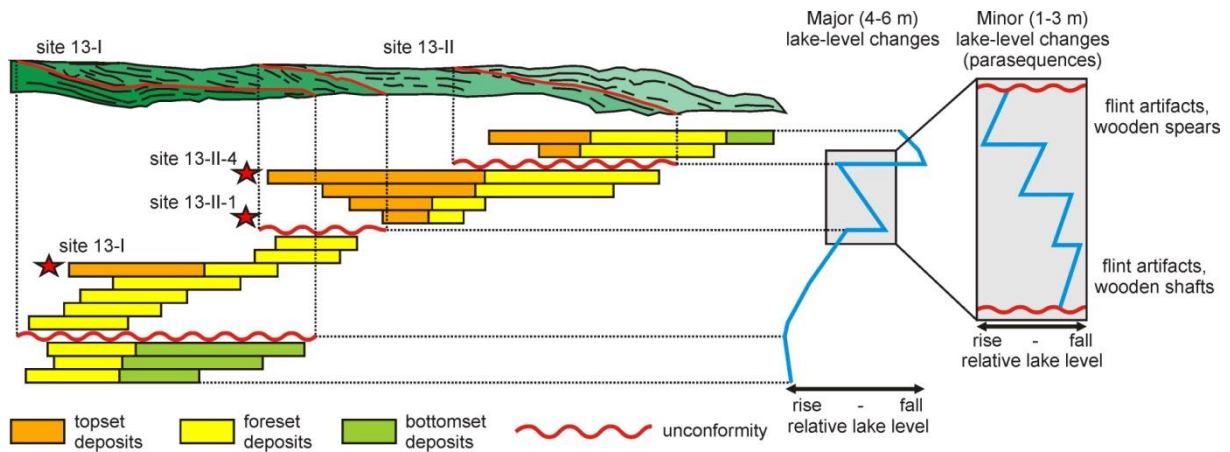


Fig. 2: Reconstruction of the lake-level curve for the Holsteinian interglacial succession, based on the topset-foreset-transitions in seismic section S-1. Minor lake-level changes are based on outcrop observations. The main archaeological horizons are indicated.

individual parasequences. Subsequently shallowing-upwards successions were deposited, comprising lake-bottom to delta-plain deposits, until the next cycle triggered another lake-level rise.

The spatial and temporal distribution of the archaeological sites is explained by the sequence stratigraphic analysis. The spatially adjacent sites 13-I and 13-II are separated by an unconformity caused by major regression (Fig. 2). The stacking patterns of the parasequences indicate that sites 12-II and 13-II formed contemporaneously, as the pollen record confirms (Urban & Sierralta, 2012). Archaeological artefacts mostly occur in deposits of the delta plain and form shoreline-parallel clusters, indicating activities of early humans at the lake margin and on the delta plains. The individual archaeological horizons at the different sites correspond to delta-plain deposits in the stacked parasequences.

6.2.2 Formation and preservation of the archaeological sites

The archaeological sites and their internal horizons document occupation by early humans in spite of changing environmental conditions. Early humans frequented the lake margin as well during the interglacial optimum phase as during the boreal phases at the beginning, respectively end of the interglacial (Thieme, 1999; Urban, 2007). The broad range of climatic conditions indicates that the lake margin and delta plains provided attractive sites for animals and early humans ambushing them. Especially during the rather dry and cold early and late phases of the interglacials the wetland of the delta plains may have represented a flourishing ecosystem within a rather hostile environment (cf., Preece *et al.*, 2006; Yansa, 2007; Ashley *et al.*, 2008, 2010).

In general, the preservation of interglacial successions within underfilled tunnel valleys is very common (e.g., Turner, 1970; Kuster & Meyer, 1979; Eissmann, 2002; Jørgensen & Sandersen, 2006). Tunnel valleys provide accommodation space with a high preservation potential and thus represent excellent archives for interglacial deposits, which may contain Palaeolithic sites. The conditions at the Schöningen sites favoured the preservation of the artefacts in several ways. The location of the archaeological sites within the tunnel valley prevented the erosion of the artefact-bearing strata, espe-

cially during the subsequent Saalian glaciation. Most artefacts were recovered from delta plain deposits, where they were embedded during lake-level rise. The subaquatic embedding prevented the oxidation and decomposition of the organic-rich artefact-bearing strata. Additionally, the preservation of bones was favoured by the high calcium-carbonate content of the water shed from springs in the Mesozoic bedrock of the Elm. Saalian glacetectonic processes had only a minor effect on the preservation, although the internal stratification of the archaeological horizons was locally disturbed. At least one of the hunting spears was broken and offset after embedding (Thieme, 1999), possibly by glacetectonic faulting.

6.3 Ice-marginal deposition in front of tunnel valleys

The terminations of tunnel valleys beneath an ice margin commonly correlate with the apices of subaerial or subaqueous outwash fans at the ice margin (Wingfield, 1990; Jørgensen & Sandersen, 2006; Kehew *et al.*, 2012; Van der Vegt *et al.*, 2012). Such ice-contact fans are also deposited within tunnel valleys during ice-sheet retreat, where their deposits attain higher thicknesses and have a higher preservation potential than deposits in intervalley areas (Krohn *et al.*, 2009; Janszen *et al.*, 2012a). If sediment-laden meltwater from a subglacial channel emerges at the ice-margin the competency of the flow is abruptly reduced and deposition is initiated (Russell *et al.*, 2003; Kehew *et al.*, 2012). The occurrence of high-magnitude meltwater-outburst floods is characteristic of the discharge from subglacial channels or tunnel valleys (Wingfield, 1990; Kehew *et al.*, 2012). Therefore, bedforms related to supercritical flows and hydraulic jumps are characteristic of subaqueous ice-contact fan and glacial lake-outburst flood deposits. The highly aggradational conditions established by the deceleration of highly sediment-laden meltwater flows allows for the preservation of these bedforms, which are usually considered as having a low preservation potential (cf., Fielding, 2006; Duller *et al.*, 2008). The studied successions include laterally and vertically stacked deposits of cyclic steps, chutes-and-pools, breaking antidunes, aggrading stationary antidunes and humpback dunes (Fig. 3). The lateral and vertical facies changes are controlled by (i) the temporal and spatial evolution of the initial supercritical flows on a large scale and (ii) internal short-term temporal and spatial variations of the flow conditions, as fluctuating discharge, bed topography and pulsating unstable flows.

Deposits of cyclic steps occur within the glacial lake-outburst flood succession and are characterised by lenticular scours infilled by gently to steeply dipping backsets. Deposits of chutes-and-pools and breaking antidunes comprise a variety of geometries, including steeply dipping backsets, gently dipping concave-convex foresets and concentric lens-fills, and occur within both the glacial outburst-flood and the subaqueous fan deposits. Although the deposits of cyclic steps tend to be characterised by lower aspect ratios and more gently dipping backsets than the deposits of chutes-and-pools, the distinction between cyclic steps and chutes-and-pools may be ambiguous because the formative flow conditions and depositional process are very similar (Taki & Parker, 2005; Kostic *et al.*, 2010) and the geometry of the bedforms depends also on the grain size and aggradation rate (Cartigny *et al.*, *in*

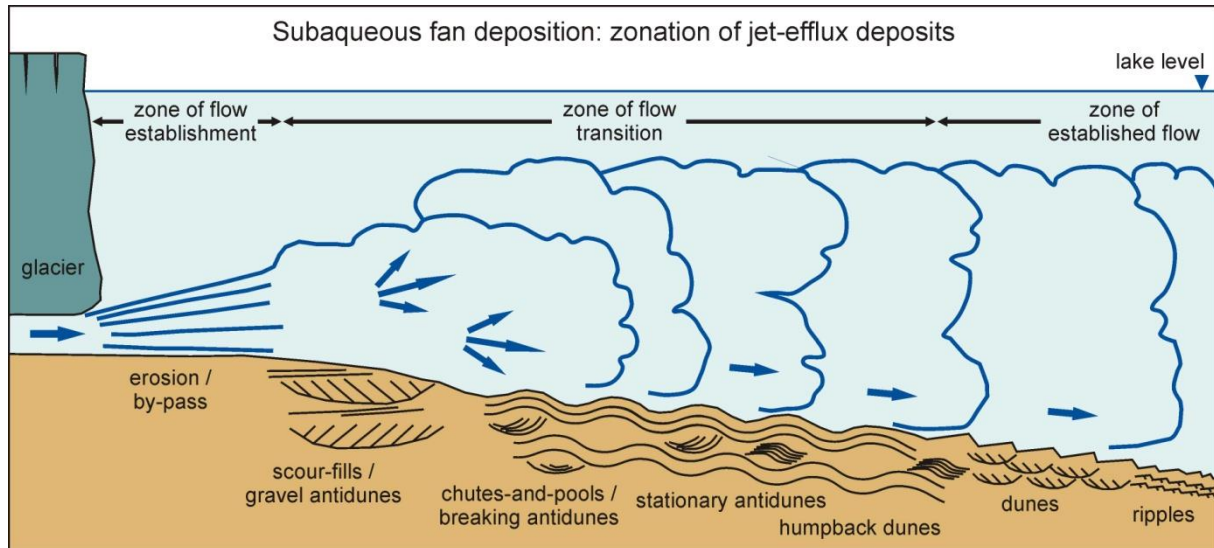


Fig. 3: Zonation of ice-marginal jet-efflux deposits (the figure is not to scale). Coarse-grained scour-fills and gravel antidunes form in the proximal zone of flow transition, passing downflow into chutes-and-pools, breaking antidunes and aggrading stationary antidunes. Intercalated deposits of aggrading stationary antidunes and humpback dunes represent deposition by flows fluctuating between super- and transcritical conditions. Dunes and ripples are deposited by subcritical flows in the zone of established flow.

press). However, a change in the grain size or aggradation rate would probably be associated with a change of the flow velocity and the mobility parameter, leading to a change of the depositional process. The presence of cyclic step deposits indicates supercritical flow conditions with Froude numbers larger than 2.2 (cf., Cartigny *et al.*, *in press*). These conditions were established when the glacial lake-outburst flood spilled over a push-moraine ridge, resulting in acceleration and thinning of the flow. Cyclic steps developed from hydraulic jumps triggered at the slope-break at the base of the push-moraine ridge and then migrated upslope, incising a broad channel into the ridge.

Deposits of chutes-and-pools, breaking antidunes, stationary antidunes, humpback dunes, 3D dunes and climbing ripples form a downflow succession within the subaqueous fan deposits (Fig. 3). The recognition of this downflow succession improves the understanding of the zonation of sedimentary facies on ice-contact subaqueous fans. Interbedded deposits of stationary antidunes and humpback dunes are characteristic of the distal zone of flow transition of supercritical plane-wall jet flows. Deposits of aggrading stationary antidunes are characterised by sheet-like sinusoidal stratified beds. Aggrading stationary antidunes are interpreted as representing deposition by quasi-steady flows at the lower limit of the upper flow stage, where an undular hydraulic jump establishes the necessary highly aggradational conditions (cf., Allen, 1984; Chanson, 2001). The hydraulic jump may occur directly in front of the meltwater conduit (Russell & Arnott, 2003) or at the mouth of a large-scale distributary channel (Winsemann *et al.*, 2009). Humpback dunes comprise downflow divergent sigmoidal foresets and are interpreted as deposited at the transition from subcritical to supercritical flow conditions or vice versa.

6.4 The reaction of salt structures to ice-sheet loading

The high thickness of the Pleistocene succession preserved in the rim syncline of the Helmstedt-Staßfurt salt wall suggests an interaction between the salt structure and ice-sheet loading. The finite-element simulations indicate that salt structures react to ice-sheet loading and thus in general support the previous conceptual models (Fig. 4; cf., Liszkowski *et al.*, 1993; Sirocko *et al.*, 2008). Diapirs will rise up to +4 m in front of an ice sheet and will be pushed down up to -36 m beneath an ice sheet. The location of the ice margin relative to the salt structures exerts the primary control on this interaction. If the diapir is transgressed by the ice sheet, the load applied to the top of the diapir forces the diapir to move downwards. Most of this subglacial downward displacement of the salt structure is reversed by upward salt flow during and after unloading, causing the diapir to rise. If the diapir is not transgressed by the ice sheet but remains outside the ice margin, the load applied to the source layer causes salt flow from the source layer into the diapir and rise of the diapir. Larger magnitudes of displacement are observed in models with larger diapirs, thicker ice sheets, longer loading phases, thicker salt source layer, lower yield strength of the overburden and lower viscosity of the salt. The results show that the amount of rise in front an ice sheet is considerably exceeded by the downward displacement beneath an ice sheet. This is probably caused to the higher mobility of the large salt body of the diapir compared to the relatively thin salt source layer.

6.4.1 Implications of the modelling results

The reactivation of salt structures by ice-sheet loading will influence the depositional architecture and preservation potential of glacial deposits in proglacial and subglacial environments and may also affect subsequent interglacial deposition. Uplifted sections will cause successions to become thin and incomplete, will subsiding areas will accommodate thick and more complete successions (cf., Kurzawa, 2003). The models indicate strong deformation above a reactivated salt structure, which is likely to trigger the reactivation of faults in the overburden and will thus affect the integrity of structural hydrocarbon reservoirs related to salt structures. Fractures due to faulting above reactivated salt structures will contribute to the erodibility of the substratum and represent zones of preferential incision (Dobracki & Krzyszkowski, 1997; Huuse & Lykke-Andersen, 2000; Grim & Sirocko, 2012). In the models, most internal deformation of a salt body during ice coverage is focussed in the upper part of the salt structures (i.e. shallower than ~2.5 km). This ice-load induced salt flow in will affect the stability of waste-disposal sites within salt structures, if these ever are transgressed by ice sheets during future glaciations.

Previous field-based studies observed a correlation between salt structures and push-moraine ridges (Gripp, 1952; Schirrmeister, 1999; Lehné & Sirocko, 2007). Actively rising salt structures were interpreted to act as a buttress for push-moraine formation (Lehné & Sirocko, 2007; Sirocko *et al.*, 2008). Alternatively, push-moraine formation above salt structures may be related to the influence of salt structures on the subglacial conditions. The high thermal conductivity of salt causes thinning of per-

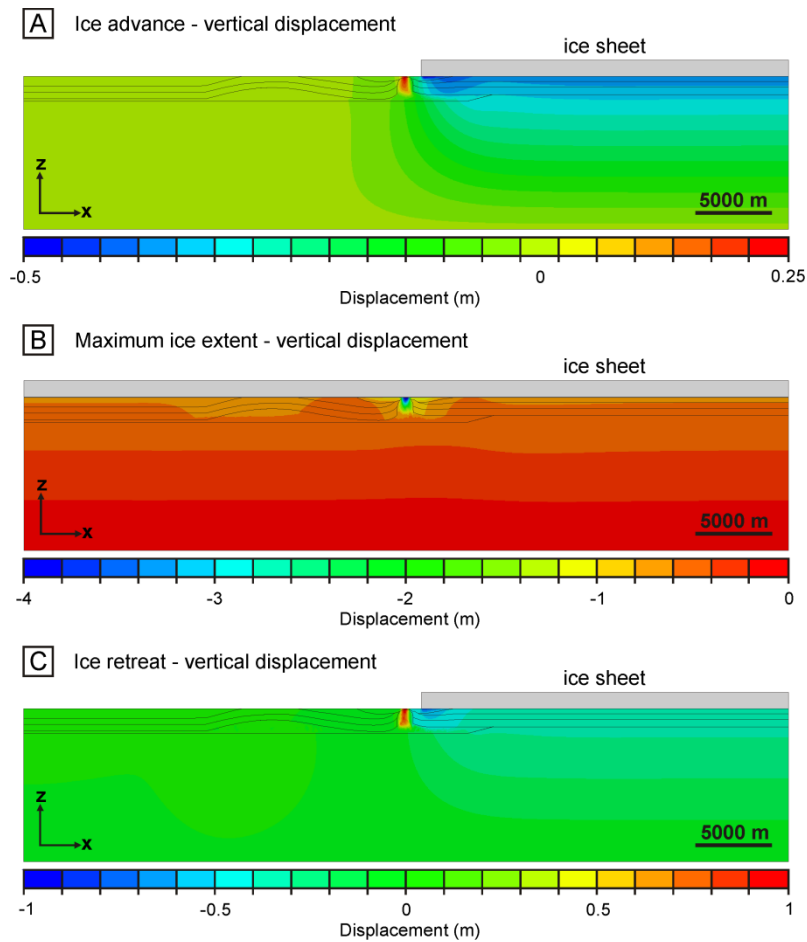


Fig. 4: Vertical displacement in models based on the geometry of the Helmstedt-Staßfurt salt wall. **A)** Rise of the salt structure during ice-sheet advance. **B)** The salt structure is pushed down beneath the ice sheet during maximum ice coverage. **C)** Rise of the salt structure during ice-sheet retreat.

mafrost above salt structures (Delisle *et al.*, 2007; Grassmann *et al.*, 2010), which in turn may raise the drainage capacity of the glacier bed and increases the basal coupling (Narloch *et al.*, 2013), eventually promoting the development of glacitectonic thrusts and the formation of push moraines at the advancing ice margin (Van der Wateren, 2002; Passchier *et al.*, 2010).

Creation of accommodation space

The Pleistocene depocentre at Schöningen is located at the margin of the southwestern rim syncline of the Helmstedt-Staßfurt salt wall. The unconsolidated Palaeogene infill of the rim syncline favoured the incision of the Elsterian tunnel valley. The results of the finite-element simulation suggest that ice-load induced salt movement had only a very minor or no influence on the Pleistocene evolution of the rim synclines and the formation of the depocentre at Schöningen. During the rise of the salt structure in front of the ice sheet, some subsidence is observed in the rim syncline beneath the ice margin (Fig. 4A, B). However, measurements of the displacement in the model show that this subsidence is not

related to salt expulsion from the source layer, but to compaction of the rim-syncline fill by the ice load. The opposite rim syncline is even slightly uplifted together with the rising diapir.

Up to ~7 m thick Holocene peat bog deposits were observed in the innermost parts of the rim synclines and above the salt wall, and interpreted as pointing to ongoing salt rise (Manger, 1952). The accommodation space for these peat bogs may have been provided by the downwards displacement of the salt wall beneath the ice sheet of the Saalian glaciation (Fig. 4B) or, alternatively, by rise of the salt wall in front of the ice sheet during ice retreat (Fig. 4B) and subsequent subsurface salt dissolution, leading to a relief reversal. Such complete or partial post-glacial relief reversals have been observed at most salt structures that rose during cold and dry glacial phases (Gripp, 1952; Sirocko *et al.*, 2002; Stackebrandt, 2005). Subsurface salt dissolution may be amplified by ice-sheet loading and unloading due to enhanced compaction and expulsion of pore water (Anderson & Hinds, 1997).

7. Conclusions

- The Middle Pleistocene succession of Schöningen was deposited within an Elsterian tunnel valley, which provided the accommodation space for subsequent glacial and interglacial deposition. The incision of the tunnel valley was favoured by the unconsolidated Palaeogene infill of the rim syncline, which provided a preferential meltwater pathway with low resistance to erosion. The tunnel valley remained underfilled after deglaciation and an elongated lake formed during the subsequent Holsteinian (MIS 9) interglacial. The interglacial succession consists of lacustrine delta and lake-bottom deposits. The long-lived interglacial lake attracted animals and early humans ambushing them. Artefacts were embedded on the delta plains and were preserved during lake-level rise. The sequence stratigraphic analysis of the delta deposits, which were affected by repeated climatically controlled lake-level changes, explains the spatial and temporal distribution of the individual archaeological sites. During the Saalian Drenthe glaciation the remnant tunnel valley was completely filled by meltwater deposits. The tunnel valley kept the Middle Pleistocene succession below the base level of both glacial and interglacial erosional processes.
- Outwash successions at ice margins are deposited by meltwater, emerging from subglacial channels or tunnel valleys. The discharge of meltwater is characterised by the occurrence of sediment-laden high-magnitude outburst floods. Bedforms related to highly aggradational supercritical flows and hydraulic jumps are therefore characteristic of deposits of subaqueous ice-contact fans and meltwater outburst floods. Bedforms include cyclic steps, chutes-and-pools, breaking antidunes, aggrading stationary antidunes and humpback dunes. The lateral and vertical successions of bedforms deposited by supercritical to transcritical flows are interpreted as representing both (i) the temporal and spatial evolution of the initial supercritical flows on a large scale, which are in general characterised by waning flow conditions, and (ii)

internal short-term temporal and spatial variations of the flow conditions. Small-scale lateral and vertical facies changes are interpreted as controlled by fluctuating discharge, bed topography and pulsating unstable flows.

- The finite-element simulation indicates that salt structures react to ice-sheet loading. If the diapir is transgressed by the ice sheet, the load applied to the top of the diapir will force the diapir to move downwards. If the diapir is not transgressed by the ice sheet and load is only applied to the source layer, the diapir will rise. Larger displacements are observed in models with larger diapirs, thicker ice sheets, longer loading phases, higher thickness of the salt source layer, lower yield strength of the overburden and lower viscosity of the salt. The rise or fall of diapirs triggered or amplified by ice-sheet loading will affect glacigenic erosion and deposition above the diapir and within the rim synclines. Some accommodation space may be created in the rim syncline and above the salt structure beneath the ice margin. Further, the long-term stability of waste-disposal sites within salt structures and the integrity of structural hydrocarbon reservoirs related to salt structures are likely to be affected by ice-induced salt flow. However, the results of the simulations indicate that ice-load induced salt flow had only a marginal or no influence on the formation of the depocentre at Schöningen.

8. References

- Allen, J.R.L., 1984: Sedimentary structures: their character and physical basis. *Developments in Sedimentology* 30, 1-663.
- Anderson, N.L., Hinds, R.C., 1997: Glacial loading and unloading: a possible cause of rock salt dissolution in the Western Canada Basin. *Carbonates and Evaporites* 12, 43-52.
- Ashley, G.M., Tactikos, J.C., Owen, R.B., 2008: Hominin use of springs and wetlands: Paleoclimate and archaeological records from Olduvai Gorge (~1.796-1.74 Ma). *Palaeogeography, Palaeoclimatology, Palaeoecology* 272, 1-16.
- Ashley, G.M., Dominguez-Rodrigo, M., Bunn, H.T., Mabulla, A.Z.P., Baquedano, E., 2010: Sedimentary geology and human origins: a fresh look at Olduvai Gorge, Tanzania. *Journal of Sedimentary Research* 80, 703-709.
- Beer, J., Mende, W., Stellmacher, R., 2000: The role of the sun in climate forcing. *Quaternary Science Reviews* 19, 403-415.
- Böhme, G., 2000: Reste von Fischen, Amphibien und Reptilien aus der Fundstelle Schöningen 12 bei Helmstedt (Niedersachsen) ó Erste Ergebnisse. *Praehistoria Thuringica* 4, 18-27.
- Bond, G., Showers, W., Cheseby, M., Lotti, R., Almasi, P., DeMenocal, P., Priore, P., Cullen, H., Hajdas, I., Bonani, G., 1997: A pervasive millennial-scale cycle in North Atlantic Holocene and glacial climates. *Science* 278, 1257-1266.

- Bond, G., Kromer, B., Beer, J., Muscheler, R., Evans, M.N., Showers, W., Showers, S., Lotti-Bond, R., Hajdas, I., Bonani, G., 2001: Persistent solar influence on North Atlantic climate during the Holocene. *Science* 294, 2130-2136.
- Boulton, G.S., Lunn, R., Vidstrand, P., Zatzepin, S., 2007: Subglacial drainage by groundwater-channel coupling, and the origin of esker systems: Part 1 ó glaciological observations. *Quaternary Science Reviews* 26, 1067-1090.
- Brandes, C., Pollok, L., Schmidt, C., Riegel, W., Wilde, V., Winsemann, J., 2012: Basin modelling of a lignite-bearing salt rim syncline: insights into rim syncline evolution and salt diapirism in NW Germany. *Basin Research* 24, 699-716.
- Broecker, W.S., 2003: Does the trigger for abrupt climate change reside in the ocean or in the atmosphere? *Science* 300, 1519-1522.
- Cartigny, M.J.B., Ventura, D., Postma, G. and van den Berg, J.H., *in press*: Morphodynamics and sedimentary structures of bedforms under supercritical-flow conditions: new insights from flume experiments. *Sedimentology*, doi: 10.1111/sed.12076.
- Chanson, H., 2001: Current knowledge in hydraulic jumps and related phenomena. A survey of experimental results. *European Journal of Mechanics B/Fluids* 28, 191-210.
- Dansgaard, W., Johnsen, S.J., Clausen, H.B., Dahl-Jensen, D., Gundestrup, N.S., Hammer, C.U., Hvdberg, C.S., Steffensen, J.P., Sveinbjörnsdottir, A.E., Jouzel, J. Bond, G., 1993: Evidence for general instability of past climate from a 250-kyr ice-core record. *Nature* 364, 218-220.
- Delisle, G., Grassmann, S., Cramer, B., Messner, J., Winsemann, J., 2007: Estimating episodic permafrost development in northern Germany during the Pleistocene. *In: Hambrey, M., Christoffersen, P., Glasser, N., Hubbard, B. (Eds.), Glacial Processes and Products. International Association of Sedimentologists Special Publications* 39, pp. 109-119.
- Desprat, S., Sánchez Goñi, M.F., Naughton, F., Turon, J.L., Duprat, J., Malaizé, B., Cortijo, E., Peypouquet, J.P., 2007: Climate variability of the last five isotopic interglacials: Direct land-sea-ice correlation from the multiproxy analysis of North-Western Iberian margin deep-sea cores. *In: Sirocko, F., Claussen, M., Goni, M.F.S., Litt, T. (Eds.): The Climate of Past Interglacials; Developments in Quaternary Science* 7, pp. 375-386.
- Dobracki, R., Krzyszkowski, D., 1997: Sedimentation and erosion at the Weichselian ice-marginal zone near Golczewo, northwestern Poland. *Quaternary Science Reviews* 16, 721-740.
- Dokken, T.M., Nisancioglu, K.H., Li, C., Battisti, D.S., Kissel, C., 2013: Dansgaard-Oeschger cycles: Interactions between ocean and sea ice intrinsic to the Nordic seas. *Paleoceanography* 28, 491-502.
- Duller, R.A., Mountney, N.P., Russell, A.J., Cassidy, N.C., 2008: Architectural analysis of a volcaniclastic jökulhlaup deposit, southern Iceland: sedimentary evidence for supercritical flow. *Sedimentology* 55, 939-964.

- Eissmann, L., 2002: Quaternary geology of eastern Germany (Saxony, Saxon-Anhalt, South Brandenburg, Thuringia), type area of the Elsterian and Saalian Stages in Europe. *Quaternary Science Reviews* 21, 1275-1346.
- Fielding, C.R., 2006: Upper flow regime sheets, lenses and scour fills: Extending the range of architectural elements for fluvial sediment bodies. *Sedimentary Geology* 190, 227-240.
- Grassmann, S., Cramer, B., Delisle, G., Hantschel, T., Messner, J., Winsemann, J., 2010: pT-effects of Pleistocene glacial periods on permafrost, gas hydrate stability zones and reservoir of the Mittelplate oil field, northern Germany. *Marine and Petroleum Geology* 27, 298-306.
- Grim, S., Sirocko, F., 2012: Natural depressions on modern topography in Schleswig-Holstein (Northern Germany) indicators for recent crustal movements or only kettle holes? *Zeitschrift der Deutschen Gesellschaft für Geowissenschaften* 163, 469-481.
- Gripp, K., 1952: Inlandeis und Salzaufstieg. *Geologische Rundschau* 40, 74-81.
- Hooke, R.L., Jennings, C.E., 2006. On the formation of the tunnel valleys of the southern Laurentide ice-sheet. *Quaternary Science Reviews* 25, 1364-1372.
- Huuse, M., Lykke-Andersen, H., 2000: Overdeepened Quaternary valleys in the eastern Danish North Sea: morphology and origin. *Quaternary Science Reviews* 19, 1233-1253.
- Janszen, A., Moreau, J., Moscariello, A., Ehlers, J., Kröger, J., 2012a: Time-transgressive tunnel-valley infill revealed by a three-dimensional sedimentary model, Hamburg, north-west Germany. *Sedimentology* 60, 693-719. Janszen, A., Spaak, M., Moscariello, A., 2012b: Effects of the substratum on the formation of glacial tunnel valleys: an example from the Middle Pleistocene of the southern North Sea. *Boreas* 41, 629-643.
- Jechorek, H., 2000: Die fossile Flora des Reinsdorf-Interglazial. *Paläokarpologische Untersuchungen an mittelpleistozänen Ablagerungen im Braunkohlentagebau Schöningen. Praehistoria Thuringica* 4, 7-17.
- Jørgensen, F., Sandersen, P.B.E., 2006: Buried and open tunnel valleys in Denmark - erosion beneath multiple ice sheets. *Quaternary Science Reviews* 25, 1339-1363.
- Kehew, A.E., Piotrowski, J.A., Jørgensen, F., 2012: Tunnel valleys: Concepts and controversies ó A review. *Earth-Science Reviews* 113, 33-58.
- Kostic, S., Sequeiros, O., Spinewine, B., Parker, G., 2010: Cyclic steps: A phenomenon of supercritical shallow flow from the high mountains to the bottom of the ocean. *Journal of Hydro-environment Research* 3, 167-172.
- Koutsodendris, A. Müller, U.C., Pross, J., Brauer, A., Kotthoff, U., Lotter, A.F., 2010: Vegetation dynamics and climate variability during the Holsteinian interglacial based on a pollen record from Dethlingen (northern Germany). *Quaternary Science Reviews* 29, 3298-3307.
- Koutsodendris, A., Lotter, A.F., Kirilova, E., Verhagen, F.T.M., Brauer, A., Pross, J., 2013: Evolution of a Holsteinian (MIS 11c) palaeolake based on a 12-ka-long diatom record from Dethlingen (northern Germany). *Boreas* 42, 714-728.

- Krohn, C.F., Larsen, N.K., Kronborg, C., Nielsen, O.B., Knudsen, K.L., 2009: Litho- and chronostratigraphy of the Late Weichselian in Vendsyssel, northern Denmark, with special emphasis on tunnel-valley infill in relation to a receding ice margin. *Boreas* 38, 811-833.
- Kühl, N., Litt, T., 2007: Quantitative Time-Series Reconstructions of Holsteinian and Eemian Temperatures Using Botanical Data. *In: Sirocko, F., Claussen, M., Goni, M.F.S., Litt, T. (Eds.): The Climate of Past Interglacials; Developments in Quaternary Science* 7, pp. 239-254.
- Kuster, H., Meyer, K.-D., 1979: Glaziäre Rinnen im mittleren und nordöstlichen Niedersachsen. *Eiszeitalter und Gegenwart* 29, 135-156.
- Lehné, R., Sirocko, F., 2007: Rezente Bodenbewegungspotenziale in Schleswig-Holstein (Deutschland) ó Ursachen und ihr Einfluss auf die Entwicklung der rezenten Topographie. *Zeitschrift der deutschen Gesellschaft für Geowissenschaften* 158, 329-347.
- Liszkowski, J., 1993 The effects of Pleistocene ice-sheet loading-deloadung cycles on the bedrock structure of Poland. *Folia Quaternaria* 64, 7-23.
- Litt, T., Schmincke, H.-U., Frechen, M., Schlüchter, C., 2008: Quaternary. *In: McCann, T. (Ed.): The Geology of Central Europe, Vol. 2: Mesozoic and Cenozoic.* pp. 1287-1340.
- Manger, G., 1952: Der Zusammenhang von Salztektonik und Braunkohlenbildung bei der Entstehung der Helmstedter Braunkohlenlagerstätten. *Mitteilungen geologisches Staatsinstitut Hamburg* 21, 7-45.
- Mania, D., 1998: Zum Ablauf der Klimazyklen seit der Elstervereisung im Elbe-Saalegebiet. *Praehistoria Thuringica* 2, 5-21.
- McManus, J.F., Oppo, D.W., Cullen, J.L., 1999: A 0.5-million-year record of millennial-scale climate variability in the North Atlantic. *Science* 283, 971-975.
- Müller, U.C., Klotz, S., Geyh, M.A., Pross, J., & Bond, G.C., 2005: Cyclic climate fluctuations during the last interglacial in central Europe. *Geology* 33, 449-452.
- Narloch, W., Wysota, W., Piotrowski, J.A., 2013: Sedimentological record of subglacial conditions and ice sheet dynamics of the Vistula Ice Stream (north-central Poland) during the Last Glaciation. *Sedimentary Geology* 293, 30-44.
- Osman, A., Pollok, L., Brandes, C., Winsemann, J., *in press*: Sequence stratigraphy of a Paleogene coal bearing rim syncline: interplay of salt dynamics and sea-level changes, Schöningen, Germany. *Basin Research*, doi: 10.1111/bre.12021.
- Passchier, S., Laban, C., Mesdag, C.S., Rijdsdijk, K.F., 2010: Subglacial bed conditions during Late Pleistocene glaciations and their impact on ice dynamics in the southern North Sea. *Boreas* 39, 633-647.
- Piotrowski, J., Geletneky, J., Vater, R., 1999: Soft-bedded subglacial meltwater channel from the Welzow-Süd open-cast lignite mine, Lower Lusatia, eastern Germany. *Boreas* 28, 363-374.
- Praeg, D., 2003: Seismic imaging of mid-Pleistocene tunnel-valleys in the North Sea Basin ó high resolution from low frequencies. *Journal of Applied Geophysics* 53, 273-298.

- Preece, R.C., Gowlett, J.A.J., Parfitt, S.A., Bridgland, D.R., Lewis, S.G., 2006: Humans in the Hoxnian: habitat, context and fire use at Beeches Pit, West Stow, Suffolk, UK. *Journal of Quaternary Science* 21, 485-496.
- Ruddiman, W.F., 2006: Orbital changes and climate. *Quaternary Science Reviews* 25, 3092-3112.
- Russell, H.A.J., Arnott, R.W.C., 2003: Hydraulic jump and hyperconcentrated-flow deposits of a glacial subaqueous fan: Oak Ridges Moraine, Southern Ontario, Canada. *Journal of Sedimentary Research* 73, 887-905.
- Russell H.A.J., Arnott, R.W.C., Sharpe, D.R., 2003: Evidence for rapid sedimentation in a tunnel channel, Oak Ridges Moraine, southern Ontario, Canada. *Sedimentary Geology* 160, 33-55.
- Schirmer, L., 1999: Die Positionen weichselzeitlicher Eisrandlagen in Norddeutschland und ihr Bezug zu unterlagernden Salzstrukturen. *Zeitschrift für geologische Wissenschaften* 27, 111-120.
- Sirocko, F., Szeder, T., Seelos, C., Lehné, R., Rein, B., Schneider, W.M., Dimke, M., 2002: Young tectonic and halokinetic movements in the North-German Basin: its effect on formation of modern rivers and surface morphology. *Netherlands Journal of Geosciences* 81, 431-441.
- Sirocko, F., Reicherter, K., Lehné, R., Hübscher, Ch., Winsemann, J., Stackebrandt, W., 2008: Glaciation, salt and the present landscape. *In: Littke, R., Bayer, U., Gajewski, D., Nelskamp, S. (Eds.), Dynamics of Complex Intracontinental Basins ó The Central European Basin System*. Springer, Berlin, pp. 233-245.
- Stackebrandt, W., 2005: Neotektonische Aktivitätsgebiete in Brandenburg (Norddeutschland). *Brandenburger geowissenschaftliche Beiträge* 12, 165-172.
- Stackebrandt, W., 2009: Subglacial channels of Northern Germany ó a brief review. *Zeitschrift der Deutschen Gesellschaft für Geowissenschaften* 60, 203-210.
- Stewart, M.A., Lonergan, L., Hampson, G., 2013: 3D seismic analysis of buried tunnel valleys in the central North Sea: morphology, cross-cutting generations and glacial history. *Quaternary Science Reviews* 72, 1-17.
- Taki, K., Parker, G., 2005: Transportational cyclic steps created by flow over an erodible bed. Part 1. Experiments. *Journal of Hydraulic Research* 43, 488-501.
- Thieme, H., 1999: Altpaläolithische Holzgeräte aus Schöningen, Ldkr. Helmstedt. *Bedeutsame Funde zur Kulturentwicklung des frühen Menschen*. *Germania* 77, 451-487.
- Toucanne, S., Zaragosi, S., Bourillet, J.F., Cremer, M., Eynaud, F., Van Vliet-Lanoë, B., Penaud, A., Fontanier, C., Turon, J.L., Cortijo, E., Gibbard, P.L., 2009: Timing of massive Fleuve Manche discharges over the last 350 kyr: insights into the European ice-sheet oscillations and the European drainage network from MIS 10 to 2. *Quaternary Science Reviews* 28, 1238-1256.
- Turner, C., 1970: The Middle Pleistocene deposits at Marks Tey, Essex. *Philosophical Transactions of the Royal Society of London. Series B, Biological Sciences* 257, 373-437.

- Urban, B., 1995: Palynological evidence of younger Middle Pleistocene interglacials (Holsteinian, Reinsdorf, Schöningen) in the Schöningen open cast lignite mine (eastern Lower Saxony, Germany). *Mededelingen Rijks Geologische Dienst* 52, 175-186.
- Urban, B., 2007: Interglacial Pollen Records from Schöningen, North Germany. *In: Sirocko, F., Claussen, M., Goni, M.F.S., Litt, T. (Eds.), The Climate of Past Interglacials; Developments in Quaternary Science* 7, pp. 418-444.
- Urban, B., Sierralta, M., 2012: New palynological evidence and correlation of Early Palaeolithic sites in Schöningen 12 B and 13 II, Schöningen open lignite mine. *In: K. Behre (Ed.), Die chronologische Einordnung der paläolithischen Fundstellen von Schöningen. Forschungen zur Urgeschichte im Tagebau von Schöningen* 1, 77-96.
- Urban, B., Sierralta, M., Frechen, M., 2011: New evidence for vegetation development and timing of Upper Middle Pleistocene interglacials in Northern Germany and tentative correlations. *Quaternary International* 241, 125-142.
- Van der Vegt, P., Janszen, A., Moscariello, A., 2012: Tunnel valleys: current knowledge and future perspectives. *In: Huuse, M., Redfern, J., Le Heron, D.P., Dixon, R.J., Moscariello, A., Craig, J. (Eds.), Glaciogenic reservoirs. Geological Society of London Special Publication* 368, pp. 75-97.
- Van der Wateren, F.M., 2002: Processes of glaciotectonism. *In: Menzies, J. (Ed.), Modern and past glacial environments. Elsevier, Amsterdam*, pp. 417-443.
- Van Dijke, J.J., Veldkamp, A., 1996: Climate-controlled glacial erosion in the unconsolidated sediments of northwestern Europe, based on a genetic model for tunnel valley formation. *Earth Surface Processes and Landforms* 21, 327-340.
- Wanner, H., Brönnimann, S., Casty, C., Gyalistras, D., Luterbacher, J., Schmutz, C., Stephenson, D.B., Xoplaki, E., 2001: North Atlantic Oscillation concepts and studies. *Surveys in Geophysics* 22, 321-381.
- Wingfield, R., 1990: The origin of major incisions within the Pleistocene deposits of the North Sea. *Marine Geology* 91, 31-52.
- Winsemann, J., Hornung, J.J., Meinsen, J., Asprion, U., Polom, U., Brandes, C., Bußmann, M., Weber, C., 2009: Anatomy of a subaqueous ice-contact fan and delta complex, Middle Pleistocene, NW Germany. *Sedimentology* 56, 1041-1076.
- Wolff, E.W., Chappellaz, J., Blunier, T., Rasmussen, S.O., & Svensson, A., 2010: Millennial-scale variability during the last glacial: The ice core record. *Quaternary Science Reviews* 29, 2828-2838.
- Yansa, C.H., 2007: Lake Records of Northern Plains Paleoindian and Early Archaic Environments: The öPark Oasisö Hypothesis. *Plains Anthropology* 52, 109-144.
- Ziegenhardt, W., Kramer, H.-J., 1968: Der känozoische Sedimentationsablauf in der Egelner Südmulde - Ein Beitrag zur Kinematik und Dynamik halokinetisch angelegter Randsenken. *Geologie* 19, 902-919.

Acknowledgements

I gratefully acknowledge Prof. Dr. Jutta Winsemann and Prof. Dr. Andrea Hampel for supervision and support during all stages of this thesis. Dominik Steinmetz and Lukas Pollok did a great job with the preparation and first interpretation of the borehole data during their diploma theses. Dr. Christian Brandes is thanked for discussion and contributing to the publications. Dr. Utz Böhner, Dr. Ulrich Polom, Dr. Jordi Serangeli and Dr. Stefan Winghart are thanked for their contributions to the publications.

Financial support by the Niedersächsisches Ministerium für Wissenschaft und Kultur (MWK) is gratefully acknowledged (Project No. 51420035 and PRO Niedersachsen Project No. 11.2-76202-17-3/09). The owner of the Schöningen open-cast mine and the owners of the gravel pits are thanked for the permission to work on their property. Borehole data were generously provided by Brinkmeyer Kieswerk GmbH & Co. KG., E.ON-Kraftwerke GmbH, E.ON Westfalen Weser AG, Niedersächsisches Landesamt für Bergbau, Energie und Geologie, Geologischer Dienst NRW and Landesamt für Geologie und Bergwesen Sachsen-Anhalt.

Janine Meinsen, Ariana Osman, Julia Roskosch and Axel Weitkamp are thanked for discussions and help with fieldwork. Dr. Tao Li, Dr. Georgios Maniatis and Dr. Heidi Turpeinen patiently helped with technical problems with ABAQUS. Discussions with Dr. Falko Turner helped me to better understand the palaeo-ecological database. Dr. Matthieu Cartigny, Prof. Dr. Nicholas Conard, Prof. Dr. Lothar Eissmann, Prof. Dr. Phil Gibbard, Prof. Dr. Klaus-Dieter Meyer, Dr. Daniel Richter, Prof. Dr. Brigitte Urban and Dr. Volker Wilde are thanked for discussion. The technical assistance and support in the field by the team of the archaeological excavation at Schöningen, Wolfgang Berkemer, Neil Haycock, Manfred Kursch, Jens Lehmann, Wolfgang Mertens, Jörg Neumann-Giesen and the late Bernd Köhler, is highly appreciated. Tabea Altenbernd, Maurits Horikx and Timo Lang are thanked for proof-reading some chapters of my thesis.

CURRICULUM VITAE

Name: Jörg Lang
Geburtsdatum: 22.09.1982
Staatsangehörigkeit: Deutsch

Ausbildung

- 2002** **Abitur**, St. Ursula Schule Hannover, Gesamtnote **šgutō**
- 10/2003 - 05/2009** **Studium:** Geowissenschaften, Leibniz Universität Hannover, Diplom: 05/2009, Gesamtnote **šsehr gutō**
Titel der Diplomarbeit: *öA depositional model and sequence stratigraphic correlation for the Cambrian to Silurian succession of the Illizi Basin, Algeriaö*, Note: **šsehr gutō**, Betreuung: Dr. D. Le Heron, Prof. Dr. J. Winsemann
- 07/2010 - 11/2013** **Promotionsstudium** an der Leibniz Universität Hannover
Titel der Dissertation: *öReconstructing the Pleistocene depositional environments at Schöningen (northern Germany): Insights from 3D subsurface modelling and numerical simulationö*, Betreuung: Prof. Dr. J. Winsemann, Prof. Dr. A. Hampel

Berufserfahrung

Praktika

- 07 - 09/2005** Guy Carpenter (München)
08 - 09/2006 Gaz de France, Exploration and Production Germany (Lingen)
07/2008 BP (London)

Wissenschaftlicher Werdegang

- Seit 08/2009** Wissenschaftlicher Mitarbeiter am Institut für Geologie der Leibniz Universität Hannover

Wehrdienst

- 10/2002 - 06/2003** Deutsche Marine

List of publications

Publications in peer-reviewed journals

- Lang, J.**, Hampel, A., Brandes, C. & Winsemann, J. (*in review*) Do salt structures react to ice-sheet loading? Insights from two-dimensional finite-element modelling. *Quaternary Science Reviews*.
- Lang, J.**, Winsemann, J., Polom, U., Böhner, U. & Serangeli, J. (*in review*) The Middle Pleistocene tunnel valley at Schöningen as a Paleolithic archive. *Journal of Human Evolution*.
- Lang, J.** & Winsemann, J. (2013) Lateral and vertical facies relationships of bedforms deposited by aggrading supercritical flows: from cyclic steps to humpback dunes. *Sedimentary Geology*, 296, 36-54.
- Lang, J.**, Dixon, R.J., Le Heron, D.P. & Winsemann, J. (2012) Depositional architecture and sequence stratigraphic correlation of Upper Ordovician glaciogenic deposits, Illizi Basin, Algeria. *In*: Huuse, M., Redfern, J., Le Heron, D.P., Dixon, R.J., Moscariello, A. & Craig, J. (Eds.): *Glaciogenic reservoirs*. Geological Society of London Special Publications 368, 293-317.
- Lang, J.**, Winsemann, J., Steinmetz, D., Polom, U., Pollok, L., Böhner, U., Serangeli, J., Brandes, C., Hampel, A. & Winghart, S. (2012) The Pleistocene of Schöningen, Germany: a complex tunnel valley fill revealed from 3D subsurface modelling and shear wave seismics. *Quaternary Science Reviews* 39, 86-105.

Publications in other journals

- Lang, J.** & Winsemann, J. (2012) The 12-II DB outcrop section at Schöningen: sedimentary facies and depositional architecture. *In*: Behre, K.-E. (Ed.) *The chronological setting of the Palaeolithic sites of Schöningen*. *Forschungen zur Urgeschichte im Tagebau von Schöningen* 1, 39-59.
- Serangeli, J., Bigga, G., Böhner, U., Julien, M.-A. **Lang, J.** & Stahlschmidt, M. (2012) Ein Fenster in das Altpaläolithikum. *Archäologie in Deutschland* 2012/4, 6-12.

Conference contributions (Abstracts)

- Lang, J.**, Hampel, A., Brandes, C. & Winsemann, J.: Interaction between salt structures and ice-sheet loading: Insights from two-dimensional numerical modelling. *Sedimentary Basins - Research, Modelling, Exploration*, 2013, Jena.
- Lang, J.** & Winsemann, J.: Lateral and vertical facies relationships of aggrading supercritical bedforms: from cyclic steps to humpback dunes. 30th IAS Meeting of Sedimentology, 2013, Manchester, UK.
- Lang, J.**, Winsemann, J., Steinmetz, D., Polom, U., Pollok, L., Böhner, U., Serangeli, J., Brandes, C., Hampel, A. & Winghart, S.: Depositional architecture of a complex Middle Pleistocene tunnel valley fill, Schöningen, Germany. 30th IAS Meeting of Sedimentology, 2013, Manchester, UK.
- J. Winsemann, P. Alho, N. Goseberg, **J. Lang**, J. Meinsen, F.S. Busschers & W. Westerhoff: Middle Pleistocene megafloods in northern central Europe: integrating field data and hydraulic modelling. 10th International Conference on Fluvial Sedimentology, 2013, Leeds, UK.
- J. Serangeli, G. Bigga, U. Böhner, M.-A. Julien, T. van Kolfschoten, **J. Lang**, C. Miller, M. Stahlschmidt, N.J. Conard: Fortsetzung der Ausgrabungen in Schöningen im Jahr 2012. 6 Hugo-Obermaier-Gesellschaft, 55th Annual Meeting, 2013, Wien, Österreich.
- Lang, J.**, Winsemann, J., Steinmetz, D., Polom, U., Pollok, L., Böhner, U., Serangeli, J., Brandes, C., Hampel, A. & Winghart, S.: Anatomy of a complex tunnel valley fill revealed from 3D subsurface modelling and shear wave seismics: the Pleistocene of Schöningen, Germany. 6 GeoHannover, 2012, Hannover.

- Lang, J.** & Winsemann, J.: Stationary waves and humpback dunes: evidence for highly aggradational supercritical flow conditions on glacial subaqueous fans. ó GV & Sediment Meeting, 2012, Hamburg.
- Lang, J.**, Winsemann, J., Steinmetz, D., Polom, U., Pollok, L., Böhner, U., Serangeli, J., Brandes, C., Hampel, A. & Winghart, S.: Insights into a complex Middle Pleistocene tunnel valley fill, Schöningen, Germany. ó GV & Sediment Meeting, 2012, Hamburg.
- Lang, J.**, Dixon, R.J., Le Heron, D.P. & Winsemann, J.: Upper Ordovician glacial deposits of the Illizi Basin (Algeria): facies architecture and sequence stratigraphic correlation. ó GV & Sediment Meeting, 2012, Hamburg.
- Lang, J.**, Winsemann, J., Steinmetz, D., Polom, U., Pollok, L., Böhner, U., Serangeli, J., Brandes, C., Hampel, A. & Winghart, S.: Sequence stratigraphic correlation of the Palaeolithic sites of Schöningen (Germany). - Umwelt ó Mensch ó Georisiken im Quartär: 35. Hauptversammlung der deutschen Quartärvereinigung (DEUQUA), 2012, Bayreuth.
- Winsemann, J., Meinsen, J., Alho, P., Busschers, F., Westerhoff, W., **Lang, J.** & Klostermann, J.: Reconstruction of the Weser Lake outburst flood pathway: integrating field data and hydraulic modelling. - Umwelt ó Mensch ó Georisiken im Quartär: 35. Hauptversammlung der deutschen Quartärvereinigung (DEUQUA), 2012, Bayreuth.
- Lang, J.**, & Winsemann, J.: Humpback-dunes and aggrading standing waves: Characteristic features of glacial subaqueous fans. ó 74th EAGE Conference & Exhibition, 2012, Kopenhagen, Dänemark.
- Lang, J.**, Dixon, R.J., Le Heron, D.P. & Winsemann, J.: Depositional architecture and sequence stratigraphy of Upper Ordovician glacial deposits, Illizi Basin, Algeria. ó 74th EAGE Conference & Exhibition, 2012, Kopenhagen, Dänemark.
- Lang, J.**, Winsemann, J., Polom, U., Serangeli, J. & Böhner, U.: The Pleistocene of Schöningen, Germany: implications for palaeoenvironments and palaeolithic archaeology. ó Society for American Archaeology, 77th Annual Meeting, 2012, Memphis, TN, USA.
- Lang, J.**, Winsemann, J., Steinmetz, D., Polom, U., Pollok, L., Böhner, U., Serangeli, J., Brandes, C., Hampel, A., Conard, N. & Winghart, S.: The famous findings of Schöningen, Germany: a new geological model for the embedding and preservation of palaeolithic artefacts. ó Hugo Obermaier-Gesellschaft, 54th Annual Meeting, 2012, Toulouse, Frankreich.
- Lang, J.**, Steinmetz, D., Pollok, L., Brandes, C., Hampel, A., Polom, U., Winghart, S. & Winsemann, J.: The Middle Pleistocene succession of Schöningen, Germany: A complex tunnel valley fill inferred from 3D subsurface modeling. ó INQUA, 2011, Bern, Schweiz.
- Lang, J.**, Steinmetz, D., Pollok, L., Böhner, U., Brandes, C., Hampel, A., Polom, U., Winghart, S., & Winsemann, J.: Integrating modern geological tools and archaeology: a case study from the famous Middle Pleistocene succession of Schöningen, Germany. ó INQUA, 2011, Bern, Schweiz.
- Lang, J.**, Steinmetz, D., Brandes, C., Polom, U. & Winsemann, J.: A depositional model for the Middle Pleistocene succession of Schöningen, NW Germany: facies analysis, seismic stratigraphy and 3D subsurface modeling (GOCAD). ó Ice, Water, Humans: 35. Hauptversammlung der deutschen Quartärvereinigung (DEUQUA), 2010, Greifswald.
- Serangeli, J., Böhner, U., van Kolfschoten, T., Schoch, W.H., **Lang, J.**, Bigga, G., Miller, C. & Conard, N.J.: New Organic Artifacts From the 2008-2009 Excavations in Schöningen (Lower Saxony, Germany). ó Paleoanthropology Society Meeting, 2010, St. Louis, MO, USA.
- Lang, J.**, Dixon, R.J., Le Heron, D.P. & Winsemann, J.: Facies characteristics and depositional architecture of Upper Ordovician glacial fan systems, Illizi Basin, Algeria. ó Glaciogenic Reservoirs and Hydrocarbon Systems, The Geological Society, 2009, London, UK.
- Lang, J.**, Dixon, R.J., Le Heron, D.P. & Winsemann, J.: A depositional model and sequence stratigraphic correlation for Ordovician glacial deposits, Illizi Basin, Algeria. ó Frühjahrstagung der DGMK, 2009, Celle.

- Lang, J.**, Dixon, R.J., Le Heron, D.P. & Winsemann, J.: A sequence stratigraphic model for Ordovician glacial deposits, Illizi Basin, Algeria. ó 4th North African/Mediterranean Petroleum and Geosciences Conference and Exhibition, 2009, Tunis, Tunesien.
- Greb, M., **Lang, J.**, Fritschka, N., Bieg, U., Hornung, J., Friedrich, A., Bruhn, R. & Hinderer, M.: Sedimento-logic and geomorphologic analysis of alluvial fans in the southern Death Valley, California (SW-USA). ó Sediment 2007, Brixen, Italien.
- Fritschka, N., **Lang, J.**, Greb, M., Bieg, U., Hornung, J, Friedrich, A. & Hinderer, M.: Application of ground-penetrating radar in the Death Valley field site: Influence of ferromagnetic minerals on the propagation of electromagnetic waves send out by GPR. ó Sediment 2007, Brixen, Italien.
- Bieg, U., Hornung, J., Greb, M., Fritschka, N., **Lang, J.**, Friedrich, A. & Hinderer, M.: Three dimensional ground-penetrating radar analysis of alluvial fan deposits (Death Valley, SW USA). ó Sediment 2007, Brixen, Italien.
- Bieg, U., Hornung, J., Greb, M., Fritschka, N., **Lang, J.**, Friedrich, A. & Hinderer, M.: Three-dimensional ground penetrating radar analysis of alluvial fan deposits (Death Valley, SW USA). ó Alluvial Fans 2007, Banff, Kanada.